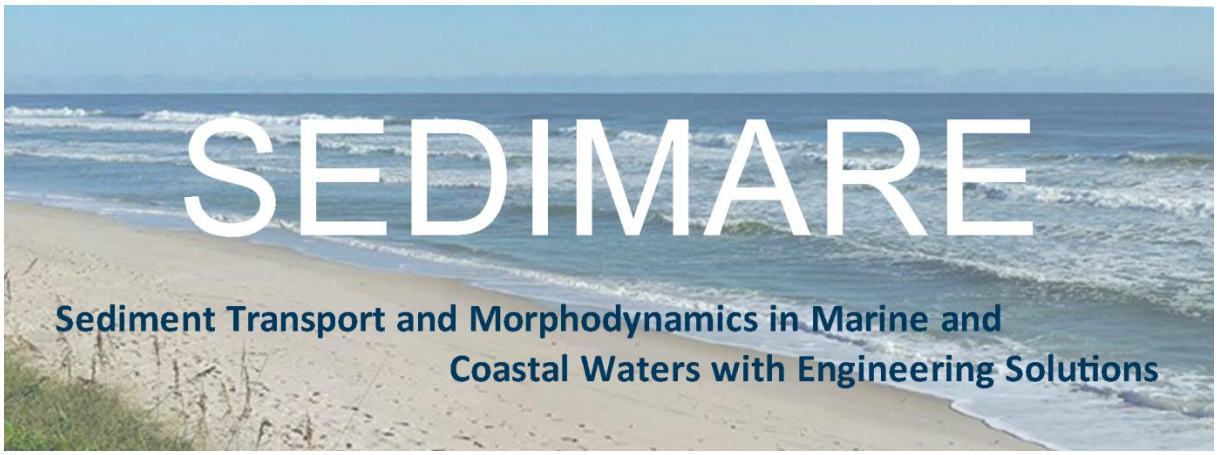

Project Number: 101072443

2nd NETWORK WORKSHOP

Dissemination level: PU - Public

Prepared by:

Athanassios Dimas, Coordinator, University of Patras

This project has received funding from the European Union's (EU) Horizon Europe Framework Programme (HORIZON) under Grant Agreement No. 101072443 as a MSCA Doctoral Network (HORIZON-MSCA-2021-DN-01).

Document Information

Project Title	Sediment Transport and Morphodynamics in Marine and Coastal Waters with Engineering Solutions
Project Acronym	SEDIMARE
Grant Agreement No.	101072443
Call	MSCA Doctoral Networks 2021 (HORIZON-MSCA-2021-DN-01)
Start Date of Project	01-02-2023
Duration of Project	48 months
Document	2nd NETWORK WORKSHOP
No. of pages including cover	263

Version	Publication Date	Author(s)	Change
1.0	25.09.2025	Athanassios Dimas	Initial version

Date and Signature of Author(s): ATHANASIOS DIMAS
25/09/2025 18:21

Table of Contents

1. Program

The SEDIMARE "2nd Network Workshop" was organized by HR Wallingford at its facilities in the UK (Howbery Park, Wallingford, Oxfordshire) on 10-11 September 2025. Local organizers were Dr. M. Knaapen and Dr. R. Whitehouse. All DCs participated with presentations of their research.

Day 1 –Wednesday 10 September

Morning

- 8:45 Walk-in
- 9:00–9:30 Welcome by **Ridha Bentiba** (Joint Chief Executive Officer)
- 9:30–10:30 Presentation of *"The evolution of tsunami physical modelling since 2004"* by **Ian Chandler** (Principal Engineer)
- 10:30 Coffee Break
- 11:00–12:40 DCs presentations (15 min presentation + 10 min discussion)
    - 11:00–11:25 DC Evangelos Petridis
    - 11:25–11:50 DC Quan Nguyen
    - 11:50–12:15 DC Ioannis Gerasimos Tsipas
    - 12:15–12:40 DC Saeed Osouli
- 12:40 Lunch

Afternoon

- 14:00–15:00 Presentation of "*Development of a new openFoam solver for scour and sediment transport simulations*" by **Sina Haeri** (Technical Director - CFD)
- 15:15–17:15 **Supervisory Board meeting**

Evening

- 19:30 Project social dinner

Day 2 – Thursday 11 September

Morning

- 8:45 Walk-in
- 09:00–10:30 Visiting HR Wallingford Facilities.
- 10:30 Coffee Break
- 11:00–12:40 DCs presentations (15 min presentation + 10 min discussion)
    - 11:00–11:25 DC Eloah Rosas
    - 11:25–11:50 DC Siyuan Wang
    - 11:50–12:15 DC Van Thi To Nguyen
    - 12:15–12:40 DC Muhammed Said Parlak
- 12:40 Lunch

Afternoon

- 14:00–15:00 Presentation of "*Insights on flow-structure-seabed interaction gained from laboratory testing*" by **Richard Whitehouse** (Technical Director - Sediment Dynamics)
- 15:00–16:40 DCs presentations (15 min presentation + 10 min discussion)
    - 15:00–15:25 DC Nishchay Tiwari

- 15:25–15:50 DC Nasim Soori
- 15:50–16:15 DC Jowi Miranda
- 16:15–16:40 DC Buckle Subbiah Elavazhagan

2. Presentations

The abstracts and the presentations of all the DCs, are shown in the next pages.

Large-eddy simulation of turbulent oscillatory flow and sediment transport induced by waves

Tsipas, I.G., Dimas, A.A.

Understanding the dynamics of turbulent oscillatory flow and wave-induced sediment transport is essential for predicting and managing key coastal processes such as shoreline erosion and pipeline or cable exposure. This study develops and applies a large-eddy simulation (LES) framework to model oscillatory flows over sand beds of mixed-grain sizes. The approach solves the Navier–Stokes equations with subgrid-scale modeling and sediment transport equations that account for both bed and suspended load. Sediment fractions are defined through the size distribution curve, using representative diameters D_{10}, D_{30}, D_{50}, D_{70}, and D_{90} to capture mixed-grain dynamics. Simulations are performed at a geometric scale of 1/4.5, based on existing experiments, with three fixed ripples, span- and streamwise periodicity, rigid-lid conditions at the top, and the immersed boundary method for bottom wall boundary dondition. The computational grid includes over 14 million cells. Results show that fractions coarser than D_{50} dominate bed load transport, while finer grains are more concentrated in suspension. Suspended load is further evaluated using two empirical formulas for the bottom boundary conditions. From the results, D_{40} is identified as a representative diameter for suspended transport. Future work will integrate a law of the wall model and extend the Exner equation with size fractions to improve predictions of bed evolution in coastal environments.

Investigation of nearshore dynamics by utilising remote sensing tools

Parlak, M.S., Postacchini, M., Brocchini, M.

The nearshore is a coastal zone where hydro-morphodynamic processes are primarily driven by nonlinear mechanisms, with waves acting as one of the main forcing factors directly shaping sea state conditions. Collecting in-situ wave data, however, is challenging due to complex physical interactions and high operational costs. Remote sensing tools (RSTs) offer an effective alternative, providing broader spatial coverage with relatively low maintenance requirements. Two RSTs, an X-Band Radar (XBR) and a video monitoring system (SGS), were deployed at the Senigallia Harbour. A novel image assimilation framework has been developed to process data from RSTs. The approach is based on advanced image and signal processing methods (e.g., Radon transformation, continuous wavelet transformation) to retrieve wave characteristics and the bathymetry. The results are compared with the observations and outputs of alternative processing tools. The method demonstrated promising performance for nearshore wave characteristics and the bathymetry. Current research efforts are aimed at refining the methodology and advancing the study of nearshore wave dynamics by integrating SGS system. Future work is focused on the incorporation of phase-resolving model which can be fed by RSTs to conduct various coastal resilience analyses. Consequently, a complete framework, which is a combination of RSTs, observations and numerical models, can be established.

Initial observations of wave ripples and suspended concentrations in sand–silt mixtures

Nguyen, T.T.V., Roos, P.C., van der Werf, J.J., Raadschelders, L.T.

The suspended concentrations and bedforms of sand–silt mixtures under oscillatory flow conditions were observed via a laboratory experiment using the AOFT (Aberdeen Oscillatory Flow Tunnel). Specifically, two groups of sand–silt mixtures were created by mixing the base material, fine sand ($D_{50} \approx 150$ μm, where D_{50} indicates median grain size), with: (1) coarse silt ($D_{50} \approx 50$ μm) and (2) medium silt ($D_{50} \approx 30$ μm). These mixtures were tested under three skewed-velocity conditions with root-mean-square velocities of 0.2, 0.3, and 0.4 m/s. Concentration and velocity profiles were measured using the ABS (Acoustic Backscatter Sensor), the TSS (Traverse Suction System), and the ADVP (Acoustic Doppler Velocity Profiler). Bedforms were measured in 2D with the LBP (Laser Bed Profiler) before and after the experiments, and in 1D over time with the SRP (Sand Ripple Profiler). The concentration of sand–medium silt (SaMs) mixtures was higher compared to sand–coarse silt (SaCs) mixtures for most conditions, except at 0.2 m/s. Most cases produced 3D ripples. Ripple dimensions were largest at 0.2 m/s ($\eta > 8$ mm, where η is ripple height), while the smallest ripples ($\eta < 3$ mm, nearly absent) occurred at 0.4 m/s, due to the transition to sheet flow conditions.

Eulerian–Lagrangian modelling of current-driven transport and PTV analysis of wave-induced particle dynamics in shallow water

Soori, N., Brocchini, M., Dimas, A.A., Postacchini, M.

The study of mass transport processes provides valuable understanding of sediment dynamics, such as particle motion, bed resistance, and the mechanisms that influence sediment modification, retention, and accumulation. This research examines sediment transport under the action of currents and waves through both numerical modelling and laboratory experiments. In the numerical modelling using MATLAB, the focus was placed on the behaviour of massive particles in shallow water conditions. A custom MATLAB code was developed based on a coupled Eulerian–Lagrangian framework. In this approach, hydrodynamic flow fields are first generated by solving the NSWEs. These fields are then applied as inputs to a particle tracking routine, where the Lagrangian module calculates particle trajectories. At each time step, local flow velocities are interpolated from the 2DH hydrodynamic solution, and particle positions are updated using numerical integration. This method allows the quantification of particle pathways, residence times, dispersion, and connectivity within the domain. Complementing the modelling, laboratory tests using PTV were performed, where neutral seeding particles acted as optical tracers to resolve trajectories and velocity profiles,with emphasis on vertical distributions. Analysis of trajectories and drift velocities provides essential knowledge of wave-driven transport mechanisms, advancing understanding of sediment and particle dynamics in coastal systems.

Cross-shore hydro-morphodynamics in a beach protected by submerged vegetation meadow under erosive wave conditions

Elavazhagan, B., Maza, M., Lara, J.

Coastal areas face immense threat by means of beach erosion driven primarily by storm waves. Nature based solutions are explored for their role in ecosystem benefits and coastal protection benefits. Notable is the P. *Oceanica*, commonly seagrass quite prevalent in coastal areas around the world. Understanding the processes like bed evolution, wave and velocity attenuation in different beach types including vegetated ones are of scientific interest which helps enabling protection measures, proper ecosystem restoration and NBS designs. IH2VOF-SED is a RANS based 2DV one phase sediment transport model developed to provide accurate morphological predictions efficiently in different beach states. The model includes vegetation effects via drag force as a momentum sink term in Navier-Stokes equation, via dispersive fluxes as source terms in k-Ɛ equation and plant motion effects via Morrsion's equation. Two experiments conducted in Southeast China University wave flume with vegetations mimicking P. *Oceanica* and S. *Alterniflora* are used to validate the model. The model is able to demonstrate accurately the hydrodynamics and the bed evolution furthering its application. Subsequently, different hydro-morphodynamic processes influenced by the presence of different vegetation types at the toe and the breaking zone of the beach profile are studied providing insights into their role.

Mathematical modeling and numerical simulations of water-saturated granular materials with emphasis on sediment transport

Petridis, E.A., Papalexandris., M.V.

Underwater dunes are dynamic bedforms that emerge from the interaction between fluid flow and sediment transport. Their migration and evolution influence local hydrodynamics, alter seabed topography, and affect engineering and ecological processes. In this work, we investigate dune formation and dynamics using a two-pressure, two-velocity continuum model for saturated fluid–granular mixtures. The governing equations couple conservation laws for the fluid and solid phases with interphasial momentum exchange, non-Newtonian stress closures for the granular medium, and a compaction equation for the solid volume fraction. The numerical scheme employs a predictor–corrector time integration combined with a generalized projection method for the phasic pressures. Simulations are performed in a two-dimensional domain representative of subaqueous sediment transport, initialized with a parabolic velocity profile and solid packing fraction of $\phi s = 0.59$. Different flow velocities and oscillation amplitudes are explored to assess their influence on bedform development. The results capture dune initiation, nonlinear growth, and flow–sediment feedback mechanisms, including the formation of recirculation zones and vorticity structures. Comparisons across cases highlight the sensitivity of dune morphology to flow strength and sediment compaction. The study provides a computational framework for analyzing sedimentary patterns and sets the stage for future validation against experimental data and extension to more realistic dune geometries.

Development of erosion threshold formulas for different sand-mud bed types

Miranda, P.S., van der Werf, J.J., Hulscher S.J.M.H.

Estuarine and deltaic evolution is influenced by sediment composition, particularly sand-mud mixtures, because different combinations are governed by distinct initiation of motion processes. To capture this variability, previous studies have estimated erosion thresholds using single bulk parameters (e.g. mud content, median grain size, bulk density). This study isolated dominant processes across sand-mud mixtures by bed type classification following the framework of Van Ledden et al. (2004), and applied multiple parameterizations to represent initiation of motion. The resulting equations provided improved fits across bed types as well as for the full dataset when compared with existing formulations. These findings offer a practical method for estimating initiation of motion from bulk parameters, with implications for sand-mud experiments and numerical modeling research.

Numerical investigations of bottom boundary layer hydrodynamics under a dam-break-driven swash event

Nguyen, Q.T., Kranenborg, J.W.M., Dodd, N., Briganti, R., van der Werf, J.J., Roos, P.C., Zhu, F.

In swash zone modelling, the nonlinear shallow water equations (NSWE) are commonly applied with a hydrostatic pressure assumption. While this assumption is generally valid in the swash zone, it neglects the minor, non-hydrostatic vertical pressure gradients that involve vertical accelerations occurring during wave run-up and rundown. This study aims at establishing whether these non-hydrostatic terms are significant enough to be included in the NSWE. The methodology consists in aims to approximate the dynamic pressure gradients efficiently using a depth-averaging model equipped with a bottom boundary layer (BBL) model. A dam-break case from the literature is used to test the model. The numerical results from the present model are compared to the experimental ones and to the simulations provided by a more computationally expensive, depth-resolving Computational Fluid Dynamics (CFD) model based on the Reynolds Averaged Navier-Stokes. In the depth integrated model, the dynamic pressure in the horizontal momentum equation is approximated by calculating terms involving accelerations in the vertical velocity. This is reconstructed in the BBL using a sub-model, originally proposed by Briganti et al. (2011). The findings show that the reconstructed vertical velocity is more accurate than that from the CFD model when compared to the measurements. The reconstructed terms involving accelerations in the vertical velocity are generally greater than the non-hydrostatic pressure contribution estimated from the CFD model. However, results show that the reconstructed vertical acceleration terms contribute minimally to the overall pressure gradient, and the hydrostatic term are several orders of magnitude higher.

A multi-layer shallow water framework for the modelling of submarine landslide

Rosas, E., Spinewine, B., Soares, S.

Sedimentary density flows, particularly submarine landslides, is important in marine sediment transport and pose major geohazards to offshore infrastructure. These flows are typically characterized by unsteady, high-sediment concentrations, and strong vertical stratification. Studying their behaviour presents significant challenges, as the transition from slope failure to runout and fluidization involves complex changes in material strength. This strain-softening process, driven by particle breakage, water entrainment, and structural remoulding, progressively reduces shear resistance, directly impacting flow velocity and dynamics. To better capture this process, this study suggests a novel multilayer shallow water framework that incorporates the approximation of Herschel–Bulkley rheological model for bed shear stress. The model distinguishes between yielded (sheared) and unyielded (plug) zones within the flow, with a new implementation for yield stress that degrades with strain, known as strain softening. By resolving vertically varying yield stress across multiple layers, the model more accurately captures nonlinear shear behaviour, including yield stress, shear thinning/thickening, and rate-dependent effects. Consequently, it improves predictions of vertical velocity profiles and flow trajectories while integrating key processes like water entrainment and sediment erosion/deposition. This approach provides a refined tool for hazard assessment of submarine landslides and their impact on subsea structures.

Overtopping Breakwater For Energy Conversion (OBREC)

Osouli, S., Postacchini, M., Sabbioni, I., Brocchini, M., Zitti, G.

The aim of this project is to assess the feasibility of installing OBRECs on shore revetments considering water discharge to the inshore part of the structure. A prototype of this system will be installed in the port of Ancona in Italy. To design the device, waves offshore were selected based on PDF (probability density function) diagrams, then they were transferred to the shallow waters using Goda approach which is an analytical model. FUNWAVE-TVD was used to track wave characteristics inside the port and near the structure. This numerical model chain reached to the FLOW-3D software to analyse wave-structure interactions, turbine performance and flow conditions in the convey system with different discharge boundary conditions (inshore or offshore). For the FUNWAVE-TVD section, bathymetry was created by combining two datasets, and wave energy spectrum was extracted from FUNWAVE-TVD outputs as the wave maker boundary conditions in FLOW-3D. Different ramp slopes under two freeboard conditions were compared with the CFD tool. Results for overtopping and reflection coefficients were compared with experimental results. An Archimedes turbine was modelled as a low head turbine in a pipe to define an optimal rotation speed to maximise efficiency to impose in real condition, if it is applicable. Finally, energy across the convey system was estimated considering different discharge conditions such as no waves, tides and waves boundary condition.

Experimental and numerical investigation of overtopping-induced breaching in non-cohesive dams

Wang, S., Roos, P.C., Soares, S.

Breach formation and development in earthen dams is a complex and highly dynamic process, with critical implications for flood risk assessment and mitigation. This study investigates overtopping-induced breaching in small-scale, non-cohesive sand dams through an integrated programme of physical experiments and numerical simulation. Laboratory tests were conducted in a small-scale flume using two different uniform sands under constant inflow conditions. Breach morphodynamics was monitored with close-range photogrammetry, allowing high-resolution reconstruction of the three-dimensional breach evolution, while ultrasonic sensors continuously measured upstream water levels, to determine the breach outflow discharge. Such experiments are needed to validate numerical simulations tools aimed at predicting breaching events. In this study, numerical simulations were performed using a depth-averaged two-dimensional morphodynamic model that solves the coupled shallow-water and Exner equations. The model is complemented with a bank erosion module, accounting for the lateral erosion and enlargement of the breach. The experimental results were used to verify the performance of the numerical model and offered further calibration. This study highlighted the value of combining experimental studies with numerical modelling to improve understanding of the mechanisms governing dam breaching.

Multi-model approach to scour in dynamic areas

Tiwari, N., Knaapen, M., Haeri, S., Whitehouse, R.

Scour around vertical marine structures is a critical design challenge for offshore wind and coastal infrastructure. This work applies a multi-model approach using the Eulerian three-phase solver *SedInterFoam* within OpenFOAM, coupled with *waves2Foam*, to simulate scour development under currents, waves, and combined wave–current conditions. The computational domain is scaled to replicate flume experiments conducted at HR Wallingford's Fast Flow Facility, with mesh resolution and boundary conditions carefully designed to capture near-bed processes. Reflection analysis using a least-squares method confirms strong agreement between simulated and experimental wave spectra, particularly when employing weighted relaxation zones. Current-only cases correctly reproduce onset of motion at $U \approx 0.3$ m/s and full mobilisation at $U \approx 0.4$ m/s, consistent with theoretical Shields estimates. Wave–current cases reveal wider scour patterns compared to current-only scour, highlighting the amplifying role of oscillatory motion. The $\mu(I)$ rheology framework is implemented for sediment stress, though sensitivity studies indicate a persistent underestimation of the angle of repose, pointing to limitations in the current model formulation. Overall, the simulations demonstrate robust predictive skill in replicating experimental scour trends, while also identifying areas for solver development. Future work will focus on vorticity dynamics, sediment heterogeneity, and scaling to prototype conditions for offshore foundations.

3rd International Conference on Design and Management of Port, Coastal and Offshore Works 2025
7-9 May, Patras, Greece

DMPCO

Large-eddy simulation of turbulent oscillatory flow and sediment transport induced by waves

Ioannis Gerasimos Tsipas

Supervisor: Athanassios A. Dimas, Professor

Funded by the European Union

This project has received funding from the European Union's Horizon Europe research and innovation programme under the Marie Skłodowska-Curie grant agreement No 101072443.

European Commission

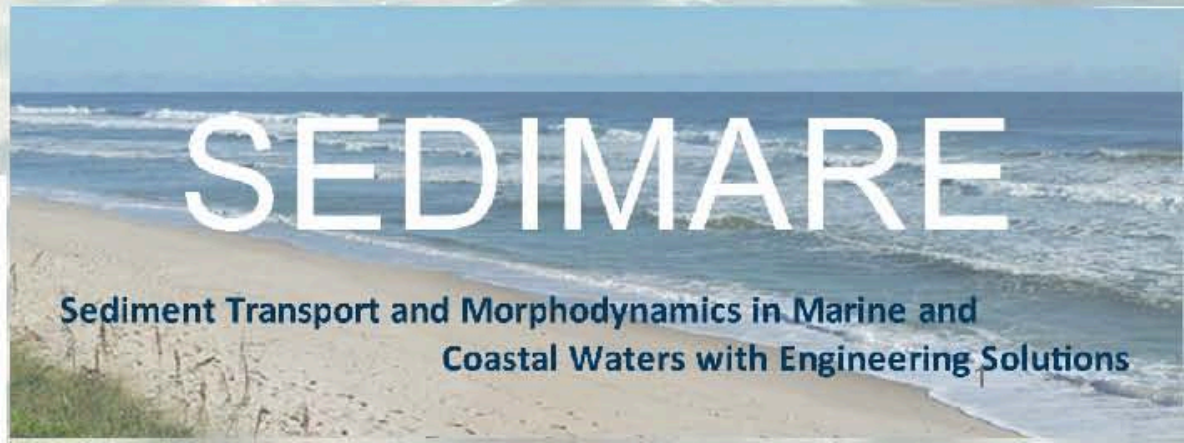

Introduction

Surface waves induce oscillatory flow at seabed

↓

Generation of bed forms (ripples, dunes, bars)

↓

Significant impact on wave propagation and sediment transport by increasing bed roughness due to vortex shedding

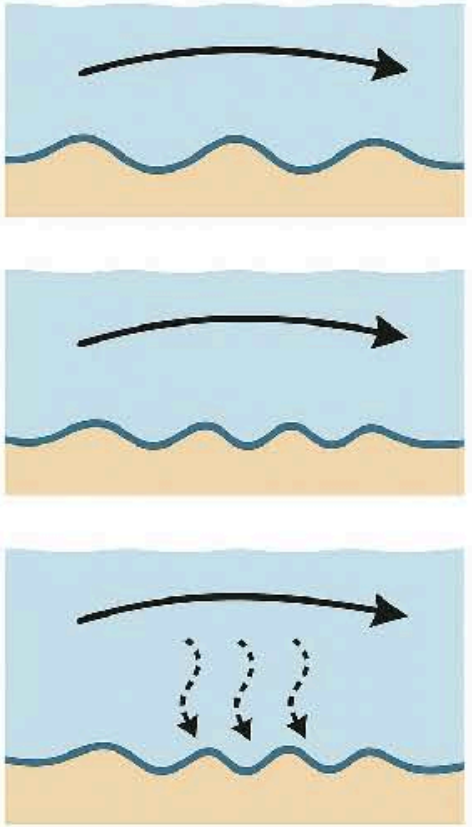

The dynamics of turbulent oscillatory flow and sediment transport over sandy beds is critical for understanding various environmental and engineering processes:

- coastal erosion
- Pipeline and cable exposure
- habitat formation
- Harbor and channel siltation

Objectives

- Development of large-eddy simulation (LES) software to model turbulent oscillatory flow and mixed-grain sediment transport induced by waves.

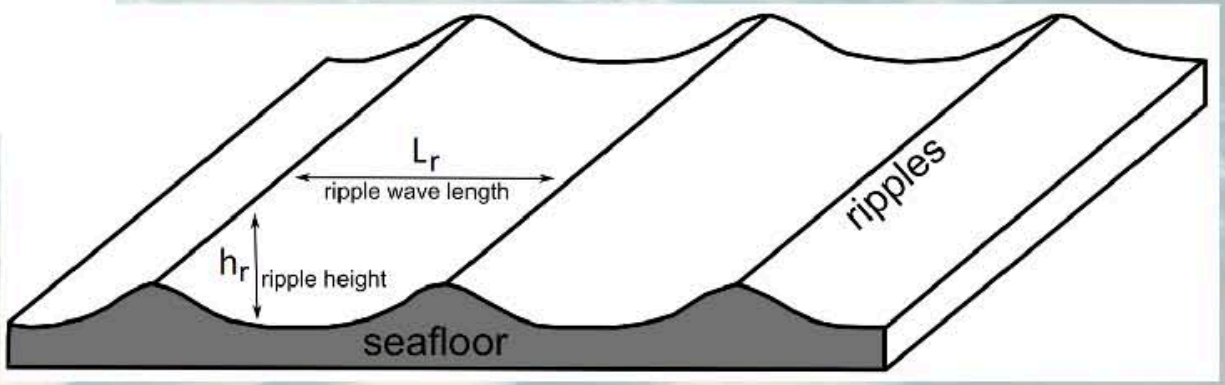

https://www.vhv.rs/viewpic/hbJbwRw_transparent-water-ripples-png-ripple-of-water-diagram/

Methodology

Key points along the CDF curve are labeled:

D10, D30, D50, D70, and **D90 that will be used later in the simulation set-up as the number of diameters (nd).**

- **D10:** Particle size at which 10% of the sediment is finer.
- **D30:** Particle size at which 30% of the sediment is finer.
- **D50:** Median particle size, where 50% of the sediment is finer.
- **D70:** Particle sizes where 70% of the sediment is finer.
- **D90:** Particle sizes where 90% of the sediment is finer.

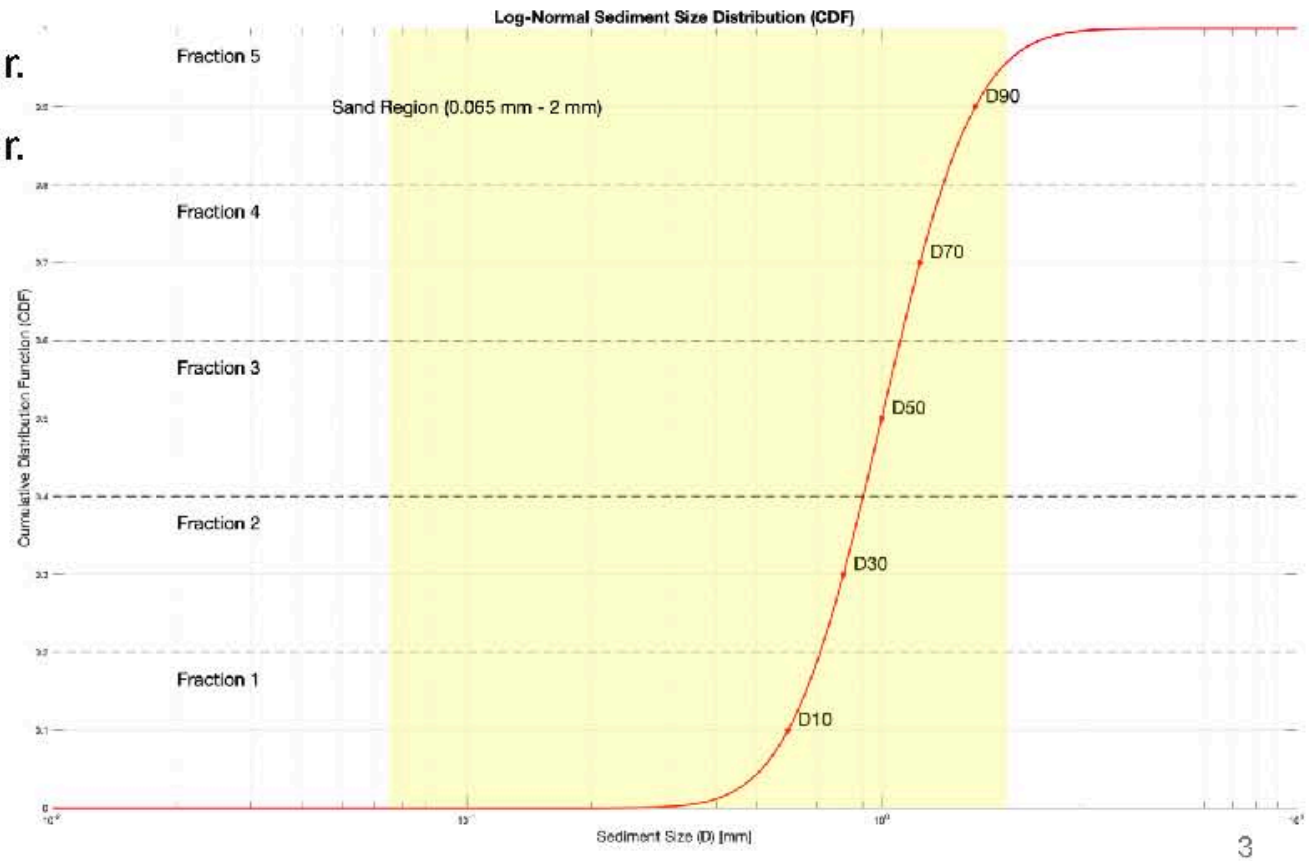

Flow Equations

Continuity equation: $\frac{\partial u_i}{\partial x_i} = 0$

Navier-Stokes equations: $\frac{\partial u_i}{\partial t} + \frac{\partial}{\partial x_j}\left(u_i u_j\right) = -\frac{\partial p}{\partial x_i} - \frac{\partial \tau_{ij}}{\partial x_j} + \frac{1}{\mathrm{Re}}\frac{\partial^2 u_i}{\partial x_j \partial x_j} + f_i$

$$Re = \frac{U_0 a_0}{\nu}$$

u_i is the resolved velocity field according to LES .

Dynamic pressure: $p = P_o + P$ where P_o is the externally imposed pressure field.

$$u_o(t) = U_o\left(\cos(\omega t) + B\cos(2\omega t)\right)$$

Subgrid-scale (SGS) stresses (Smagorinsky 1963) : $\tau_{ij} = -2D_{wall}\nu_{sgs}S_{ij} = -2D_{wall}\left(C_s\Delta\right)^2|S|S_{ij}$

$$S_{i,j} = \frac{1}{2}\left(\frac{\partial u_i}{\partial x_j} + \frac{\partial u_j}{\partial x_i}\right) \qquad |S| = \left(2S_{ij}S_{ij}\right)^{1/2} \qquad \Delta = \left(\Delta x_1 \Delta x_2 \Delta x_3\right)^{1/3}$$

$$D_{wall} = 1 - \exp\left(-\left(\frac{r^+}{A^+}\right)^3\right) \qquad r^+ = \frac{u_* r}{\nu_w} \qquad u_* = \sqrt{\frac{\left|\max(\tau_b)\right|}{\rho_w}} \qquad A^+ = 25$$

Sediment Transport Equations

Bed load transport rate (Engelund and Fredsøe, 1976):

$$\frac{q_{b(nd)}}{\sqrt{(S-1)gDg_{(nd)}^3}} = \begin{cases} \operatorname{sgn}(\theta)\frac{5\pi}{3}\left[1+\left(\frac{\pi}{6}\frac{\mu_d}{|\theta|-\theta_{c(nd)}}\right)^4\right]^{-\frac{1}{4}}\left(\sqrt{|\theta|}-0.7\sqrt{|\theta c_{(nd)}|}\right), (\theta > \theta c_{(nd)}) \\ 0 \qquad , (\theta < \theta c_{(nd)}) \end{cases}$$

Shields number : $\theta = \frac{\tau_b}{\rho_w(S-1)gDg_{50}^3}$

Critical Shields number: $\theta_c\left(D_{g(nd)}, S\right)$

Grain diameters: $Dg_{(nd)}$

Sediment specific gravity: S

Dynamic friction coefficient: $\mu_d \approx 0.5\mu_s$

Sediment Transport Equations

Advection-diffusion equation for the suspended sediment concentration:

$$\frac{\partial c_{(nd)}}{\partial t} + u_j \frac{\partial c_{(nd)}}{\partial x_j} - w_{s(nd)} \frac{\partial c_{(nd)}}{\partial x_3} = \frac{1}{\sigma Re} \frac{\partial^2 c_{(nd)}}{\partial x_j \partial x_j} - \frac{\partial \chi_j}{\partial x_i} + f_c$$

where $w_{s(nd)}$ is the sediment fall velocity (Hallermeier 1981) for each grain fraction:

$$\frac{w_{s(nd)} D g_{(nd)}}{\nu} = \begin{cases} \mathrm{D}_{*(nd)}^3/18 & \mathrm{D}_{*(nd)}^3 < 39 \\ \mathrm{D}_{*(nd)}^{2.1}/6 \quad for & 39 < \mathrm{D}_{*(nd)}^3 < 10^4 \\ 1.05\mathrm{D}_{*(nd)}^{1.5} & 10^4 < \mathrm{D}_{*(nd)}^3 \leq 3 \cdot 10^6 \end{cases} .where. \quad D_{*(nd)} = D g_{(nd)} \left(\frac{(S-1)g}{\nu^2} \right)^{1/3}$$

σ is the Schmidt number, χ_j is the SGS turbulent term (Zedler and Street 2001): $\chi_j = \frac{\nu_{sgs}}{\sigma_t} \frac{\partial c_{(nd)}}{\partial x_j}$

and σ_t is the turbulent Schmidt number.

Boundary conditions for bottom : $c_b = \frac{c_o}{(1+1/\lambda)^3}$ (Fredsøe & Deigaard, 1992)

$$c_b = 0.156 \frac{D_{g(nd)}}{a} \frac{(\theta - \theta_{c(nd)})^{1.5}}{D_{\cdot(nd)}^{0.3}}$$ Van Rijn(1984)

Suspended load transport rate: $q_{s1,2(nd)} = \int_{x_{3bed}}^{x_{3top}} u_{1,2} c_{(nd)} dx_3$

Simulation Set-up

Van Der Werf et al.(2007) , experiment Mr5b63

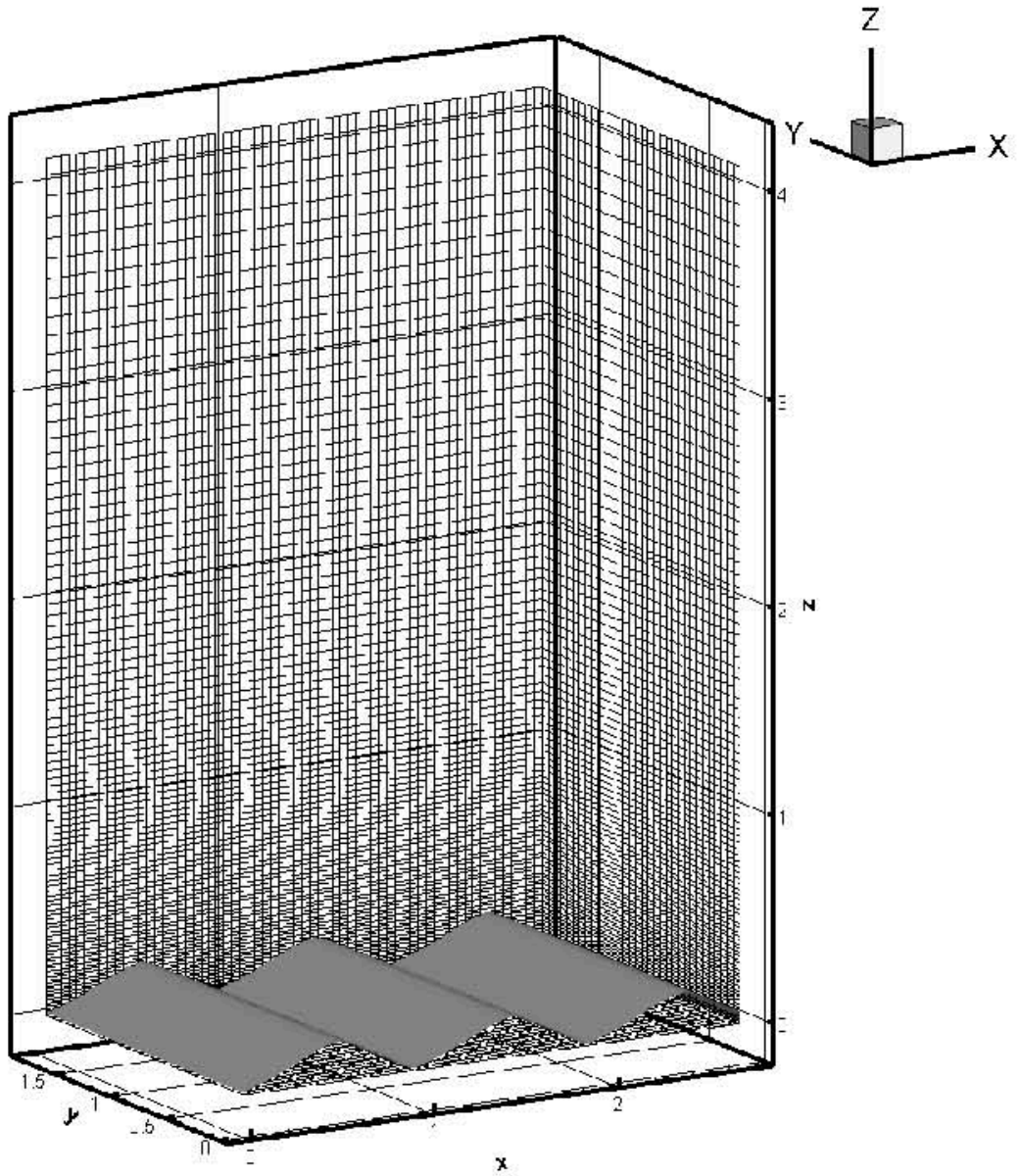

D_g(mm)	Ψ	a_0/D_g
0.25	104.4	2100
0.35	74.5	1500
0.44	59.3	1193
0.53	49.2	990
0.66	39.5	795

$\mathrm{Re} = 206000$

Numerical Simulations at Geometrical Scale 1/4.5

Numerical Parameters

Ripple characteristics

$Lr / a_0 = 0.9425$

$h_r / a_0 = 0.18$

Grid discretization

$\Delta x / a_0 = 0.00368$ m

$\Delta y / a_0 = 0.00368$ m

$\Delta z / a_0 = 0.001$ -> 0.04853 m

Grid = 256x128x430 =14.090.240 cells

Results

The period- and spanwise-averaged velocity field (vectors) and Y vorticity field

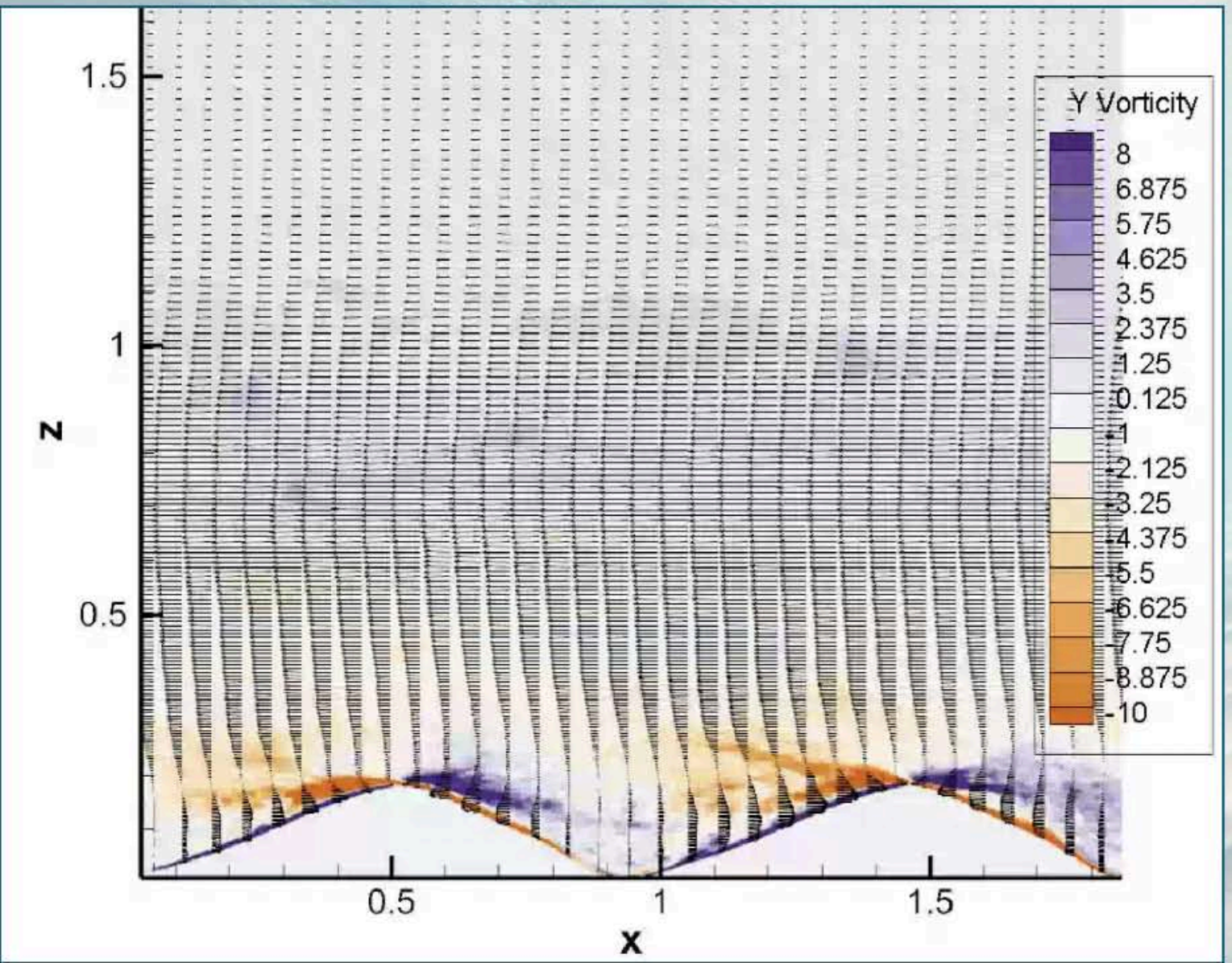

Profile of the mean streamwise velocity, u_1

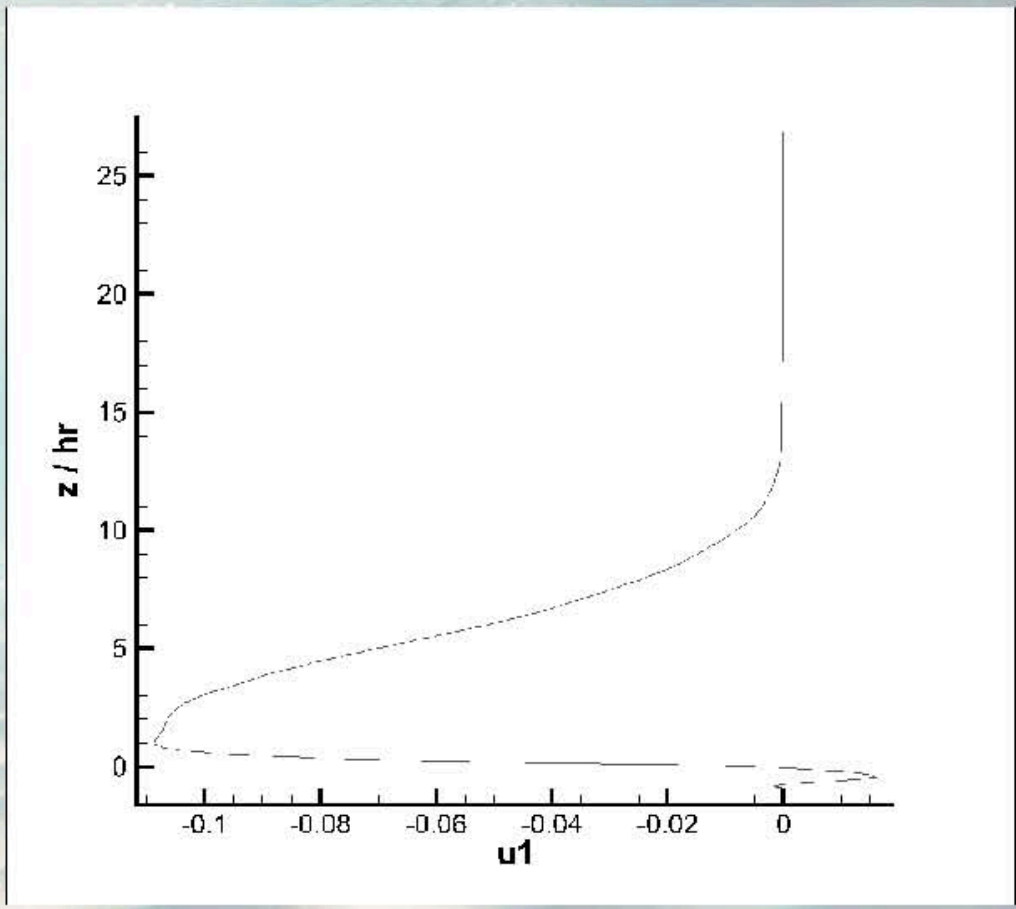

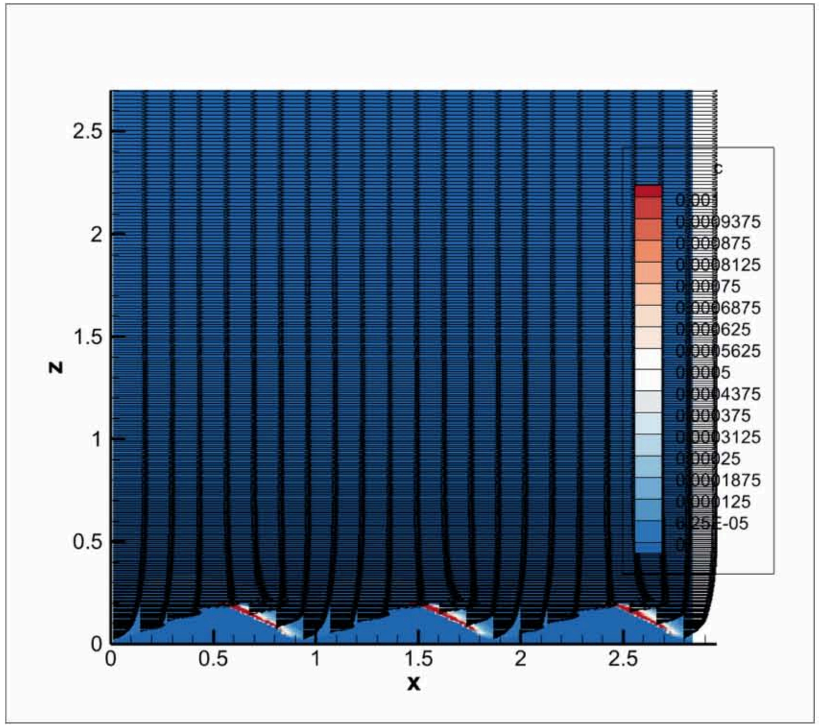
z
x
0
0.5
1
1.5
2
2.5
c
0.001
0.0009375
0.000875
0.0008125
0.00075
0.0006875
0.000625
0.0005625
0.0005
0.0004375
0.000375
0.0003125
0.00025
0.0001875
0.000125
6.25E-05
0

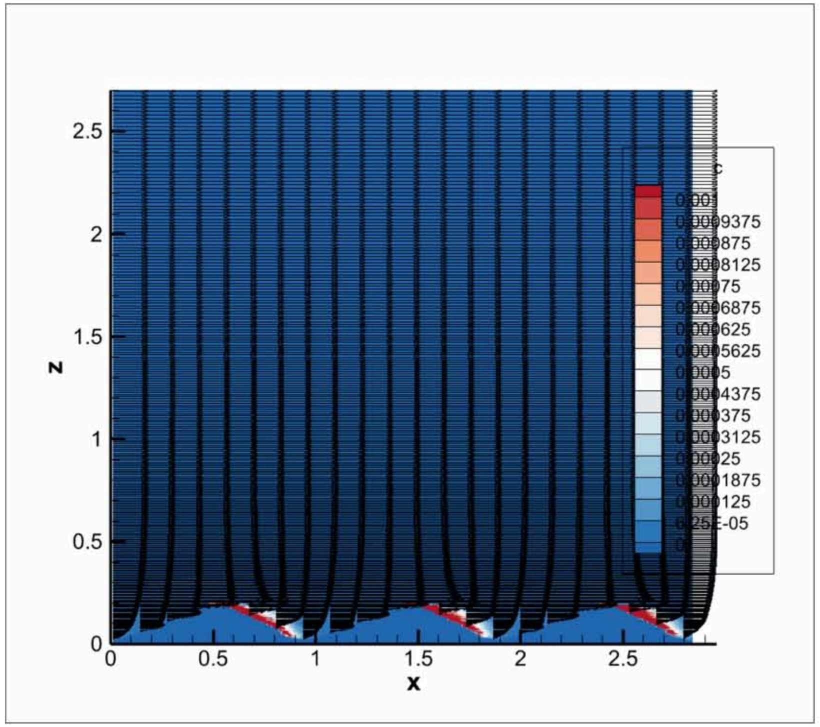
z
x
0
0.5
1
1.5
2
2.5
c
0.001
0.0009375
0.000875
0.0008125
0.00075
0.0006875
0.000625
0.0005625
0.0005
0.0004375
0.000375
0.0003125
0.00025
0.0001875
0.000125
6.25E-05
0

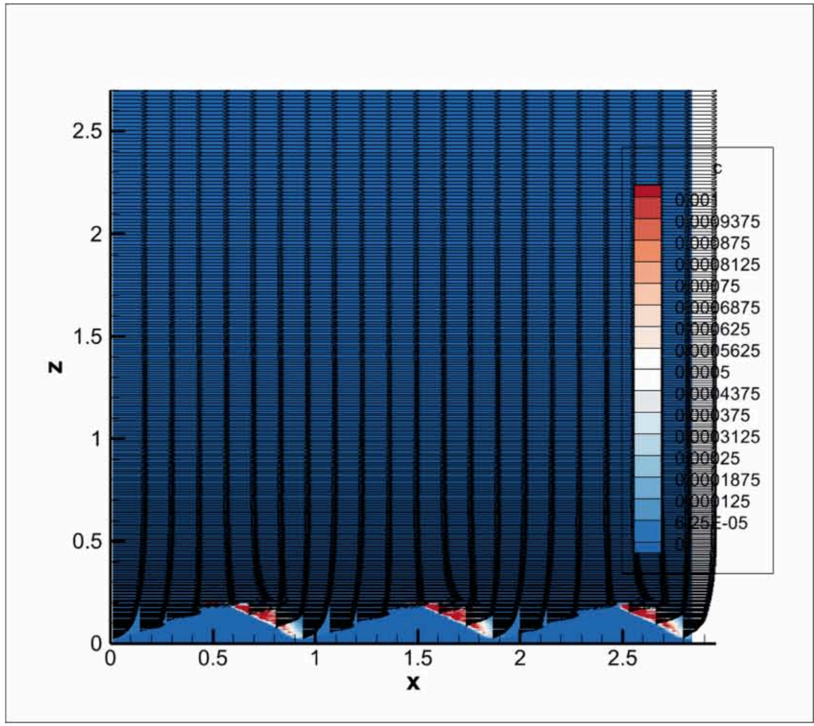
z
x
0
0.5
1
1.5
2
2.5
c
0.001
0.0009375
0.000875
0.0008125
0.00075
0.0006875
0.000625
0.0005625
0.0005
0.0004375
0.000375
0.0003125
0.00025
0.0001875
0.000125
6.25E-05
0

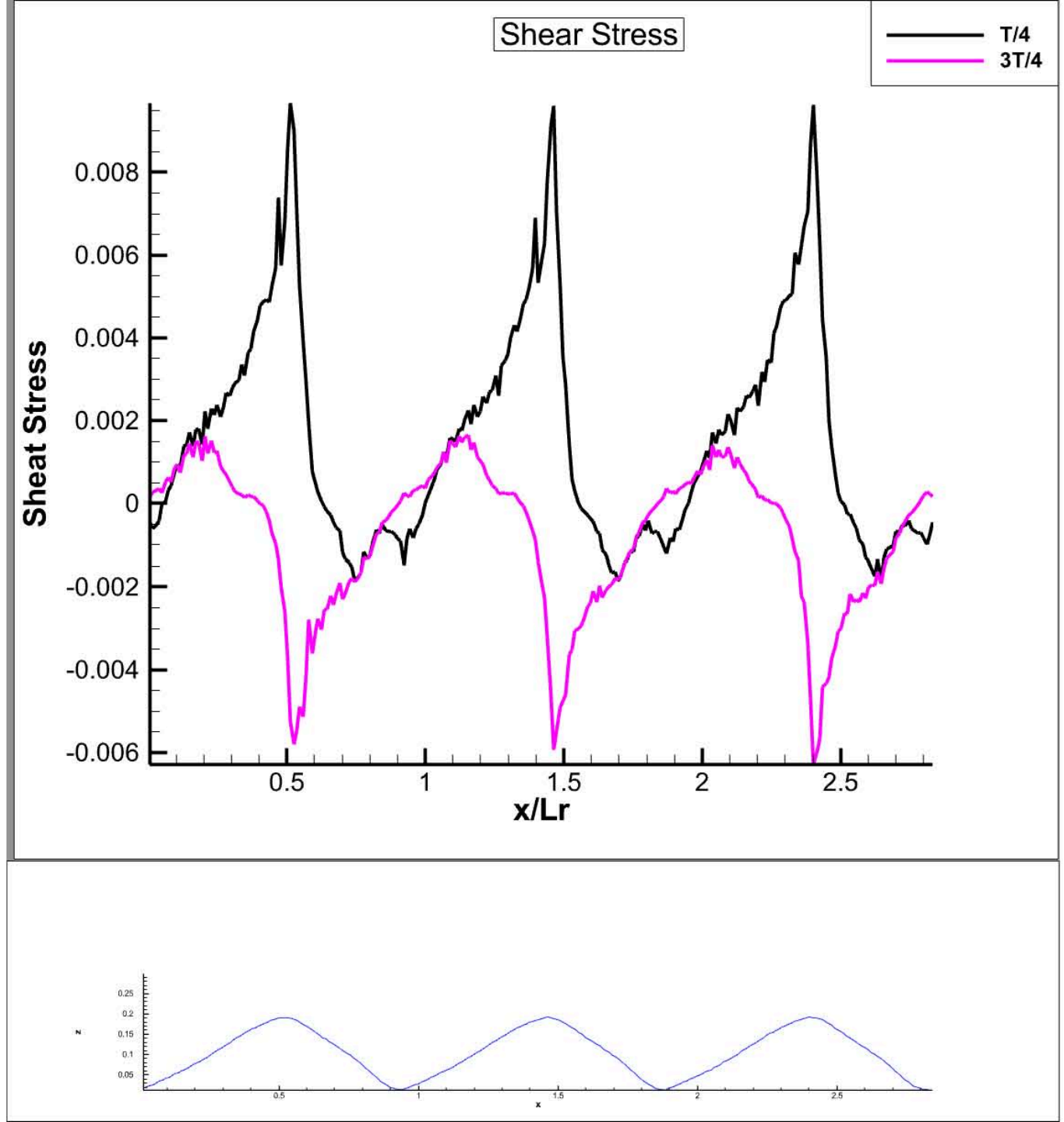
Shear Stress
T/4
3T/4
Sheat Stress
0.008
0.006
0.004
0.002
0
-0.002
-0.004
-0.006
0.5
1
1.5
2
2.5
x/Lr
z
0.25
0.2
0.15
0.1
0.05
x

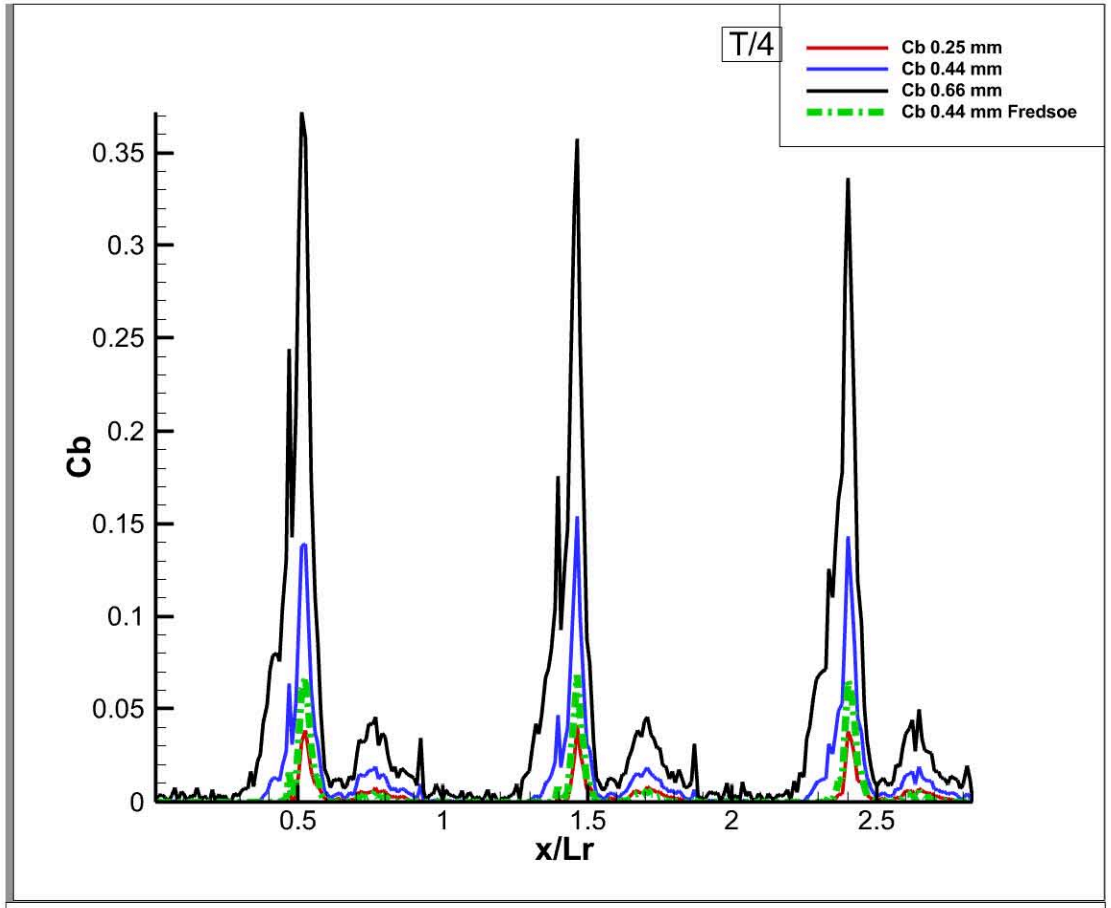
T/4
Cb 0.25 mm
Cb 0.44 mm
Cb 0.66 mm
Cb 0.44 mm Fredsoe
Cb
x/Lr
0
0.05
0.1
0.15
0.2
0.25
0.3
0.35
0.5
1
1.5
2
2.5

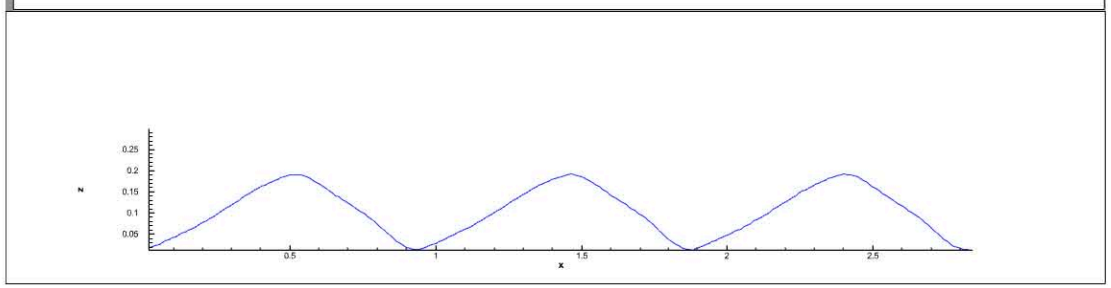

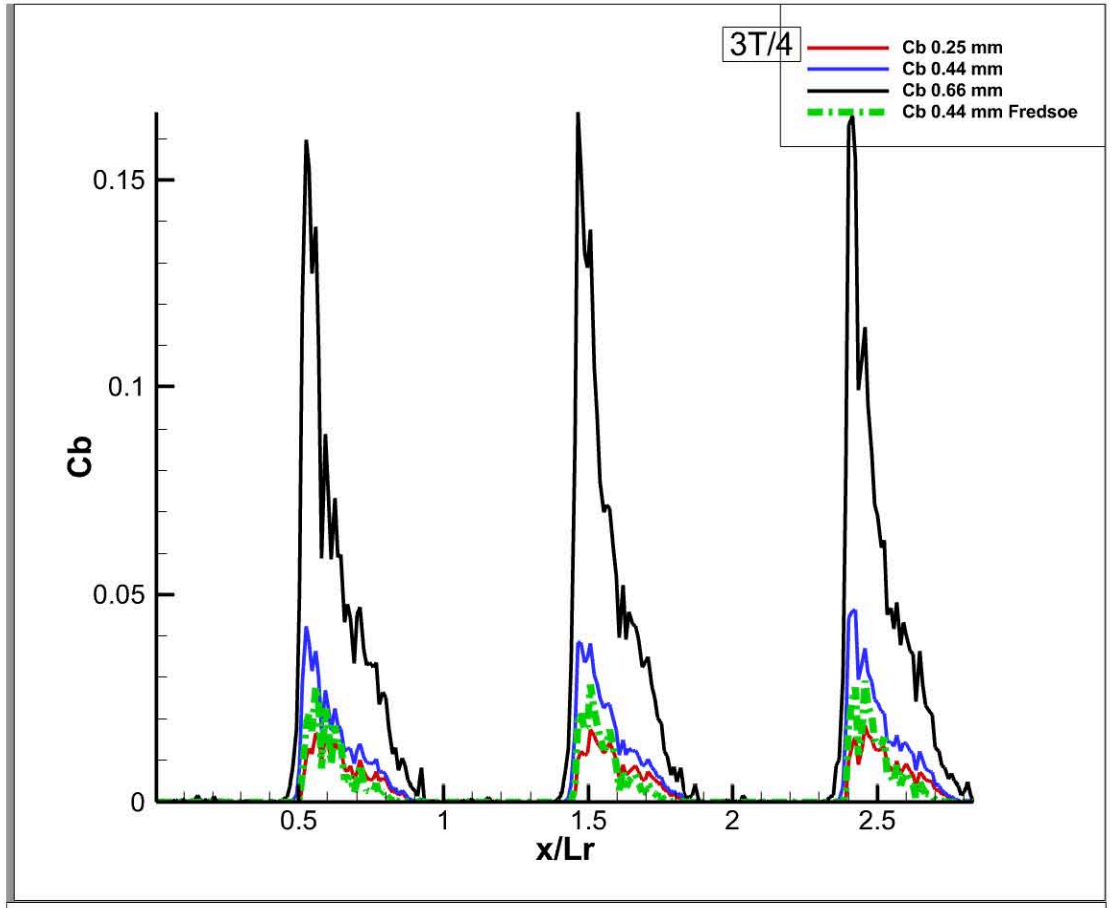
3T/4
Cb 0.25 mm
Cb 0.44 mm
Cb 0.66 mm
Cb 0.44 mm Fredsoe
Cb
x/Lr
0
0.05
0.1
0.15
0.5
1
1.5
2
2.5

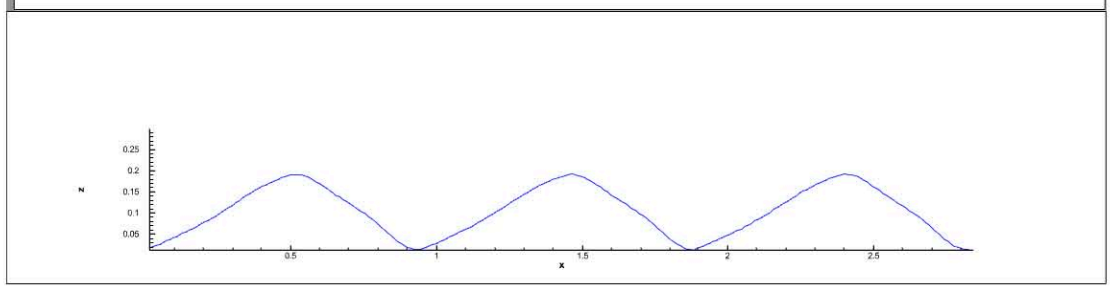

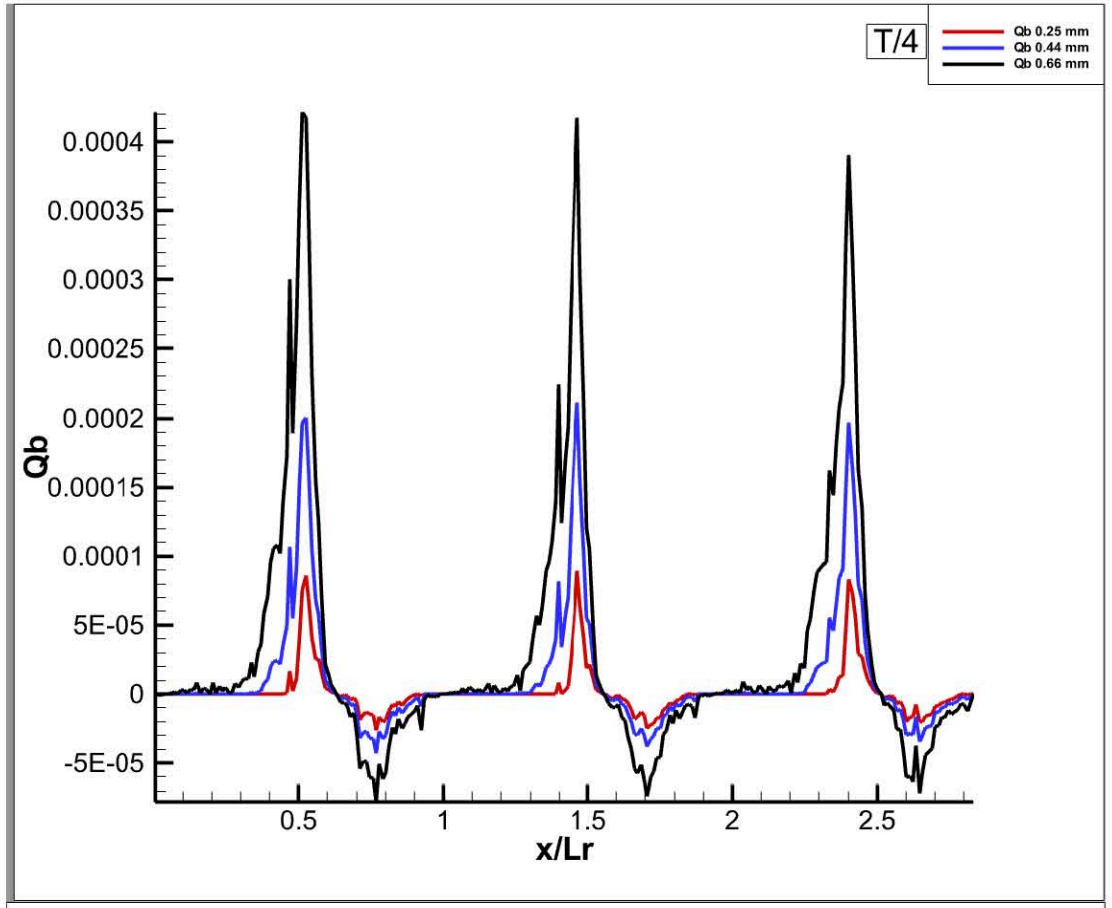
T/4
Qb 0.25 mm
Qb 0.44 mm
Qb 0.66 mm
Qb
x/Lr
0.0004
0.00035
0.0003
0.00025
0.0002
0.00015
0.0001
5E-05
0
-5E-05
0.5
1
1.5
2
2.5

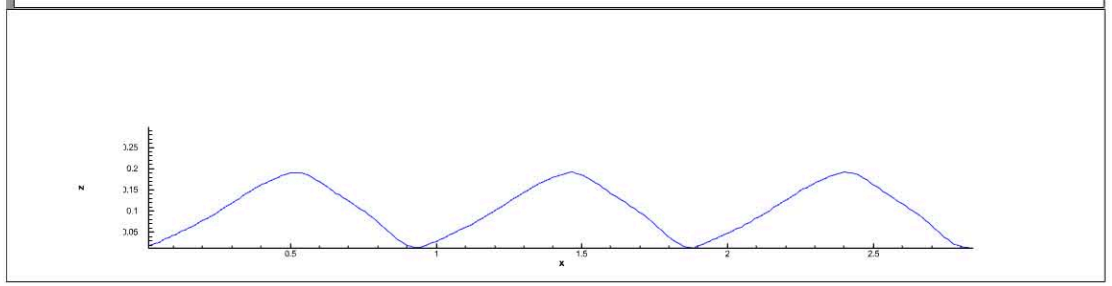

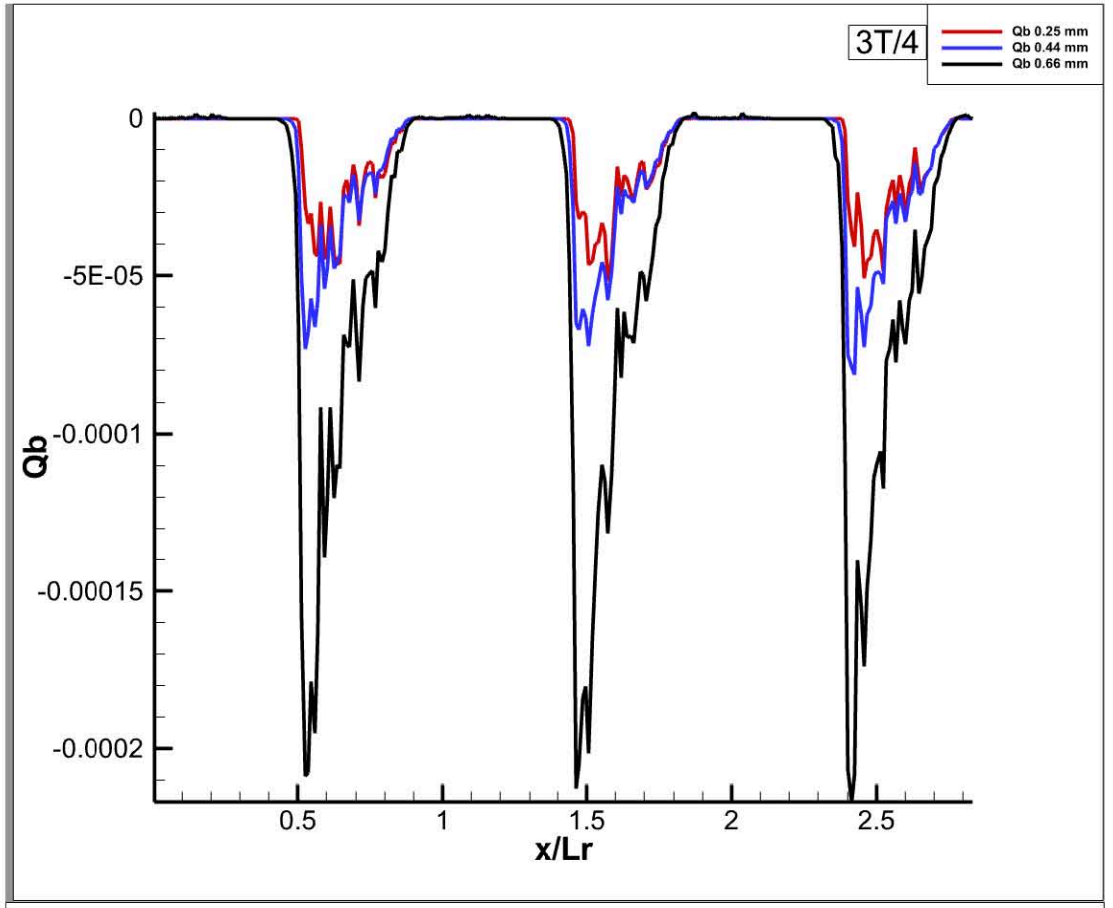
3T/4
Qb 0.25 mm
Qb 0.44 mm
Qb 0.66 mm
Qb
x/Lr
0
-5E-05
-0.0001
-0.00015
-0.0002
0.5
1
1.5
2
2.5

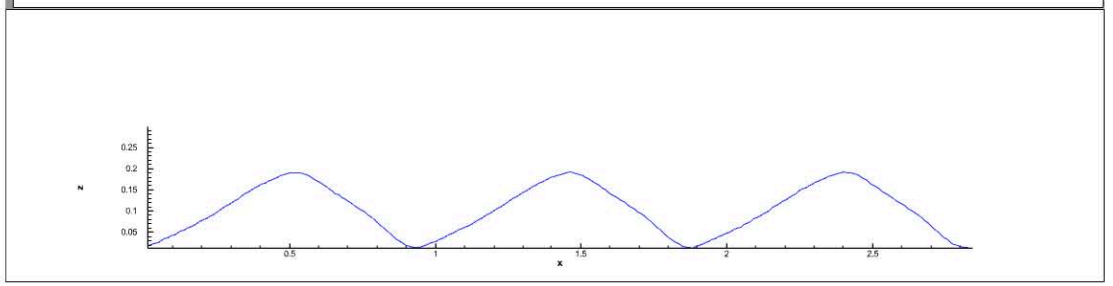

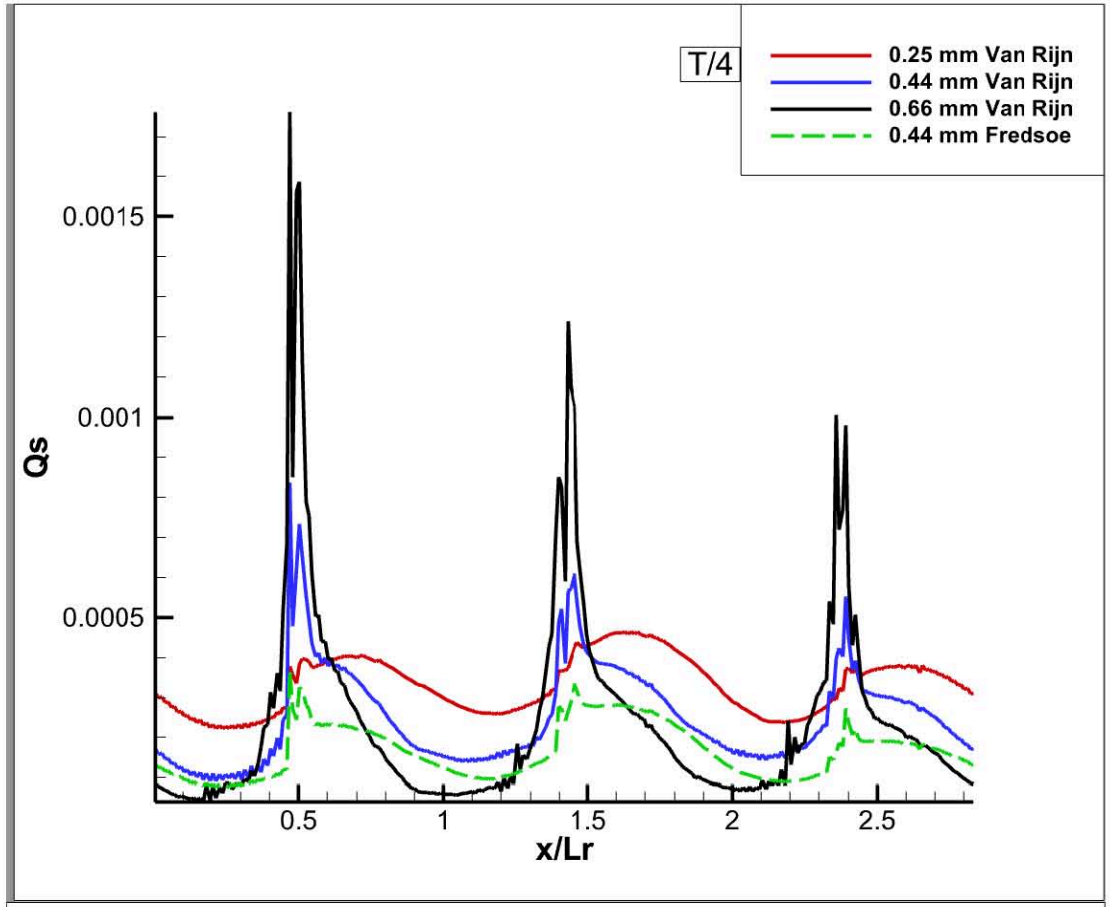
T/4
0.25 mm Van Rijn
0.44 mm Van Rijn
0.66 mm Van Rijn
0.44 mm Fredsoe
Qs
0.0015
0.001
0.0005
0.5
1
1.5
2
2.5
x/Lr

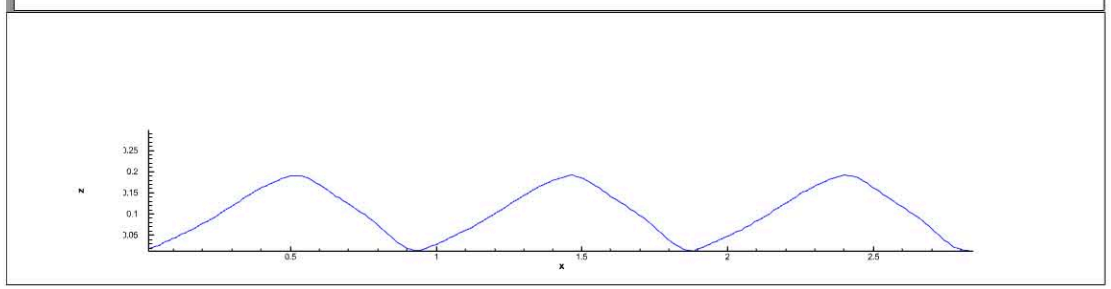

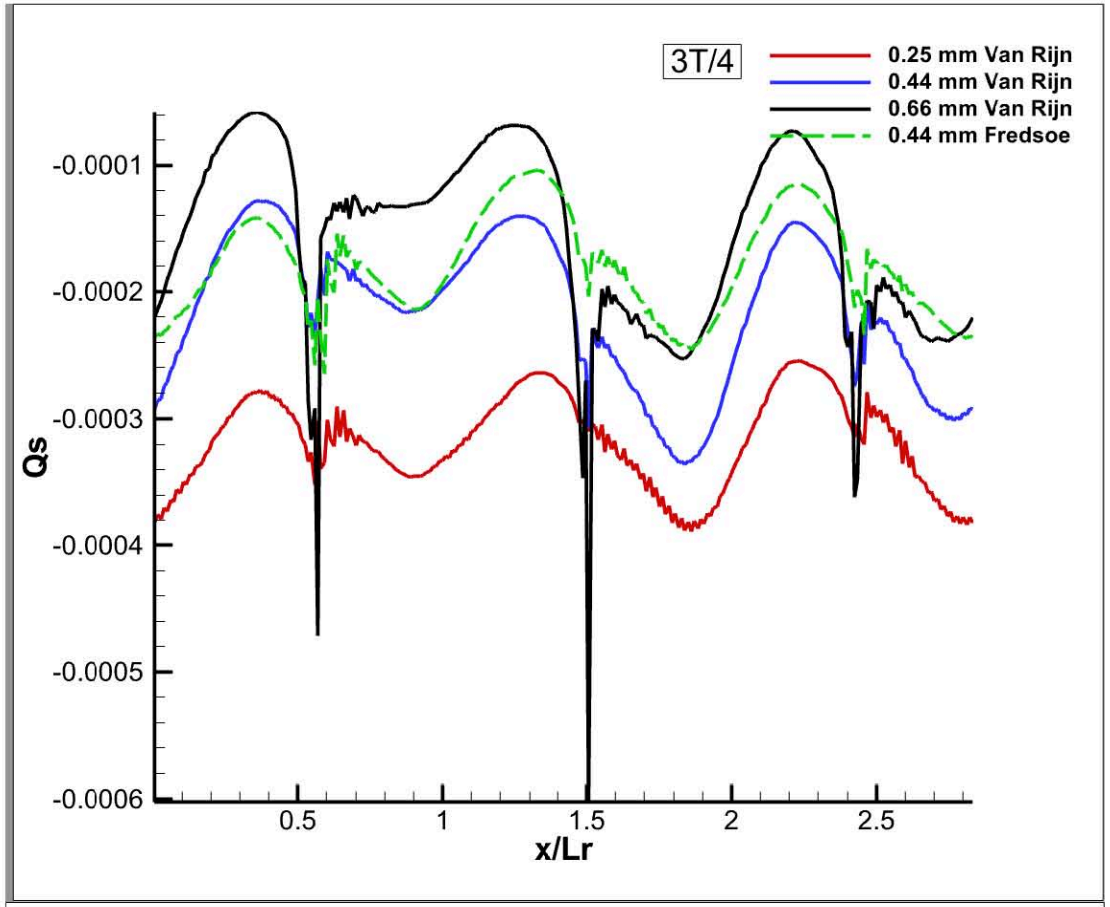
3T/4
0.25 mm Van Rijn
0.44 mm Van Rijn
0.66 mm Van Rijn
0.44 mm Fredsoe
Qs
-0.0001
-0.0002
-0.0003
-0.0004
-0.0005
-0.0006
0.5
1
1.5
2
2.5
x/Lr

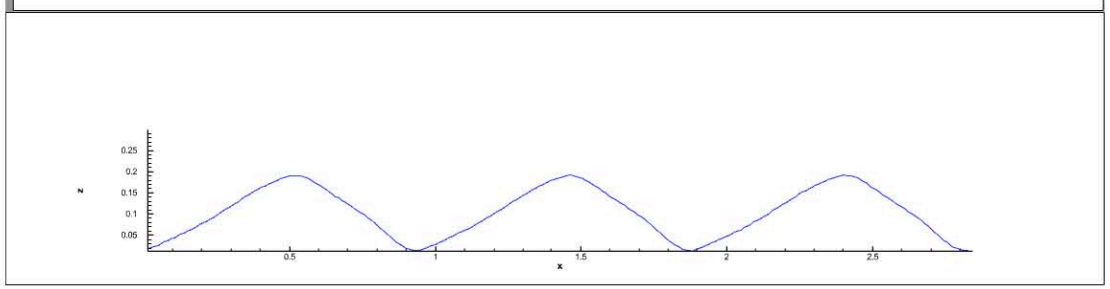

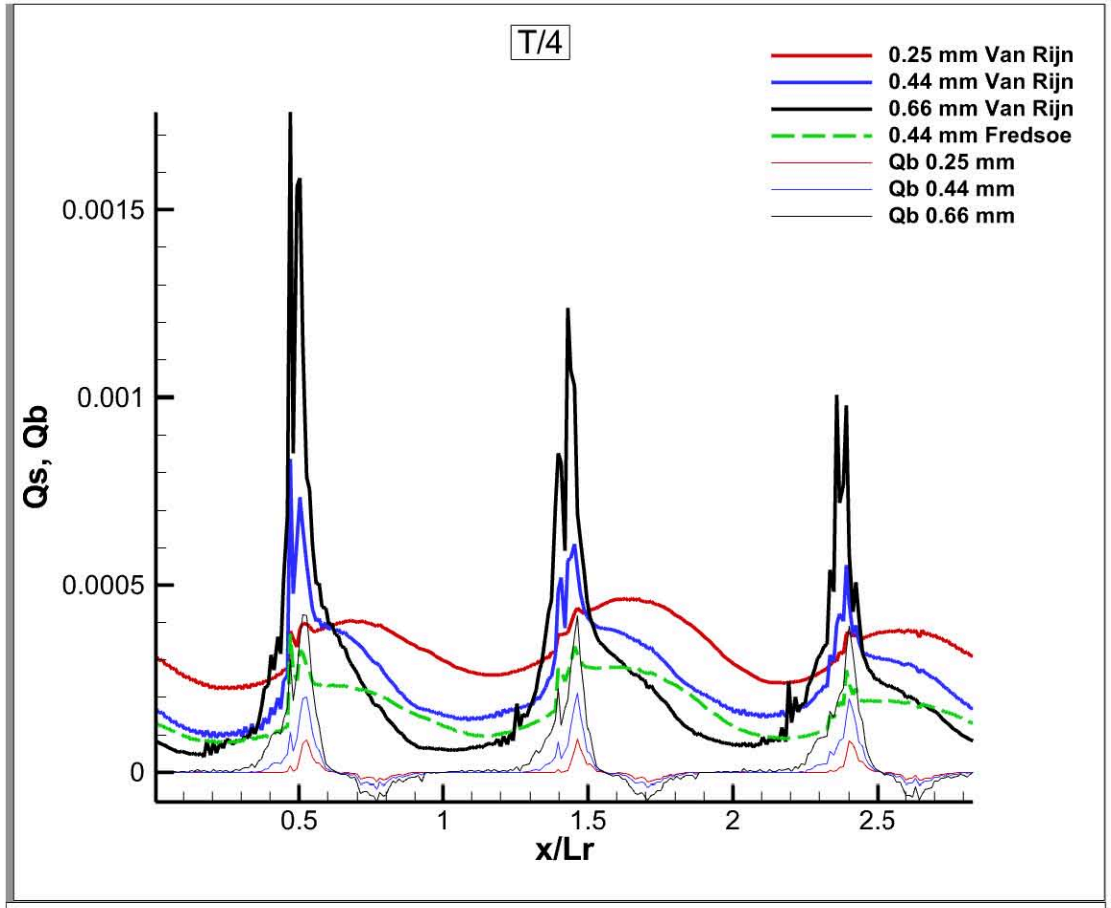
T/4
0.25 mm Van Rijn
0.44 mm Van Rijn
0.66 mm Van Rijn
0.44 mm Fredsoe
Qb 0.25 mm
Qb 0.44 mm
Qb 0.66 mm
Qs, Qb
x/Lr
0.0015
0.001
0.0005
0
0.5
1
1.5
2
2.5

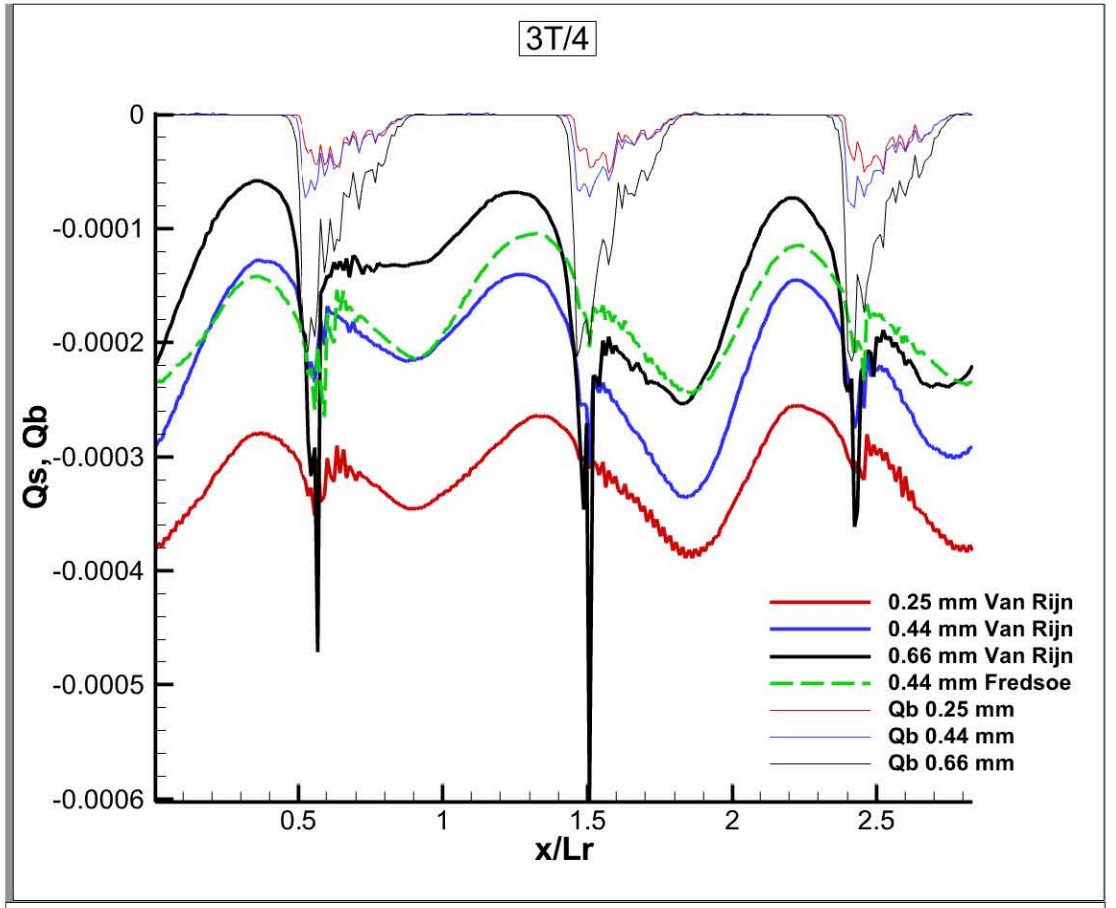
3T/4
Qs, Qb
x/Lr
0
-0.0001
-0.0002
-0.0003
-0.0004
-0.0005
-0.0006
0.5
1
1.5
2
2.5
0.25 mm Van Rijn
0.44 mm Van Rijn
0.66 mm Van Rijn
0.44 mm Fredsoe
Qb 0.25 mm
Qb 0.44 mm
Qb 0.66 mm

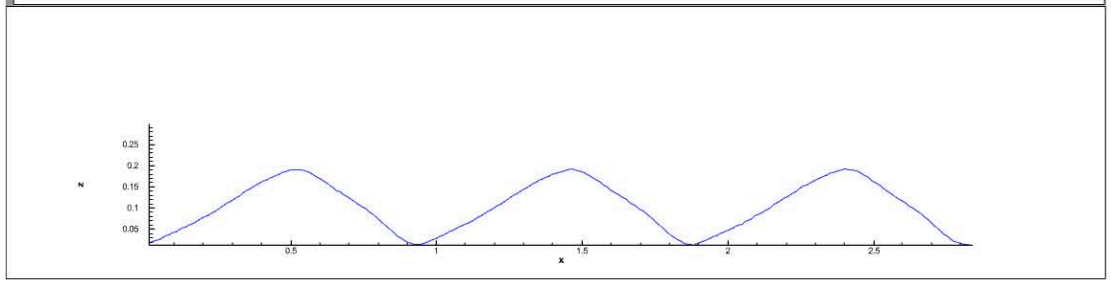

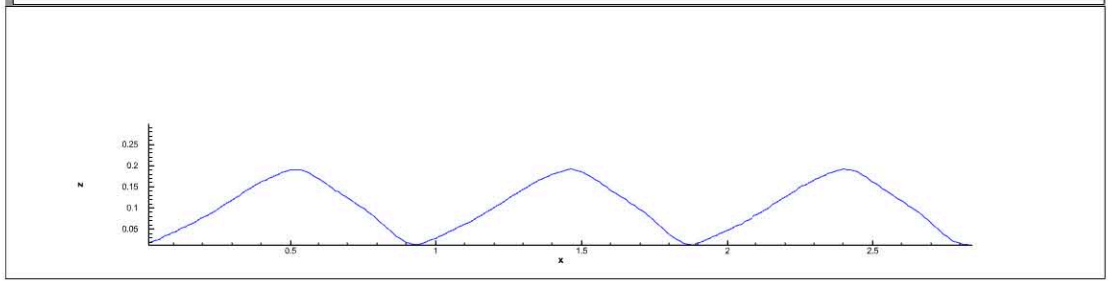

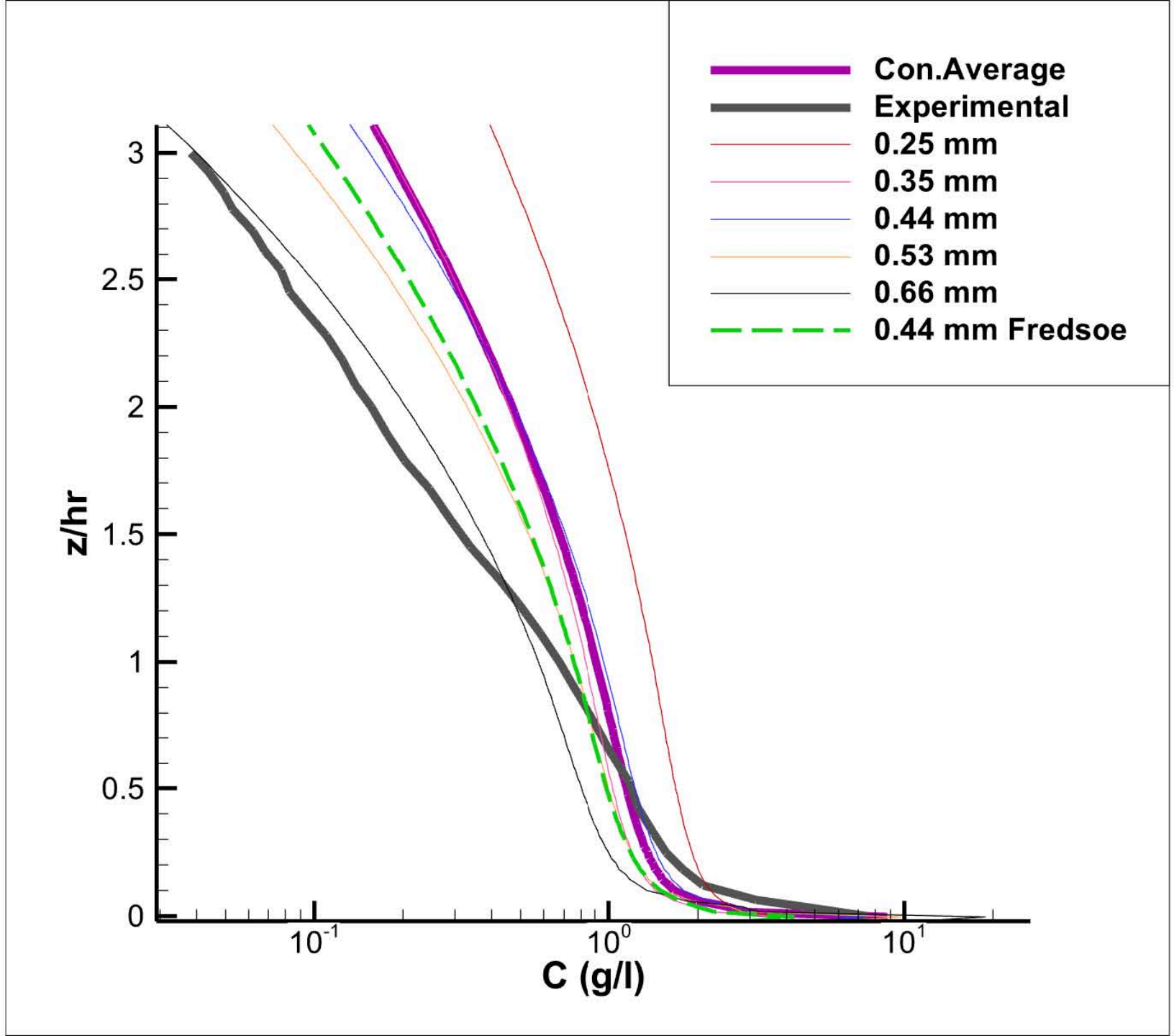
Con.Average
Experimental
0.25 mm
0.35 mm
0.44 mm
0.53 mm
0.66 mm
0.44 mm Fredsoe
z/hr
3
2.5
2
1.5
1
0.5
0
10^{-1}
10^{0}
10^{1}
C (g/l)

Conclusions

- The fractions with diameters larger than D50 contribute more to the bed load.
- Suspended Load : Depending on the bottom boundary condition, differences appear on the crest.
- Concentration : Diameter Size Decreases -> Concentration Increases
- D40 is the representative diameter for the suspended sediment transport.

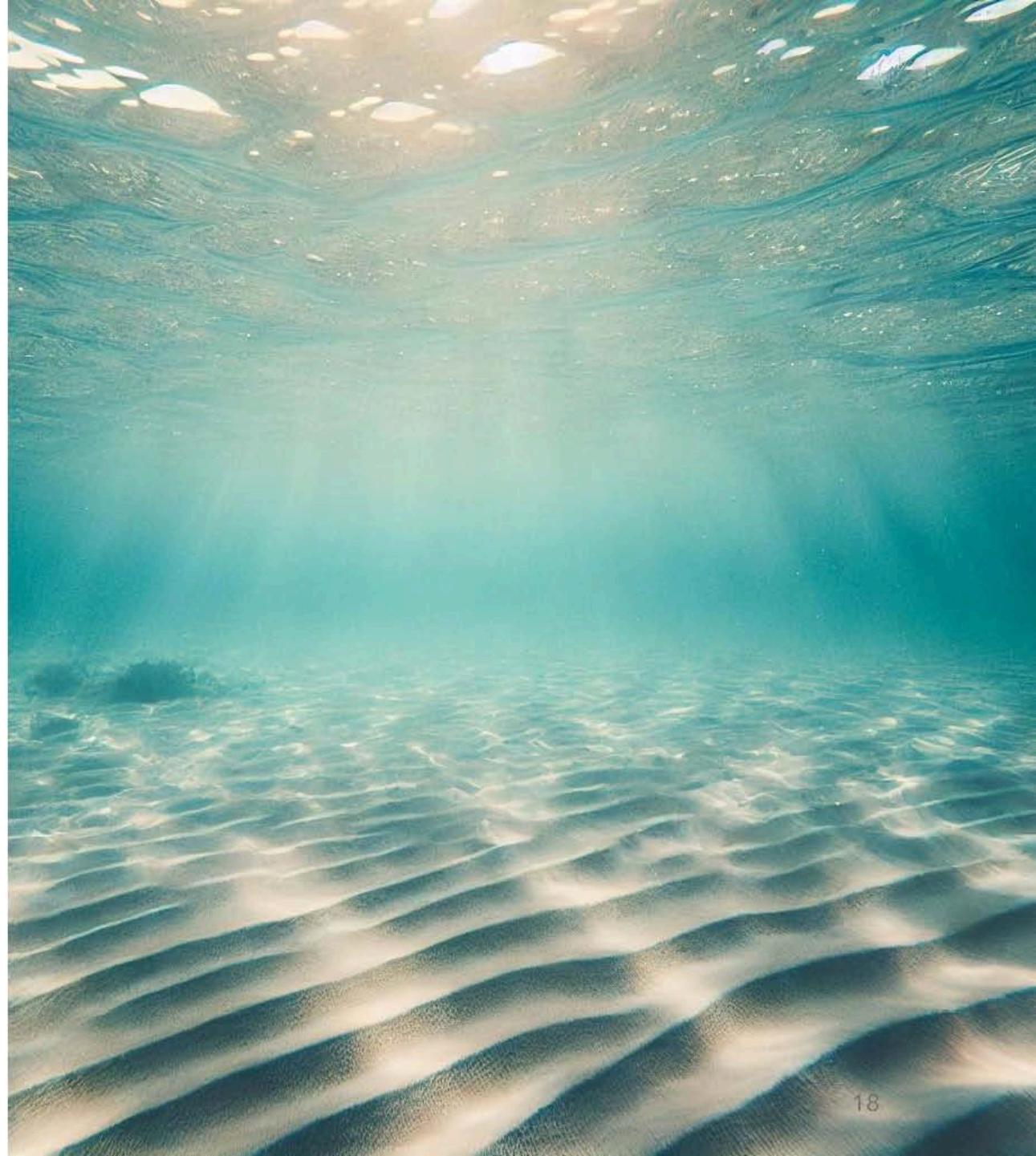

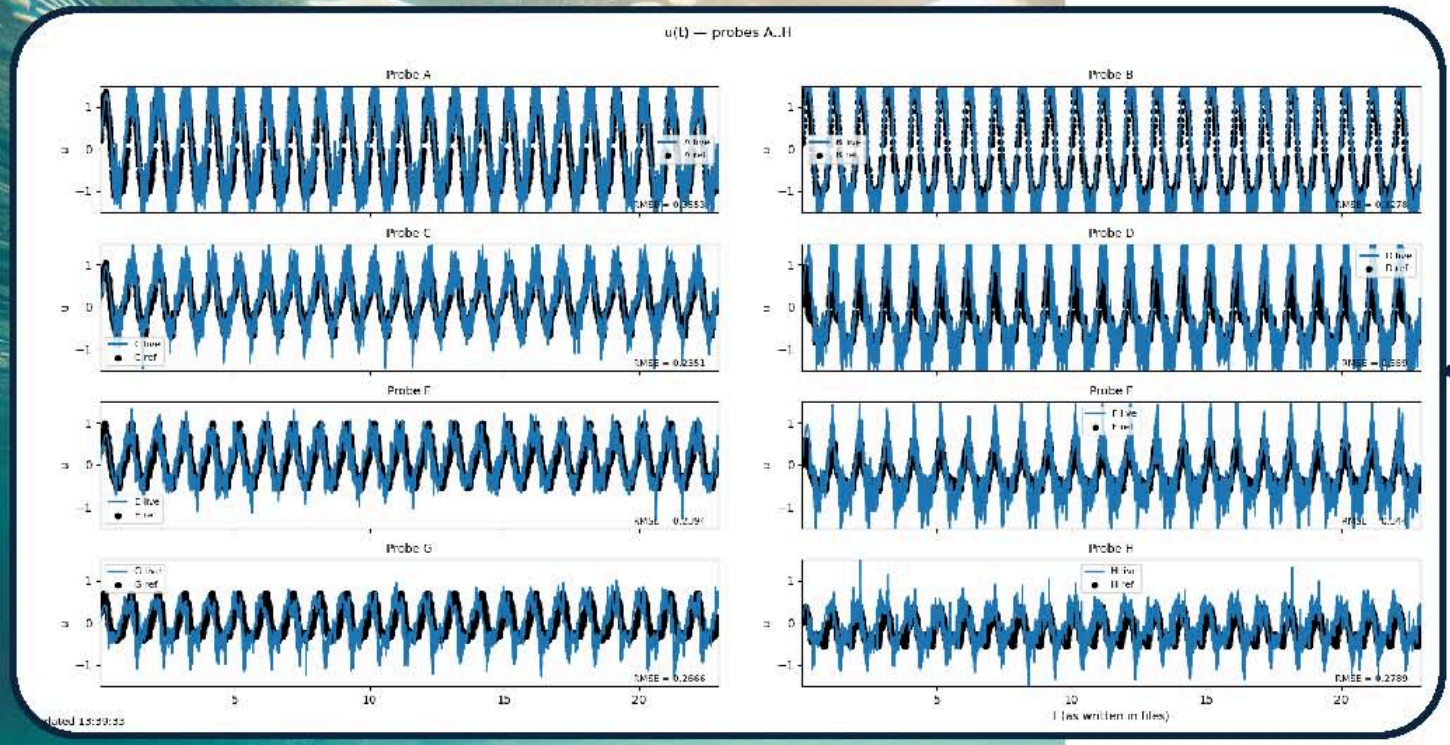

Future Work

- Implement the **law of the wall model** to resolve the turbulent boundary layer.
- Incorporate **sediment size fractions** into the **Exner equation** to improve the bed evolution model.

UNIVERSITÀ POLITECNICA DELLE MARCHE
DIPARTIMENTO INGEGNERIA CIVILE EDILE ARCHITETTURA
18|22 23|27 ECCELLENZA
Funded by the European Union

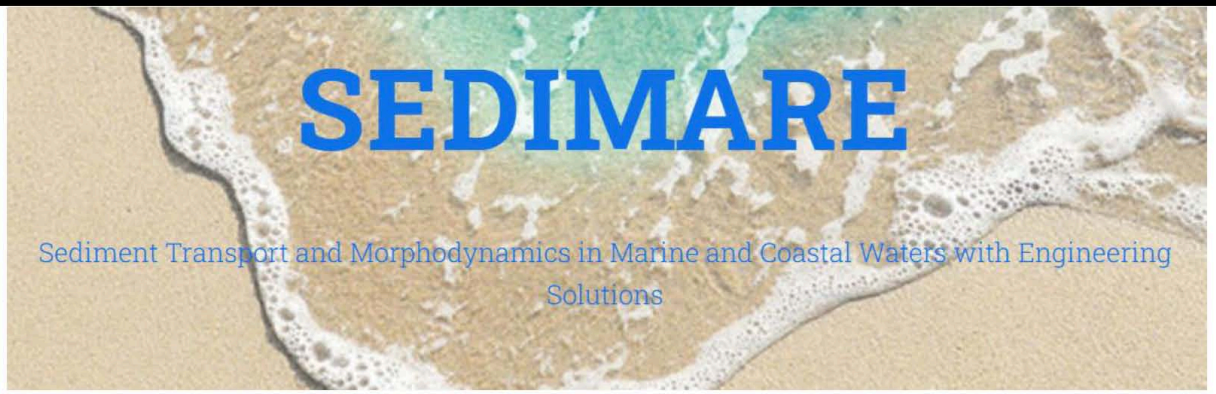

Image Assimilation for Remote Sensing Tools to Investigate Nearshore Dynamics

10-11 September 2025, HR Wallingford

M. Said Parlak
Doctoral Candidate
Università Politecnica delle Marche
Department of ICEA
m.s.parlak@univpm.it

Supervisors:
Maurizio Brocchini
m.brocchini@staff.univpm.it
Matteo Postacchini
m.postacchini@staff.univpm.it

Acknowledgement: This project has received funding from the European Union's (EU) Horizon Europe Framework Programme (HORIZON) under Grant Agreement No 101072443 as a MSCA Doctoral Network (HORIZON-MSCA-2021-DN-01) of SEDIMARE.

Why Remote Sensors

- In-situ measurements may limit the spatial coverage.
- Widely utilised in Met-Ocean fields.
- Availability of open-source processing tools.

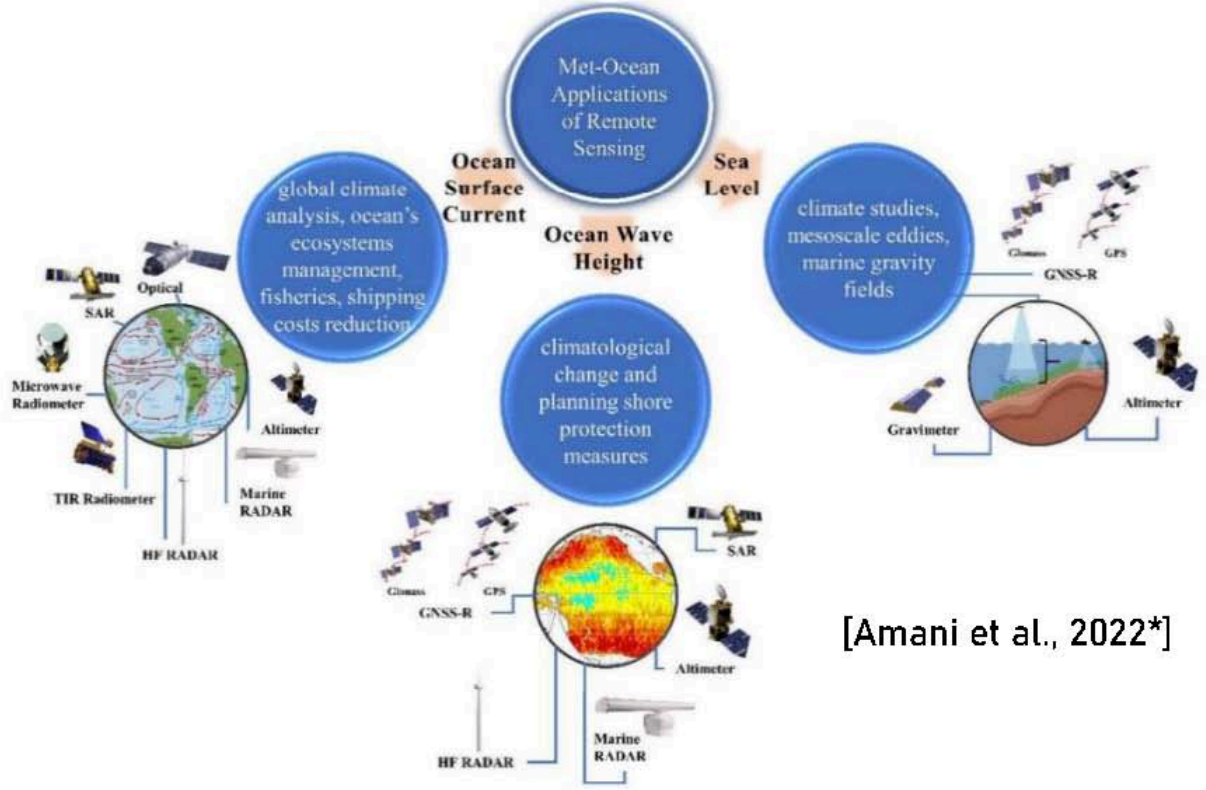

[Amani et al., 2022*]

*Amani, M., Moghimi, A., Mirmazloumi, S. M., Ranjgar, B., Ghorbanian, A., Ojaghi, S., ... & Jin, S. (2022). Ocean remote sensing techniques and applications: A review (part i). Water, 14(21), 3400.

Why Remote Sensors

- In-situ measurements may limit the spatial coverage.
- Widely utilised in Met-Ocean fields.
- Availability of open-source processing tools.

Not as an alternative but a good companion

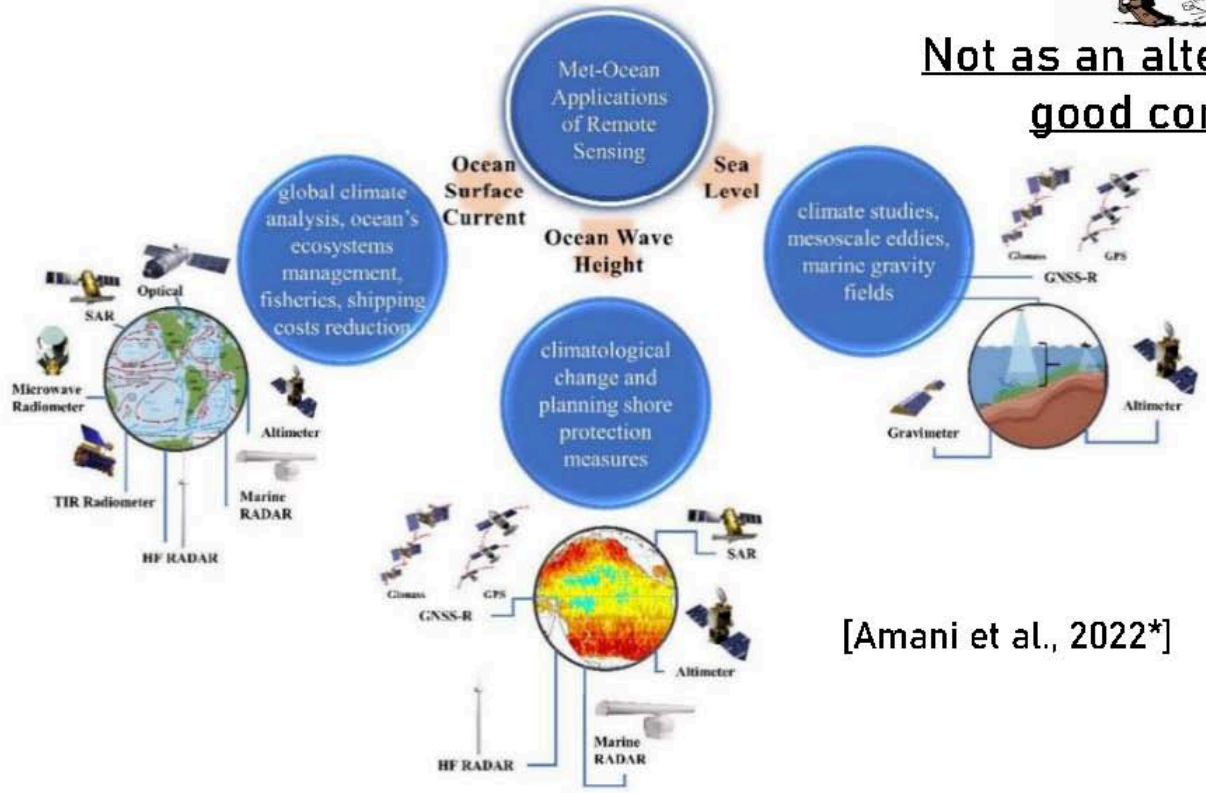

[Amani et al., 2022*]

*Amani, M., Moghimi, A., Mirmazloumi, S. M., Ranjgar, B., Ghorbanian, A., Ojaghi, S., ... & Jin, S. (2022). Ocean remote sensing techniques and applications: A review (part i). Water, 14(21), 3400.

Study Site

- Senigallia, a maritime city at the Adriatic coast, Italy.

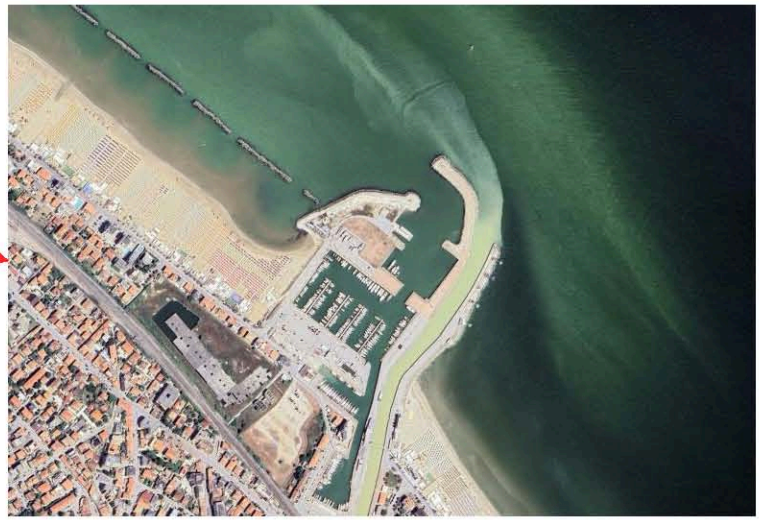

Study Site

- Senigallia, a maritime city at the Adriatic coast, Italy.
- Seasonal variabilities and strong sea-river interactions (Brocchini et al., 2017*)

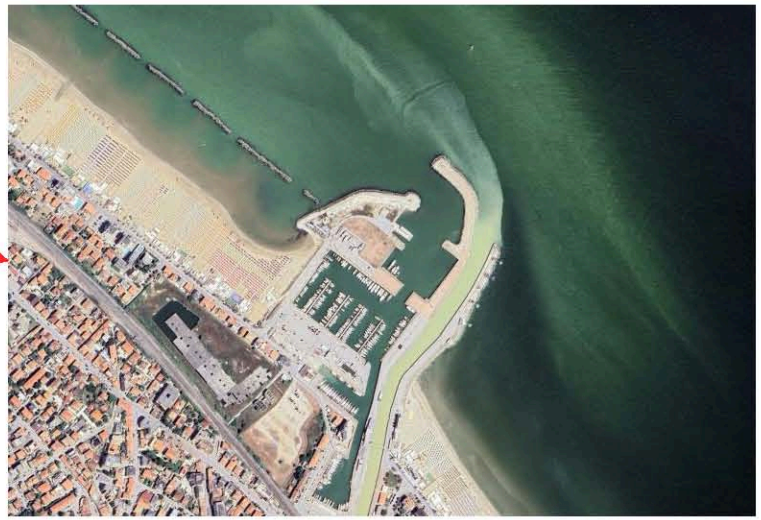

*Brocchini, M., Calantoni, J., Postacchini, M., Sheremet, A., Staples, T., Smith, J., ... & Soldini, L. (2017). Comparison between the wintertime and summertime dynamics of the Misa River estuary. *Marine Geology*, *385*, 27-40

Study Site

- Senigallia, a maritime city at the Adriatic coast, Italy.
- Seasonal variabilities and strong sea-river interactions (Brocchini et al., 2017*)
- 2 systems are deployed, X-Band Radar (XBR) and Video Camera System (SGS)

SGS: 5 cameras, ~2 Hz sampling, ~10 min-long
XBR: Single Antenna, ~0.5 Hz sampling, 63 scans

*Brocchini, M., Calantoni, J., Postacchini, M., Sheremet, A., Staples, T., Smith, J., ... & Soldini, L. (2017). Comparison between the wintertime and summertime dynamics of the Misa River estuary. *Marine Geology*, *385*, 27-40

Image Assimilation for RSTs

RST: Remote Sensing Tool

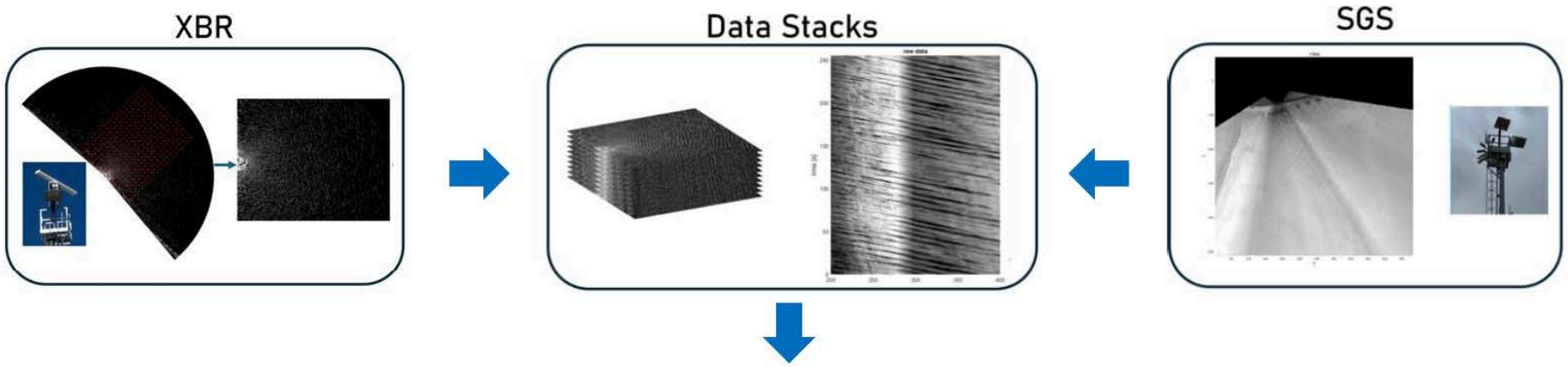

refracted_images:

Capturing the wave refraction by utilizing RADON transformation.

Image Assimilation for RSTs

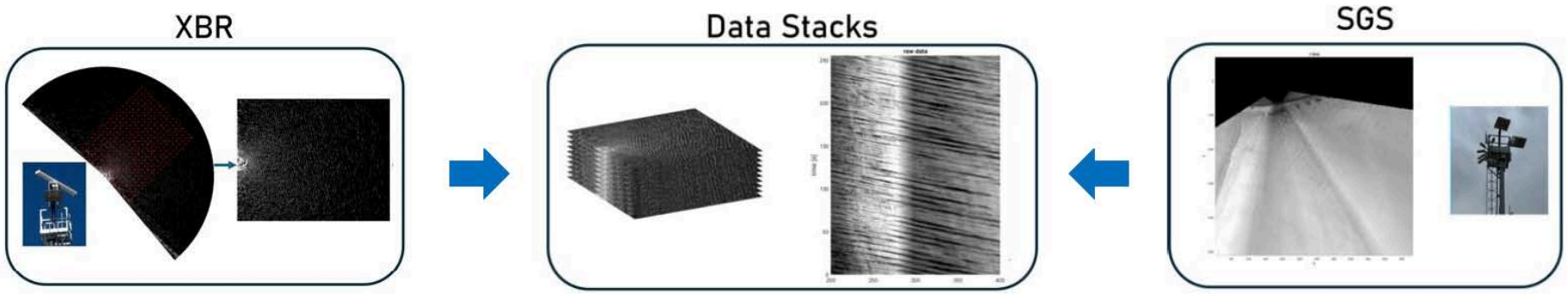

refracted_images:

Capturing the wave refraction by utilizing RADON transformation.

wavelet_k_c_f:

Evaluation of wavenumbers by Continuous Wavelet Transformation (CWT).
Evaluation of wave celerity by utilizing RADON transformation.

Image Assimilation for RSTs

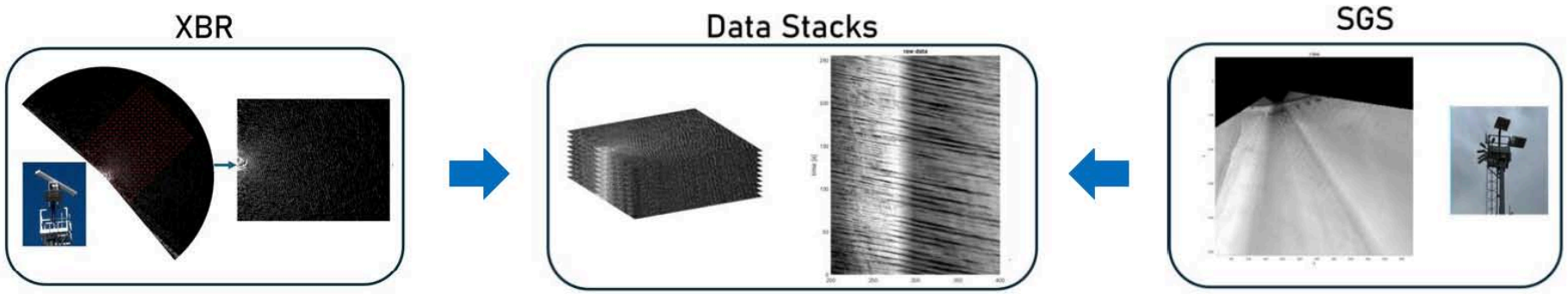

refracted_images:

Capturing the wave refraction by utilizing RADON transformation.

wavelet_k_c_f:

Evaluation of wavenumbers by Continuous Wavelet Transformation (CWT).
Evaluation of wave celerity by utilizing RADON transformation.

bathy_n_params:

Determination of bathymetry by solving the dispersion equation.
Prediction of wave characteristics to feed numerical models.

Image Assimilation for RSTs

refracted_images:

Capturing the wave refraction by utilizing RADON transformation.

highest variance for the peak direction

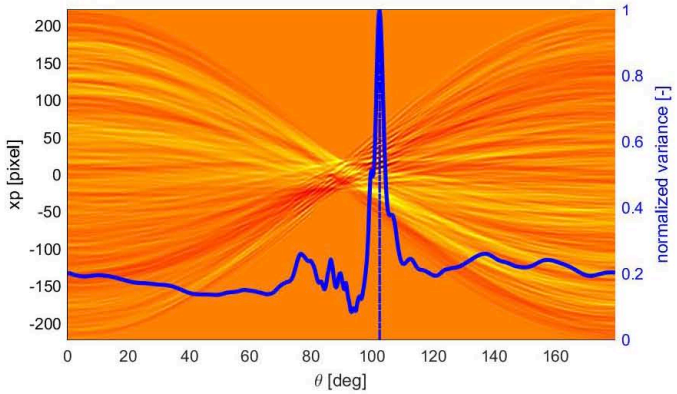

Image Assimilation for RSTs

refracted_images:

Capturing the wave refraction by utilizing RADON transformation.

highest variance for the peak direction

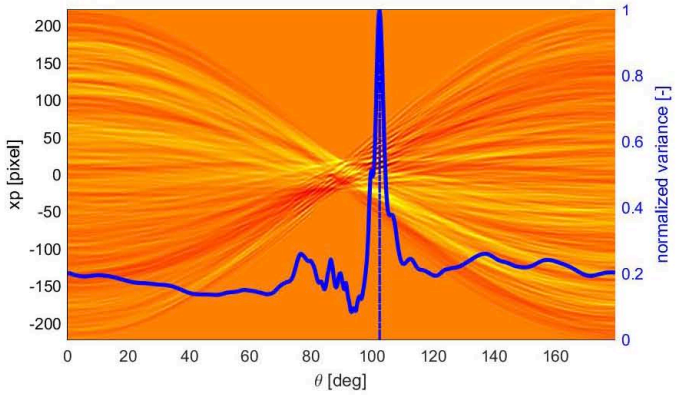

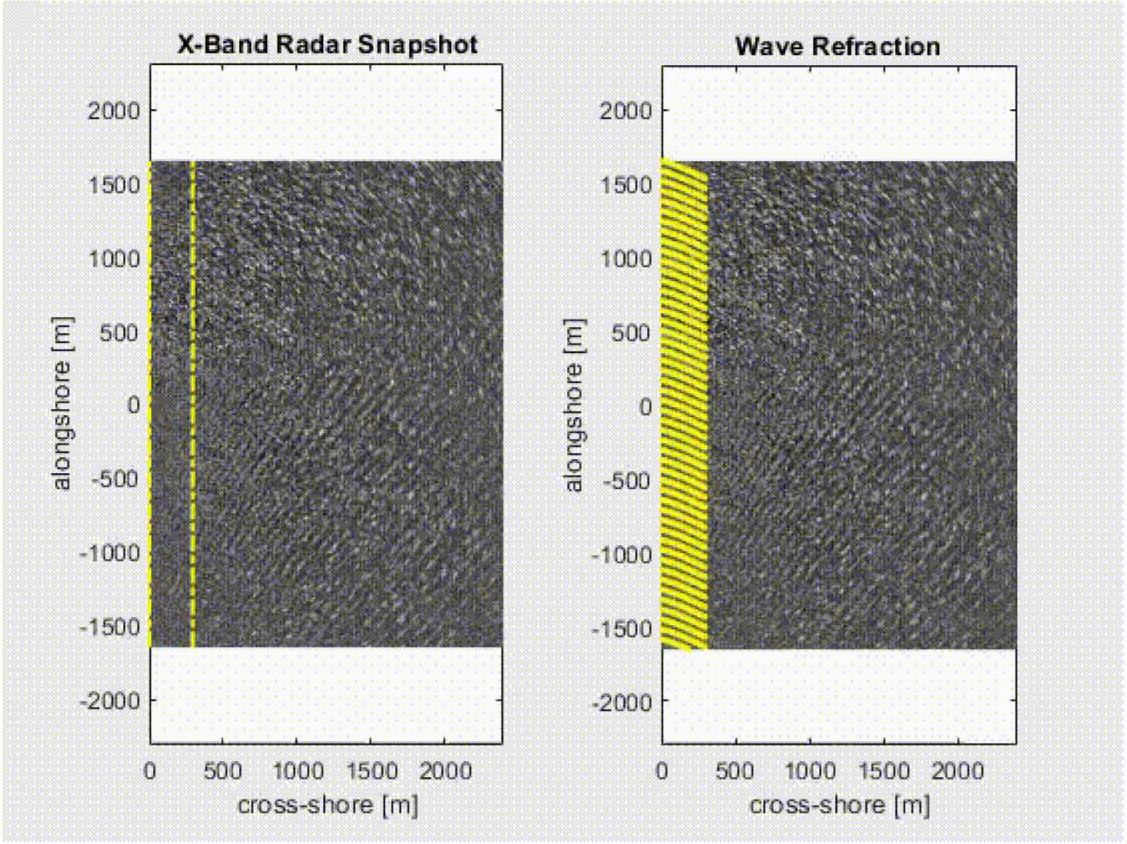

Image Assimilation for RSTs

refracted_images:

Capturing the wave refraction by utilizing RADON transformation.

highest variance for the peak direction

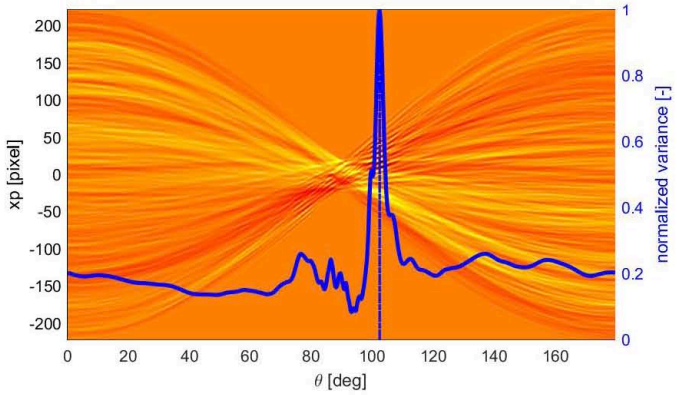

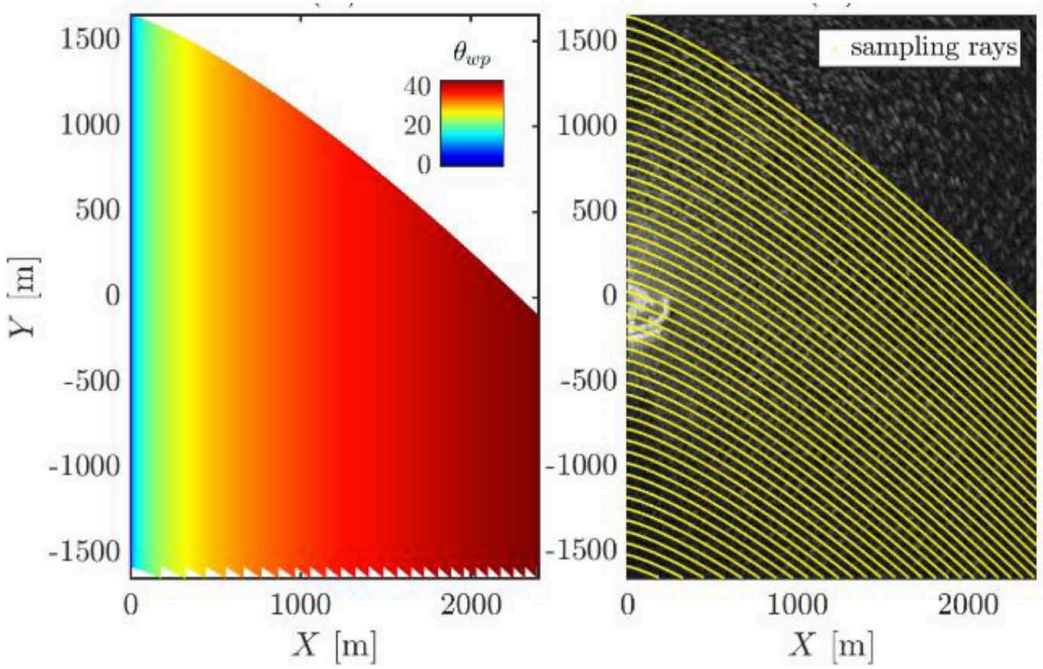

Image Assimilation for RSTs

refracted_images:

Capturing the wave refraction by utilizing RADON transformation.

highest variance for the peak direction

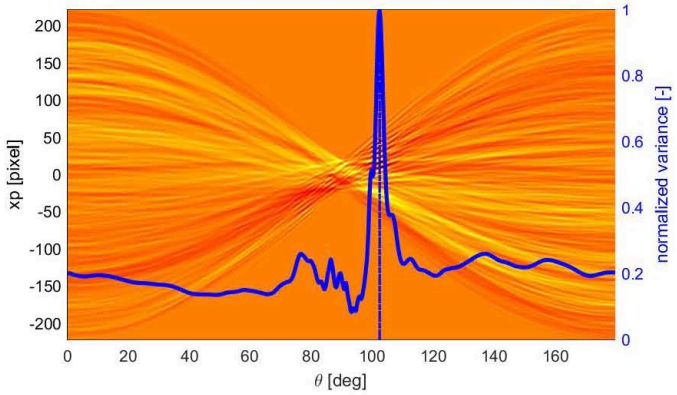

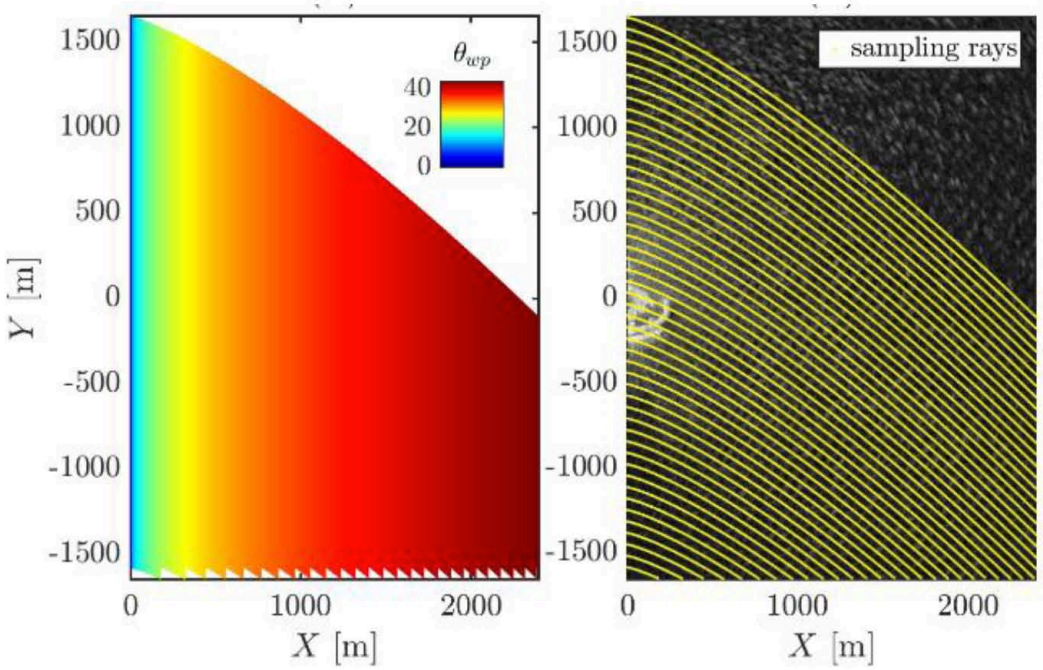

images are interpolated to sampling rays

Image Assimilation for RSTs

wavelet_k_c_f:

Evaluation of wavenumbers by Continuous Wavelet Transformation (CWT).

Evaluation of wave celerity by utilizing RADON transformation.

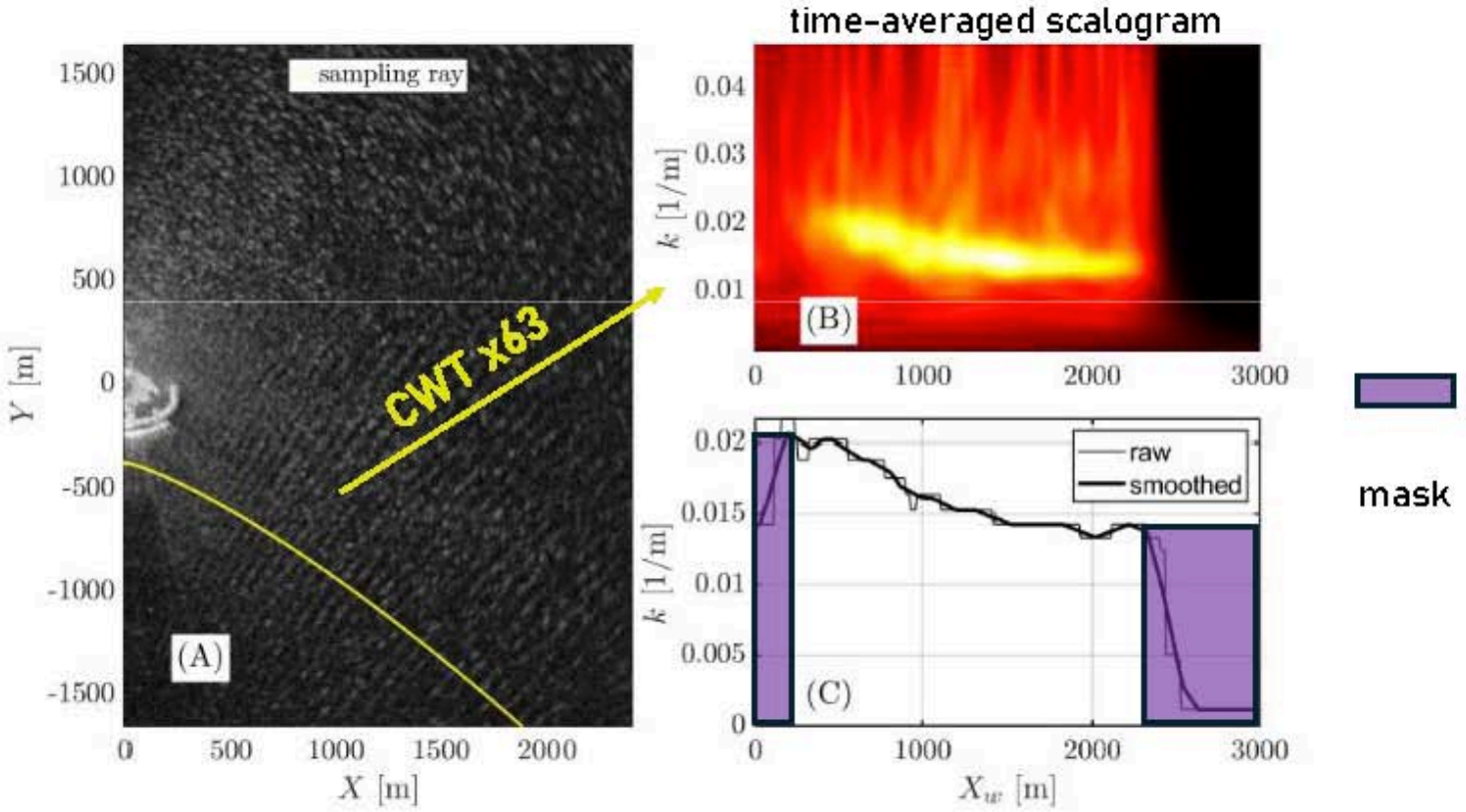

Image Assimilation for RSTs

wavelet_k_c_f:

Evaluation of wavenumbers by Continuous Wavelet Transformation (CWT).

Evaluation of wave celerity by utilizing RADON transformation.

time-stack

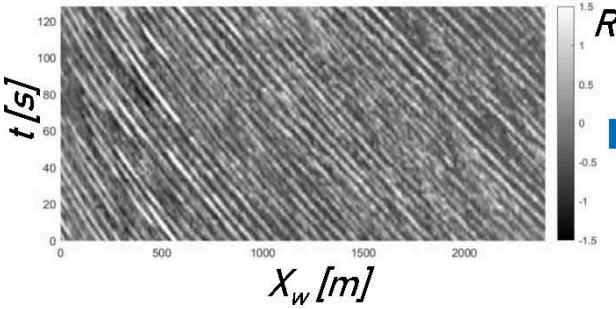

RADON

slope of crest path

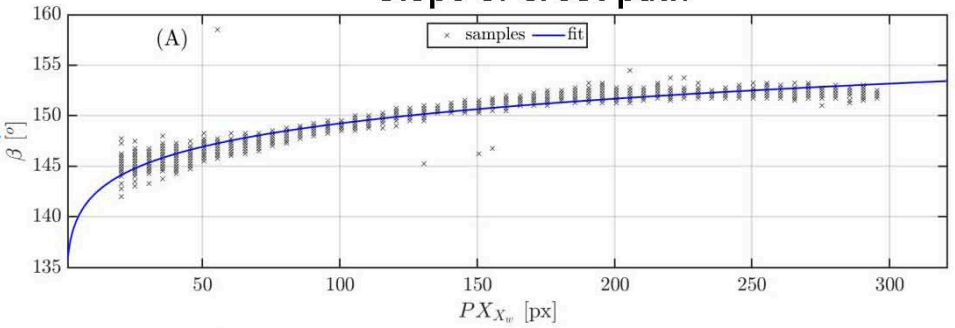

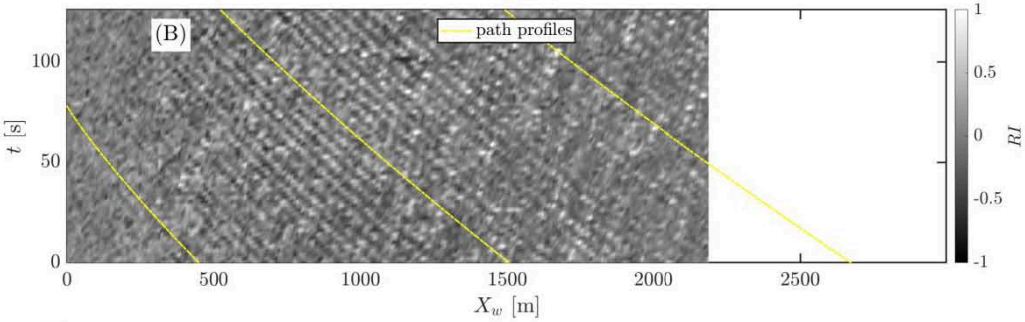

time&space relation

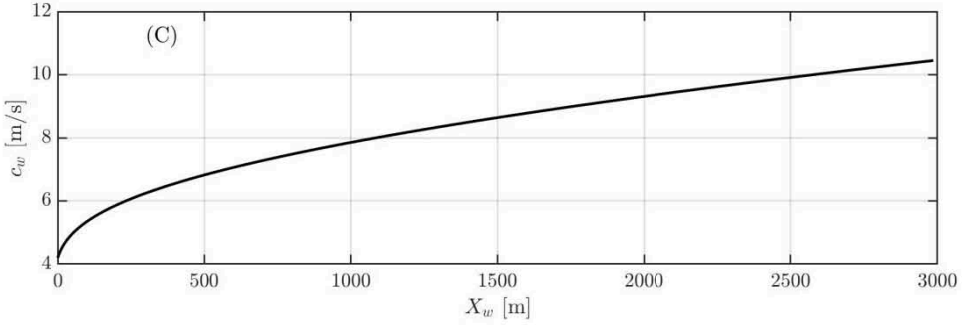

$$c_w = \frac{\partial X_w}{\partial t} = \frac{\Delta X_w}{\Delta t} \ [m/s]$$

Image Assimilation for RSTs

wavelet_k_c_f:

Evaluation of wavenumbers by Continuous Wavelet Transformation (CWT).
Evaluation of wave celerity by utilizing RADON transformation.

$$c_w = \frac{\partial X_w}{\partial t} = \frac{\Delta X_w}{\Delta t} \; [m/s]$$

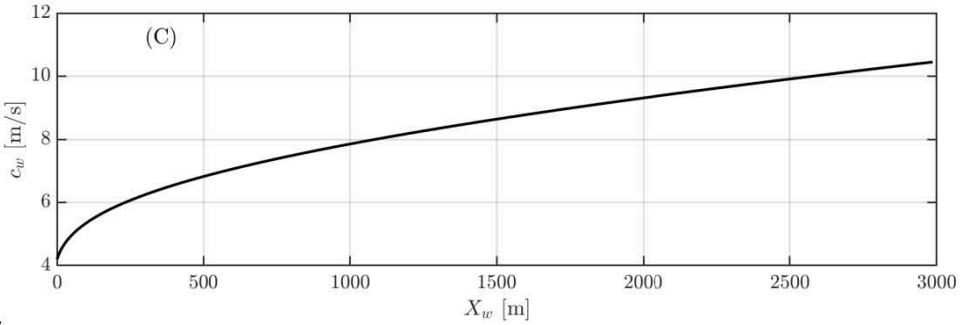

Derivation of the dominant period, T_{dom}

$$\mathbf{f} = \mathbf{c_w} * \mathbf{k}$$

$$\mathbf{k} = \frac{\mathbf{1}}{\boldsymbol{\lambda}}$$

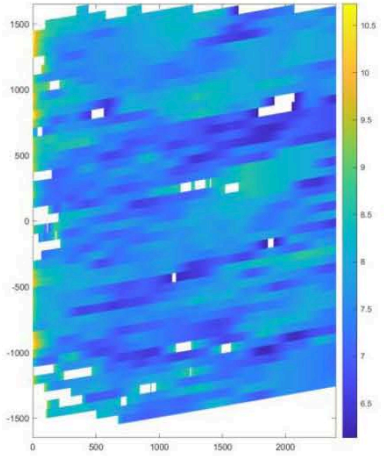

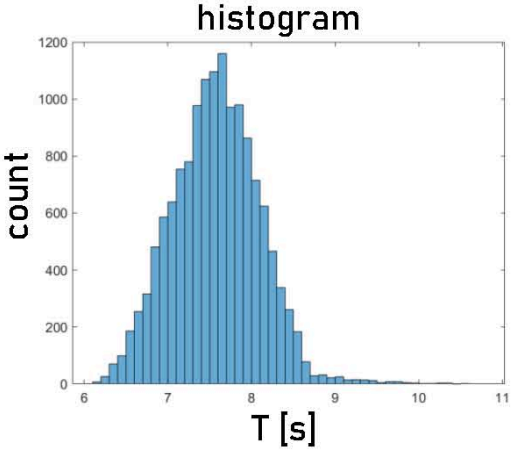

T_{dom}

Image Assimilation for RSTs

bathy_n_params:

Determination of bathymetry by solving the dispersion equation.

Prediction of wave characteristics to feed numerical models.

Celerity correction for the currents in wave direction

$$\mathbf{c_0} = \frac{f_{dom}}{\mathbf{k}} \rightarrow \Delta\mathbf{c} = \mathbf{c_0} - \mathbf{c_w} \rightarrow \mathbf{c_{cor}} = \mathbf{c_w} + \overline{\Delta c}$$ adding average current

$c_{deep} = \frac{gT_{dom}}{2\pi}$ deep water celerity $\quad c = \frac{gT}{2\pi}\tanh(kh)$ linear dispersion

$$\mathbf{h_{ini}} = \frac{\operatorname{atanh}\left(\frac{\mathbf{c_{cor}}}{c_{deep}}\right)}{2\pi\mathbf{k}}$$ initial bathymetry

$\mathbf{h_{cor}} = \mathbf{h_{ini}} - \eta_{tide}$ tide correction

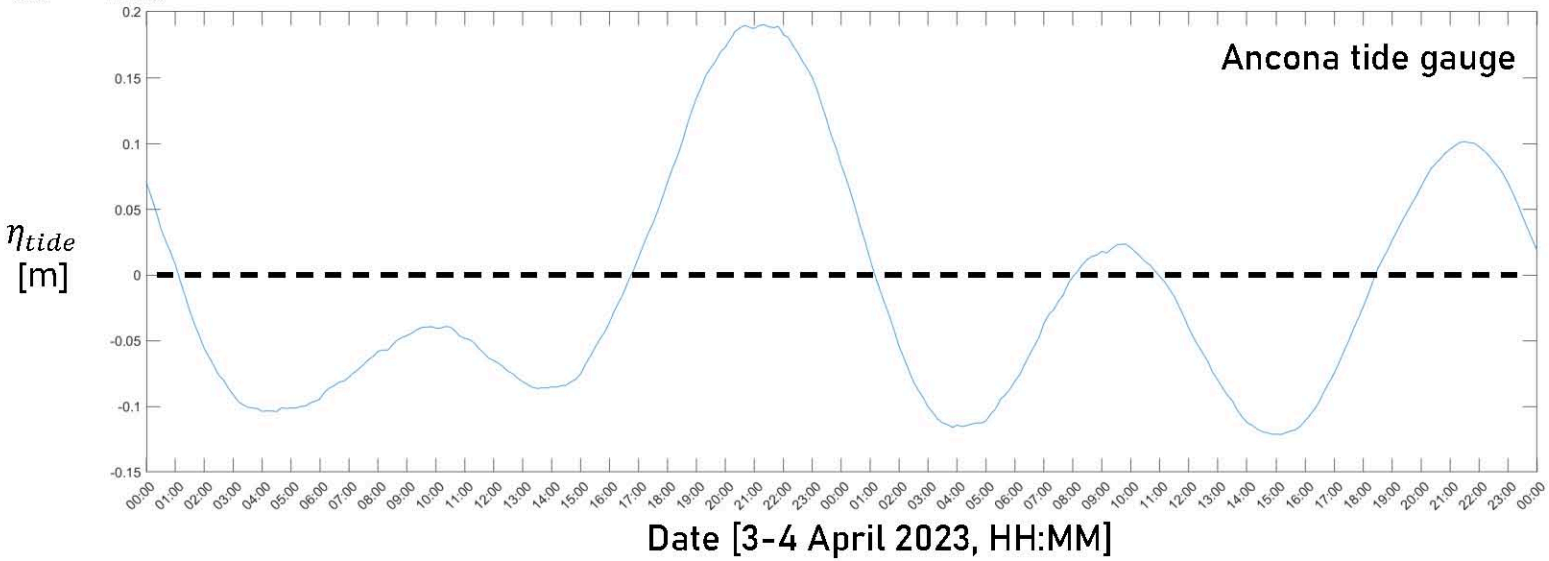

Image Assimilation for RSTs

bathy_n_params:

Determination of bathymetry by solving the dispersion equation.

Prediction of wave characteristics to feed numerical models.

refracted_images → θ_{wp}

wavelet_k_c_f → $T_{dom}, \lambda_{b,off}, \lambda_{b,on}$

? → H_s

FUNWAVE

FUNWAVE: Phase-resolving model to study inundation

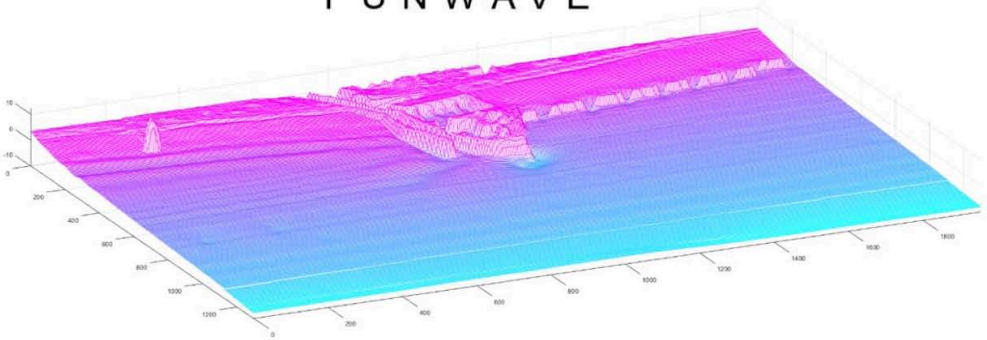

Image Assimilation for RSTs

bathy_n_params:

Determination of bathymetry by solving the dispersion equation.

Prediction of wave characteristics to feed numerical models.

For a general wave shape, the slope of the crest:

$$S = \frac{a_0 H}{\lambda}$$ where a_0 is a constant

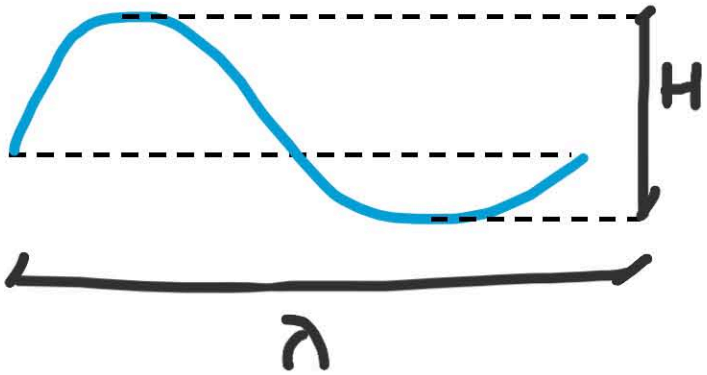

Image Assimilation for RSTs

bathy_n_params:

Determination of bathymetry by solving the dispersion equation.

Prediction of wave characteristics to feed numerical models.

For a general wave shape, the slope of the crest:

$$S = \frac{a_0 H}{\lambda}$$ where a_0 is a constant

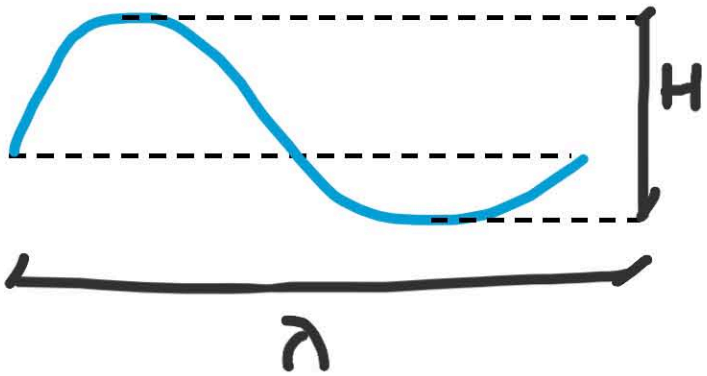

Radar signals are correlated with wave slope:

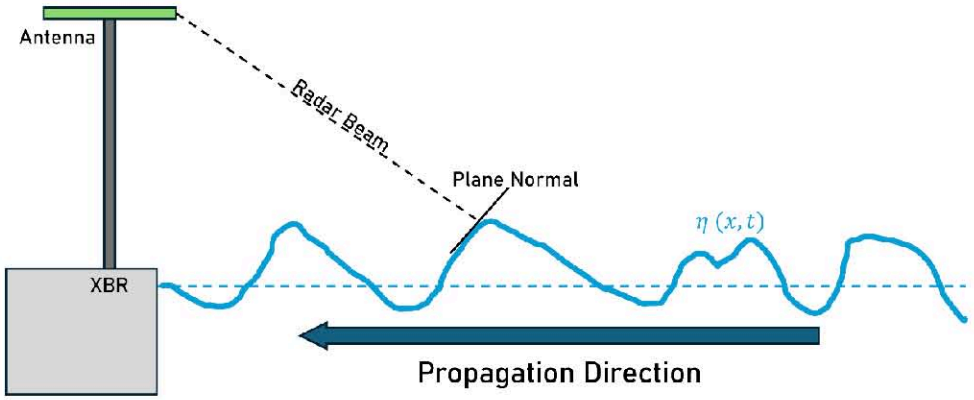

Image Assimilation for RSTs

bathy_n_params:

Determination of bathymetry by solving the dispersion equation.

Prediction of wave characteristics to feed numerical models.

For a general wave shape, the slope of the crest:

$$S = \frac{a_0 H}{\lambda}$$ where a_0 is a constant

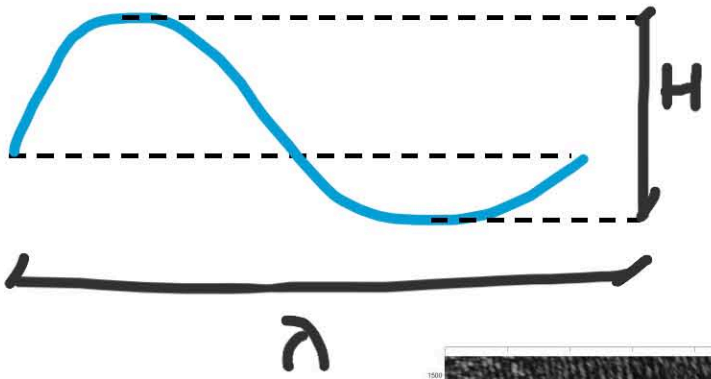

Radar signals are correlated with wave slope:

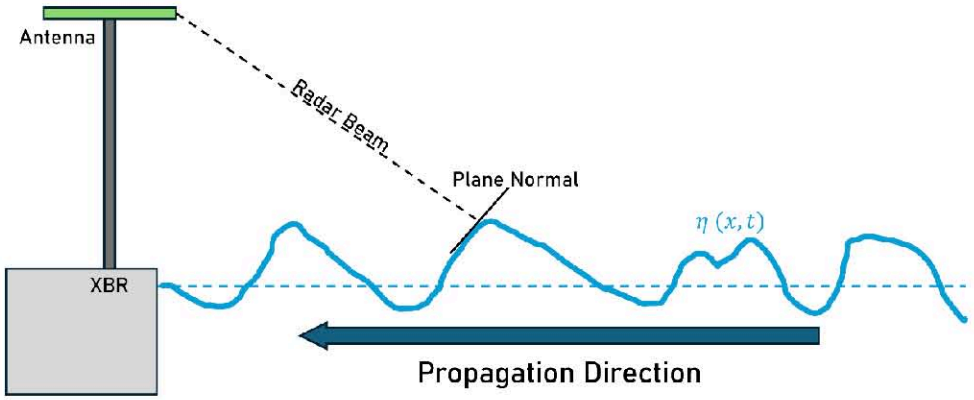

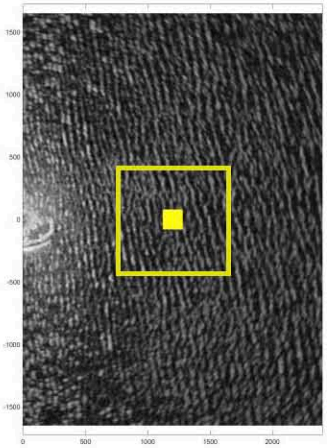

Therefore, a simple regression model can be established:

$$H_s = b_0 + b_1 \lambda \sigma_{1/3}$$

where b_0 and b_1 are regression coefficients, λ is the wavelength and $\sigma_{1/3}$ is the mean raw radar signal of the upper 33rd percentile from a patch close to the center where signals are visible

Preliminary Results

CW: Current Work

The performance of the proposed methodology has been tested by comparing to observations and alternative processing tools.

observations

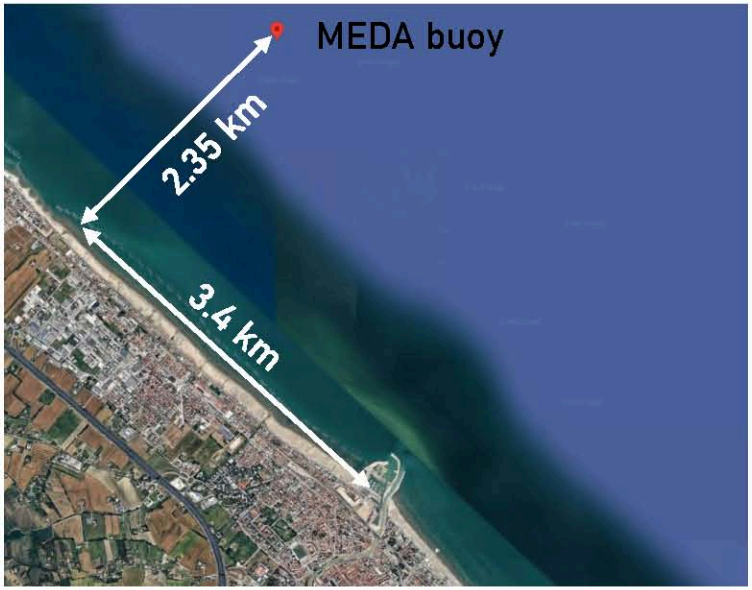

processing tools

REMOCEAN[1]

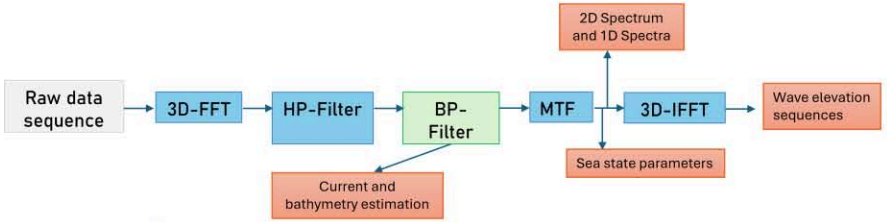

cBathy[2]

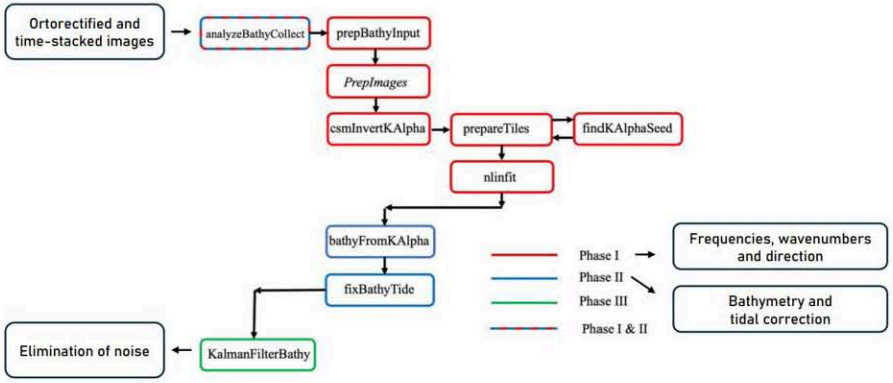

[1]Serafino, F., Lugni, C., Ludeno, G., Arturi, D., Uttieri, M., Buonocore, B., ... & Soldovieri, F. (2012). REMOCEAN: A flexible X-band radar system for sea-state monitoring and surface current estimation. IEEE Geoscience and Remote Sensing Letters, 9(5), 822-826.

[2]Holman, R., Plant, N., & Holland, T. (2013). cBathy: A robust algorithm for estimating nearshore bathymetry. Journal of geophysical research: Oceans, 118(5), 2595-2609.

Preliminary Results

CW: Current Work

CW performs well due to regression model
Remocean overestimates

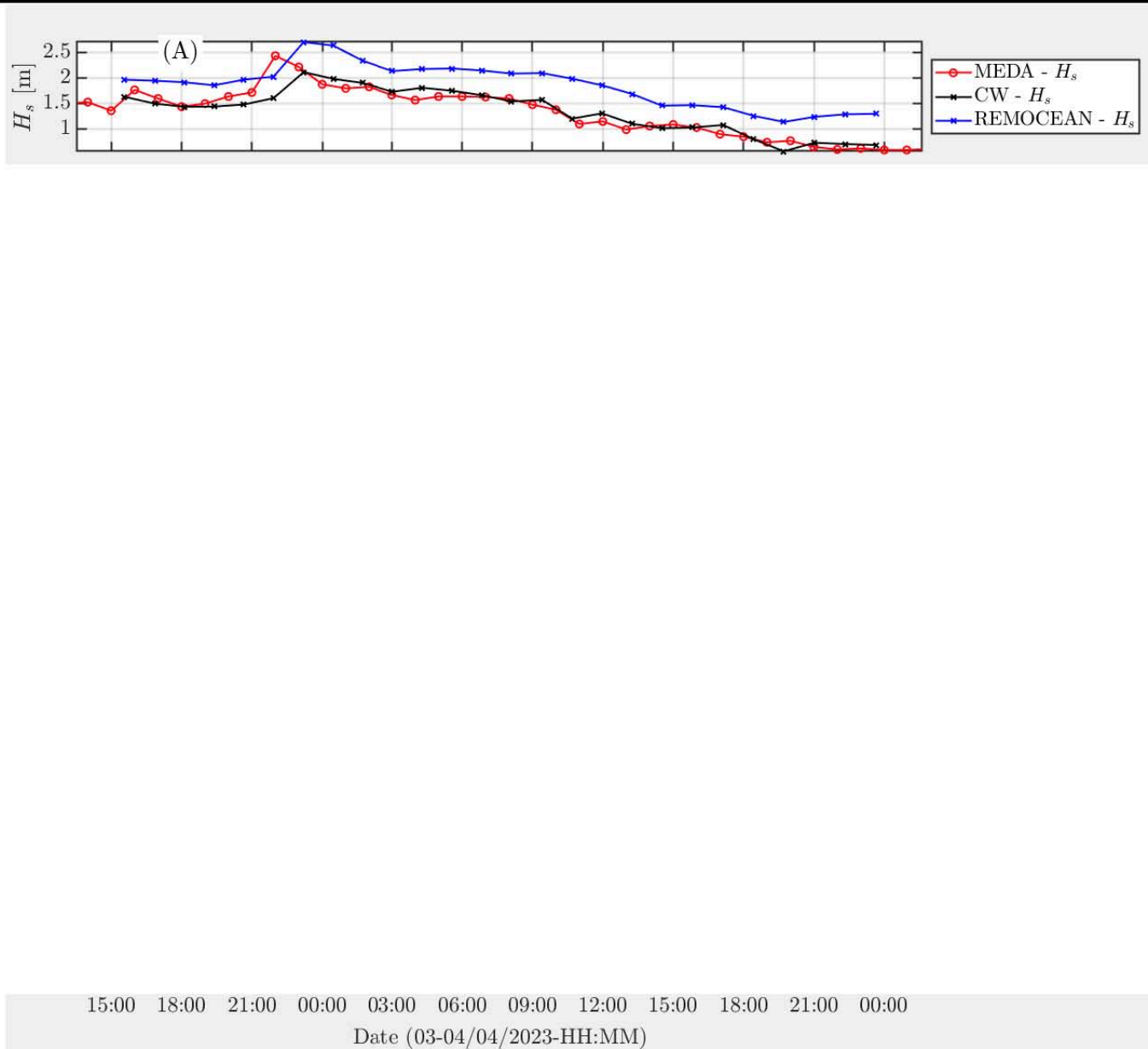

Preliminary Results

CW: Current Work

CW performs well due to regression model
Remocean overestimates

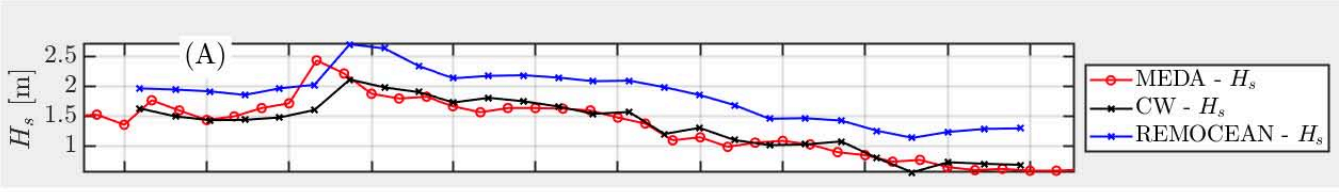

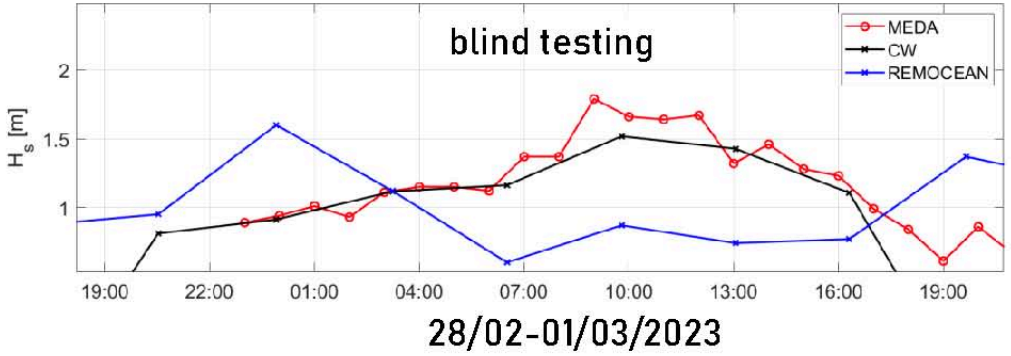

15:00 18:00 21:00 00:00 03:00 06:00 09:00 12:00 15:00 18:00 21:00 00:00
Date (03-04/04/2023-HH:MM)

Preliminary Results

CW: Current Work

CW performs well due to regression model
Remocean overestimates

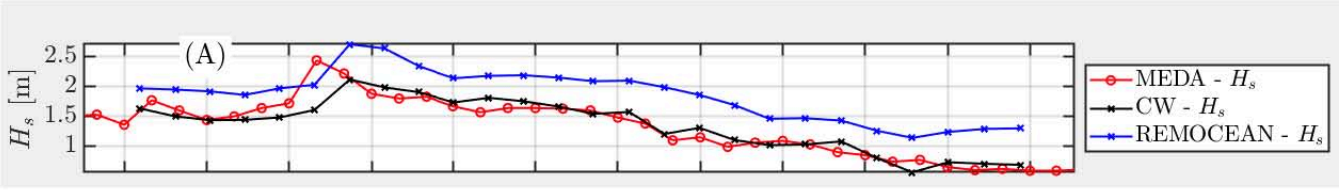

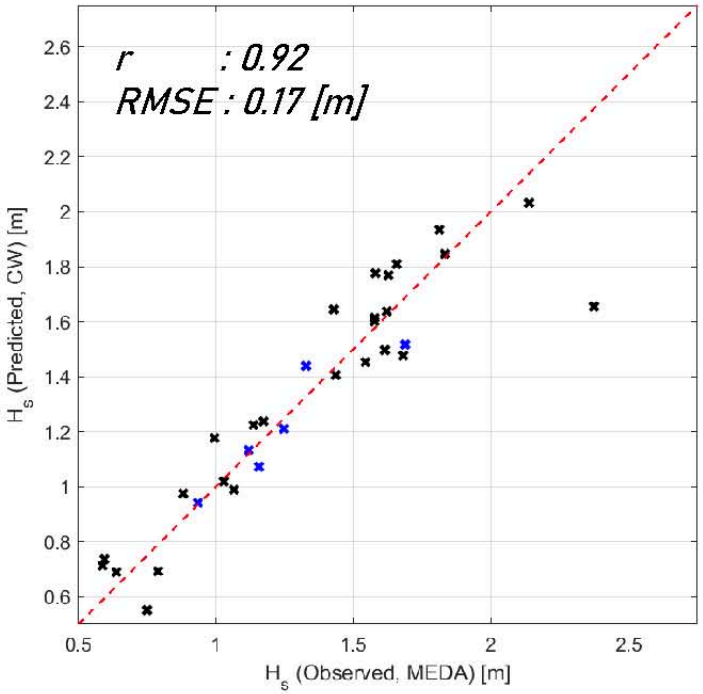

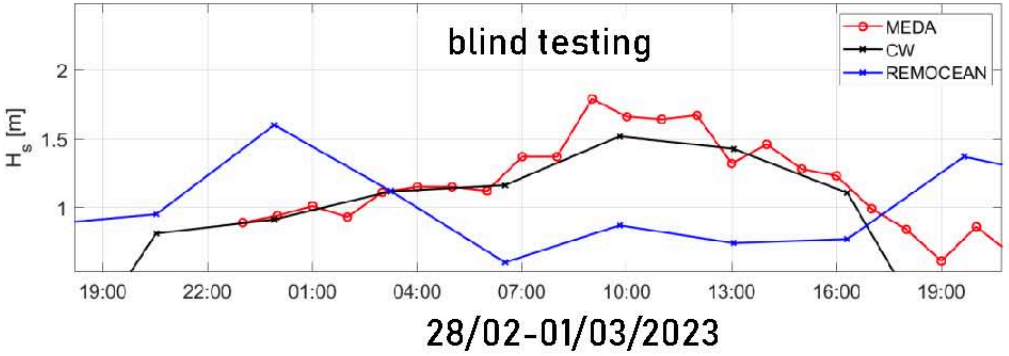

15:00 18:00 21:00 00:00 03:00 06:00 09:00 12:00 15:00 18:00 21:00 00:00
Date (03-04/04/2023-HH:MM)

Preliminary Results

CW: Current Work

CW performs well due to regression model
Remocean overestimates

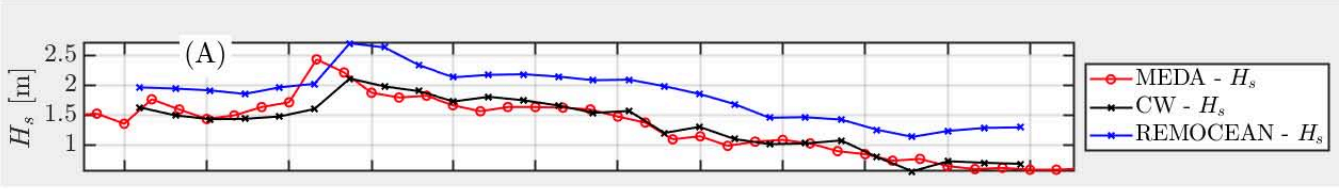

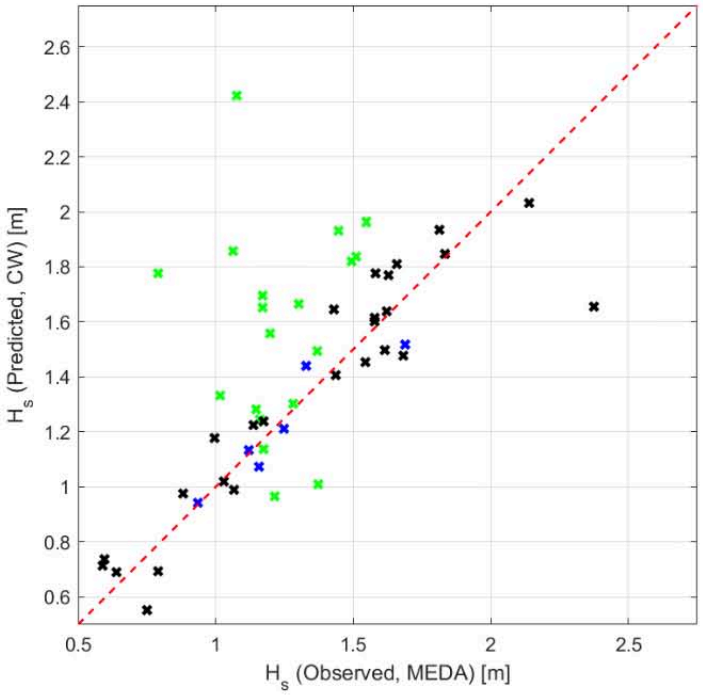

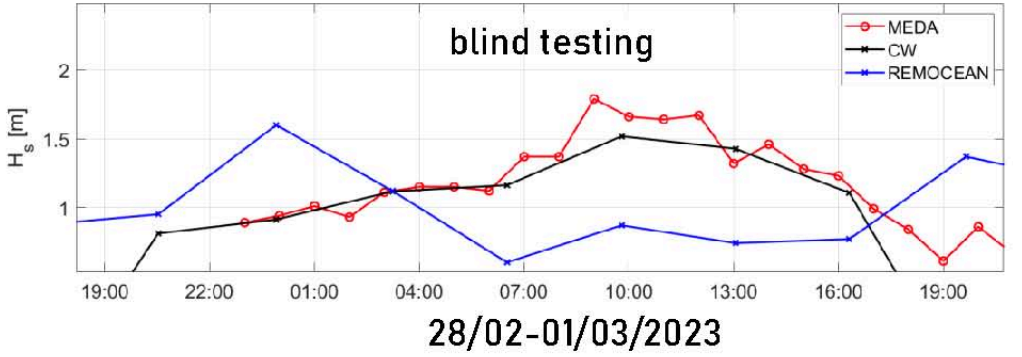

28/02-01/03/2023

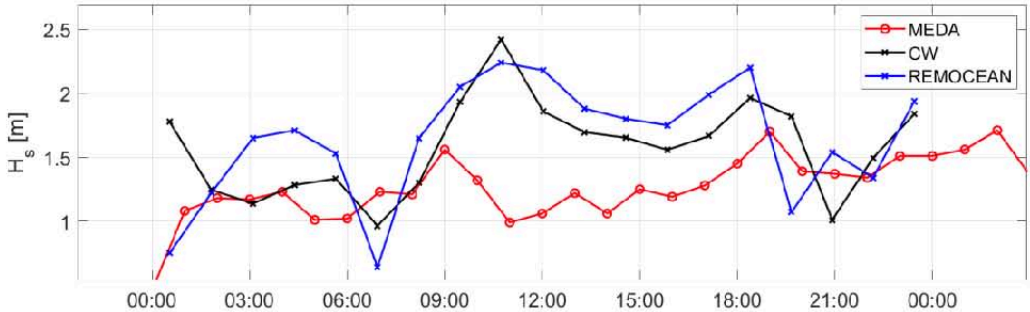

16/05/2023

Preliminary Results

CW: Current Work

CW performs well due to regression model
Remocean overestimates

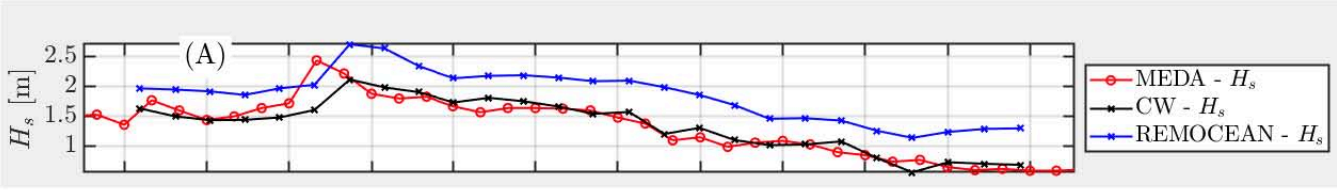

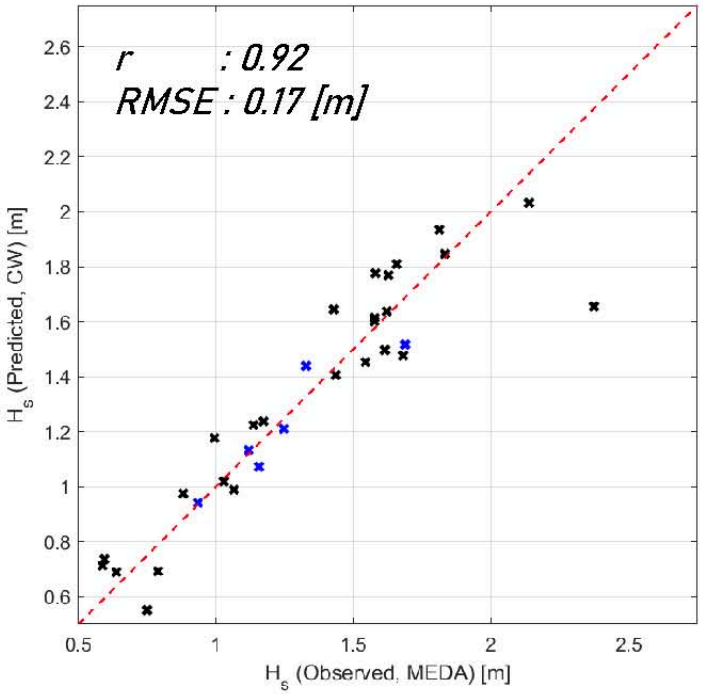

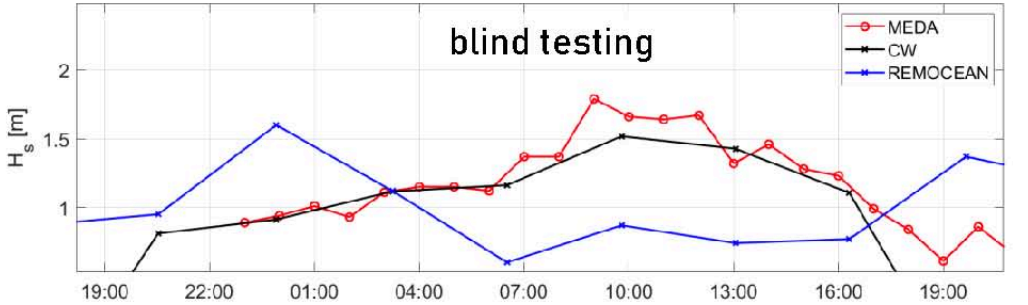

28/02-01/03/2023

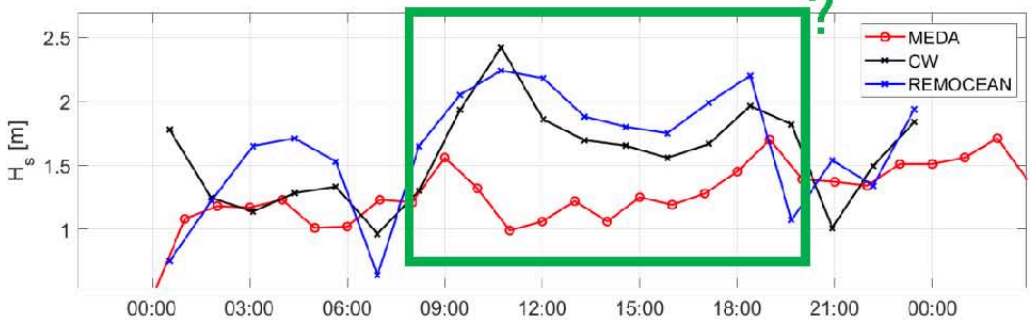

16/05/2023

15:00 18:00 21:00 00:00 03:00 06:00 09:00 12:00 15:00 18:00 21:00 00:00
Date (03-04/04/2023-HH:MM)

Preliminary Results

CW: Current Work

CW performs well due to regression model
Remocean overestimates

Remocean, cBathy and the CW are in good agreement

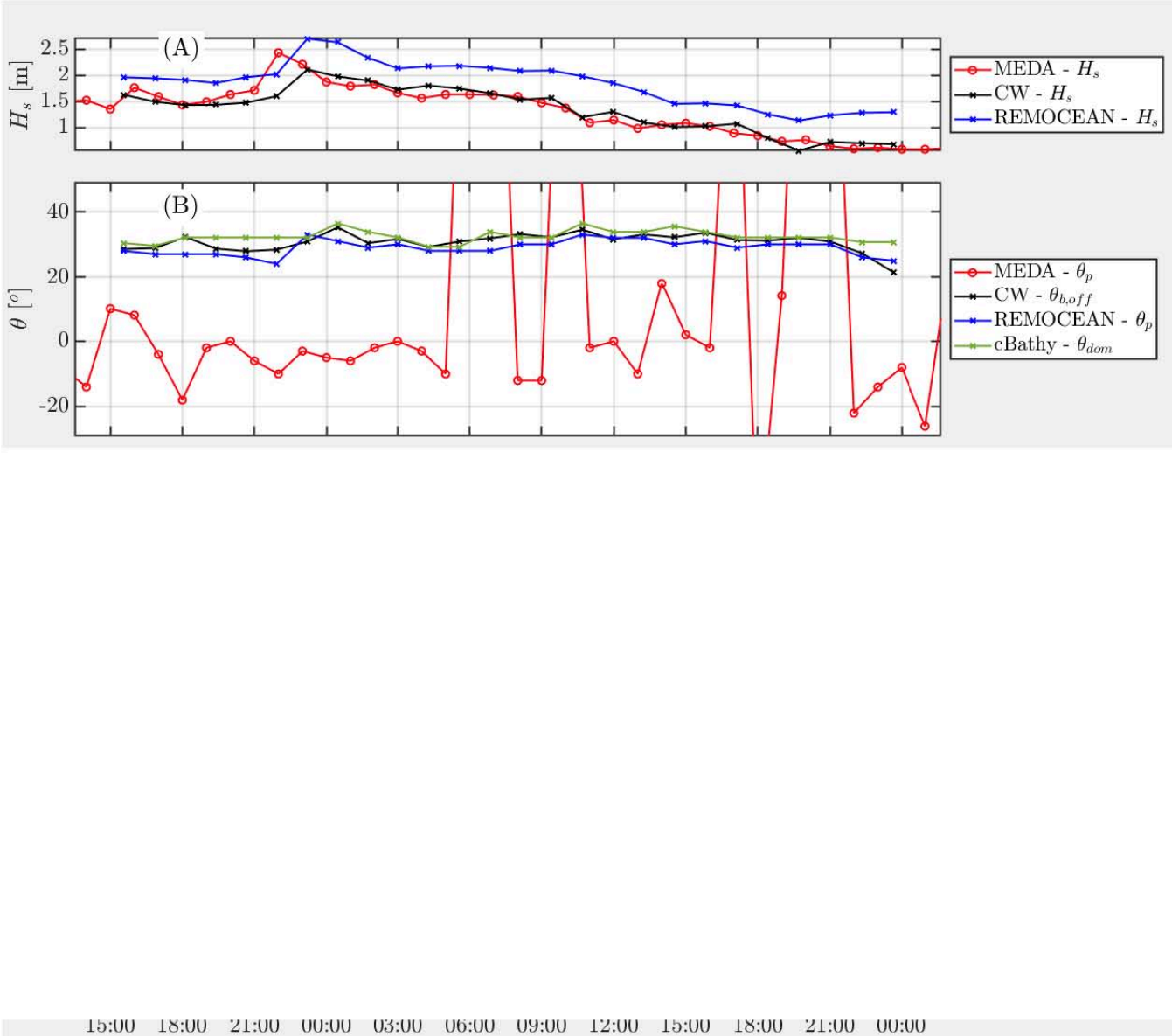

Preliminary Results

CW: Current Work

CW performs well due to regression model
Remocean overestimates

Remocean, cBathy and the CW are in good agreement

CW can capture the trend slightly better than Remocean
cBathy under- and overestimates

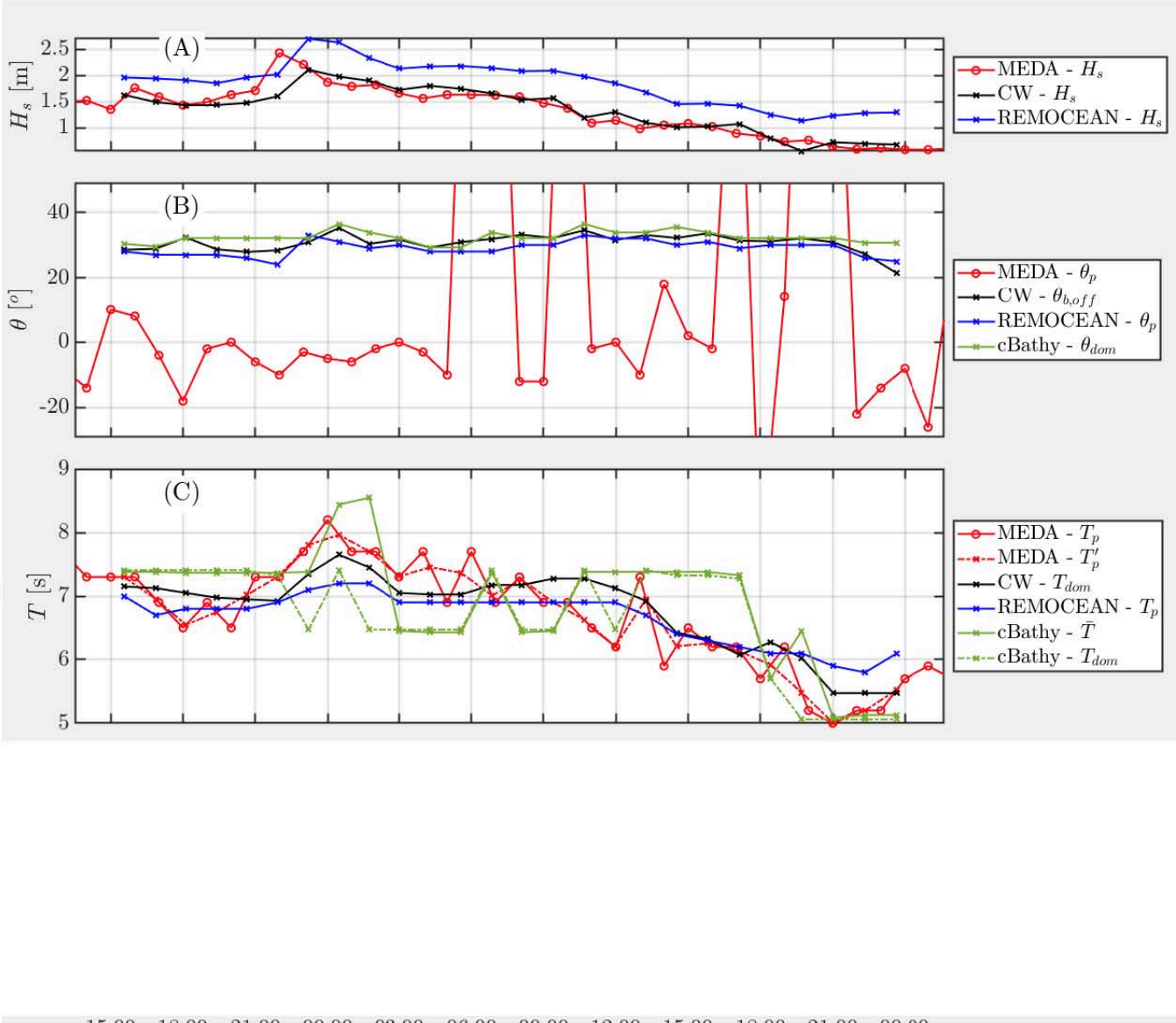

Preliminary Results

CW: Current Work

CW performs well due to regression model
Remocean overestimates

Remocean, cBathy and the CW are in good agreement

CW can capture the trend slightly better than Remocean
cBathy under- and overestimates

Remocean and CW are in good agreement
cBathy shows the average

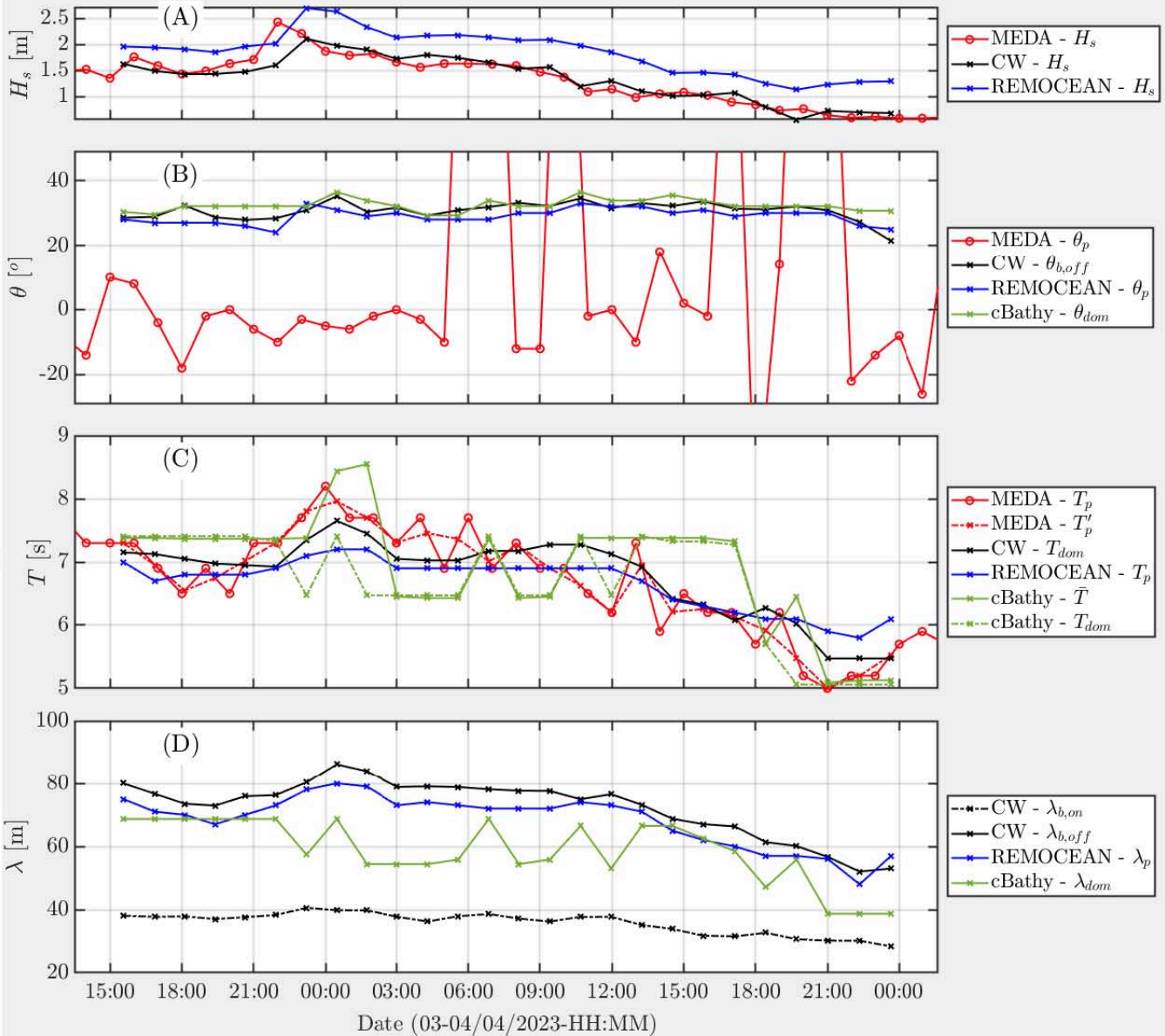

Preliminary Results

CW: Current Work

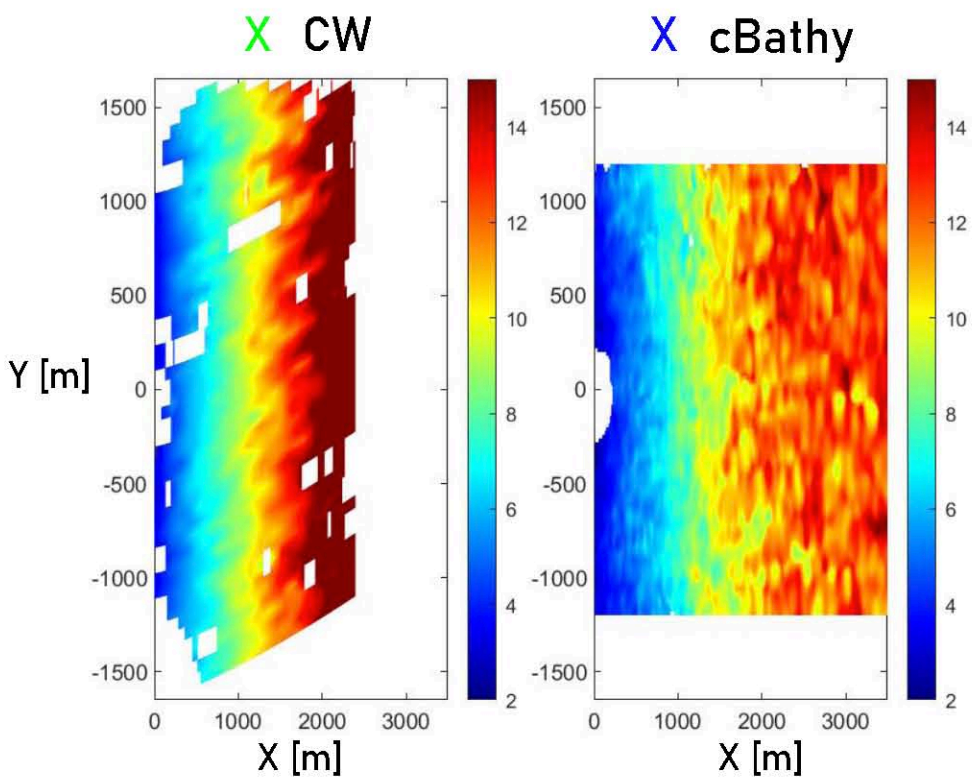

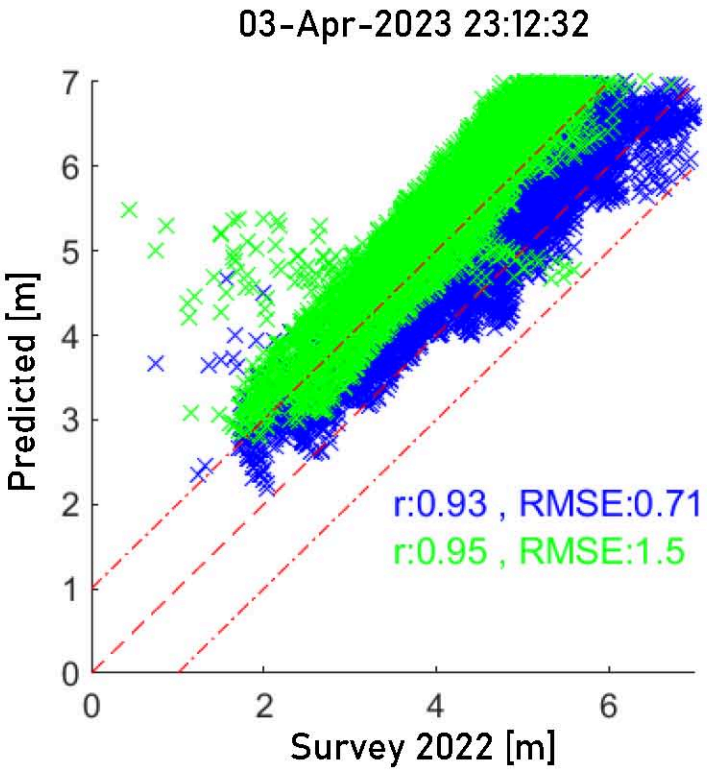

CW gives better *r*, however, higher *RMSE* than cBathy

r: Pearson number

Preliminary Results

CW: Current Work

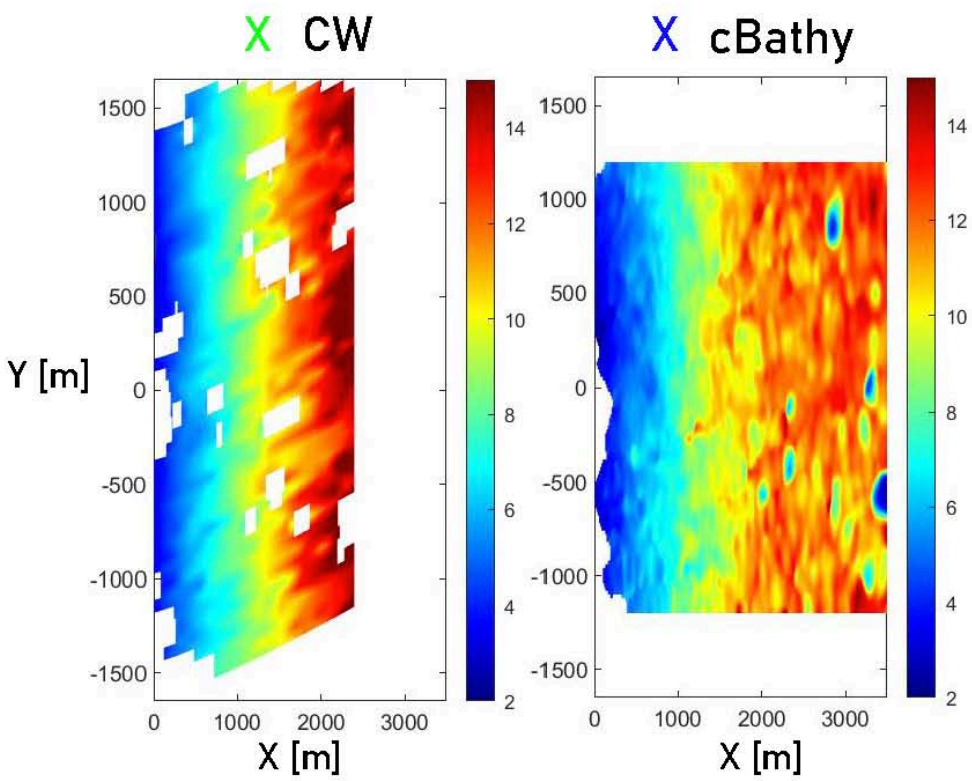

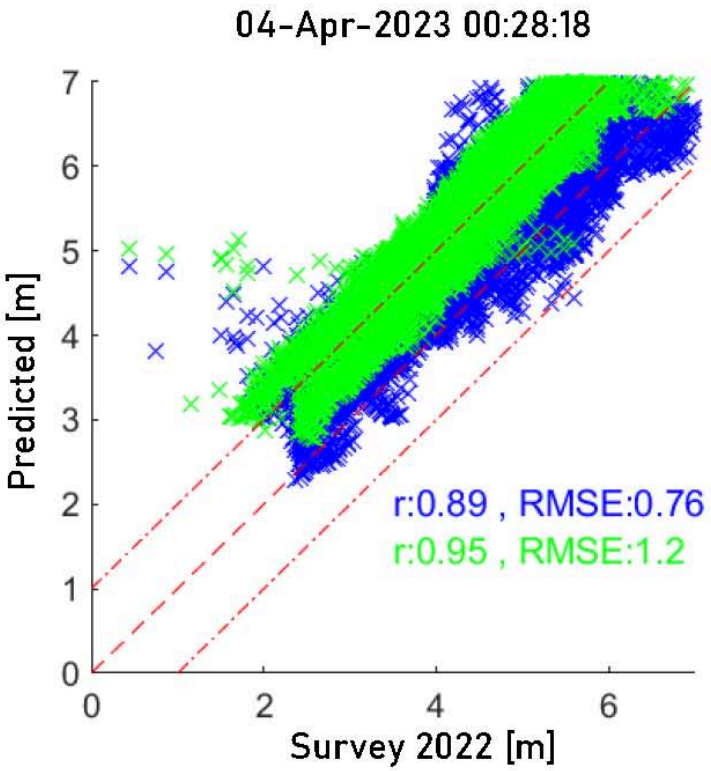

CW gives better *r*, however, higher *RMSE* than cBathy

r: Pearson number

Preliminary Results

CW: Current Work

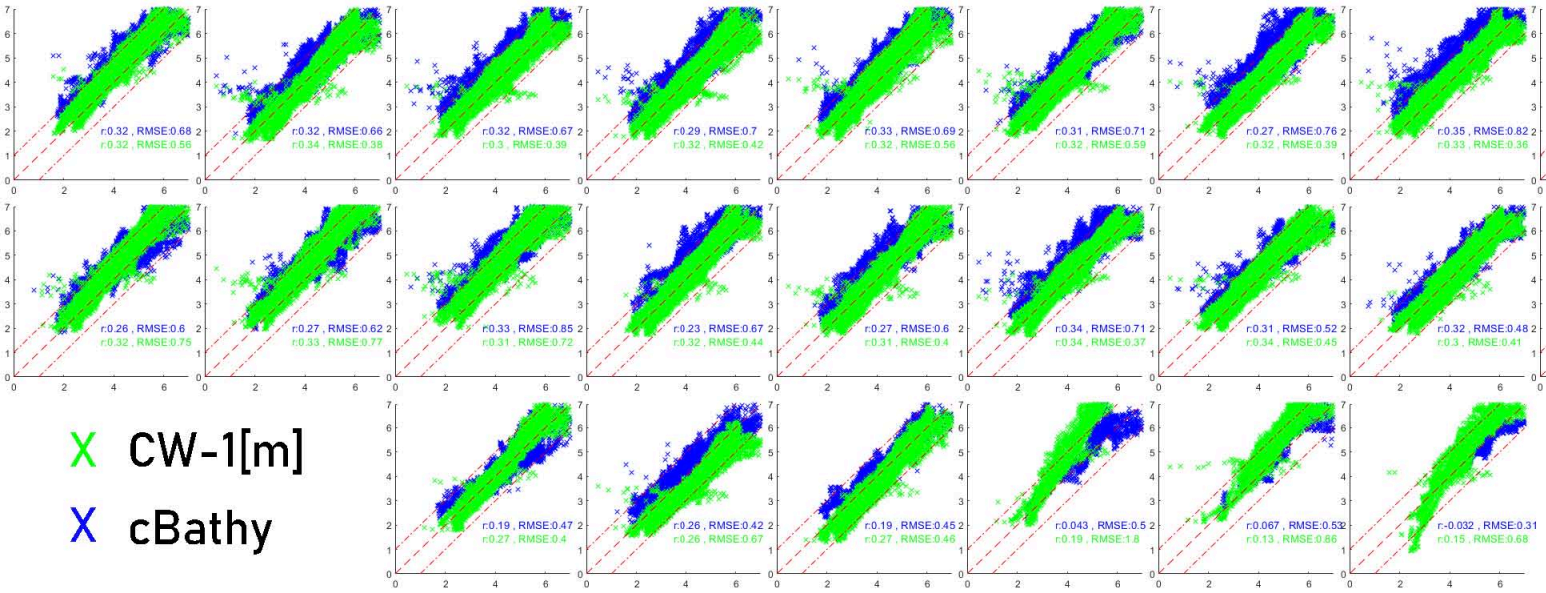

X CW-1[m]

X cBathy

CW gives better *r*, however, higher *RMSE* than cBathy
CW-1[m] increases the performance significantly

average computational time per data stack	
CW (w/out parallelization)	cBathy (w/ parallelization, 8 cores)
33 [s]	327 [s]

Model	$\bar{r}$	$\overline{RMSE}$ [m]
CW	0.95	1.37
cBathy	0.93	0.6
CW-1[m]	0.95	0.58

r: Pearson number

Ongoing Work

Investigation of the improvement on the bathymetry results.
Benchmarking the methodology with other datasets and at other sites.
Conducting inundation analyses with FUNWAVE fed by XBR derived wave characteristics.

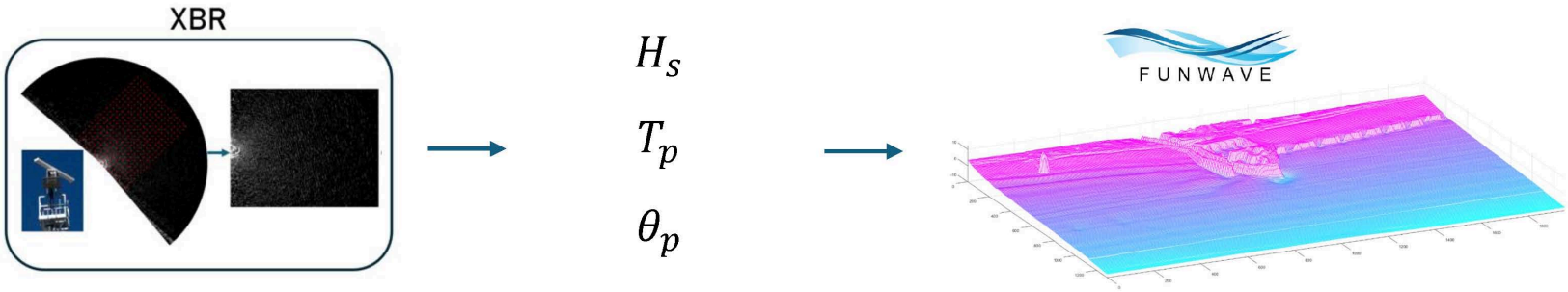

Ongoing Work

Investigation of the improvement on the bathymetry results.
Benchmarking the methodology with other datasets and at other sites.
Conducting inundation analyses with FUNWAVE fed by XBR derived wave characteristics.
Accounting for the secondary peak.

4 Apr 2023

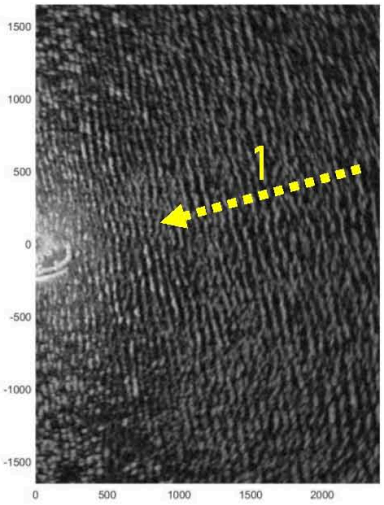

RADON

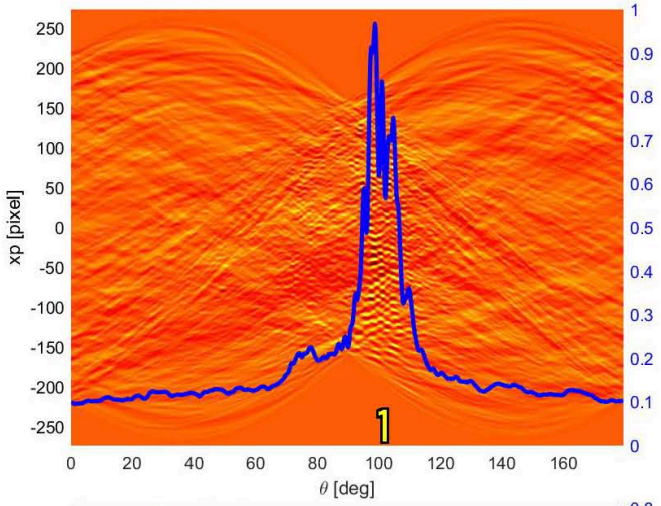

?

16 May 2023

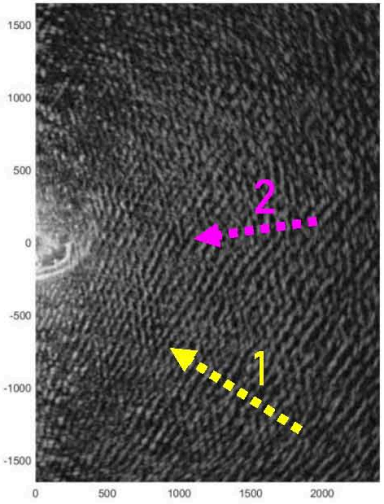

RADON

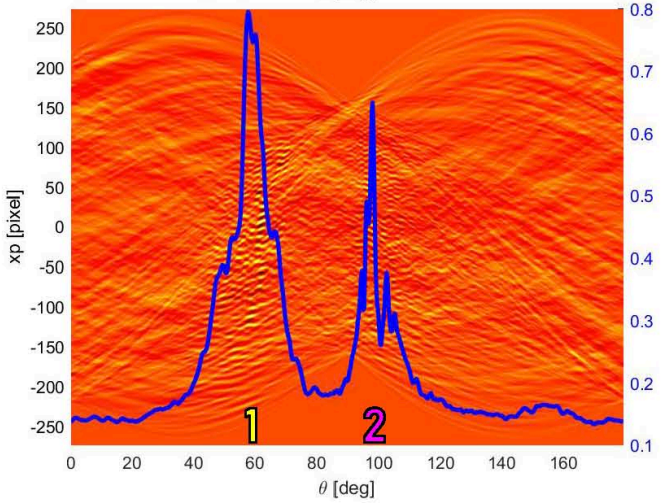

Ongoing Work

Incorporation of SGS data for further investigation on wave and nearshore dynamics

SGS

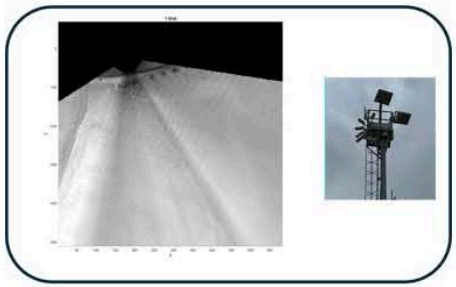

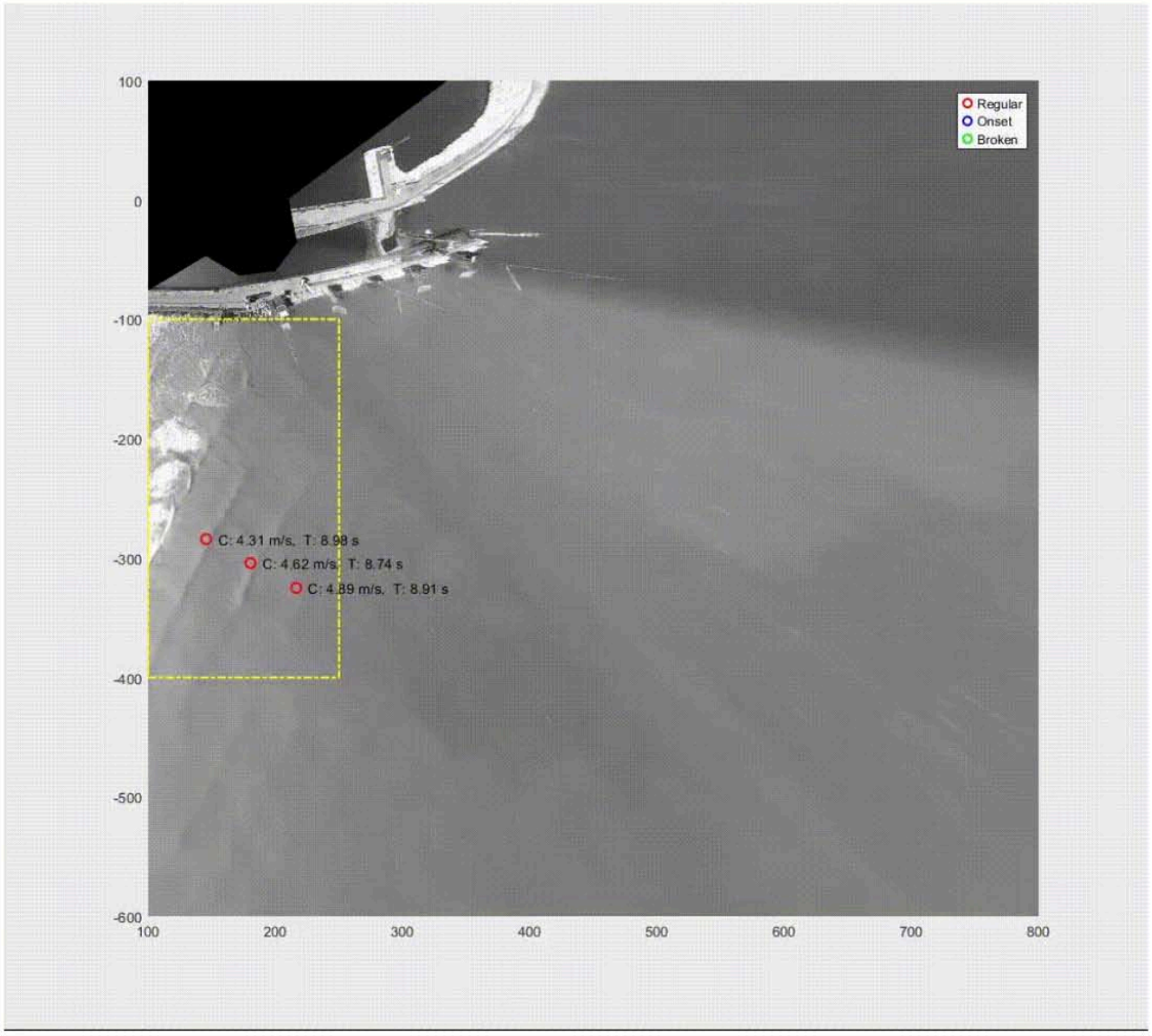

UNIVERSITÀ POLITECNICA DELLE MARCHE
DIPARTIMENTO INGEGNERIA CIVILE EDILE ARCHITETTURA
18|22 23|27 ECCELLENZA
Funded by the European Union

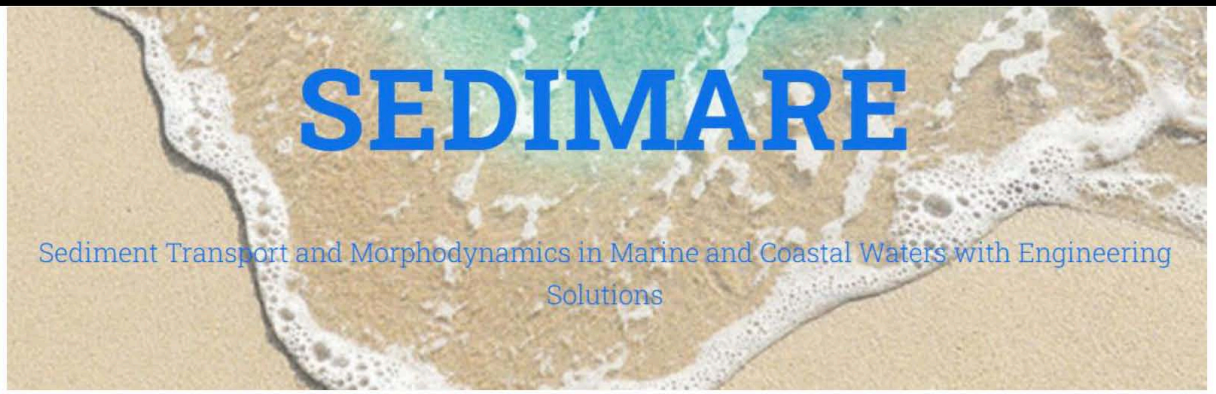

Image Assimilation for Remote Sensing Tools to Investigate Nearshore Dynamics

10-11 September 2025, HR Wallingford

M. Said Parlak
Doctoral Candidate
Università Politecnica delle Marche
Department of ICEA
m.s.parlak@univpm.it

Supervisors:
Maurizio Brocchini
m.brocchini@staff.univpm.it
Matteo Postacchini
m.postacchini@staff.univpm.it

Acknowledgement: This project has received funding from the European Union's (EU) Horizon Europe Framework Programme (HORIZON) under Grant Agreement No 101072443 as a MSCA Doctoral Network (HORIZON-MSCA-2021-DN-01) of SEDIMARE.

Preliminary Results

CW: Current Work

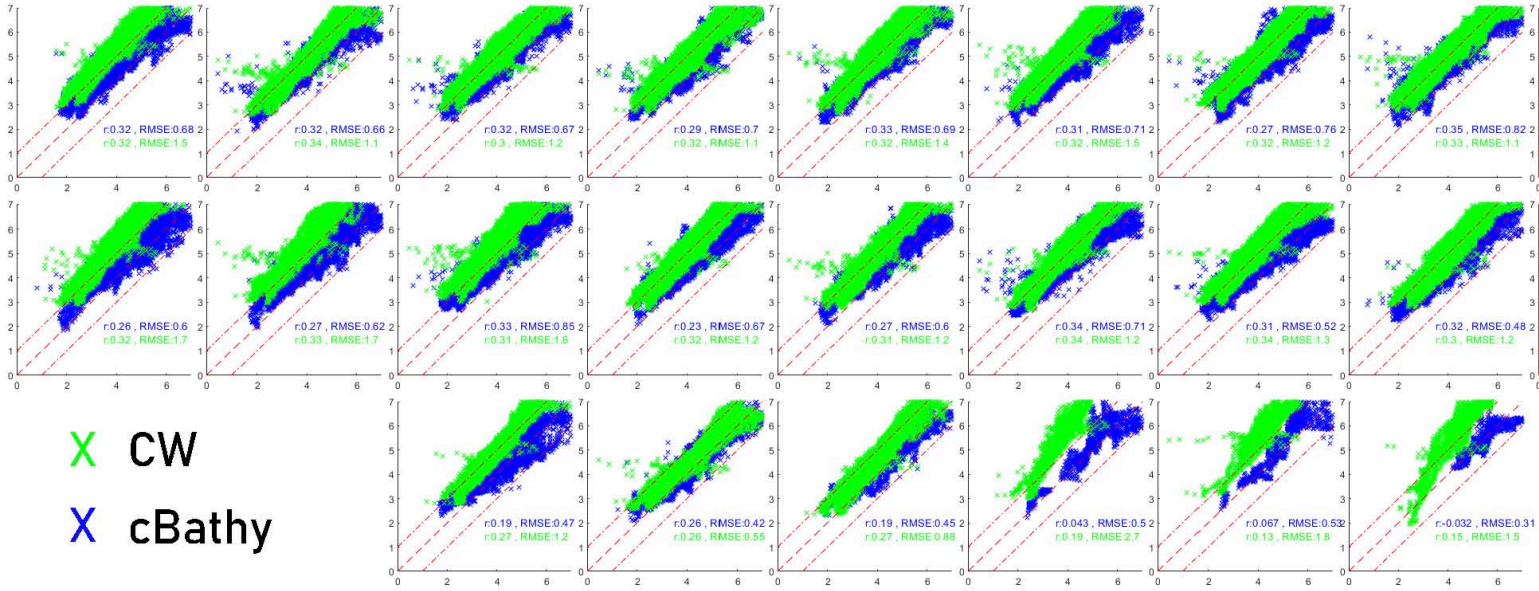

CW gives better *r*, however, higher *RMSE* than cBathy

Preliminary Results

CW: Current Work

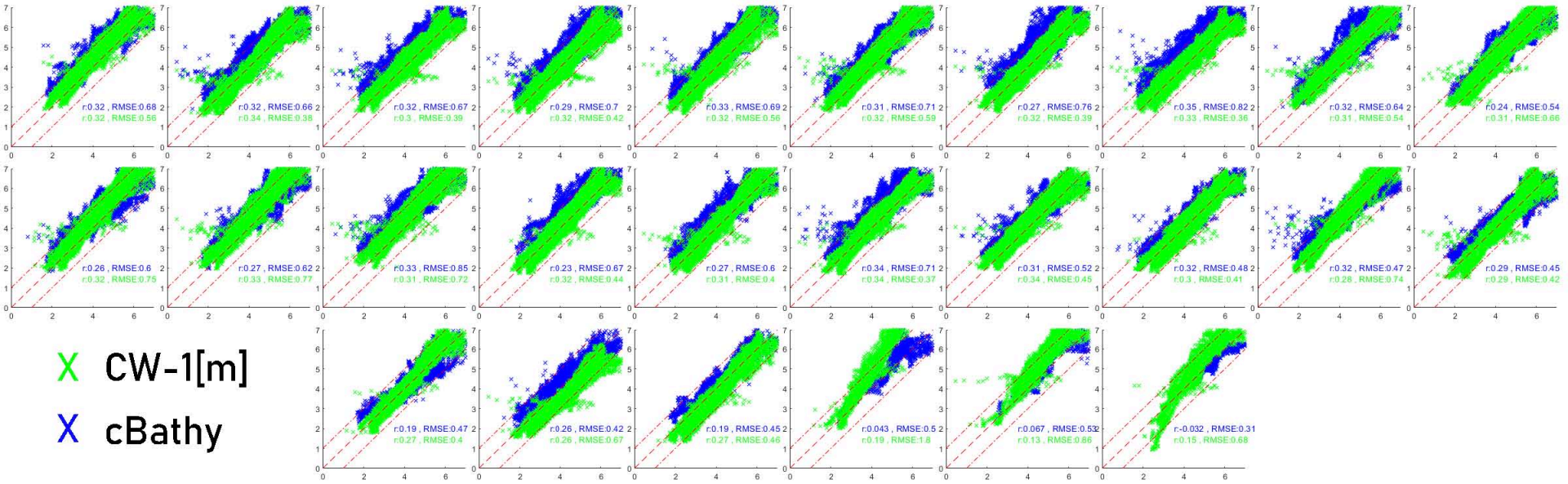

X CW-1[m]

X cBathy

CW gives better *r*, however, higher *RMSE* than cBathy
CW-1[m] increases the performance significantly

UNIVERSITÀ POLITECNICA DELLE MARCHE

Nasim Soori

Supervisors:
Prof. Maurizio Brocchini – UNIVPM
Prof. Athanassios Dimas – UPATRAS
Prof. Matteo Postacchini – UNIVPM

Eulerian–Lagrangian Modelling of Current-Driven Transport and PTV Analysis of Wave-Induced Particle Dynamics in Shallow Water

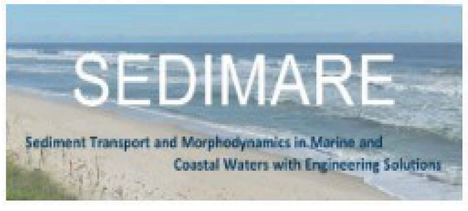

This project has received funding from the European Union's (EU) Horizon Europe Framework Programme (HORIZON) under Grant Agreement No 101072443 as a MSCA Doctoral Network (HORIZON-MSCA-2021-DN-01).

Marie Skłodowska-Curie Actions

10-11 Sept., 2025 – HR Walingford

Introduction and Significance

❑ **Numerical modelling in MATLAB** and **laboratory experiments using Particle Tracking Velocimetry (PTV)** for studying sediment transport under currents and waves.

❑ Numerical modelling in MATLAB

Study of mass transport processes; understanding sediment dynamics

Key aspects:

❑ Particle motion

❑ Bed resistance

❑ Sediment modification, retention, and accumulation

❑ Laboratory Experiments

Explore the behavior of the neutral particles, We performed some **experimental tests** in our laboratory under monochromatic and bichromatic waves.

Numerical Modelling (MATLAB Implementation)

A general outline:

❑ Flow Field Input

- Import velocity fields from hydrodynamic models (e.g., shallow water equations).
- Velocity data can be interpolated onto particle positions.

❑ Particle Tracking (Lagrangian Approach)

- Solve the particle motion equation:

$$dx/dt = u(x, t) \quad , \quad u: \text{the deterministic velocity field}$$

- Use numerical integration scheme (Euler) for trajectory computation.

❑ Mass Transport and Deposition Analysis

- Track particles to quantify sediment dispersion, retention zones, and accumulation patterns.
- Implement criteria for deposition based on bed shear stress vs. critical Shields parameter.

❑ Outputs

- Particle trajectories, residence times, spatial distribution of sediment, and transport pathways.

Numerical Modelling (MATLAB Implementation)

This example demonstrates entrainment, deposition, and resuspension of sediment moving down a straight channel within a uniform flow.

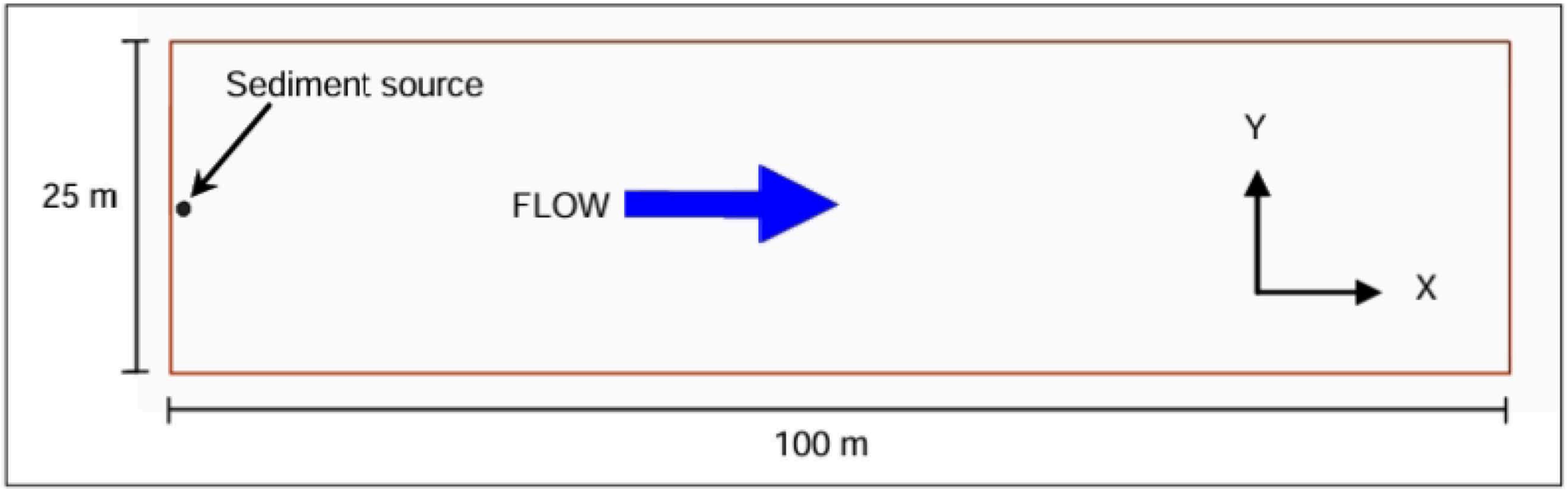

Fig 1.a Geometry

- The velocity is time dependent, changing in a sinusoidal manner.
- The velocity in the x (horizontal) direction is constant across the domain and cycles between 0 and 0.5 m/sec over a period of 2 min.
- The transverse velocity stays constant at 0 m/sec.
- Depth constant at 1 m,

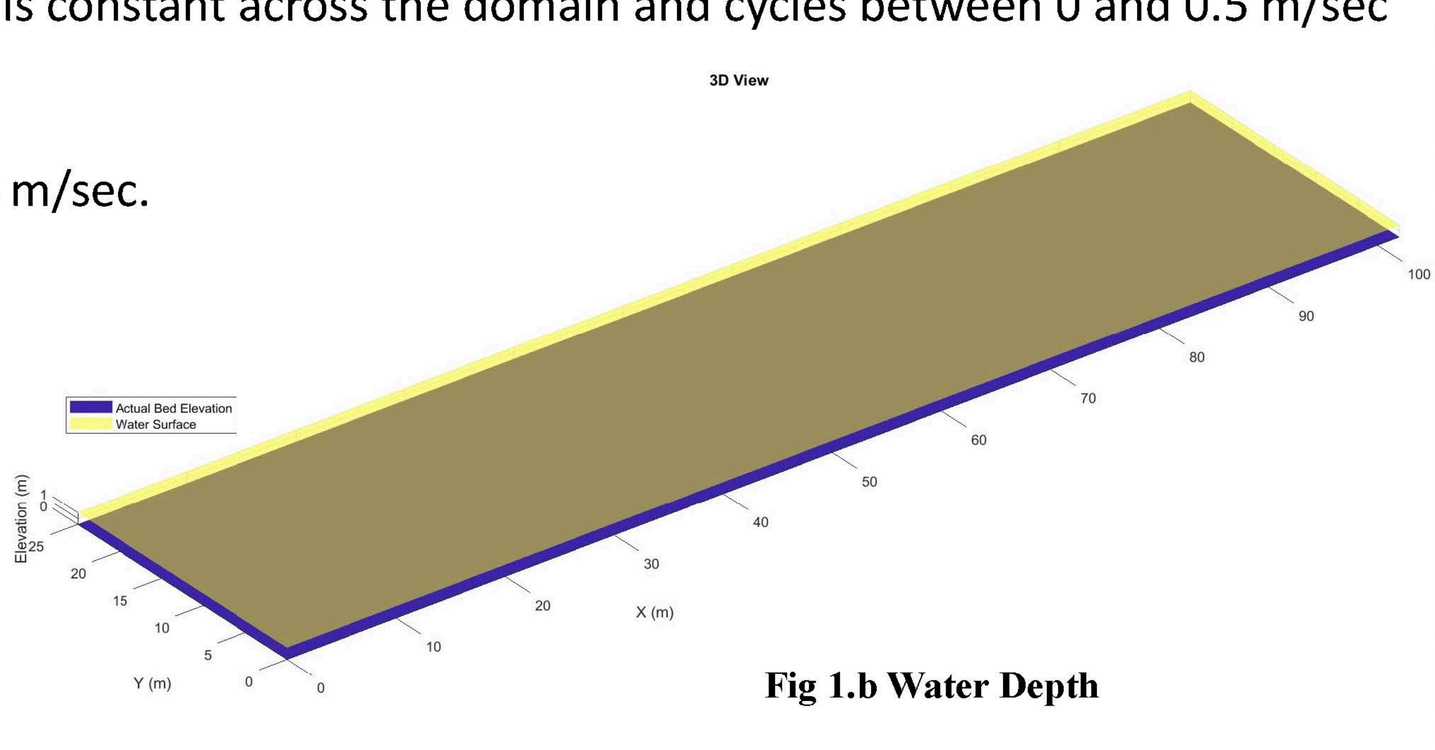

Fig 1.b Water Depth

Numerical Modelling - Velocity input

Velocities (u, v, w)

❑ Horizontal Velocities (u, v)

***u* velocity:**

- Varies sinusoidally with time (simulating wave/current oscillation) (Fig. 2)
- Zero at lateral boundaries (y-direction)
- Uniform across depth

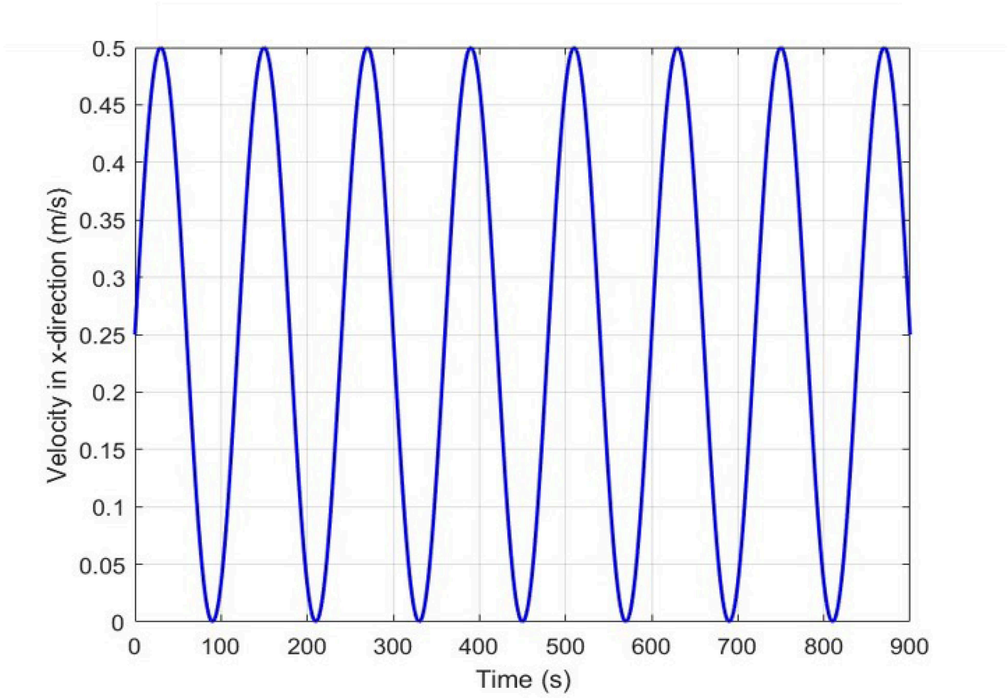

Fig 2. Input u-velocity

***v velocity*:** Set to zero everywhere

❑ Vertical Velocity (w)

Calculated from the continuity equation: (in this case; *w* everywhere is zero)

$$\frac{\partial w}{\partial z} = -\left(\frac{\partial u}{\partial x} + \frac{\partial v}{\partial y}\right)$$

Integrated vertically at each time step, assuming no flow at the bed (w = 0 at z = 0).

✓ **Critical Shields Parameter**

θ_{cr} as a function of grain Reynolds number and size.

The MATLAB code uses a simplified approximation consistent with PTM literature:

$$\theta_{cr} = \frac{0.30}{(1 + 1.2D_p)} + 0.055(1 - e^{-0.020D_p})$$

❑ Particle Fate Processes

✓ **Deposition**

When near-bed shear is insufficient ($\theta < \theta_{cr}$, the particle is deposited and immobilized at the bed (set to $z = z_0$).

✓ **Resuspension**

If bed shear exceeds critical ($\theta > \theta_{cr}$):

- A probabilistic pickup rate is applied, based on Van Rijn formulations.
- The vertical redistribution height is sampled from a **Rouse-type concentration profile**, controlled by the Rouse number:

$$R = \frac{w_s}{\kappa u_*}$$

ws= settling velocity [m/s]

κ = von Kármán constant (≈ 0.41)

u* = shear velocity (friction velocity) [m/s]

R = Rouse number

Describes the balance between particle settling and upward turbulent mixing.

✓ Large R (≫1): particles stay near the bed.

✓ Small R (≪1): particles remain suspended higher in the water column.

Laboratory Experiments (PTV)

Particle tracking is a numerical method used to simulate the movement of individual particles within a fluid system.

To explore the behavior of the particles, We performed some **experimental tests** in our laboratory under monochromatic and bichromatic waves:

✓ Physical experiments using Particle Tracking Velocimetry (PTV)

✓ Neutral seeding particles as optical tracers

✓ Emphasis on vertical distributions

❑ Experimental Setup

Wave parameters: Wave height: H= 3 cm, Period: T= 1 s, Depth: 12 cm

- Tracking at 120 fps, ~4900 frames (~40s)
- Frames divided into 3 blocks (720 frames each)

✓ Each block = **6 wave periods**

- Block 1: 1–720
- Block 2: 721–1440
- Block 3: 1441–2160

Laboratory Experiments - Pre-processing Workflow

- Runs tested with varying parameters:
  - ✓ Particle size (p_size = 7, 9, 11, 13, 15)
  - ✓ Particle Intensities (p_int = : 5000, 7000, 9000, 11000, 13000)
  - ✓ Threshold values (threshD = 2, 5, 8)

✓ Each run produces drift velocity profiles

Run	p_size	p_int	threshD
Run1	7	5000	2
Run2			5
Run3			8
Run4		7000	2
Run5			5
Run6			8
Run7		9000	2
Run8			5
Run9			8
Run10		11000	2
Run11			5
Run12			8
Run13	9	5000	2
Run14			5
Run15			8
Run16		7000	2
Run17			5
Run18			8
Run19		9000	2
Run20			5
Run21			8
Run22		11000	2
Run23			5
Run24			8

Run	p_size	p_int	threshD
Run25	11	5000	2
Run26			5
Run27			8
Run28		7000	2
Run29			5
Run30			8
Run31		9000	2
Run32			5
Run33			8
Run34	13	9000	2
Run35			5
Run36			8
Run37		11000	2
Run38			5
Run39			8
Run40	15	9000	2
Run41			5
Run42			8
Run43		11000	2
Run44			5
Run45			8
Run46		13000	2
Run47			5
Run48			8

Laboratory Experiments - Processing Workflow

Pre-processing Workflow

- Import frames and parameter scripts into MATLAB
- Sequential renumbering of frames
- Background subtraction (average background removed)
- Contrast enhancement for particle visibility
- Output stored in contrast folder for tracking

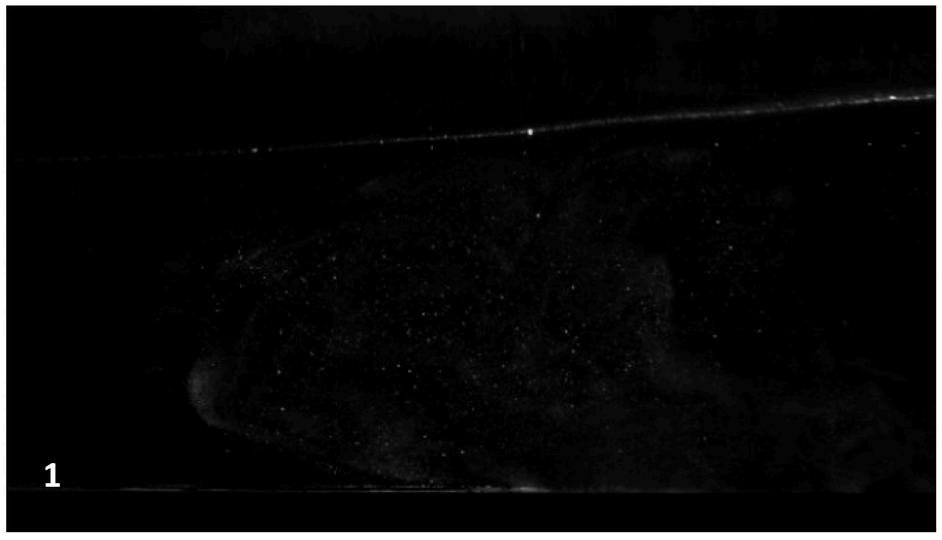

- **Fram with the background**

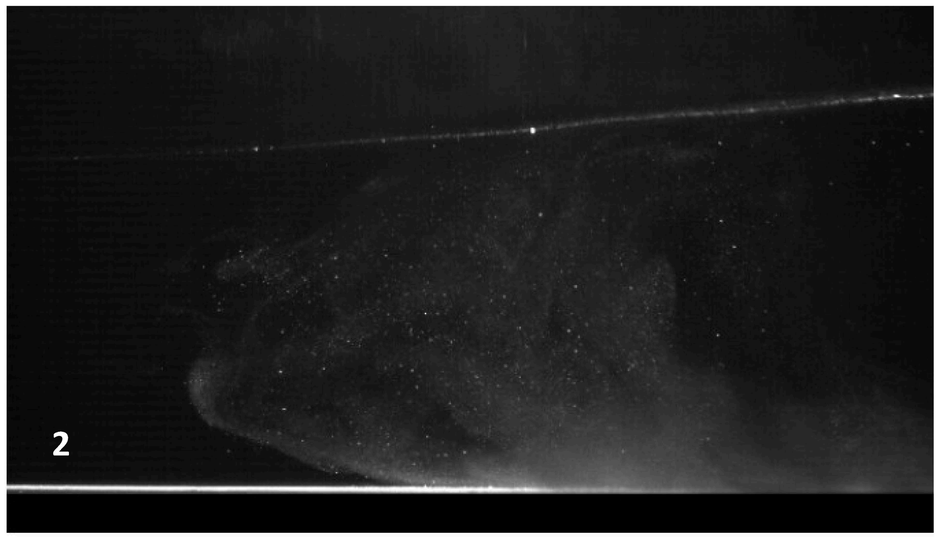

- **Fram without the background**

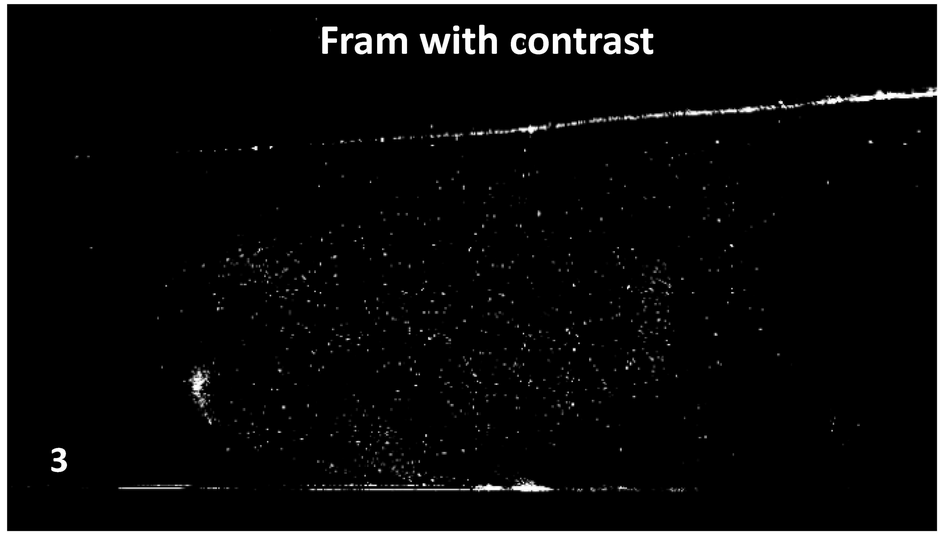

Laboratory Experiments - Processing Workflow

Contrast value 1:

Run 43 p_size=15, p_int=11000, threshD=2

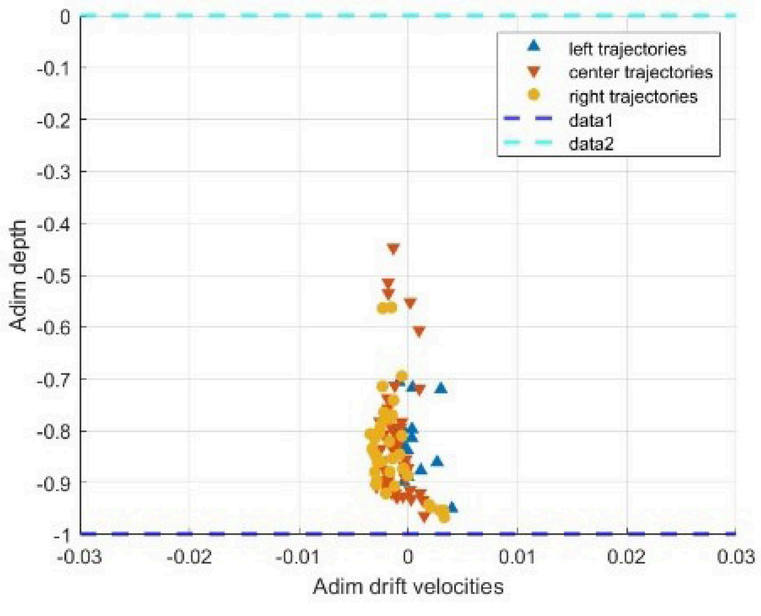

Run 44 p_size=15, p_int=11000, threshD=5

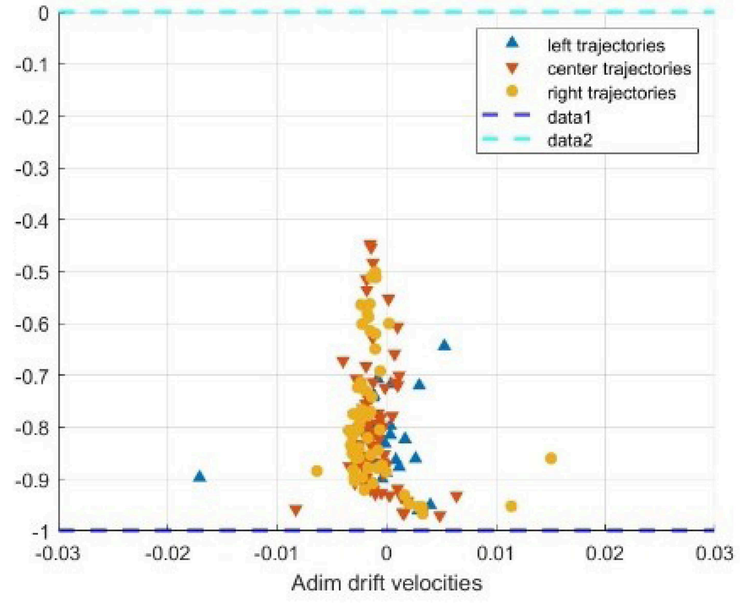

Run 45 p_size=15, p_int=11000, threshD=8

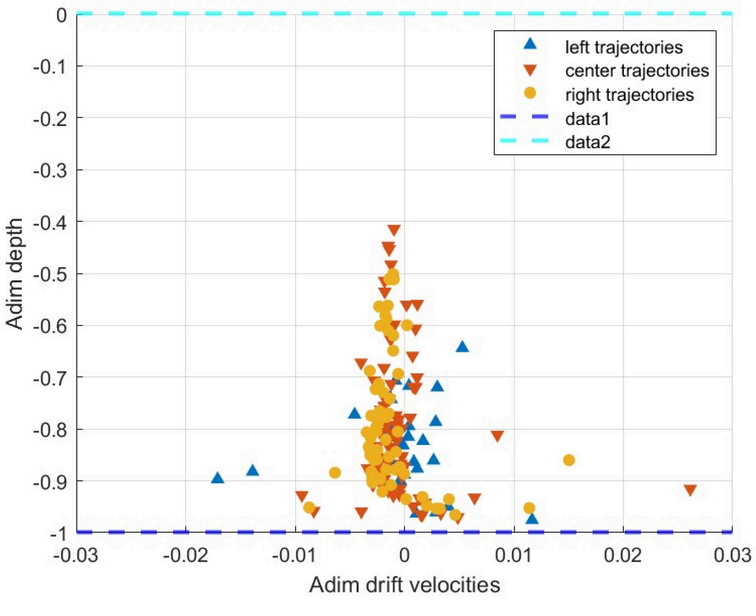

Contrast value 2:

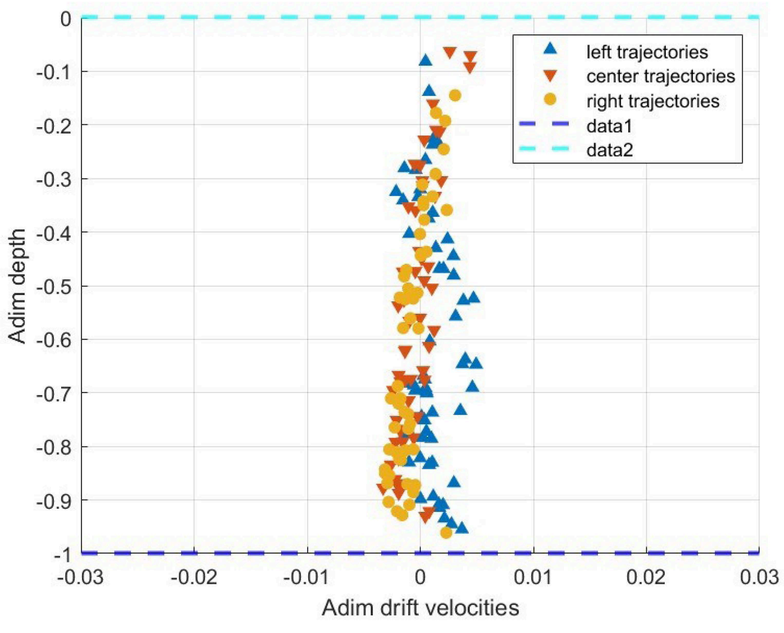

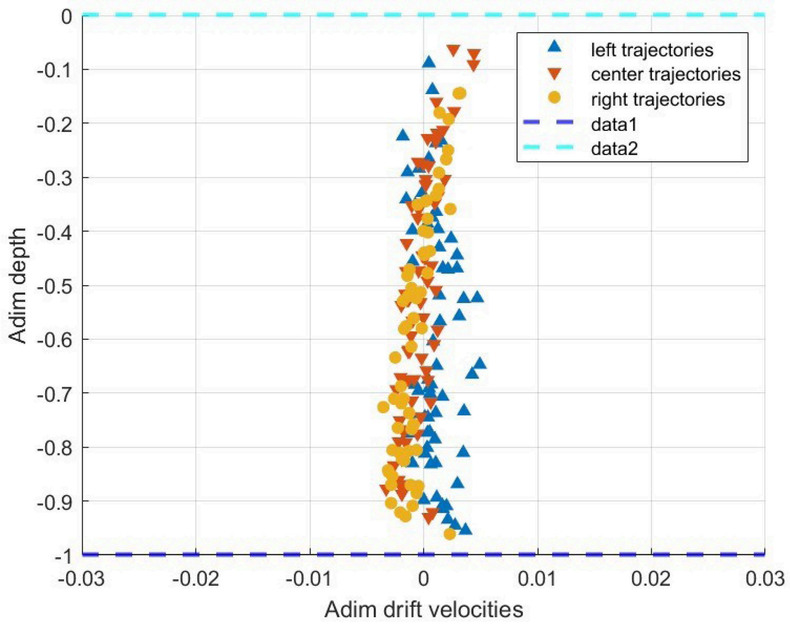

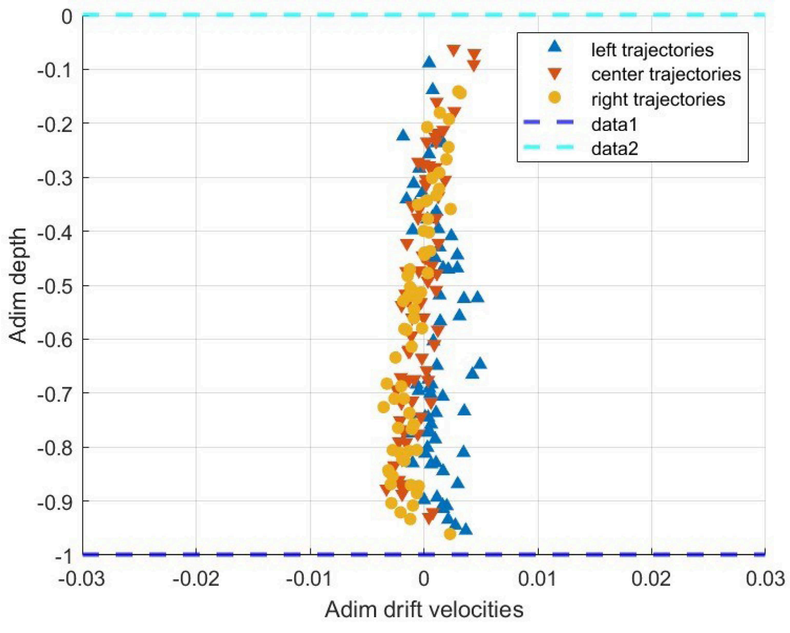

Laboratory Experiments - Post-processing Workflow

- Larger sizes (p_size= 13, 15) → best agreement

Run 1 (p_size=7, p_int=11000, threshD=8)

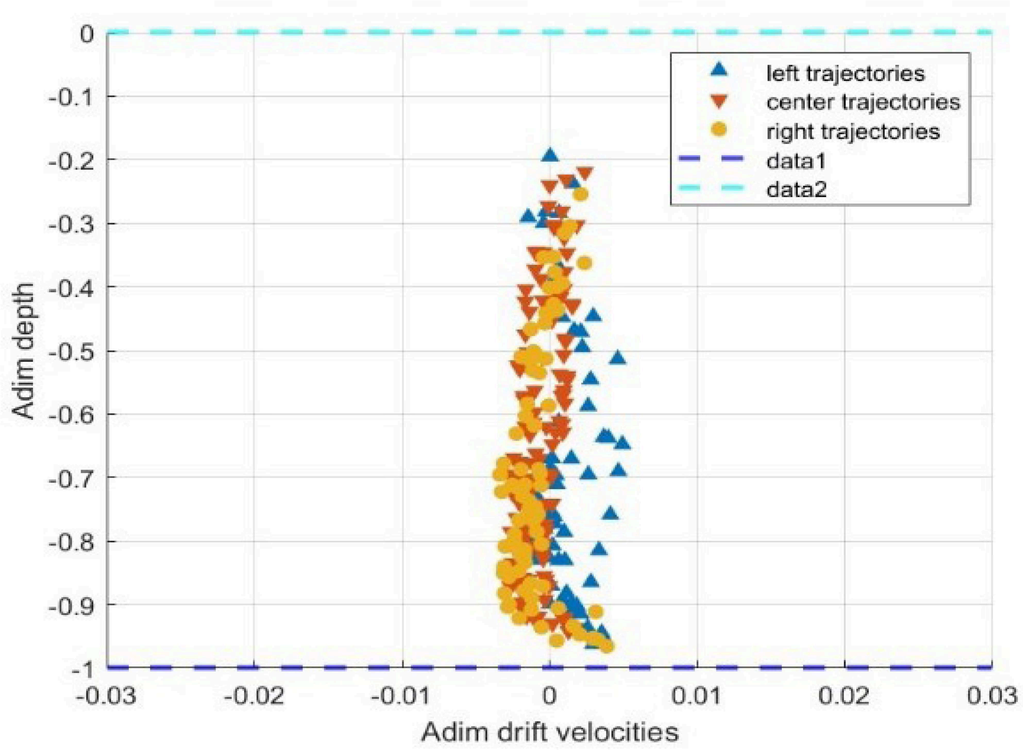

Run 20 (p_size=9, p_int=11000, threshD=8)

Run 1 (p_size=13, p_int=11000, threshD=8)

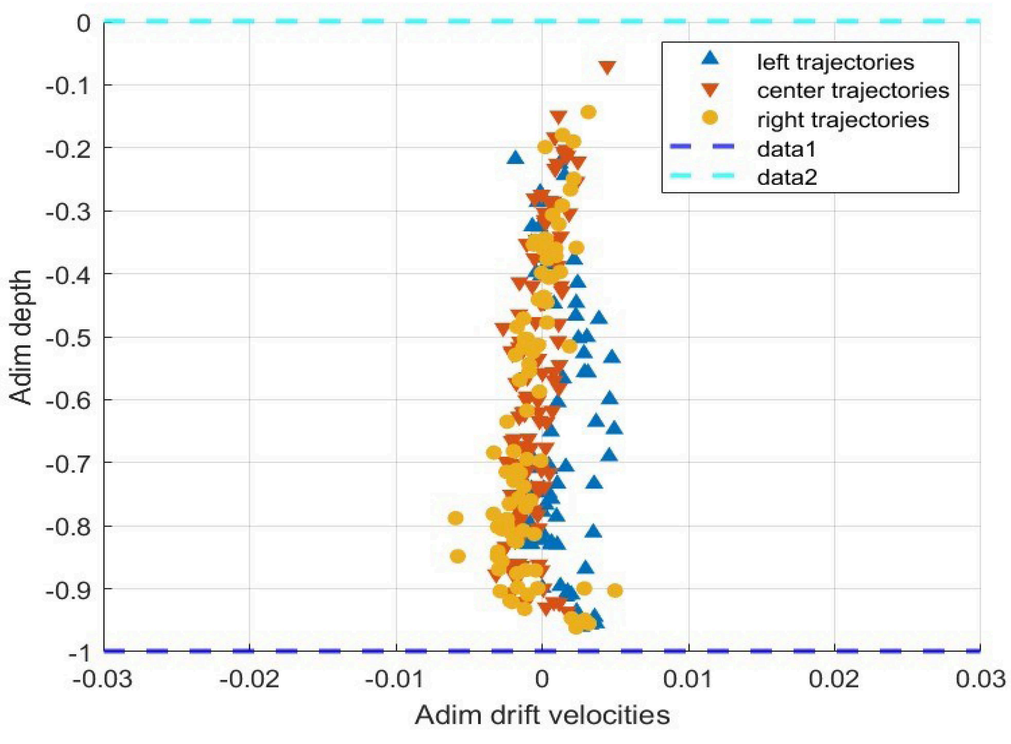

Run 1 (p_size=15, p_int=11000, threshD=8)

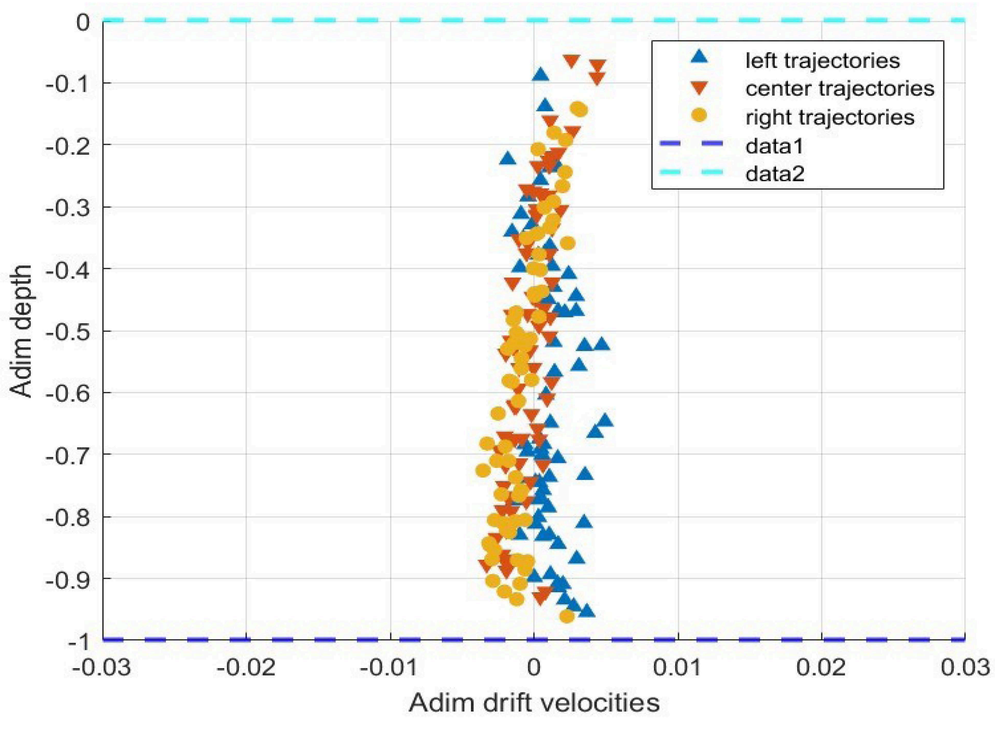

Laboratory Experiments - Processing Workflow

❑ Particles Intensity

- **particle size= 13**

✓ **particle intensity = 9000 and 11000**

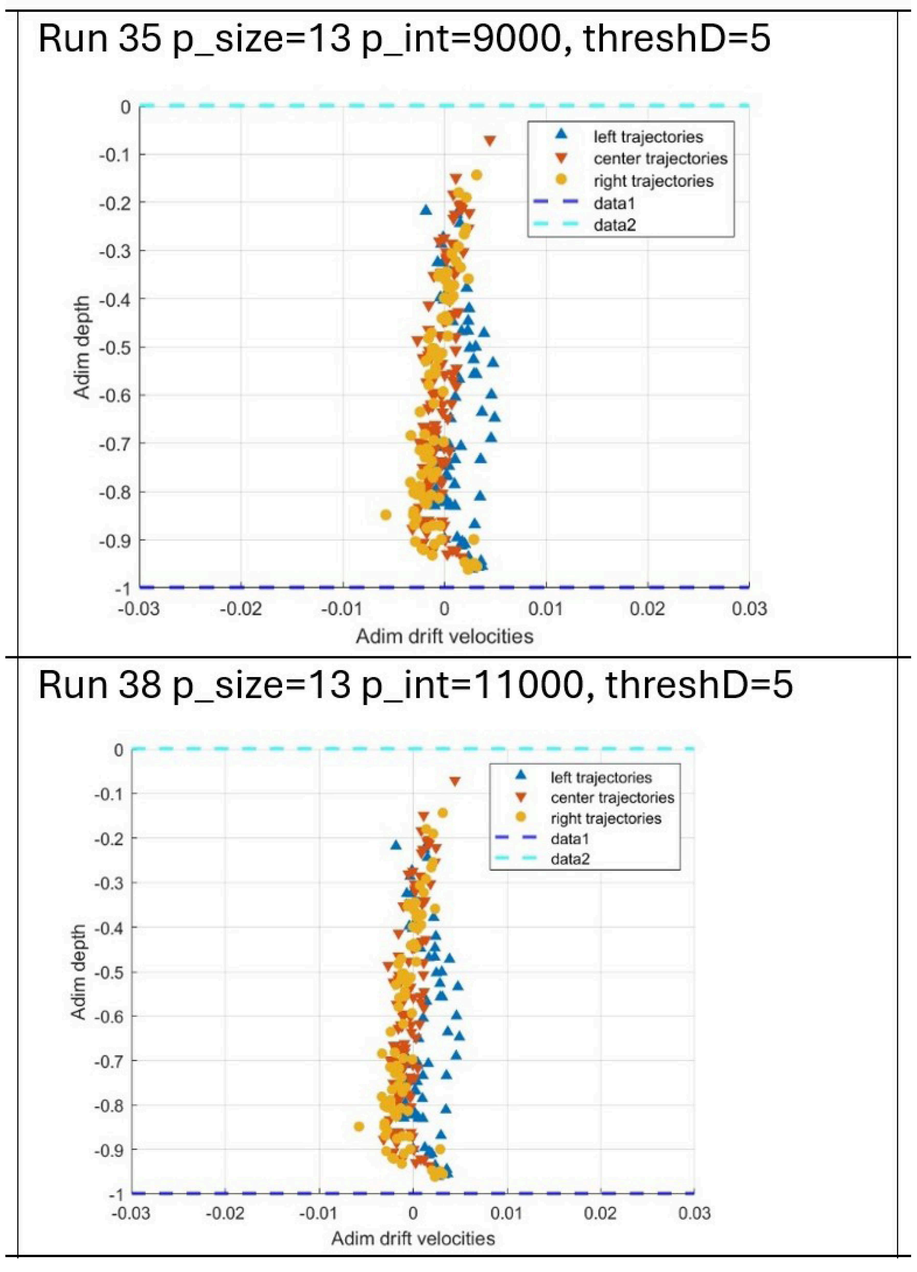

- **particle size= 15**

✓ **particle intensity = 9000, 11000**

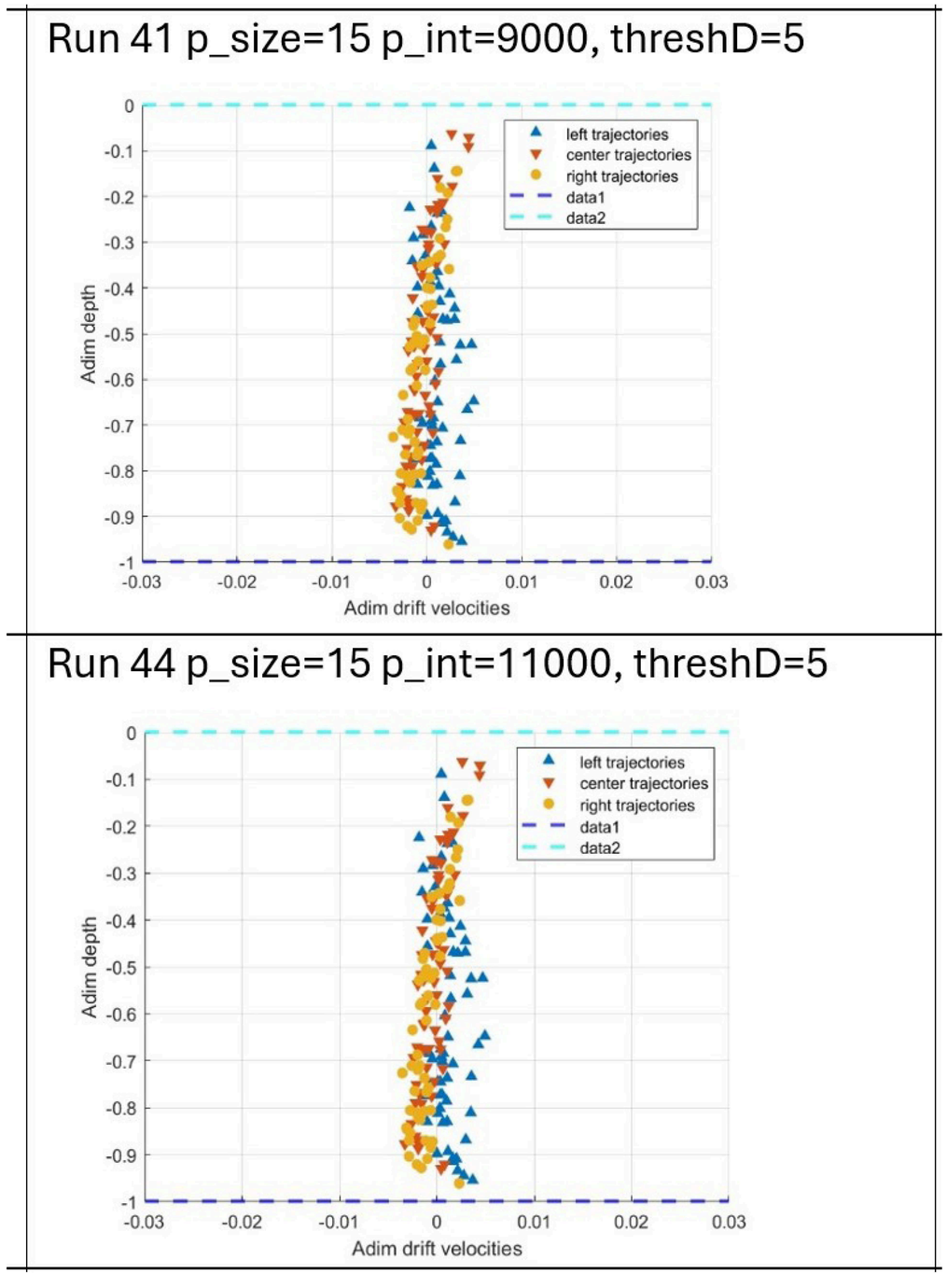

Laboratory Experiments

Find the optimal configuration

p_size=13 p_int=9000, threshD=8

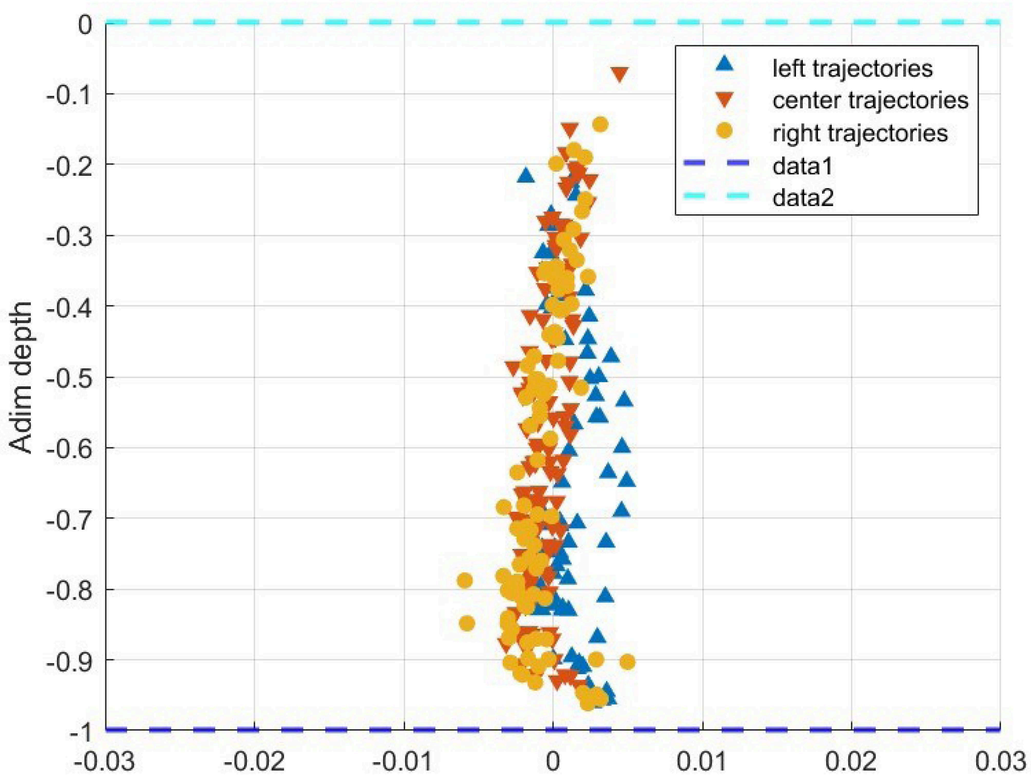

p_size=13 p_int=11000, threshD=8

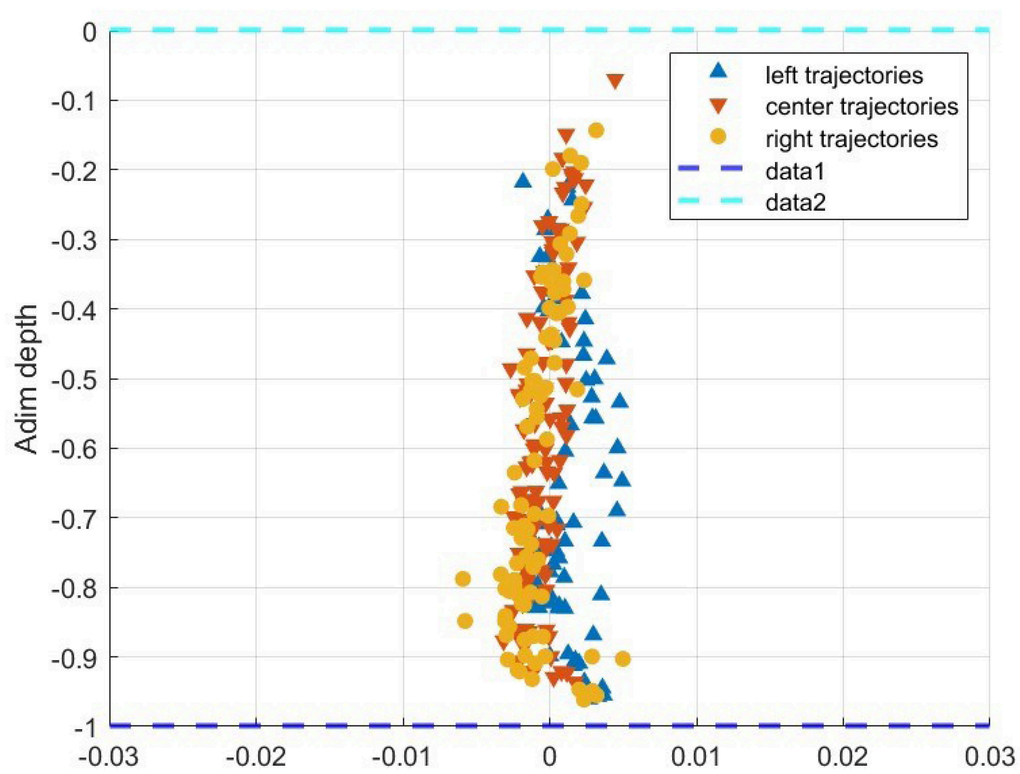

p_size=15 p_int=9000, threshD=8

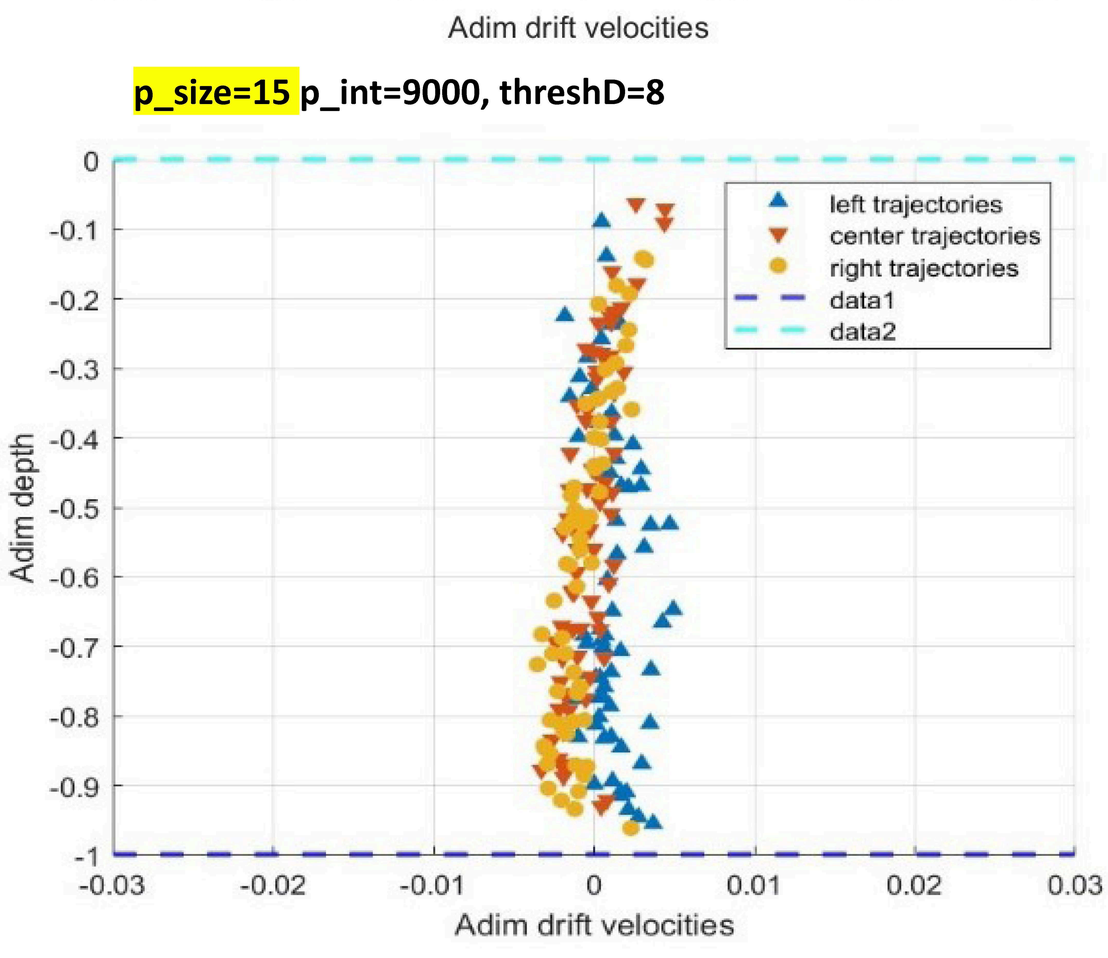

p_size=15 p_int=11000, threshD=8

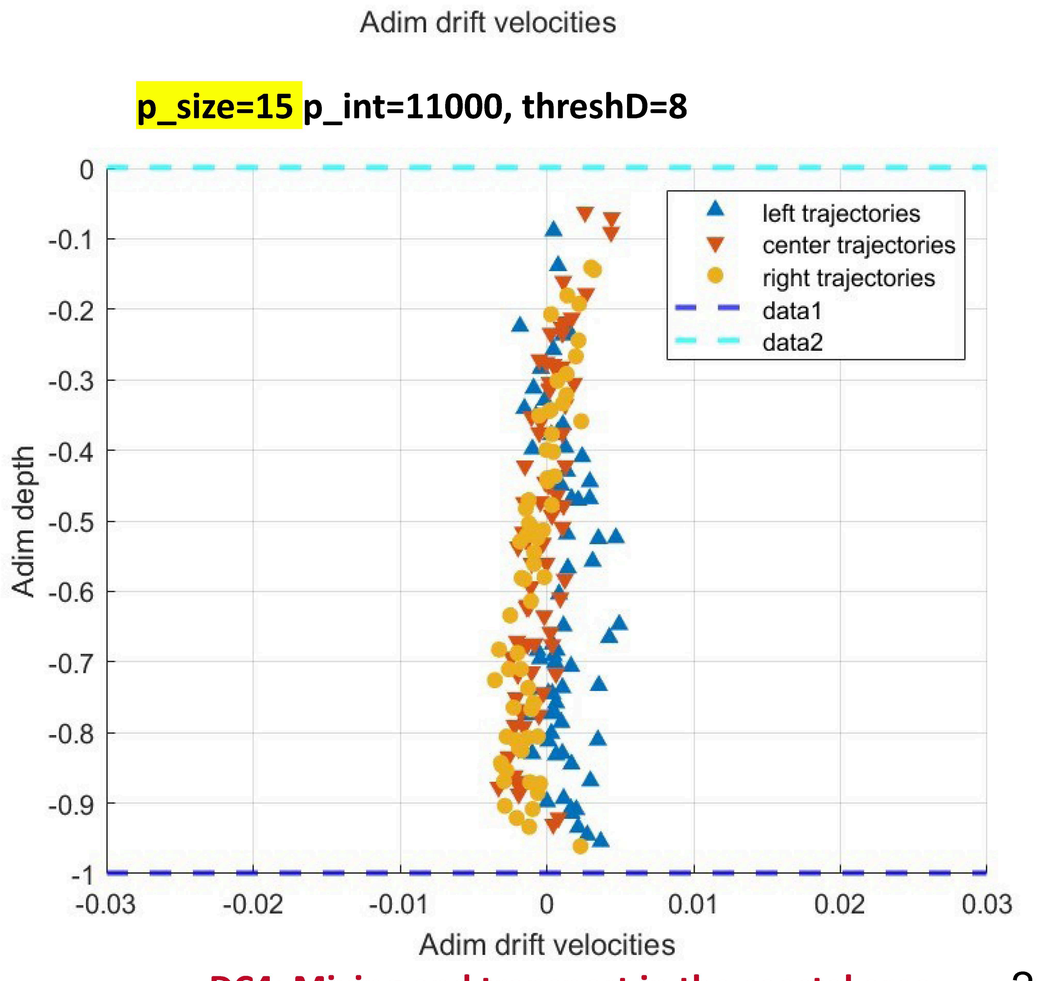

Laboratory Experiments - Processing Workflow

✓ **Compare best configurations to find the optimal**

Polynomial _ deg = 2

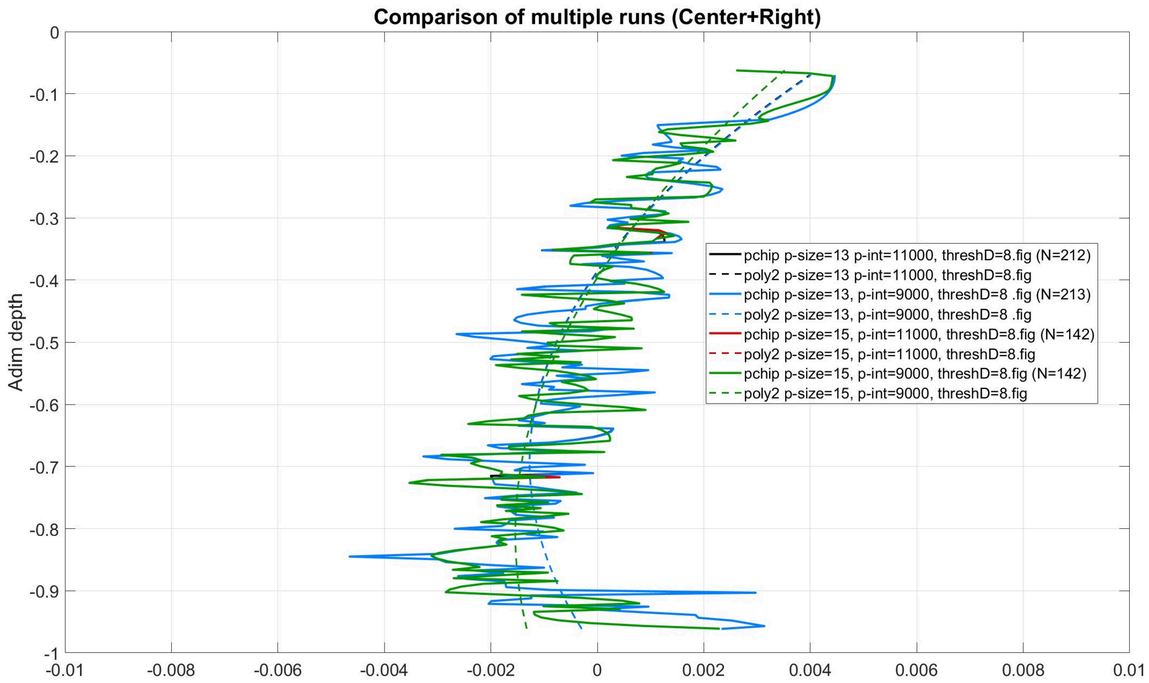

Polynomial _ deg = 3

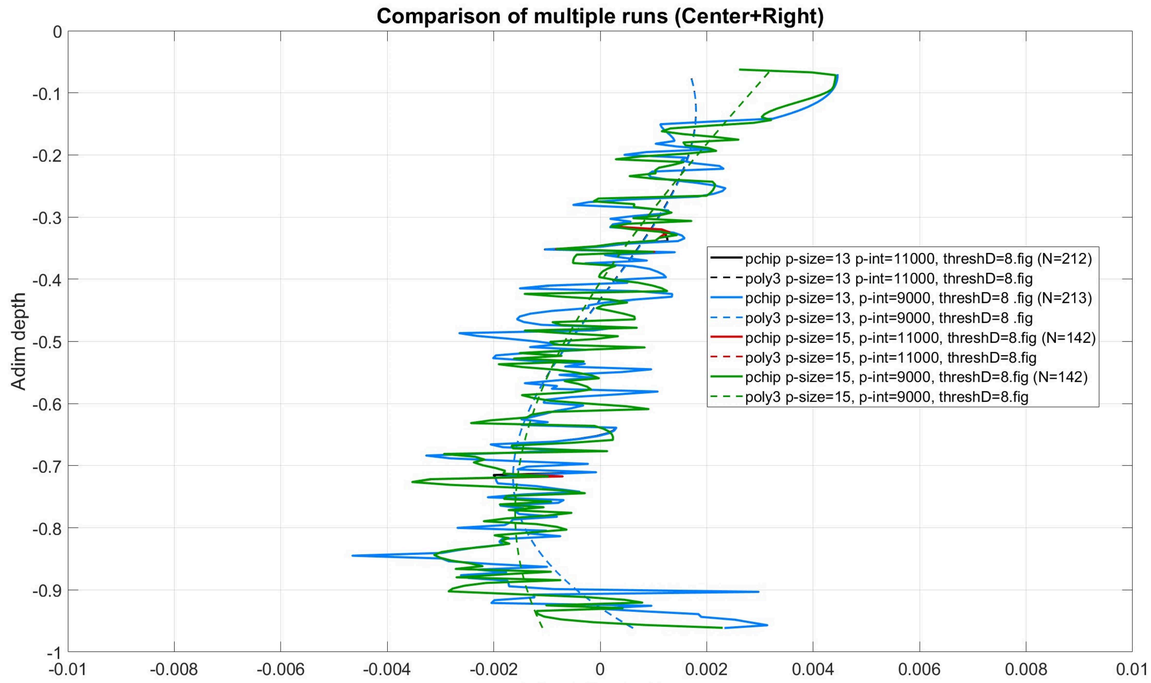

Grue and J. Kolaas 2017

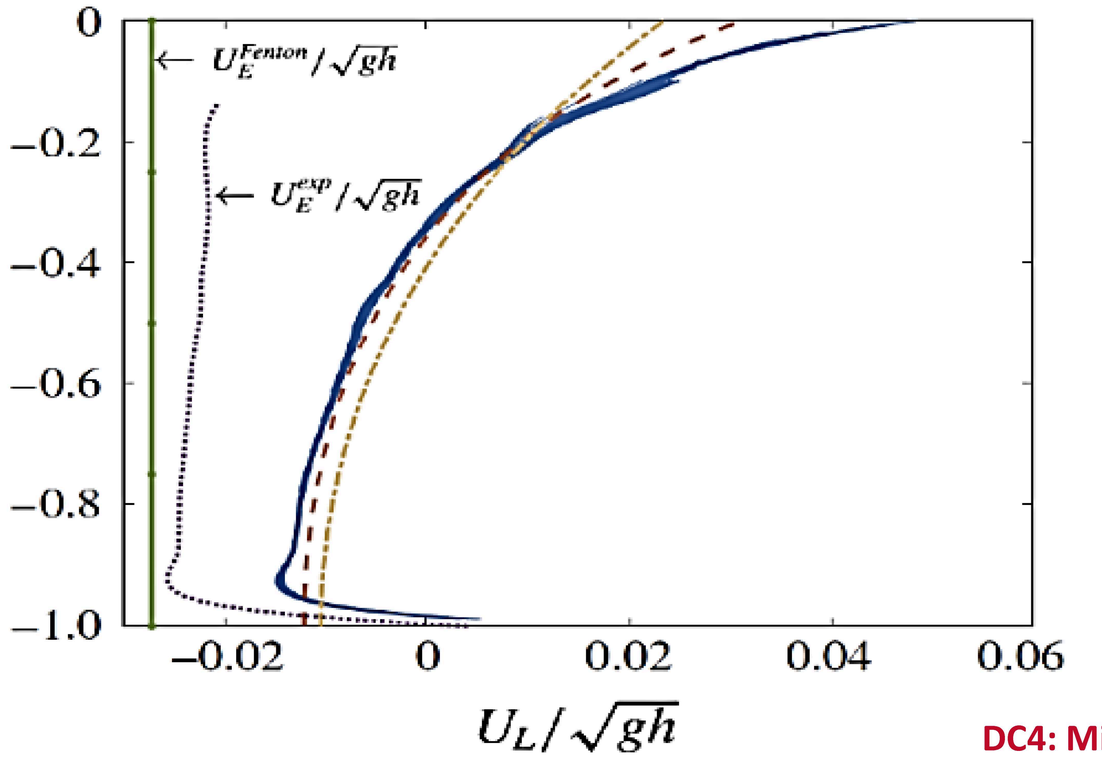

Laboratory Experiments - Processing Workflow

❑ Lagrangian Drifts

p_size=15 p_int=9000, threshD=8

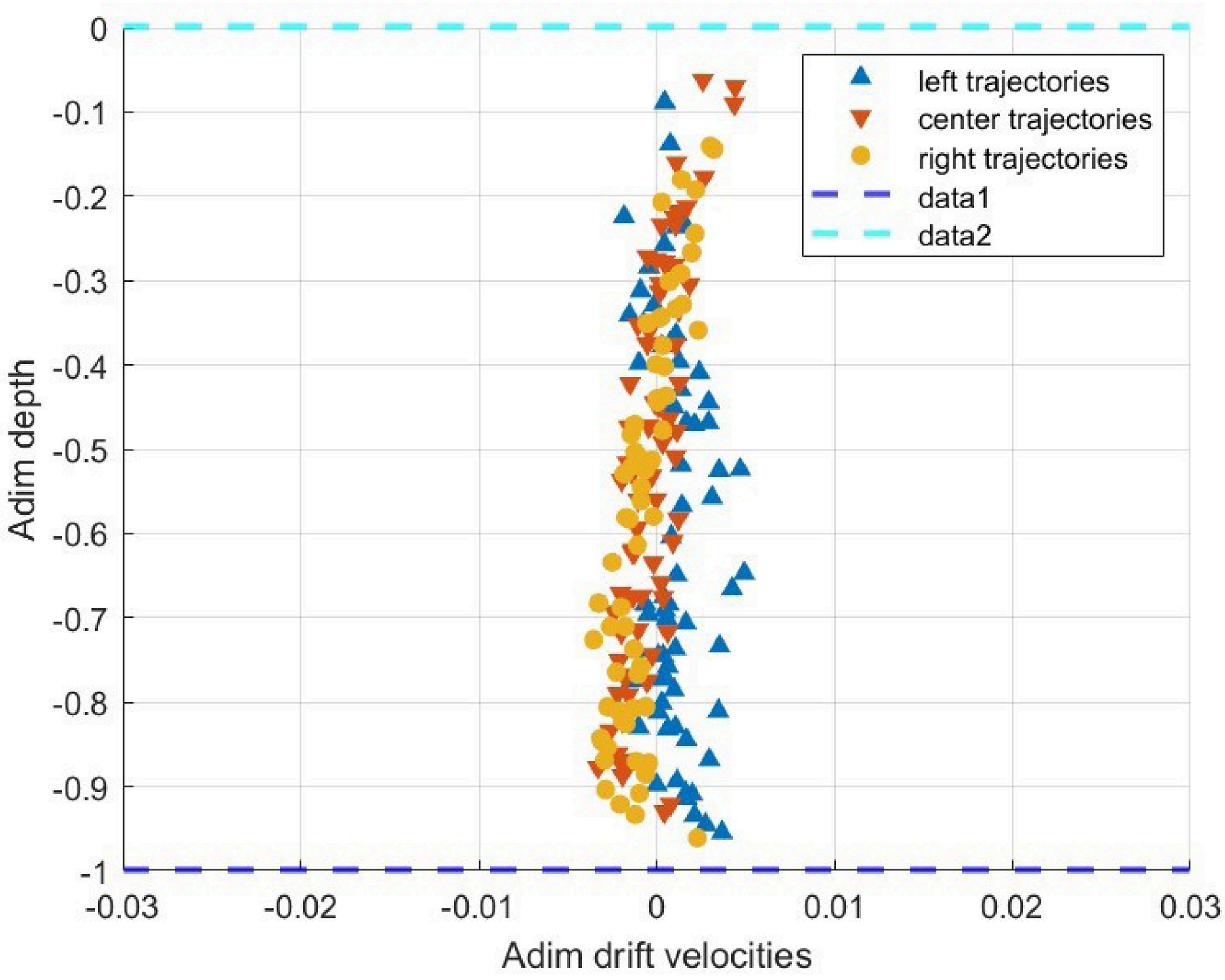

Laboratory Experiments - Processing Workflow

❑ Horizontal Velocity Profiles

p_size=15 p_int=9000, threshD=8

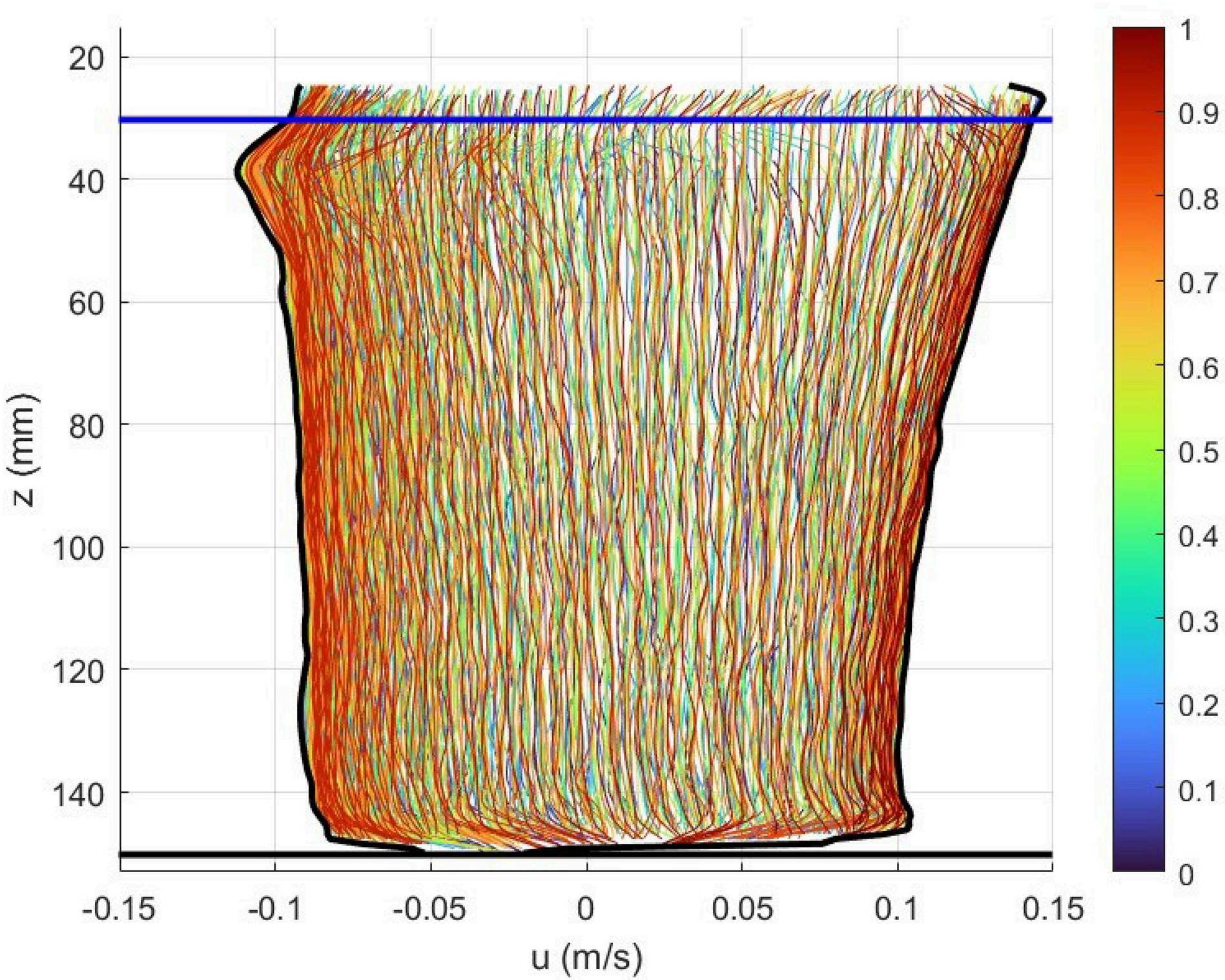

Laboratory Experiments - Results

- Such these results contribute to our understanding of how tracers, pollutants, and sediments behave in marine environments.
- Analysis of trajectories and drift velocities; undrestanding wave-driven transport

Future work

- Investigate all blocks and bichromatic wave interactions.
- Validate MATLAB particle tracking code against benchmark wave cases.

UNIVERSITY OF TWENTE. Nelen & Schuurmans UCLouvain

SEDIMARE
Sediment Transport and Morphodynamics in Marine and Coastal Waters with Engineering Solutions

SEDIMARE 2nd Workshop

EXPERIMENTAL AND NUMERICAL INVESTIGATION OF OVERTOPPING-INDUCED BREACHING IN NON-COHESIVE DAMS

Siyuan Wang

s.wang-4@utwente.nl

siyuan.wang@uclouvain.be

Supervised by:

Dr. Ir. P.C. Roos (UT)

Dr. J. J. Warmink (UT)

Prof. Dr. S. Soares-Frazão (UCLouvain)

Dr. N. D. Volp (Nelens&Schuurmans)

11 September 2025

Marie Skłodowska-Curie Actions

This project has received funding from the European Union's (EU) Horizon Europe Framework Programme (HORIZON) under Grant Agreement No 101072443 as a MSCA Doctoral Network (HORIZON-MSCA-2021-DN-01).

Overview

1. Introduction
2. Small-scale experiment
3. Numerical simulation
4. Conclusions

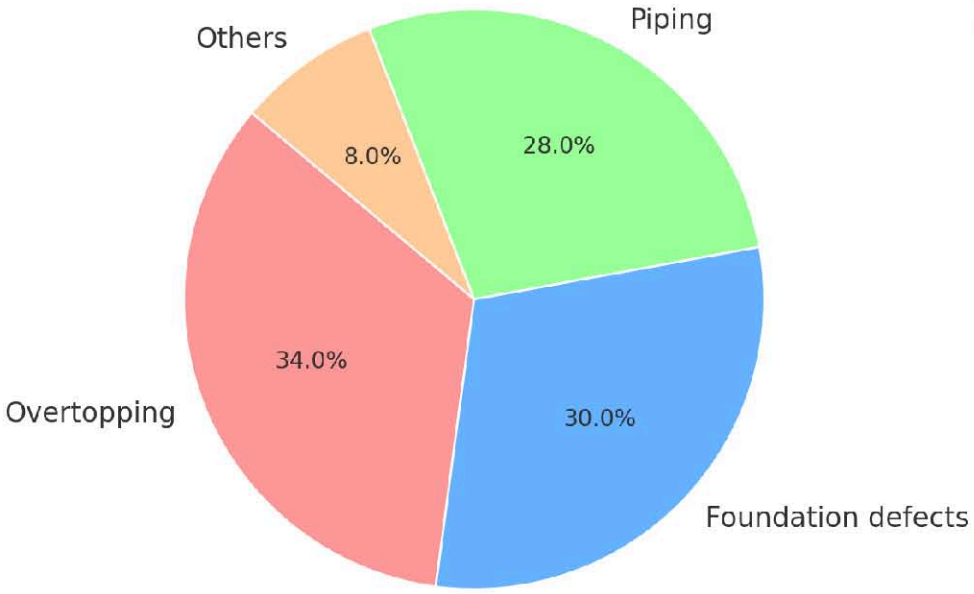
Others
Piping
8.0%
28.0%
34.0%
30.0%
Overtopping
Foundation defects

Experiment setup

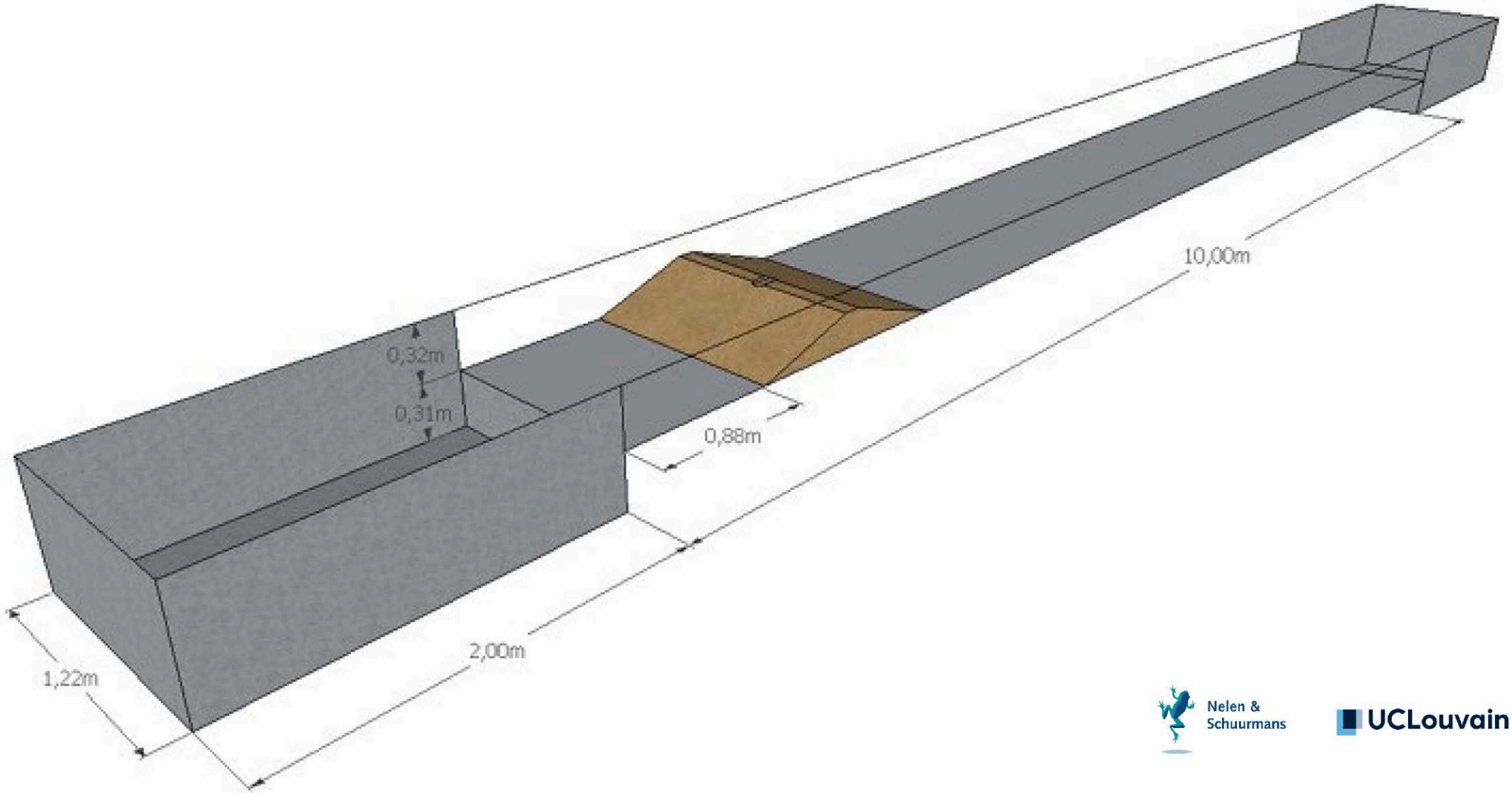

Nelen & Schuurmans UCLouvain UNIVERSITY OF TWENTE.

Experiment setup

Dimensions of dam [cm]

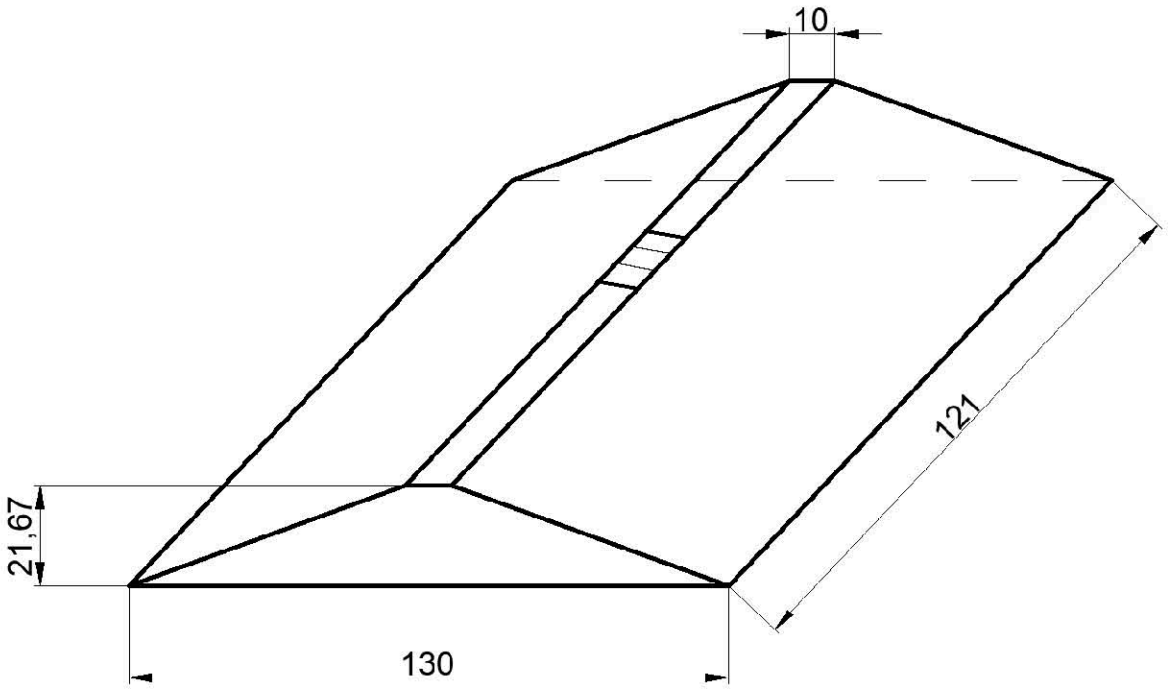

Dimensions of pilot channel [cm]

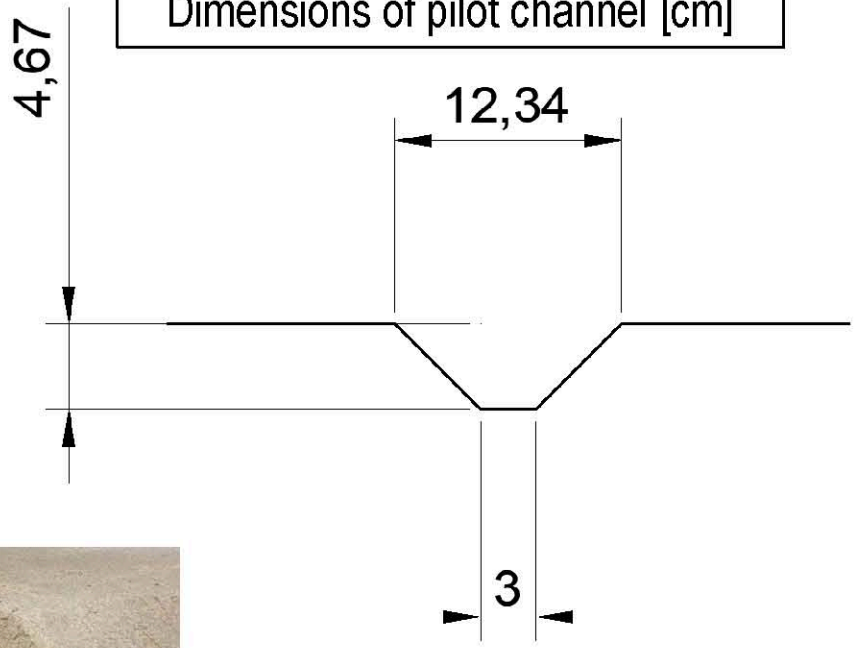

Soil properties and hydraulic conditions

Grain size: Fine sand (d_{50} = **0.31 mm**)

Medium sand (d_{50} = **0.61 mm**)

Soil moisture: **14.5%** for fine sand

15.5% for Medium sand

Overtopping: Constant inflow **4 l/s**

Measurement techniques

Instrumentation:
- Photogrammetry
- Ultrasonic sensor

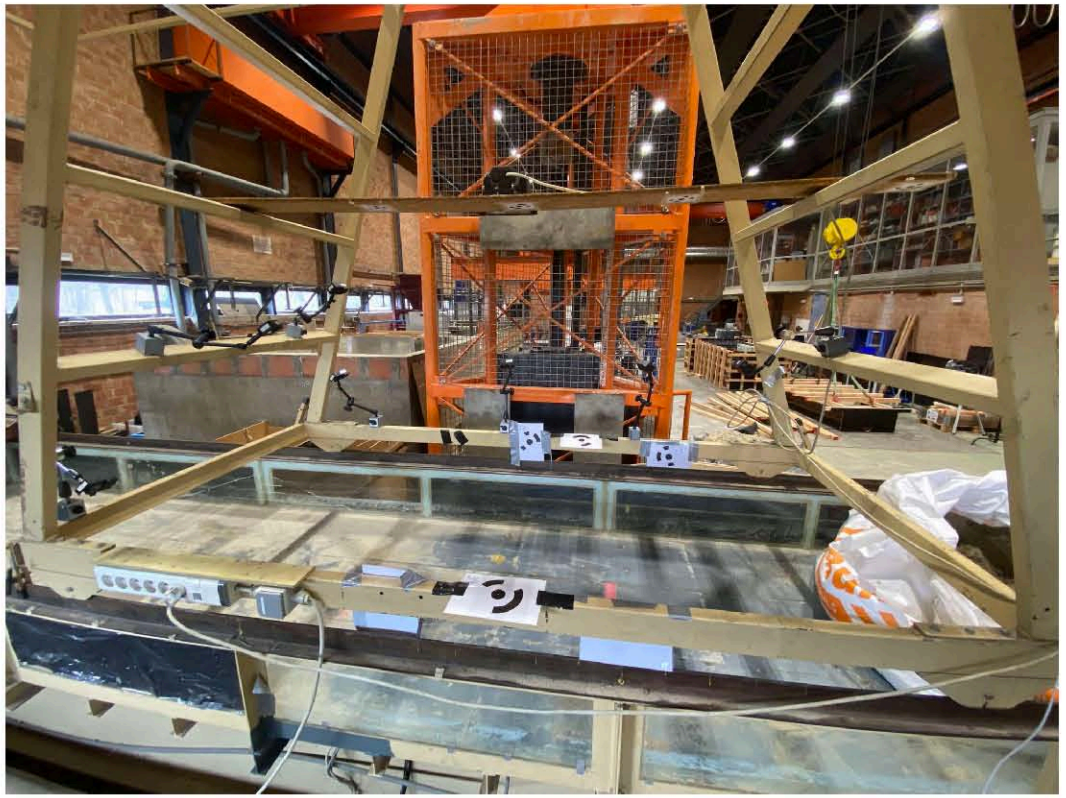

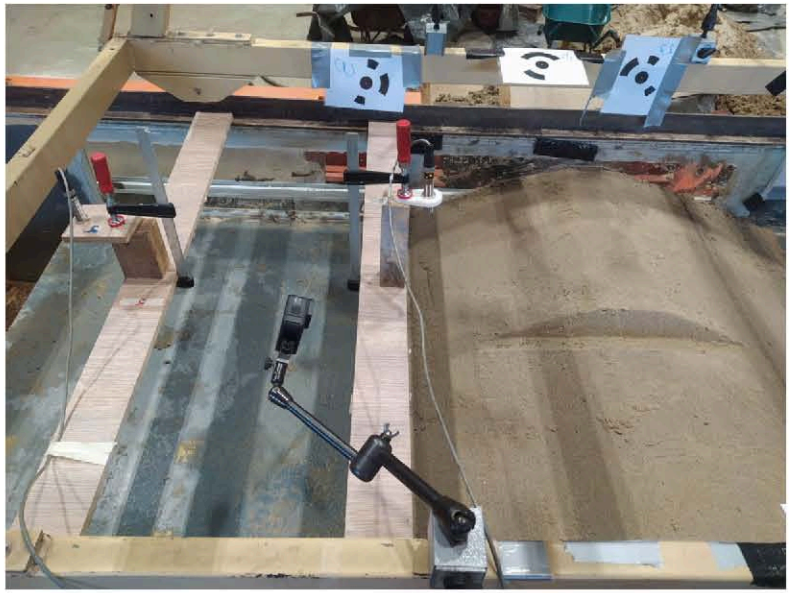

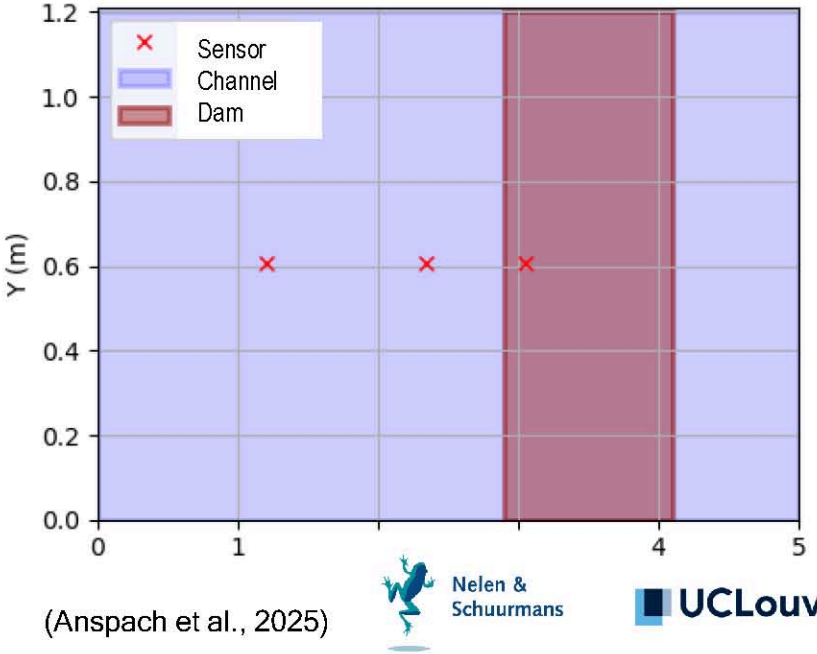

(Anspach et al., 2025)

Nelen & Schuurmans

UCLouvain

UNIVERSITY OF TWENTE.

Measurement techniques - Photogrammetry

- Image capture by cameras
- 3D dense cloud reconstruction
- Digital elevation models (DEMs)

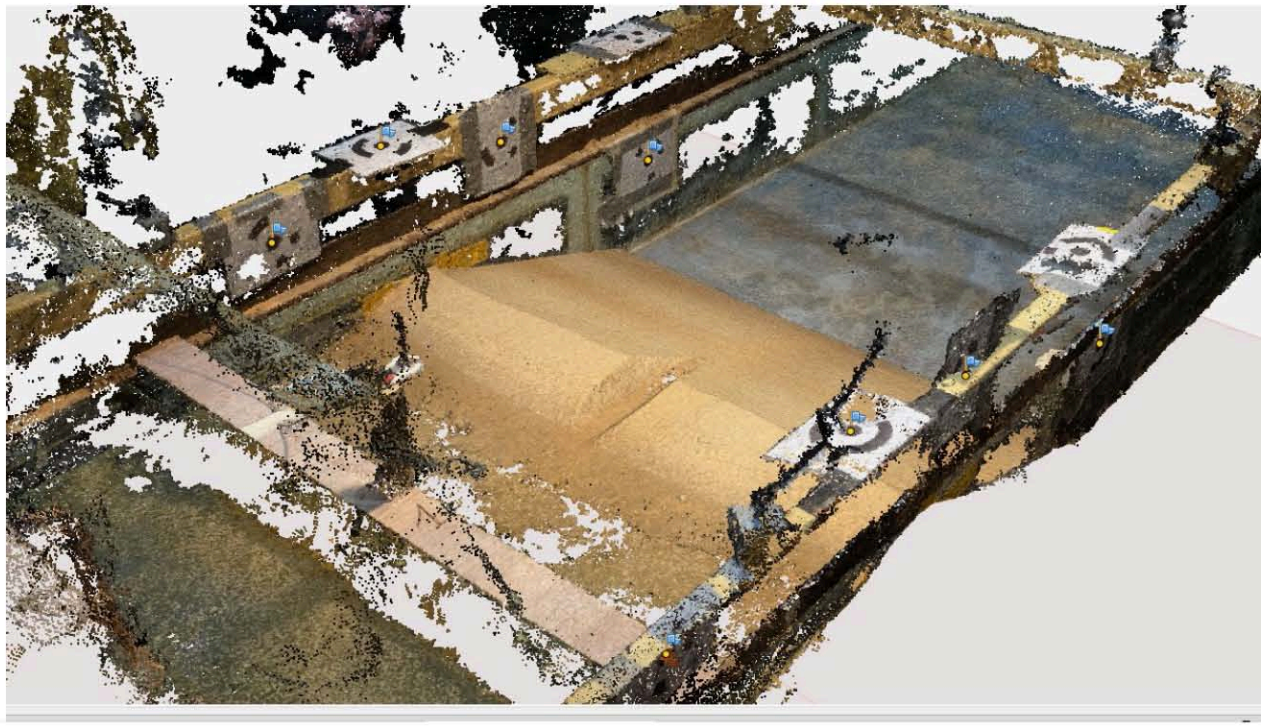

(Anspach et al., 2025)

Measurement techniques - Photogrammetry

Digital elevation models (DEMs) for fine sand (d_{50} = 0.31 mm)

T0 T60 T90 T130

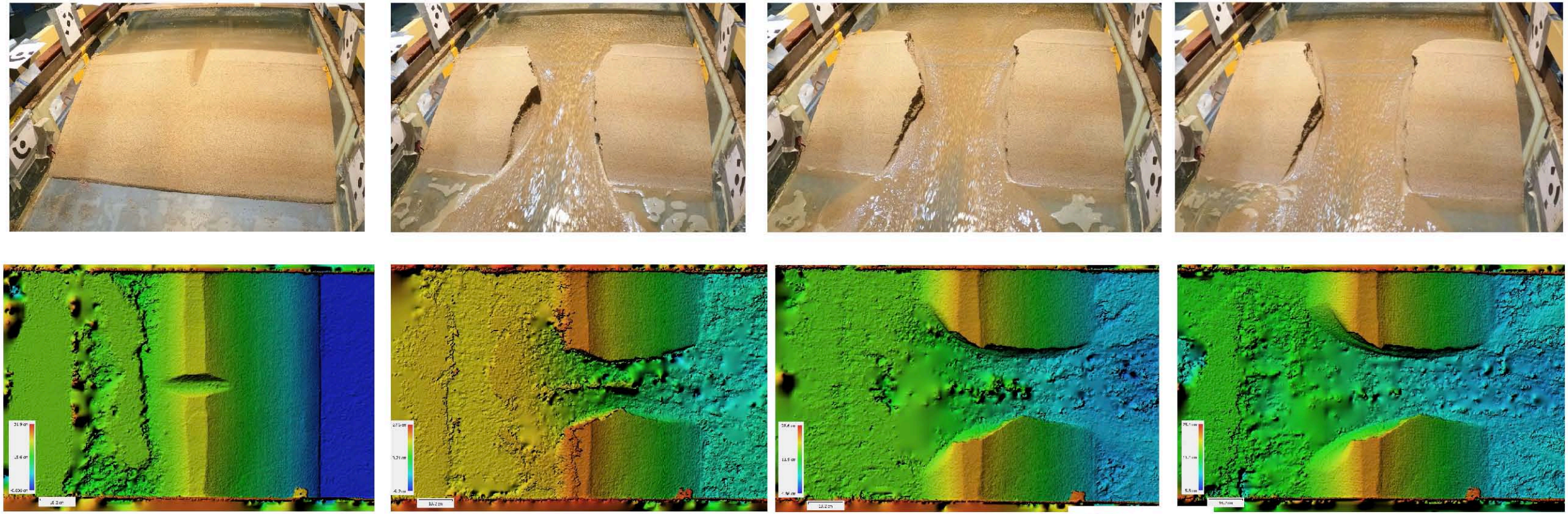

(Anspach et al., 2025)

Nelen & Schuurmans UCLouvain UNIVERSITY OF TWENTE.

Measurement techniques - Ultrasonic sensor

$$Q_{\text{out}} = Q_{in} - 1000.A_{basin}.\frac{\text{dz}}{\text{dt}}$$

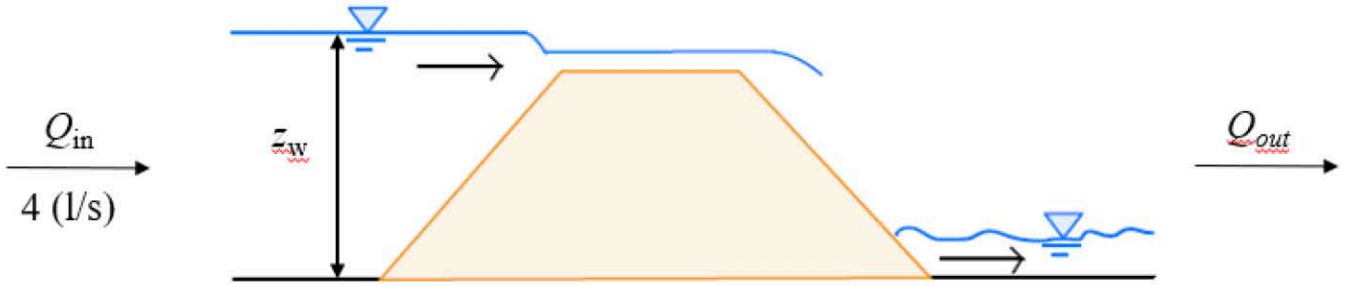

Q_{in} [l/s]

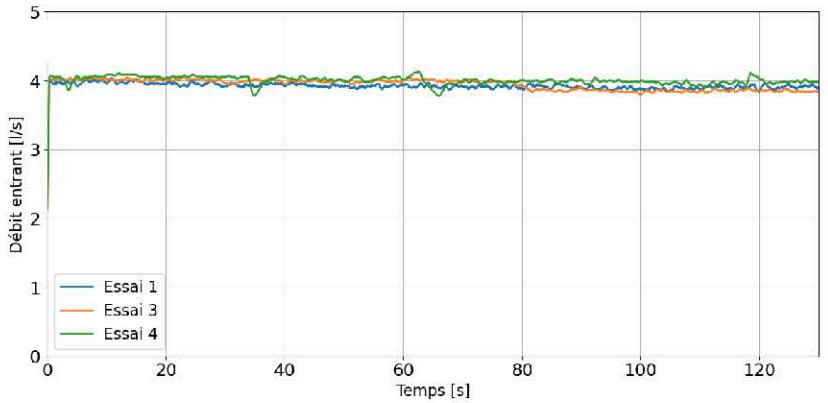

Q_{out}[l/s]

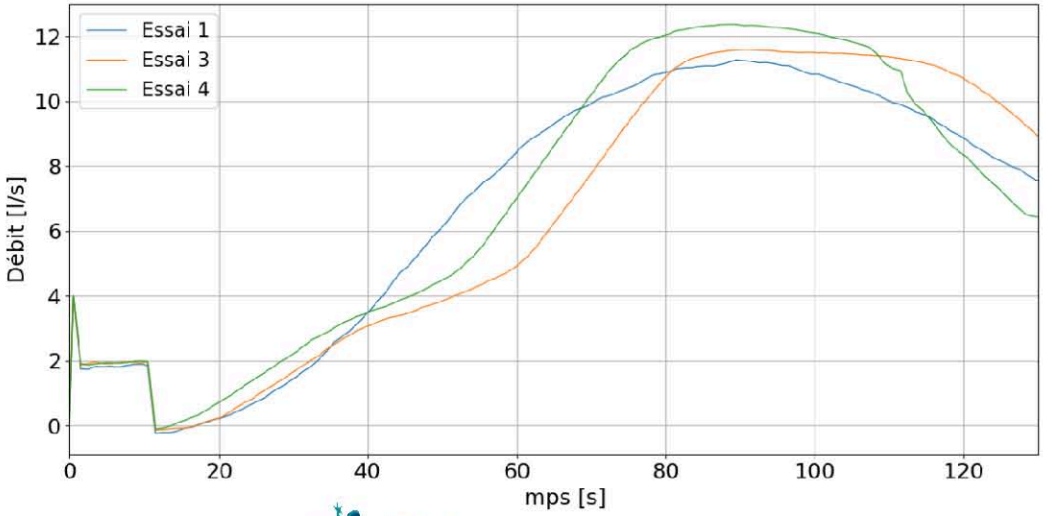

(Anspach et al., 2025)

Nelen & Schuurmans | UCLouvain | UNIVERSITY OF TWENTE.

Overtopping dam breach test- fine sand

Watlab

Governing Equations: Shallow-Water-Exner equations

Continuity equation

$$\frac{\partial h}{\partial t} + \nabla \cdot \boldsymbol{q} = 0$$

Momentum equation (2D)

$$\frac{\partial \boldsymbol{q}}{\partial t} + \nabla \cdot \left(\boldsymbol{\sigma} + \boldsymbol{\mu}_{xy}\right) = gh\left(\boldsymbol{S}_0 - \boldsymbol{S}_f\right)$$

Exner equation

$$\frac{\partial z_b}{\partial t} + \frac{1}{(1-\varepsilon_0)} \nabla \cdot \boldsymbol{q}_s = 0$$

Meyer-Peter & Müller

$$\boldsymbol{q}_s = \sqrt{g(s-1)d^3}(\tau_b - 0.047)^{1.5}$$

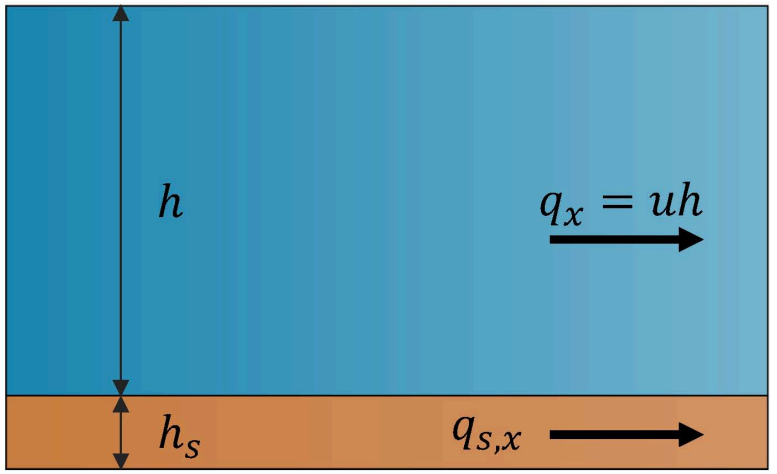

Nelen & Schuurmans UCLouvain UNIVERSITY OF TWENTE.

Watlab

Bank failure operator:

Stability angles α

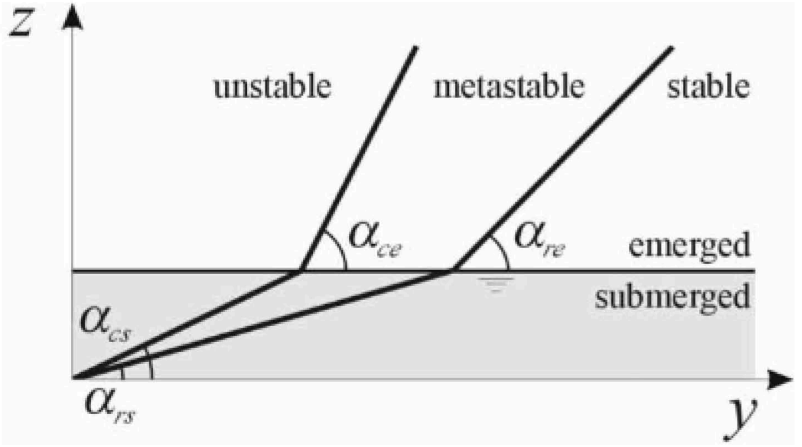

Above water	Stable: **85.0°** Unstable: **87.0°**
Under water	Stable: **30.0°** Unstable: **35.0°**

Watlab - MESCH

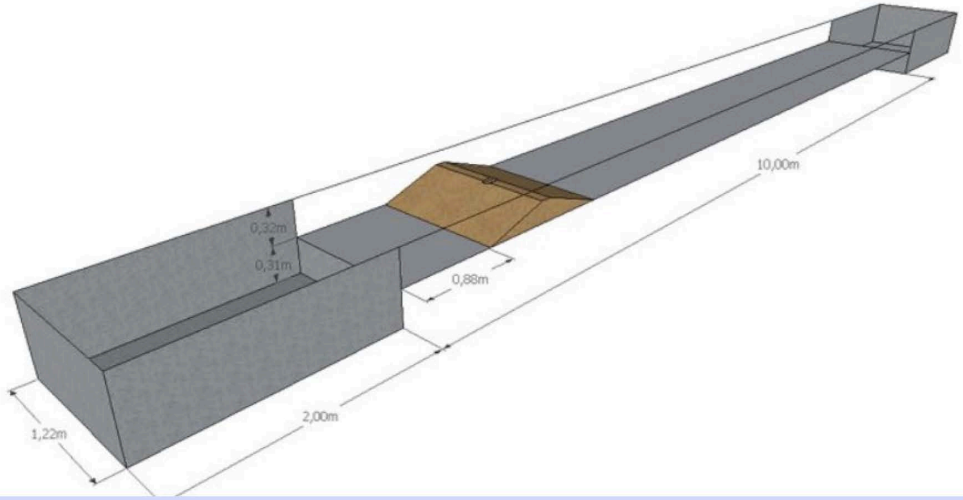

Dimensions of dam [cm]

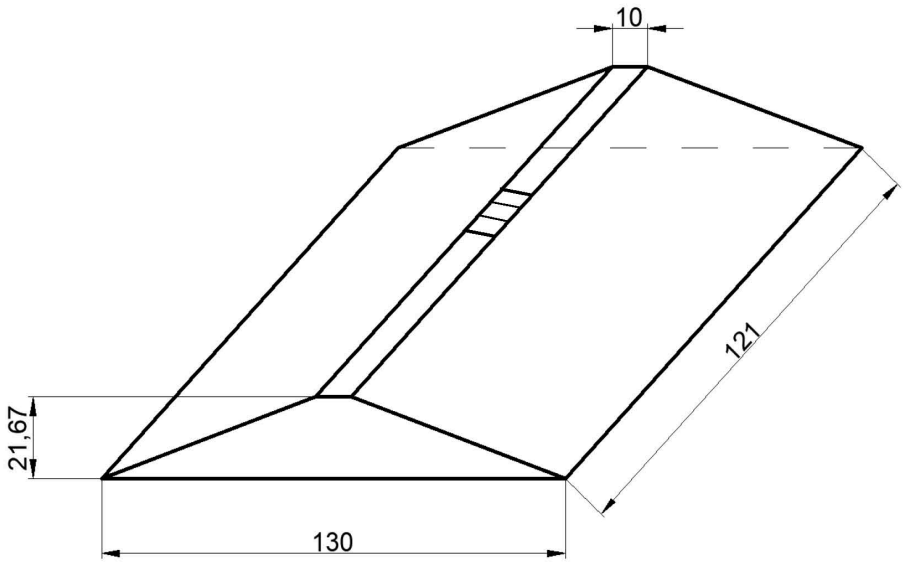

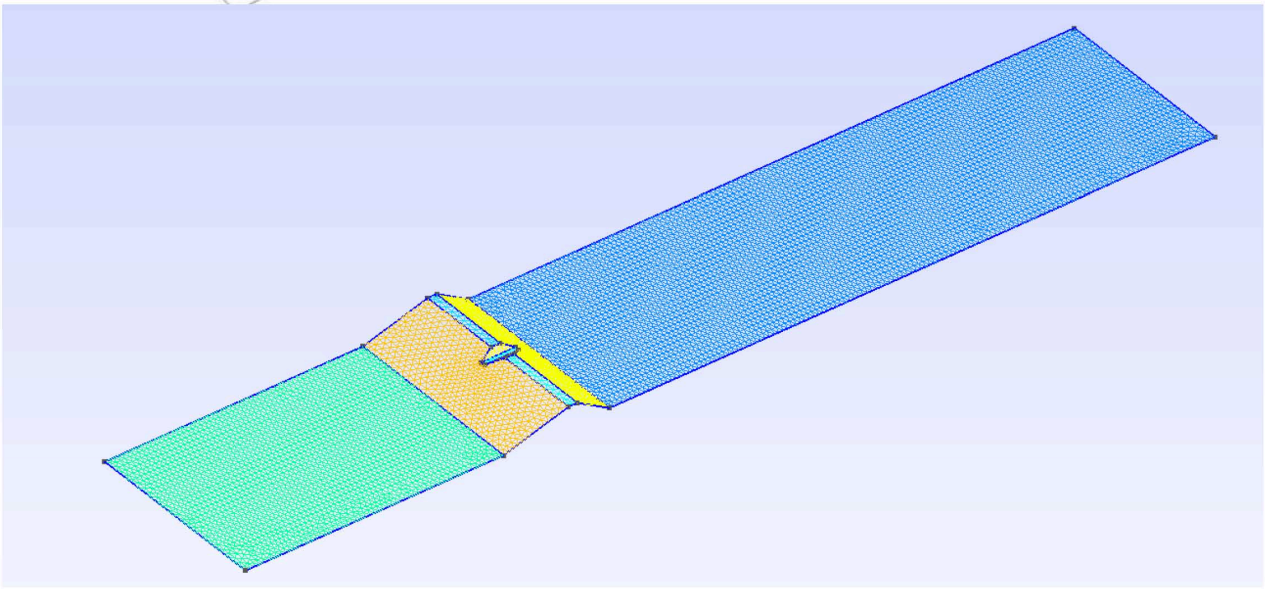

Nelen & Schuurmans UCLouvain UNIVERSITY OF TWENTE.

Watlab - MESCH

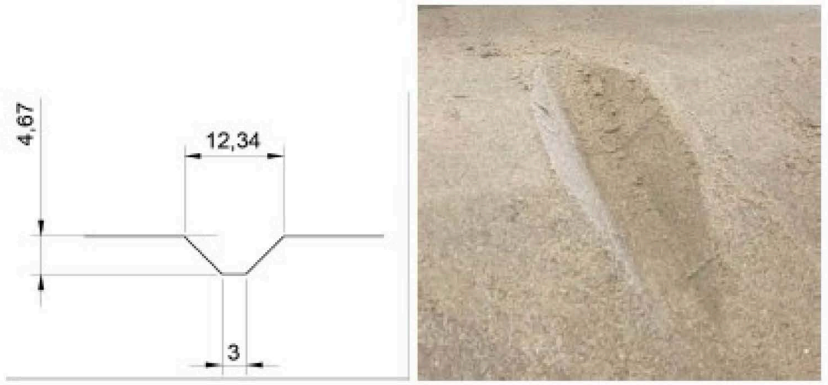

FIGURE 3.4 – Chenal pilote

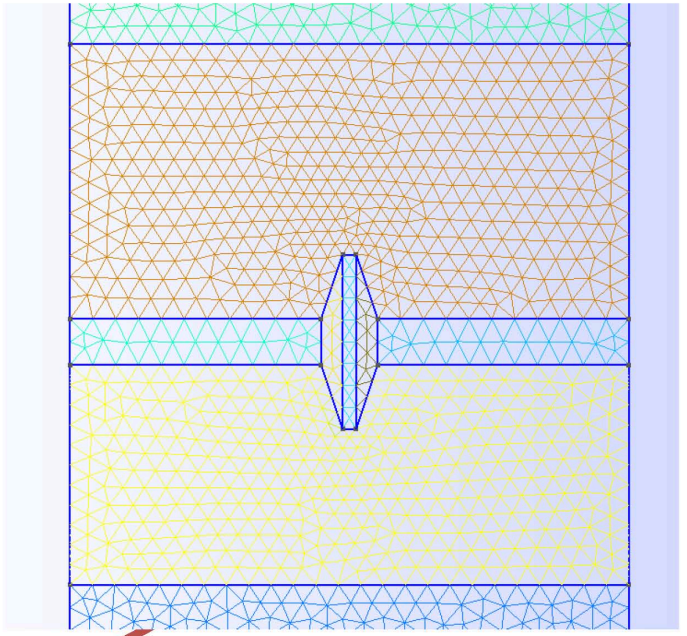

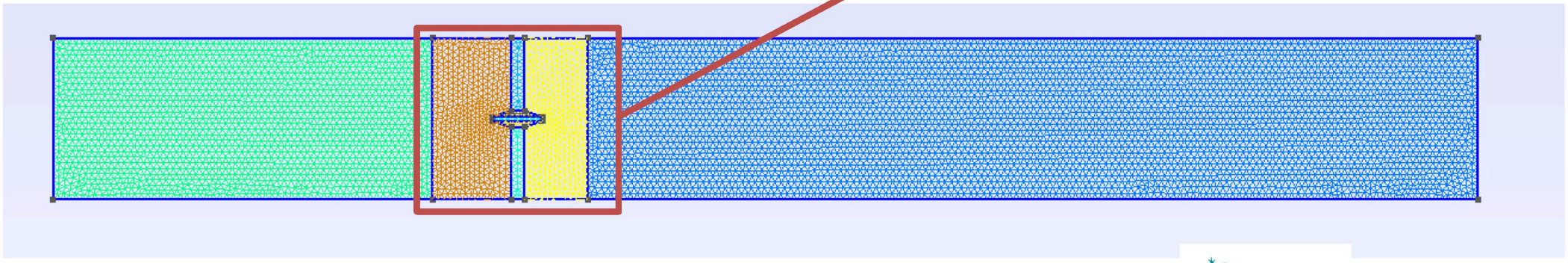

Watlab – Hydroflow model results

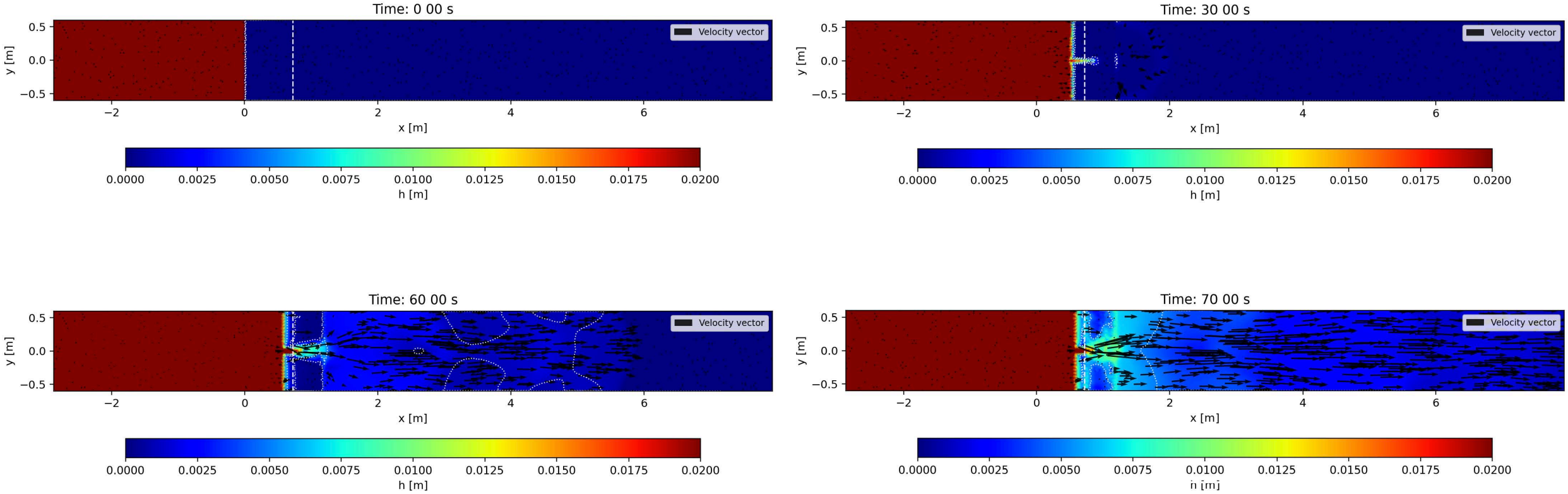

Plan view of water depth and velocity field

Watlab – Hydroflow model results

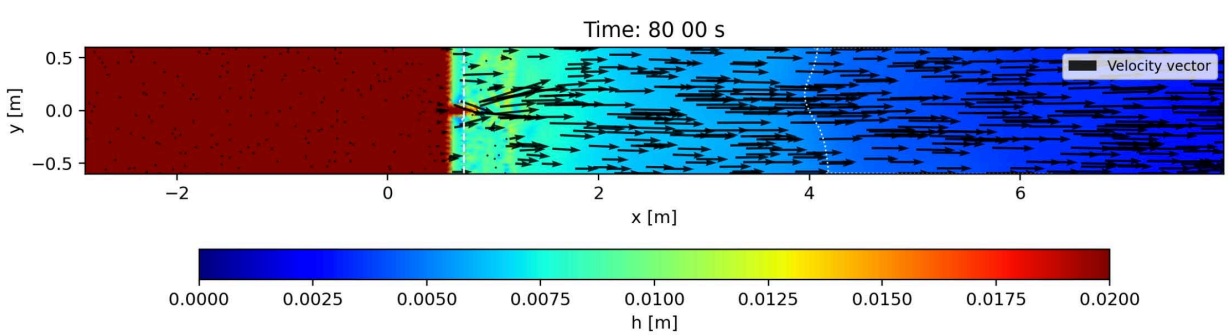

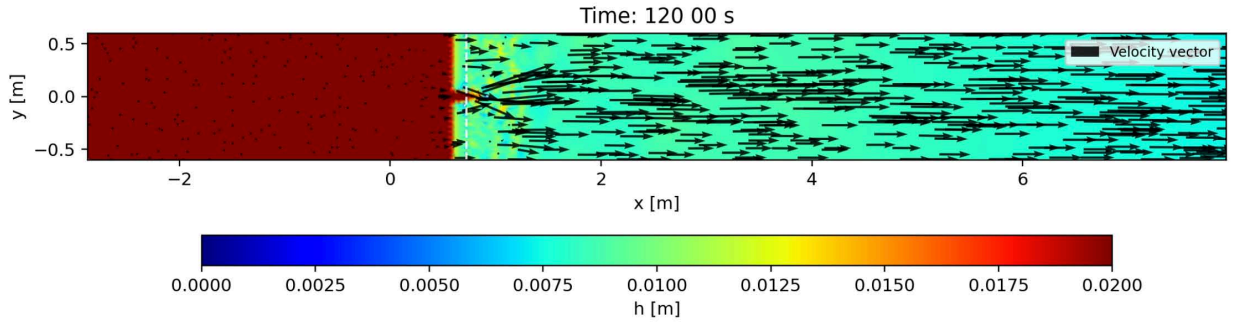

Plan view of water depth and velocity field

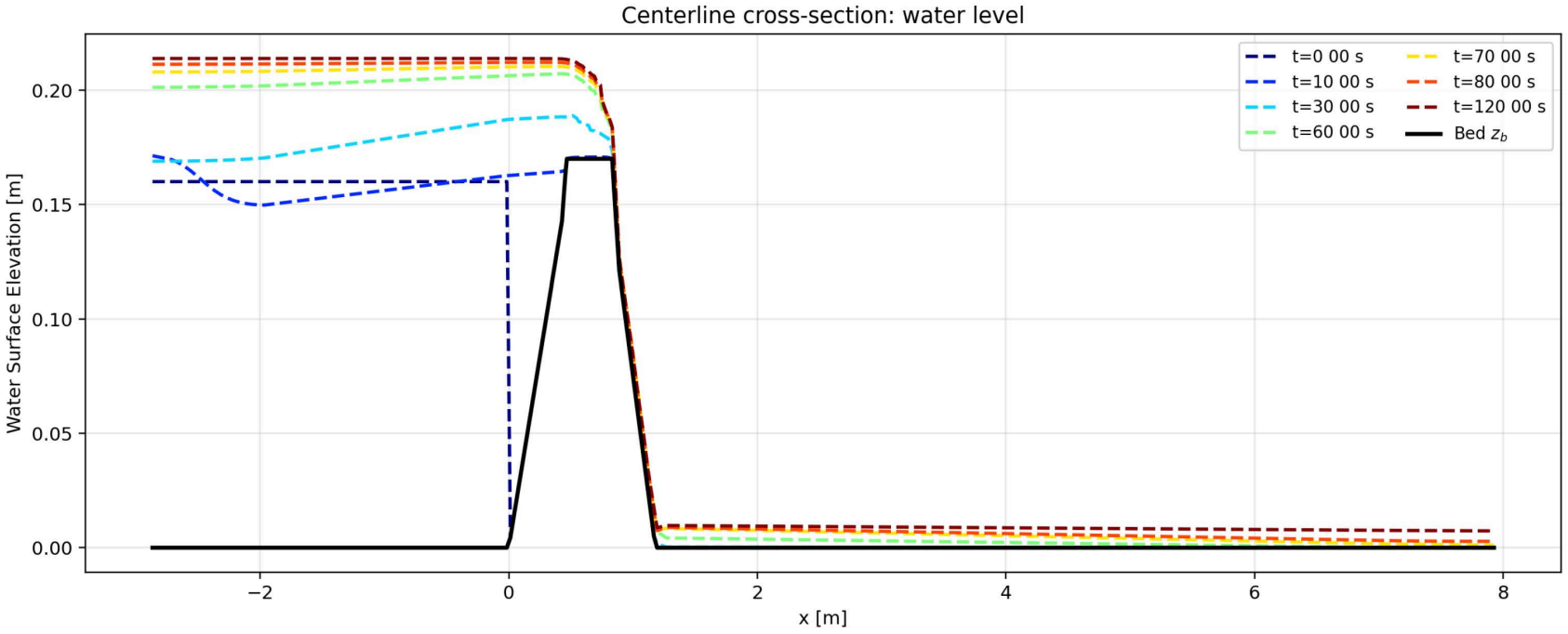

Nelen & Schuurmans

UCLouvain

UNIVERSITY OF TWENTE.

Watlab – MESCH

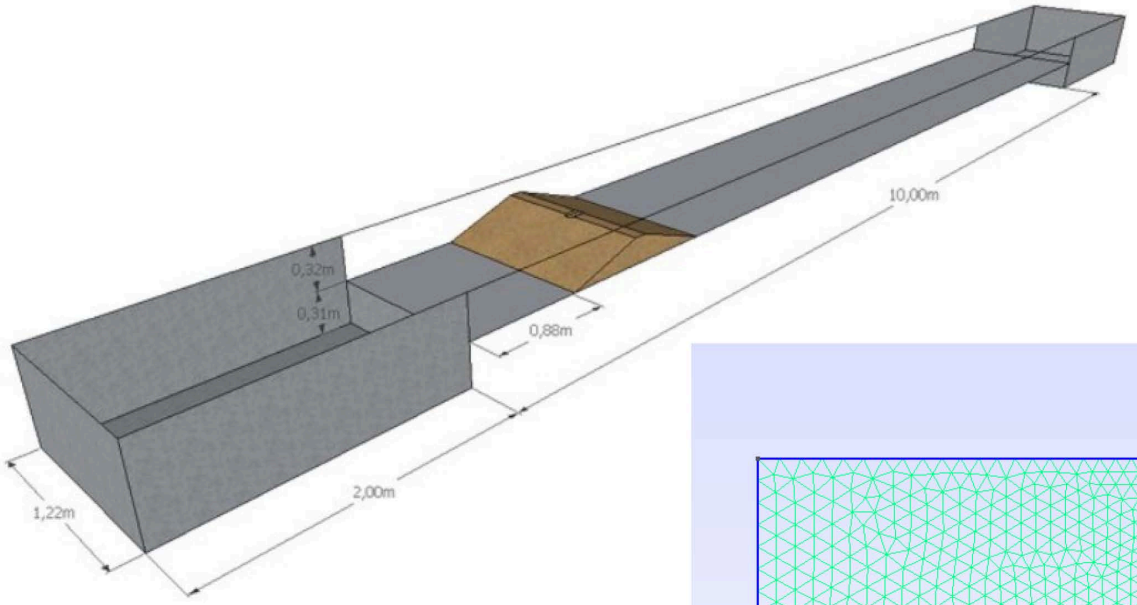

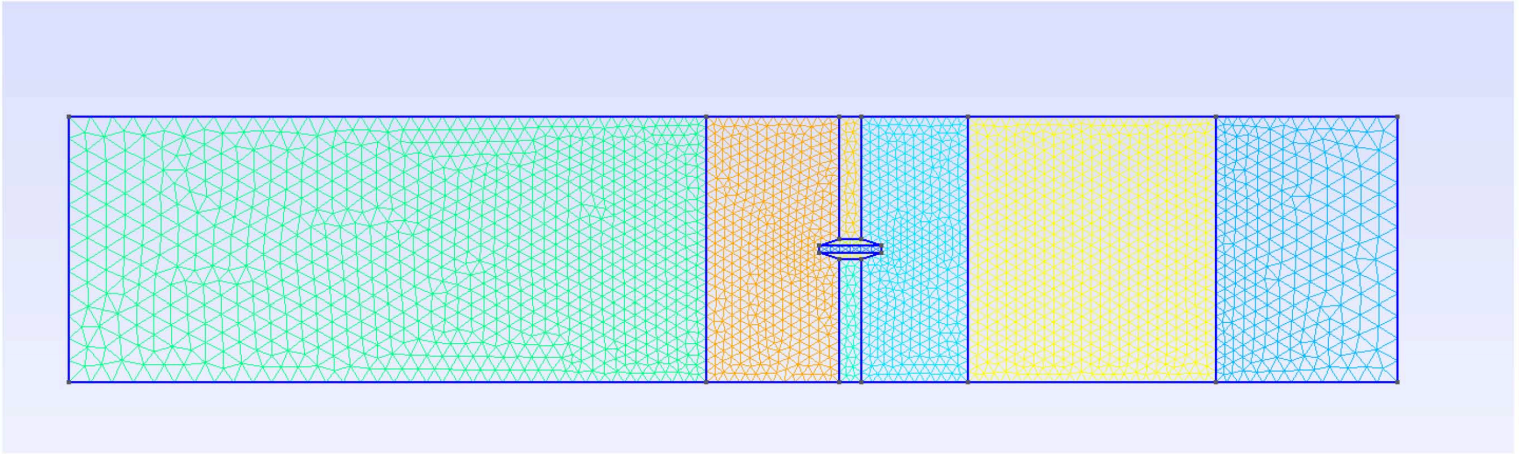

Watlab – Morphodynamic model results

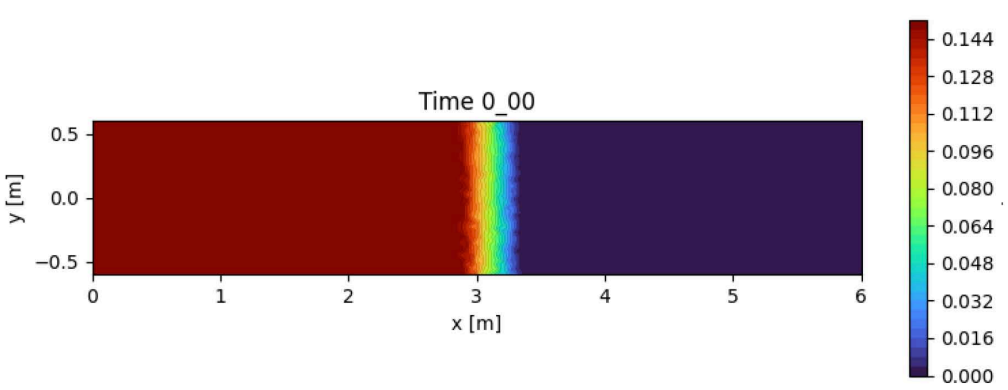

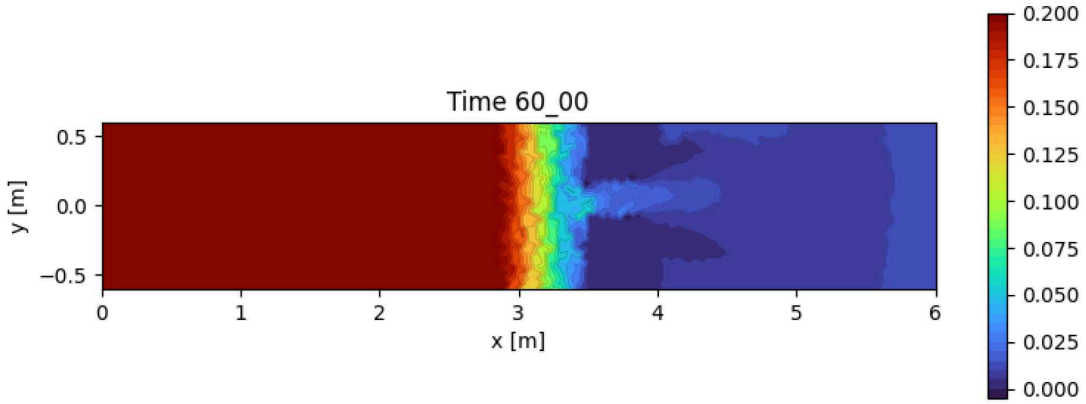

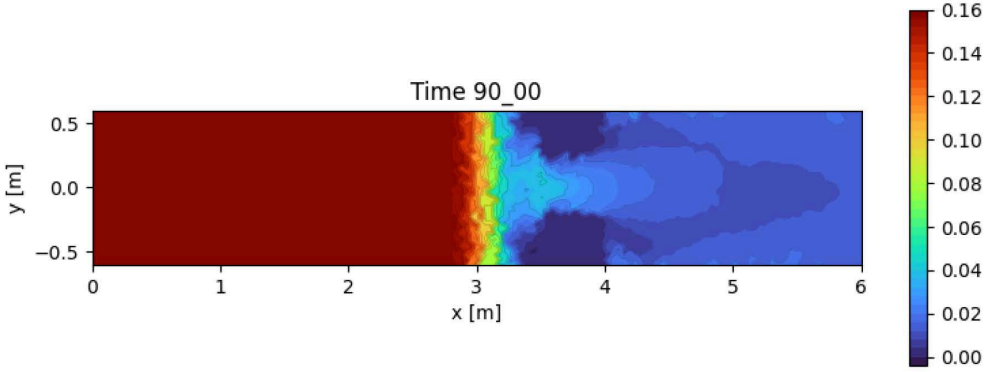

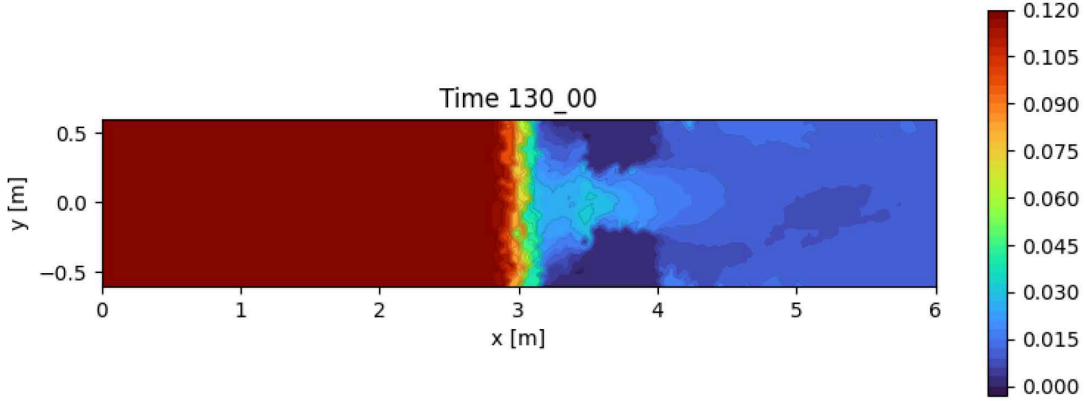

Medium sand (d_{50} = 0.61 mm)

Nelen & Schuurmans UCLouvain UNIVERSITY OF TWENTE.

Watlab – Morphodynamic model results

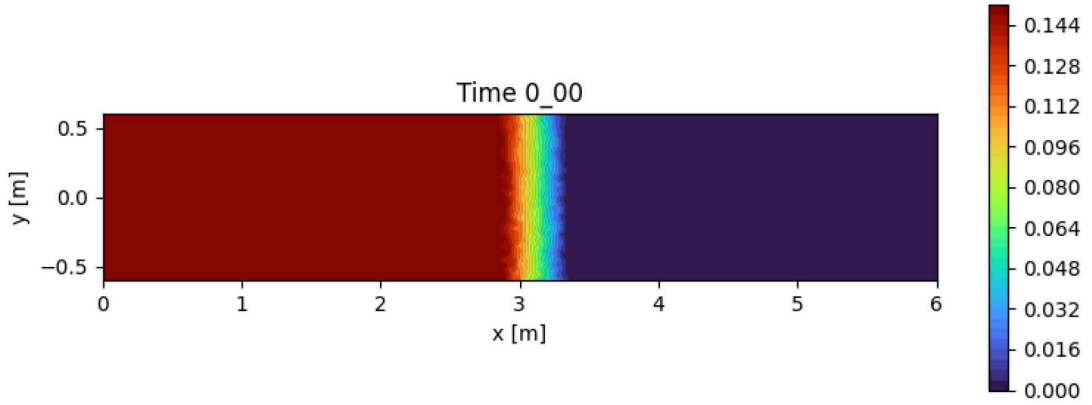

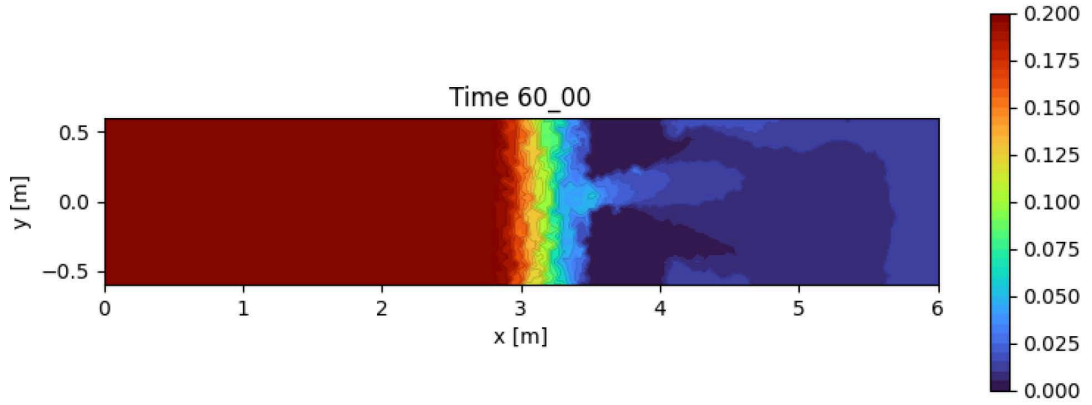

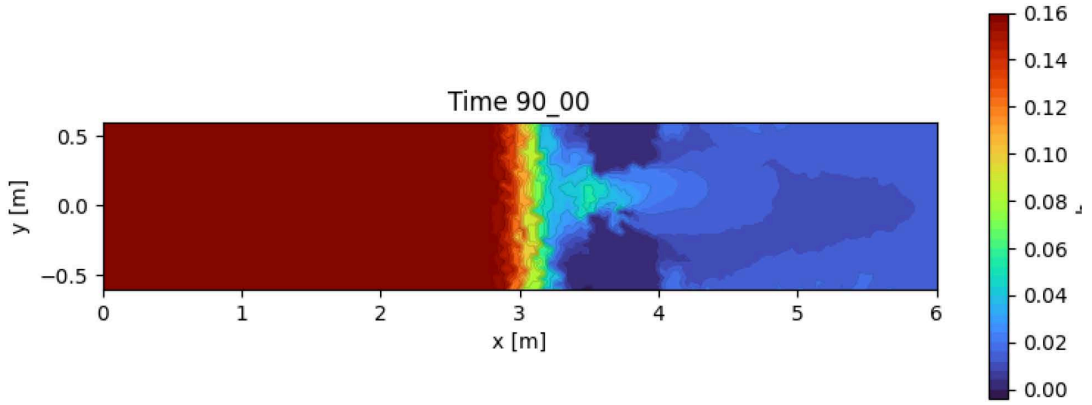

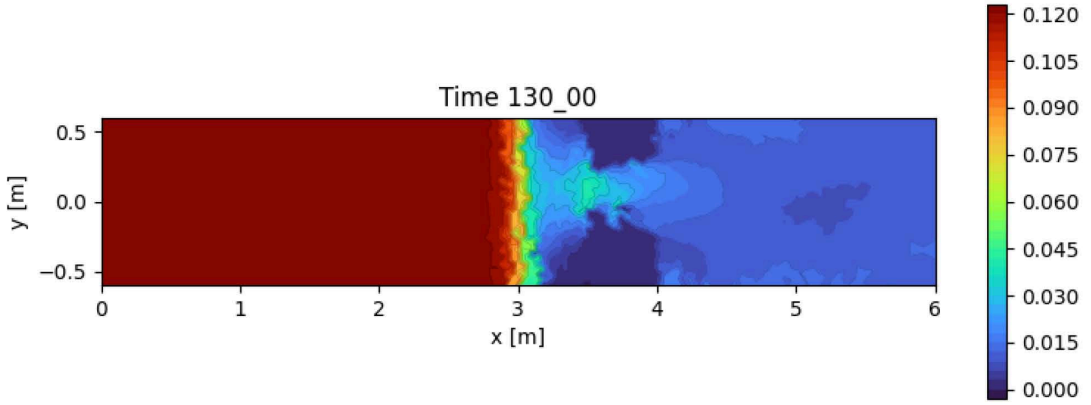

Fine sand (d_{50} = 0.31 mm)

Nelen & Schuurmans UCLouvain UNIVERSITY OF TWENTE.

Watlab – Morphodynamic model results

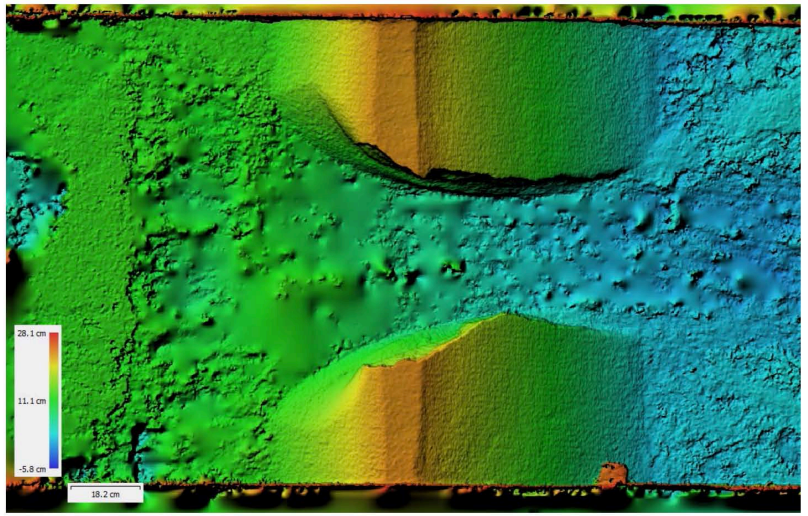

Fine sand (d_{50} = 0.31 mm)

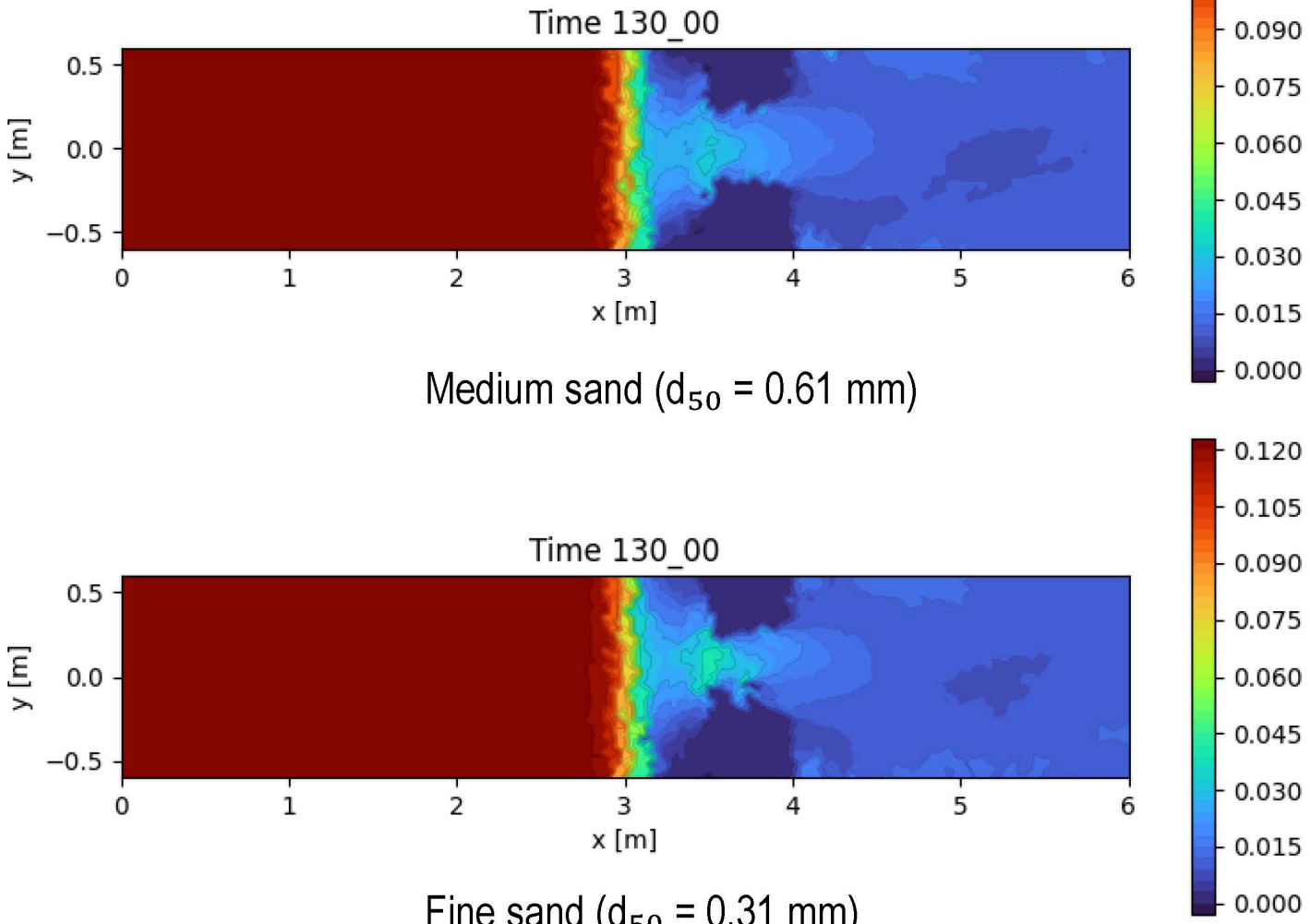

Medium sand (d_{50} = 0.61 mm)

Fine sand (d_{50} = 0.31 mm)

Nelen & Schuurmans

UCLouvain

UNIVERSITY OF TWENTE.

Conclusions

Small-scale flume experiment

- Photogrammetry
- Ultrasonic sensor

2D model with bank failure operator

- Medium sand (d_{50} = 0.61 mm)
- Fine sand (d_{50} = 0.31 mm)

Future works

- Quantitative comparison of breach width, depth (model vs experiment)
- Test different bank-failure angles
- Compare models with and without bank-failure operator

UNIVERSITY OF TWENTE. Nelen & Schuurmans UCLouvain

SEDIMARE
Sediment Transport and Morphodynamics in Marine and Coastal Waters with Engineering Solutions

SEDIMARE 2nd Workshop

EXPERIMENTAL AND NUMERICAL INVESTIGATION OF OVERTOPPING-INDUCED BREACHING IN NON-COHESIVE DAMS

Siyuan Wang
s.wang-4@utwente.nl
siyuan.wang@uclouvain.be

Supervised by:
Dr. Ir. P.C. Roos (UT)
Dr. J. J. Warmink (UT)
Prof. Dr. S. Soares-Frazão (UCLouvain)
Dr. N. D. Volp (Nelens&Schuurmans)

11 September 2025

Marie Skłodowska-Curie Actions

This project has received funding from the European Union's (EU) Horizon Europe Framework Programme (HORIZON) under Grant Agreement No 101072443 as a MSCA Doctoral Network (HORIZON-MSCA-2021-DN-01).

UNIVERSITY OF TWENTE.

SEDIMARE 2023 - 2027

Sediment Transport and Morphodynamics in Marine and Coastal Waters with Engineering Solutions

SEDIMARE PROJECT_DC #3

HR Wallingford Meeting

Sand-Silt Experiment in Aberdeen: First observations of wave ripples

PhD Candidate: *Nguyen, Thi To Van (Van)*
Promotor: *P.C. Roos (Pieter)*
Co-promotor: *J.J. van der Werf (Jebbe)*

Date: 2025 September 11th

Contents

1. Introduction

In nature, especially in coastal and fluvial systems, most of sediments are mixes of sand and fines (clay and silt).

Recently, there have been more studies focusing on the transport of sand-mud mixtures. However, most of these studies treated clay and silt collectively as mud.

Silty sediments in Mekong Delta, Vietnam
[Photo by MangLub project]

Mudflat, Wadden Sea, Netherlands.

Satellite images of the Mekong Delta taken by Envisat

1. Introduction

SILT

Apparently cohesive

Small RD

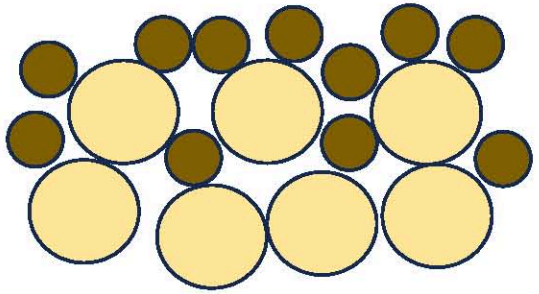

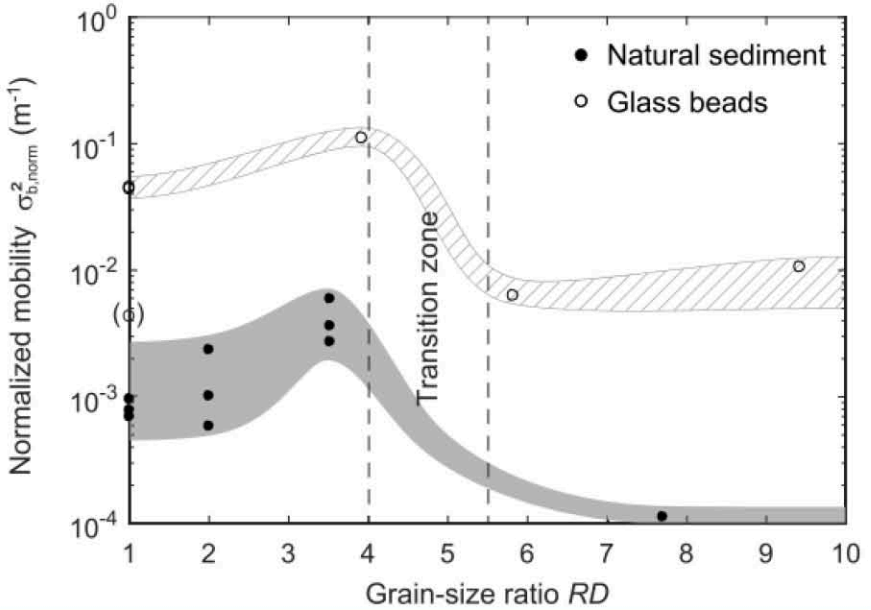

Normalized mobility (logarithmic scale), with varying grain-size ratio (Staudt et al., 2019)

4

63

Large RD (grain-size ratio)

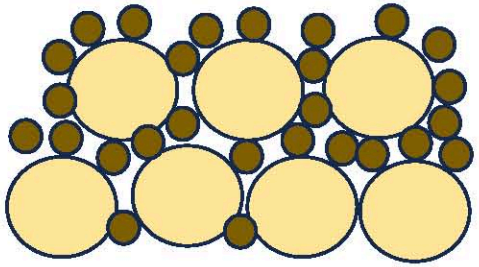

SAND

Non-cohesive

1. Introduction

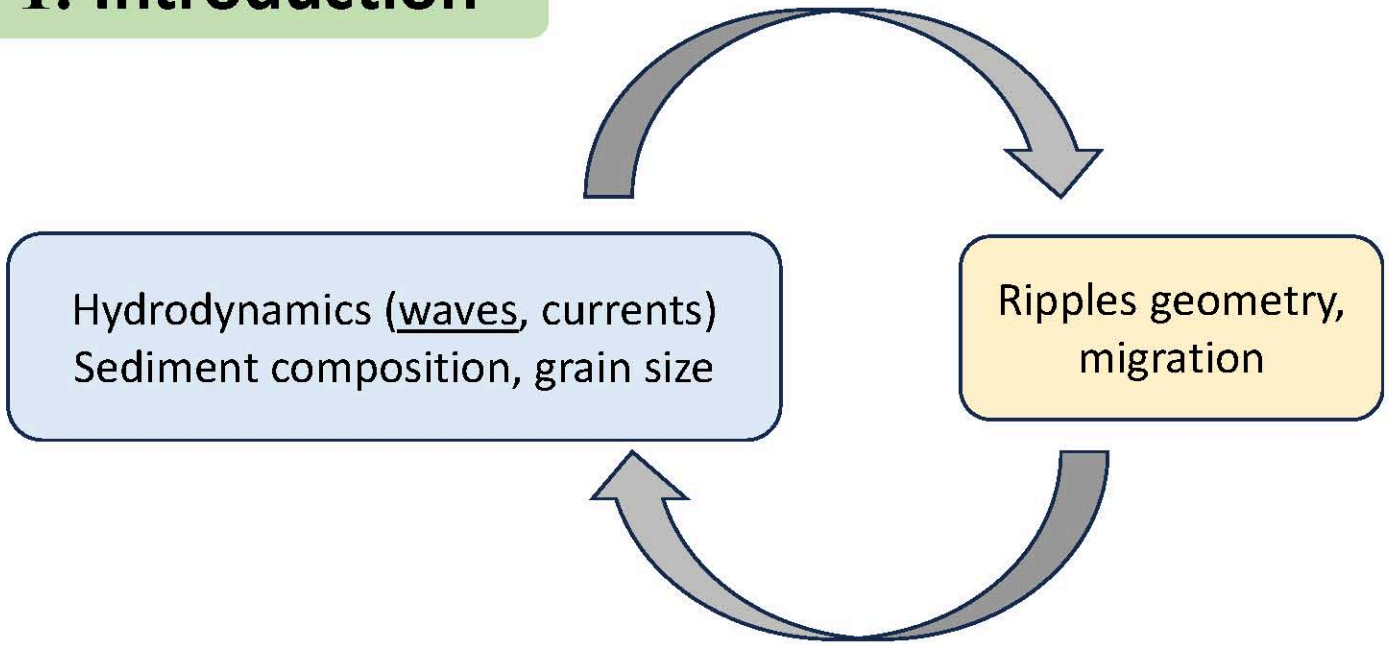

Field examples of 2D–3D ripples (percentages denote subsurface mudcontents, the scale bar is 200 mm long (Baas et al., 2019)

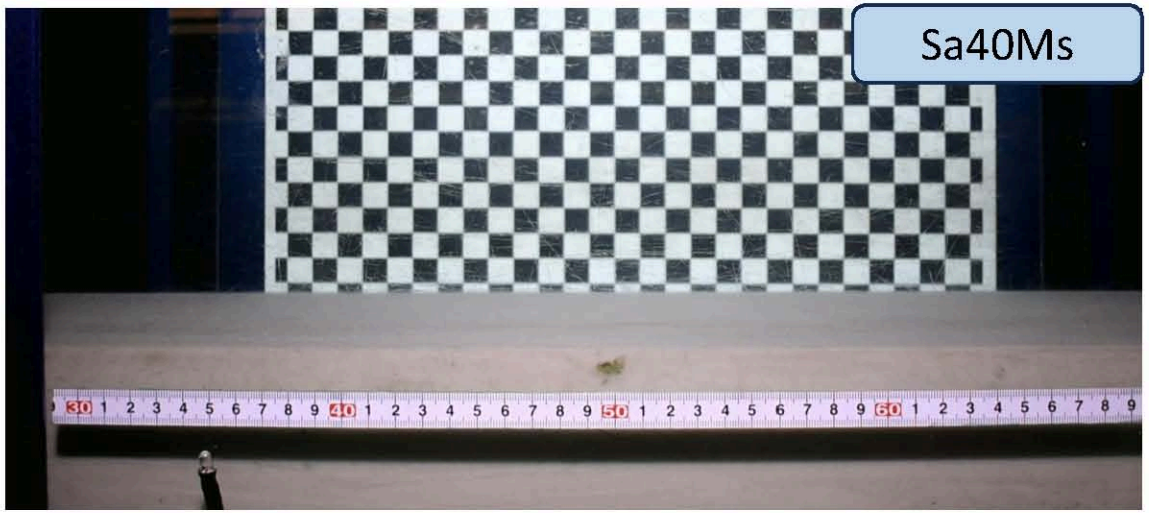

Wave ripple development in a test of sand-medium silt mixture (40% of silt by dry weight)

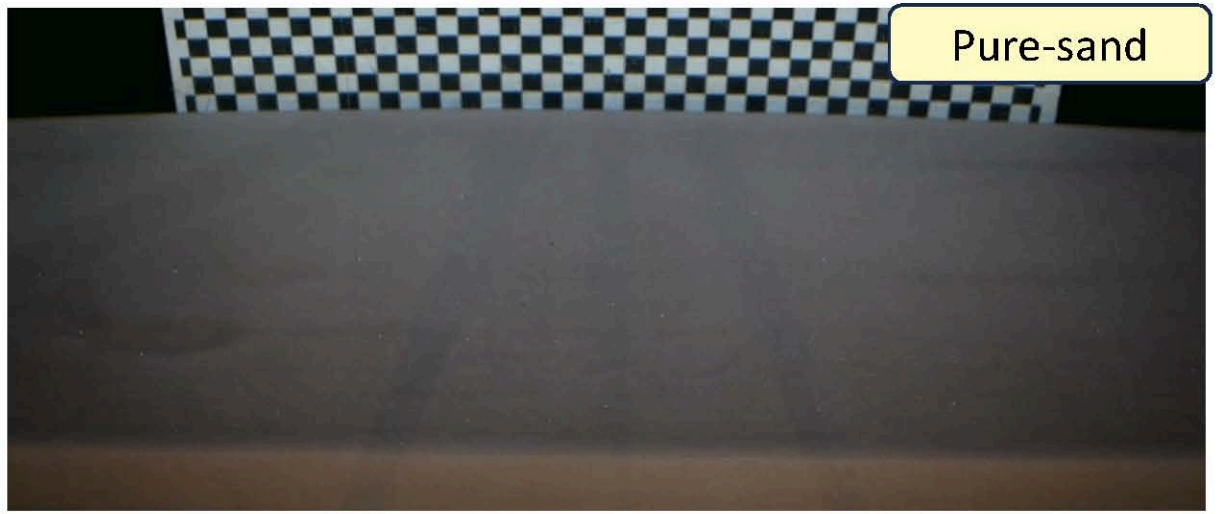

Wave ripple development in a test of pure-sand bed

2. Sand-silt experiments

Full-scale Aberdeen Oscillatory Flow Tunnel

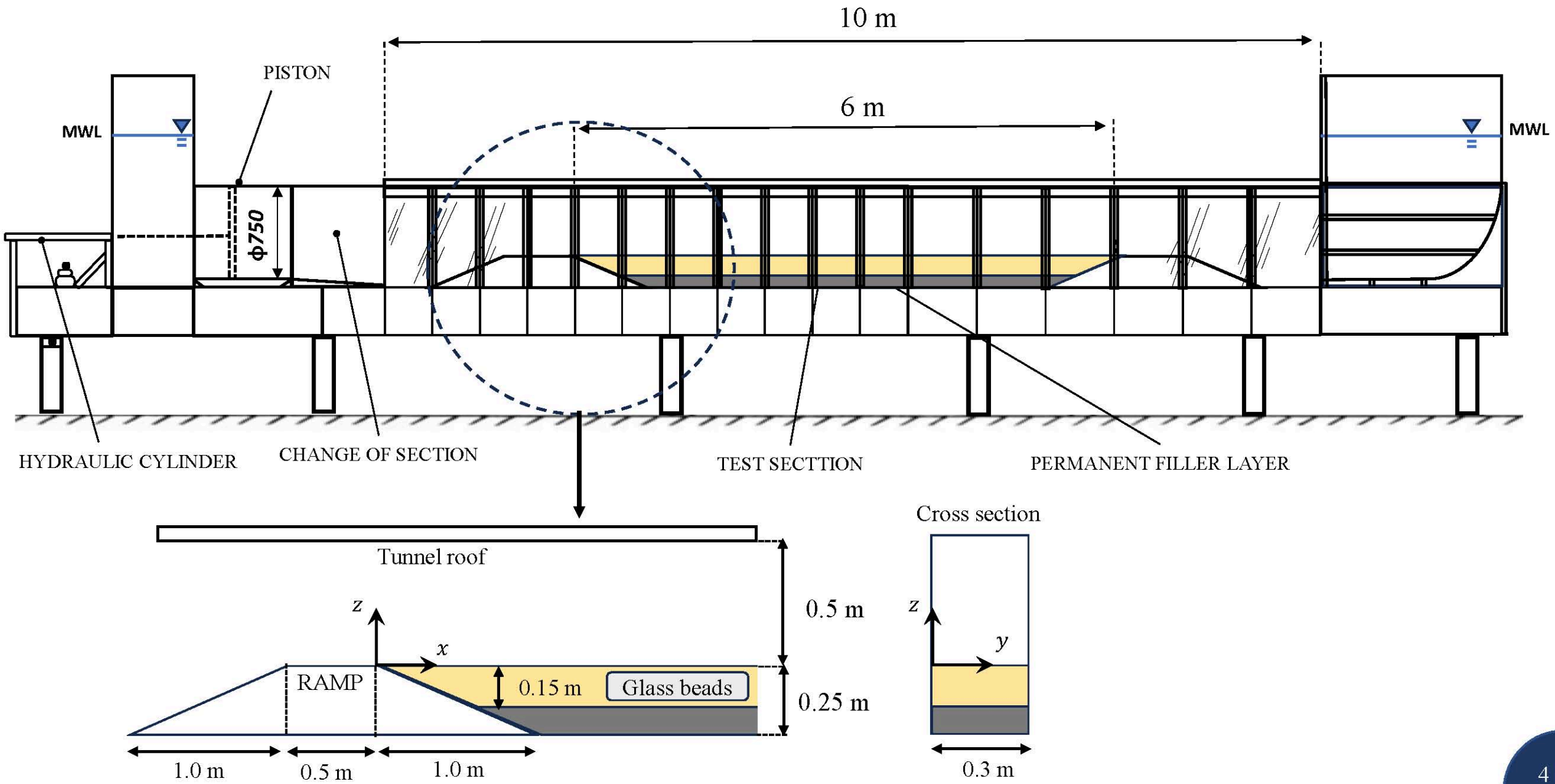

2. Sand-silt experiments

Materials in our experiment

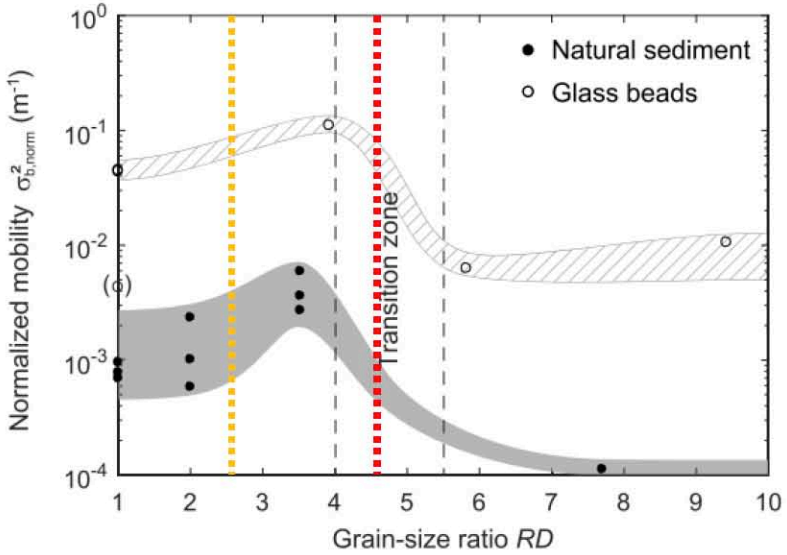

Sediment fractions	D_{50} (µm)
Medium silt	31
Coarse silt	52
Sand	144

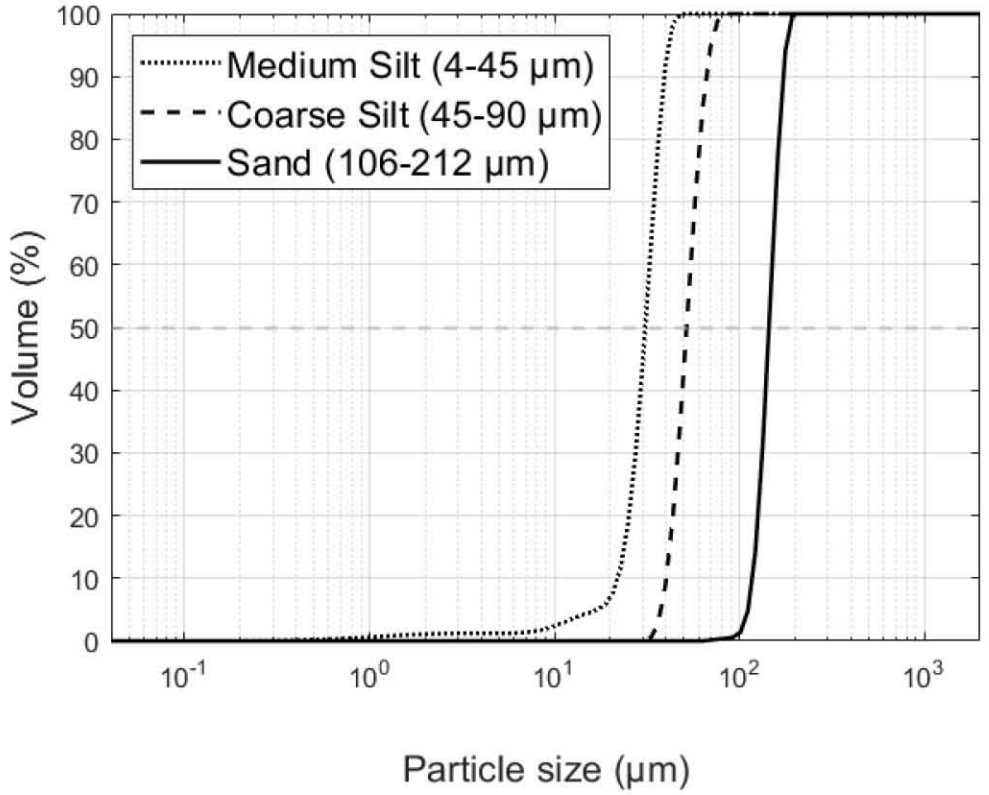

Particle-size distributions of glass beads using a laser diffraction particle size analyzer (Beckman Coulter LS13320)

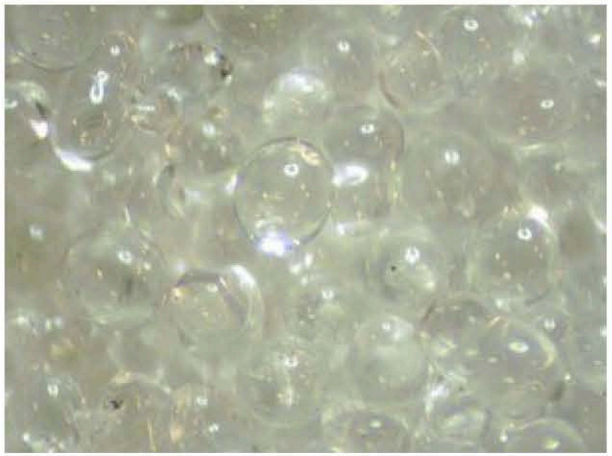

Glass Bead is a chemically inert soda lime glass that is round in shape, well-sort in distribution and has main composition is silica ($\rho_s = 2500$ kg/m^3).

2. Sand-silt experiments

Experimental conditions

Sediment fractions

Silt contents

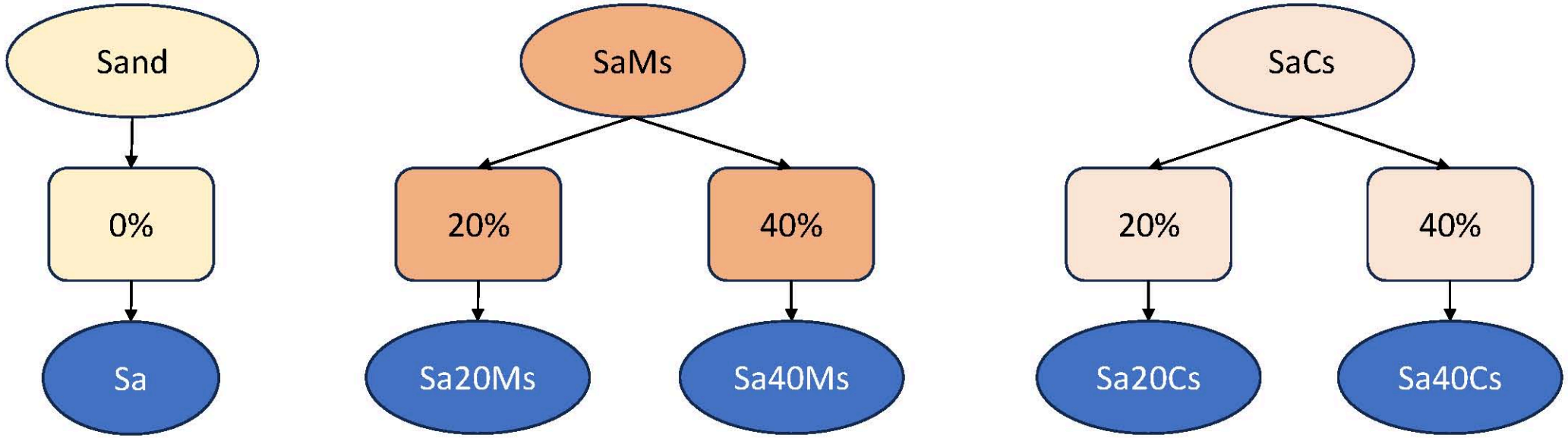

Flow period (*T*) — 4 s

Flow velocities (u_{rms}) — 0.2 m/s | 0.3 m/s | 0.4 m/s

Velocity skewness (*r*) — 0.5

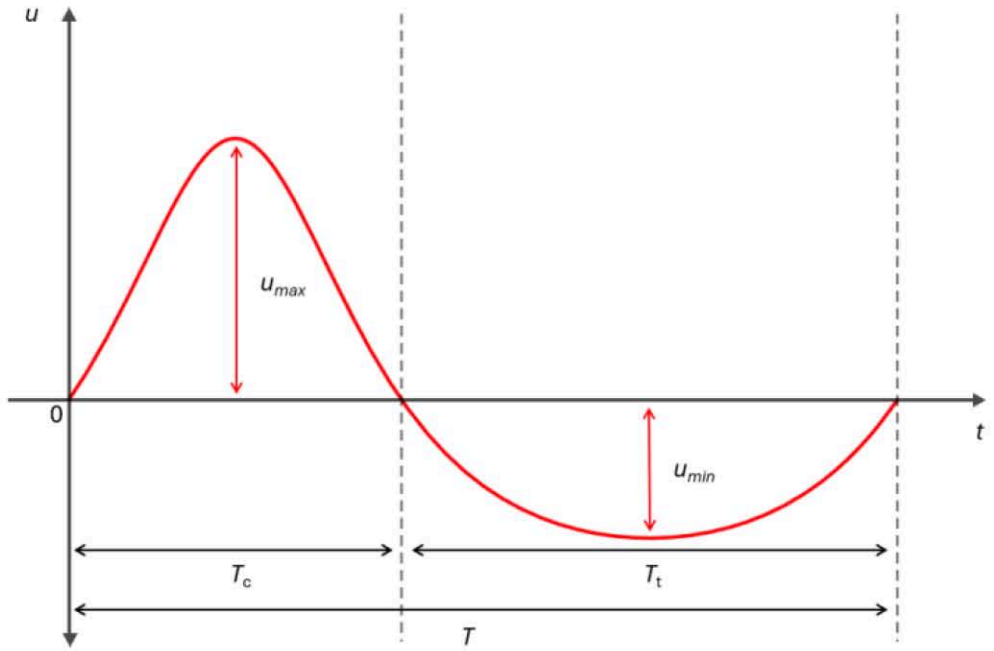

2. Sand-silt experiments

The LBP (Laser Bed Profiler) was applied to measure the bed elevation pre- and post-experiment.

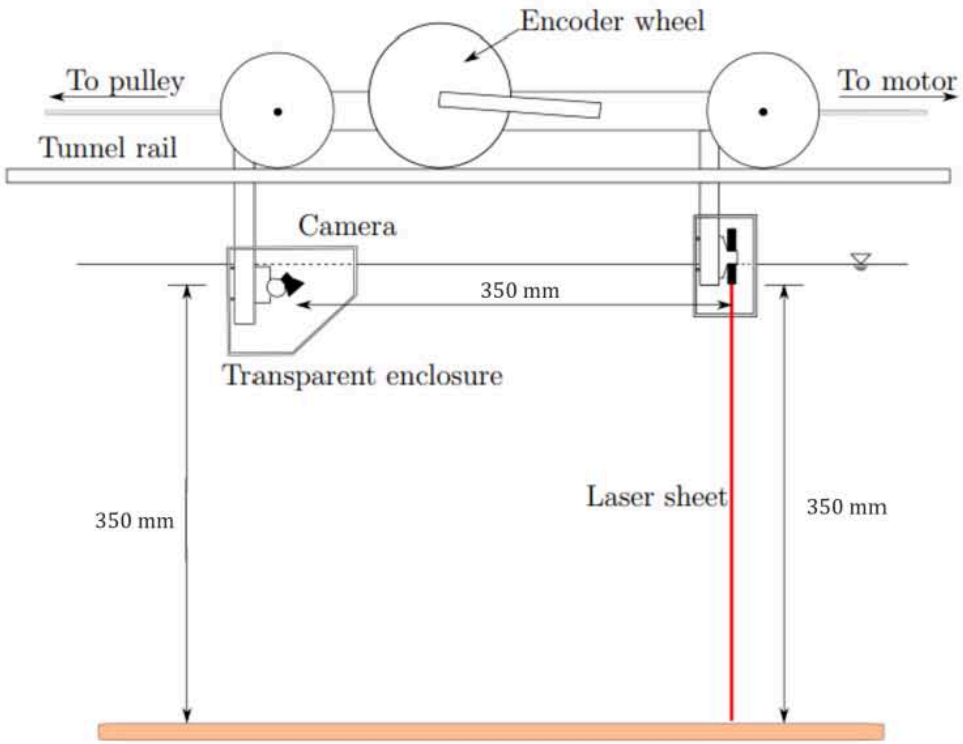

Sketch of the setup of the LBP in the AOFT (*Boscia, 2021*)

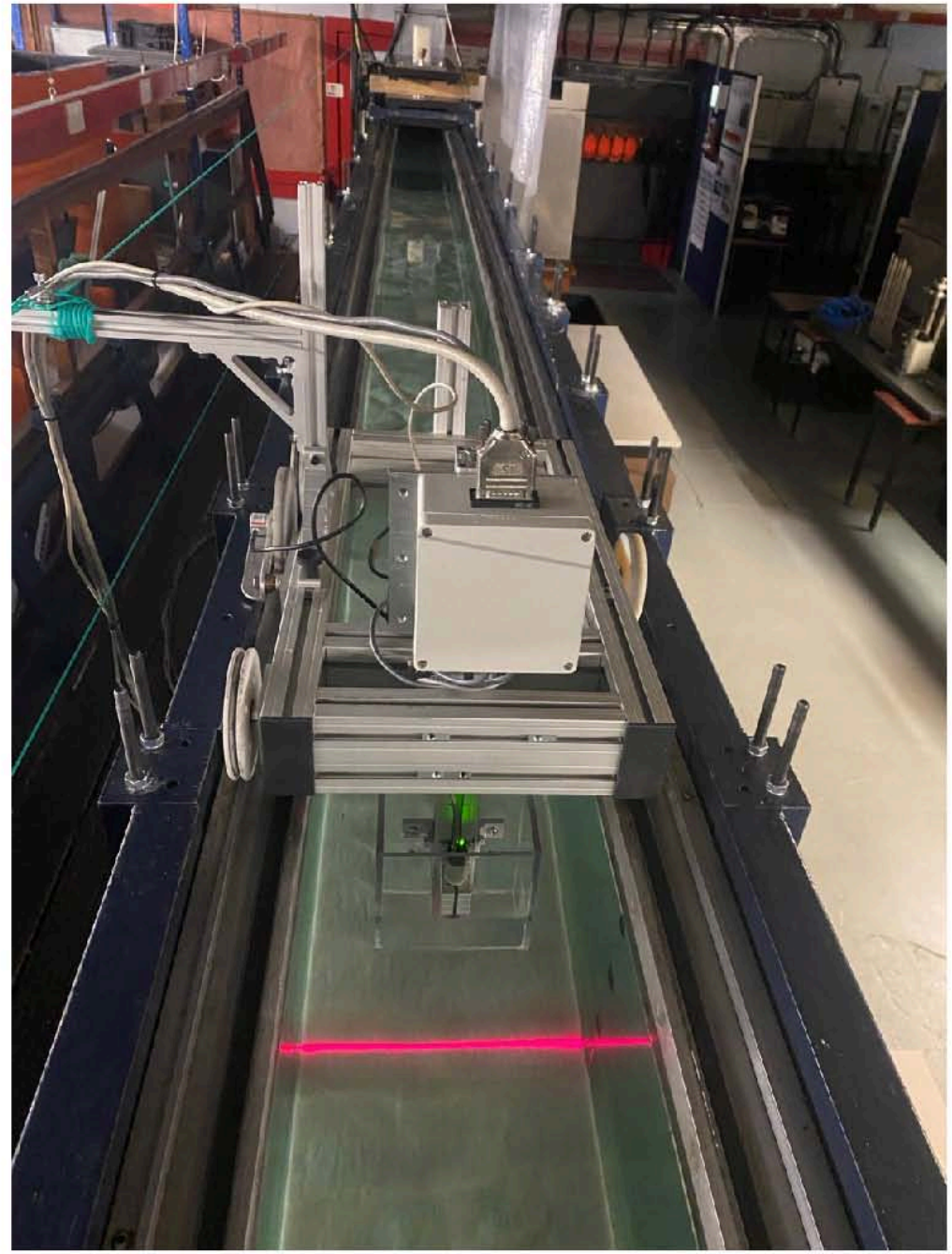

2. Sand-silt experiments

Phase 1: observe bedform development

- SRP: measure temporal 1D bed elevation
- Two cameras: observed 2D and 3D view of the bed development

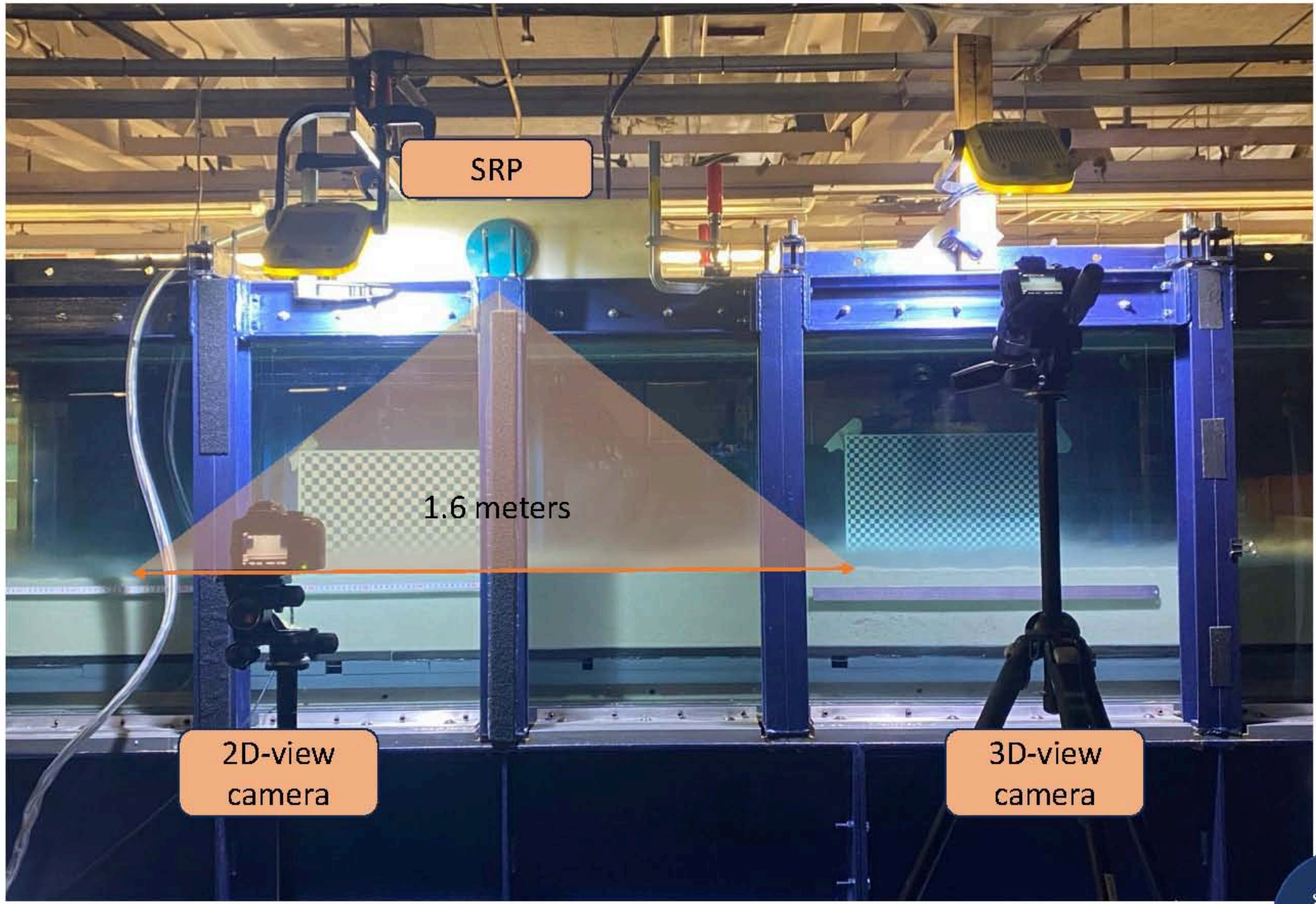

2. Sand-silt experiments

Phase 2: Measure detailed velocity and SSC profiles.

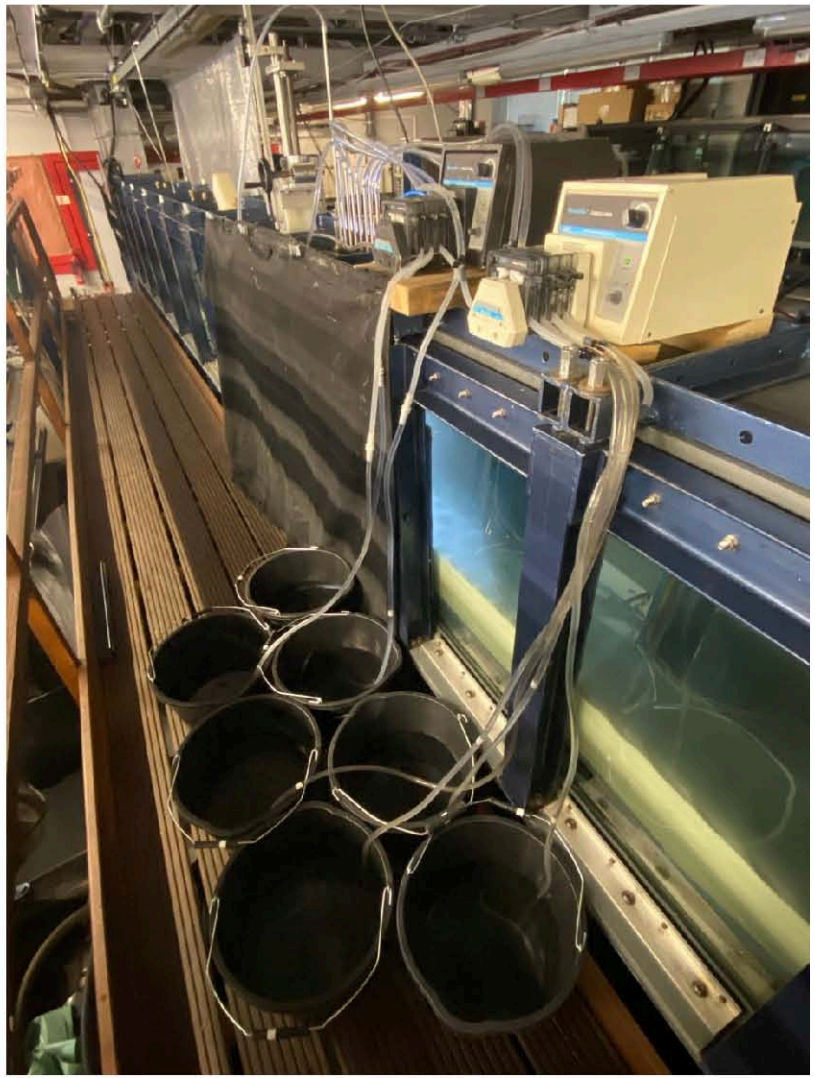

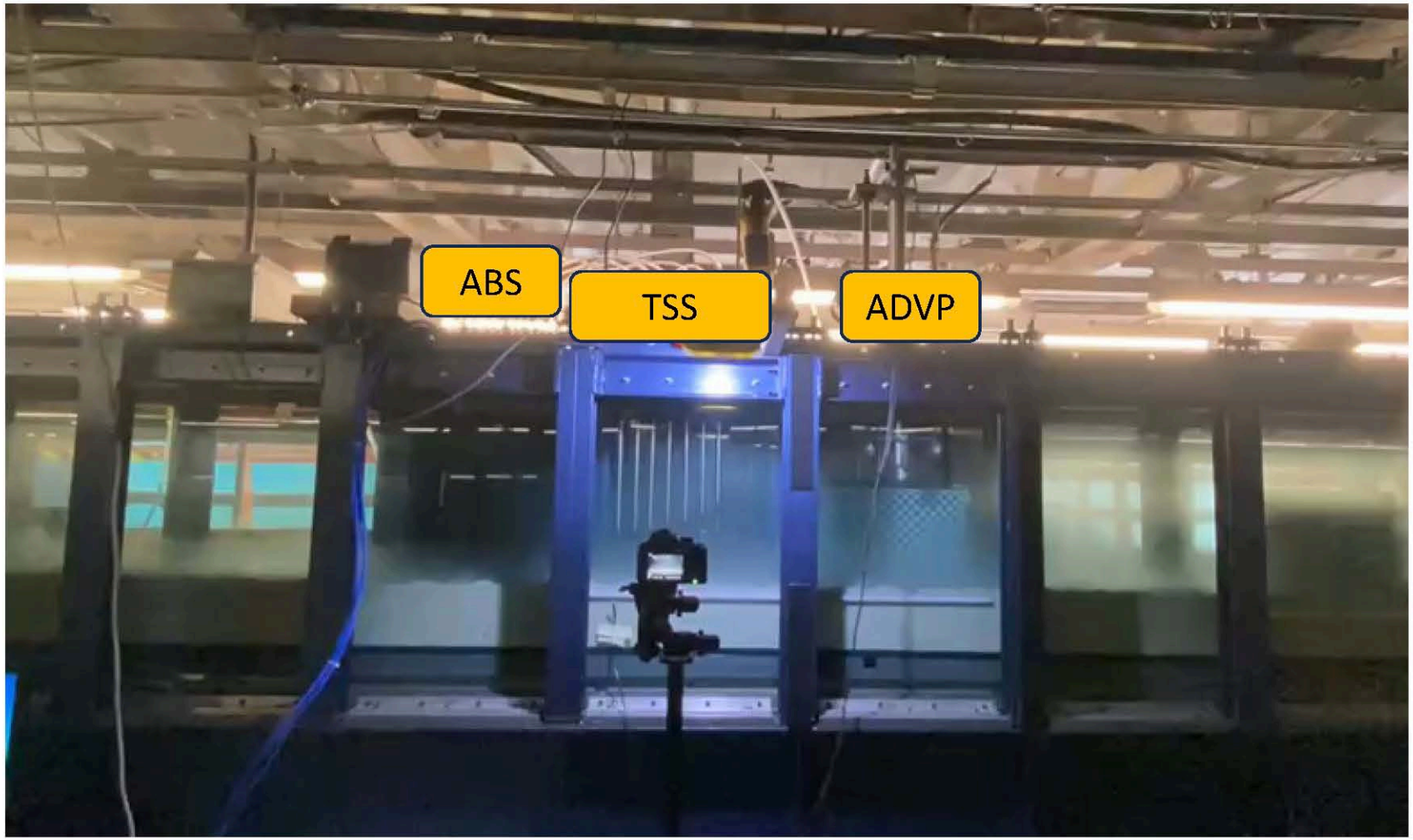

2. Sand-silt experiments

After running two phases of each experiment

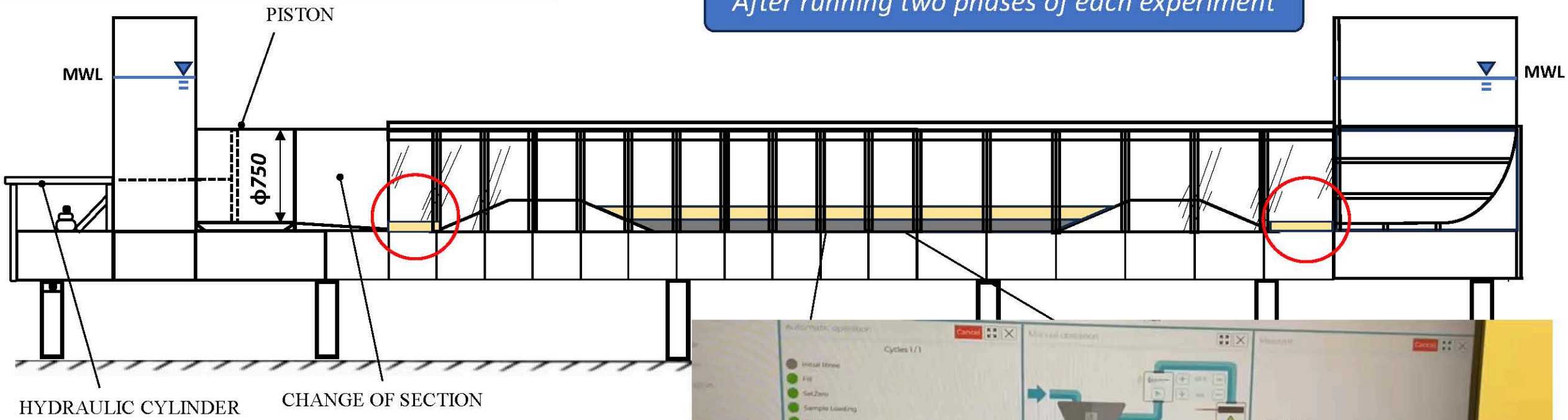

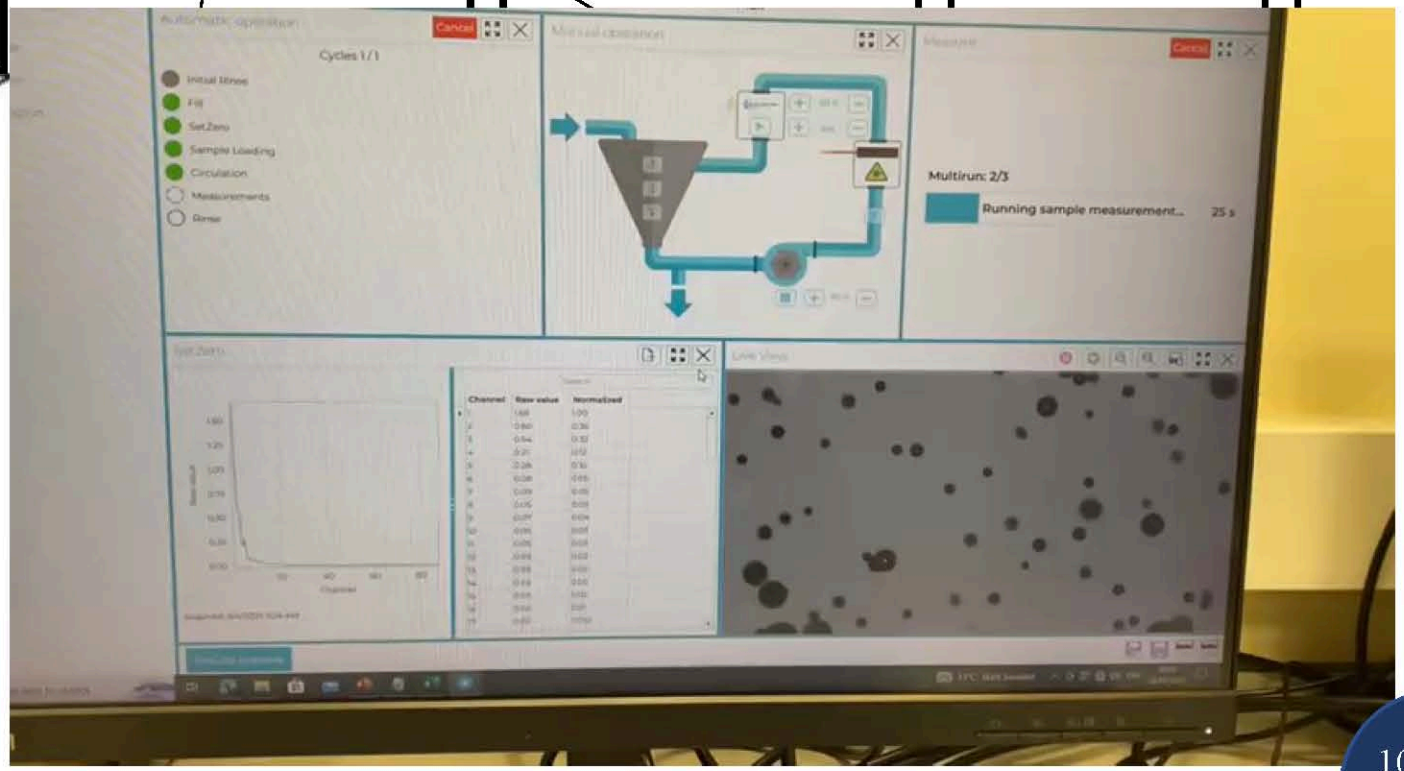

- Collected sediments in two traps to study the net transport.
- All of sediment samples were used to analyze particle size distribution.

3. First result: ripples observations

Sa40Cs02_600 cycles

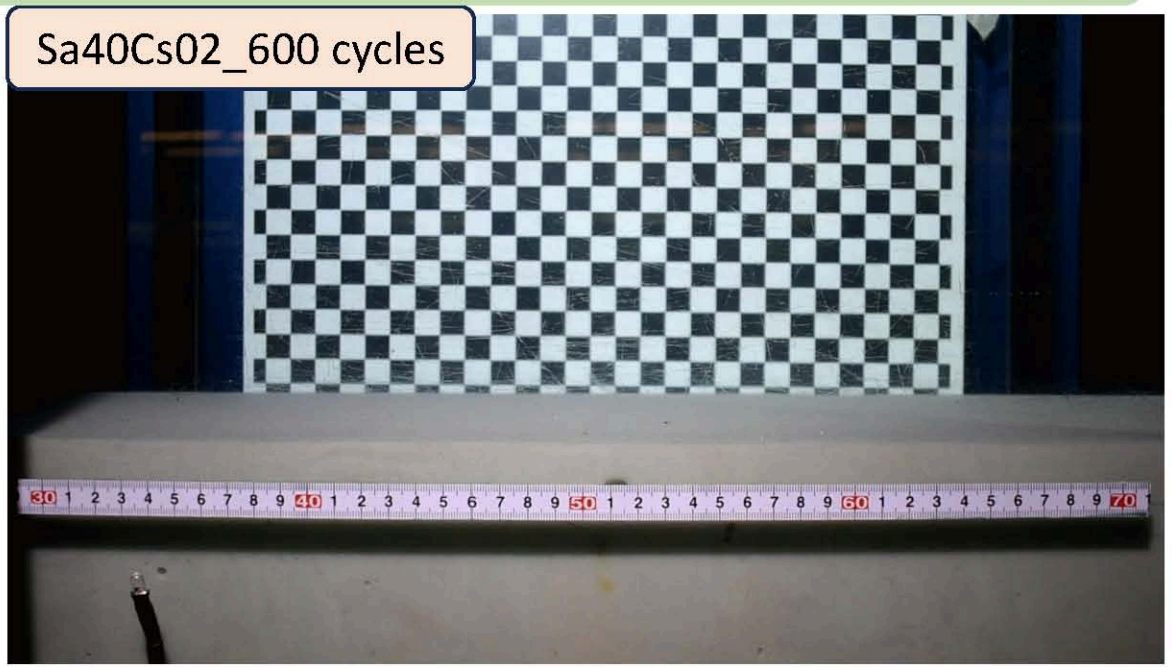

Sa40Ms02_600 cycles

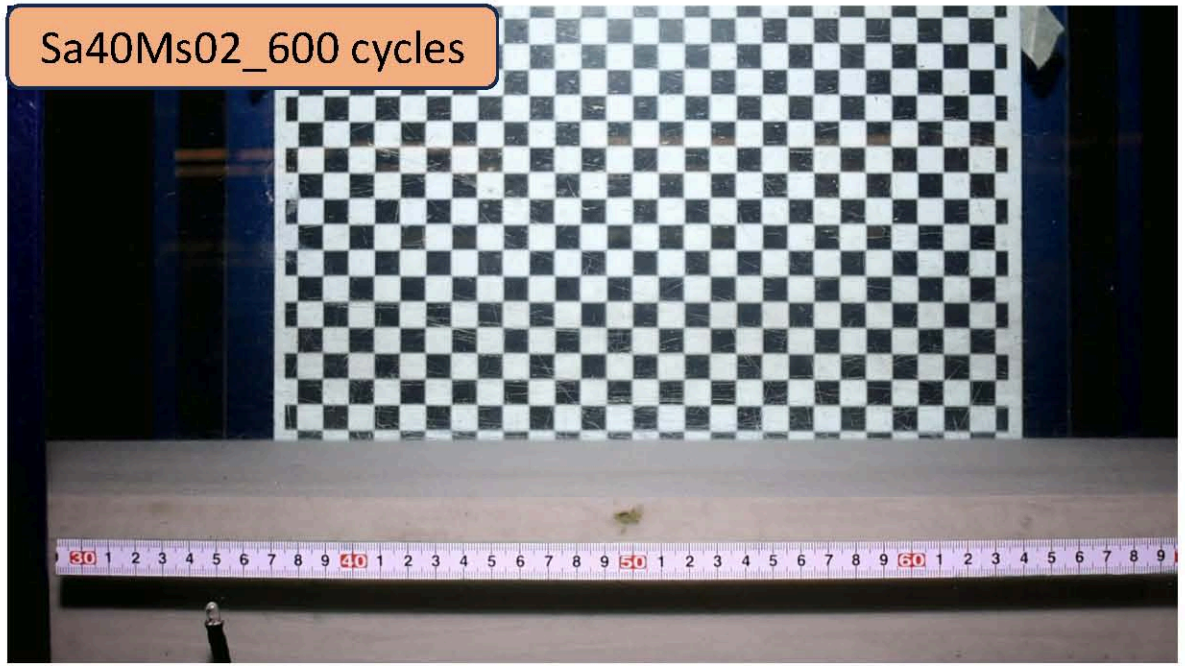

Sa02_600cycles

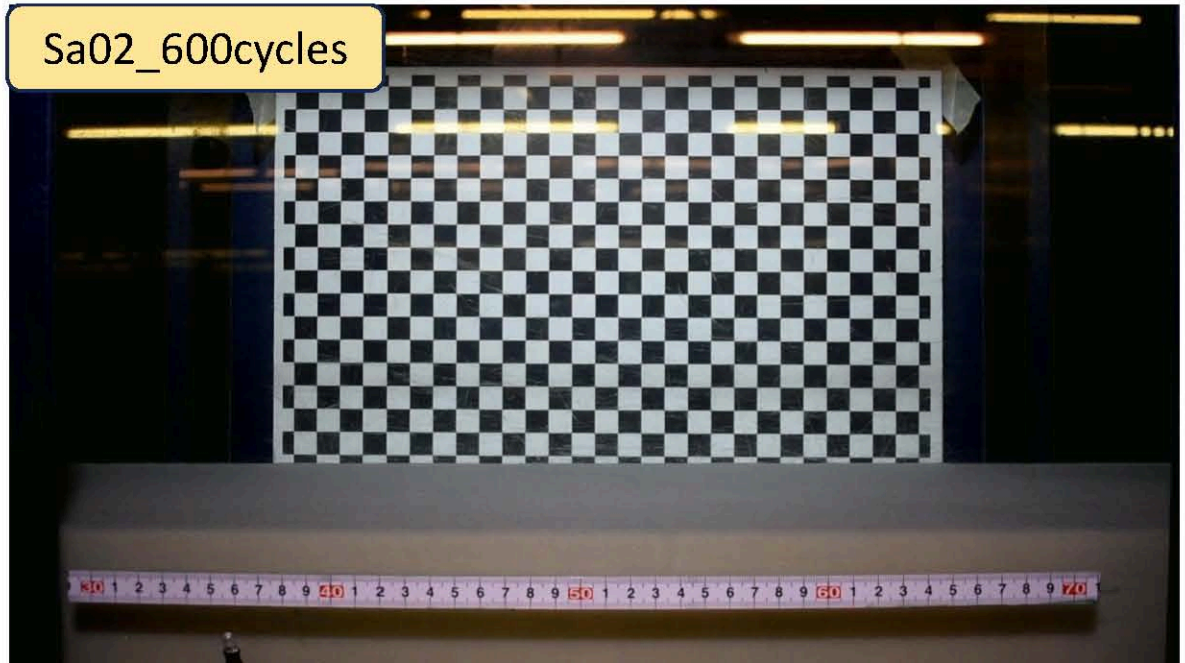

u_{rms} = 0.2 m/s condition

3. First result: ripples observations

Sa40Cs03_500 cycles

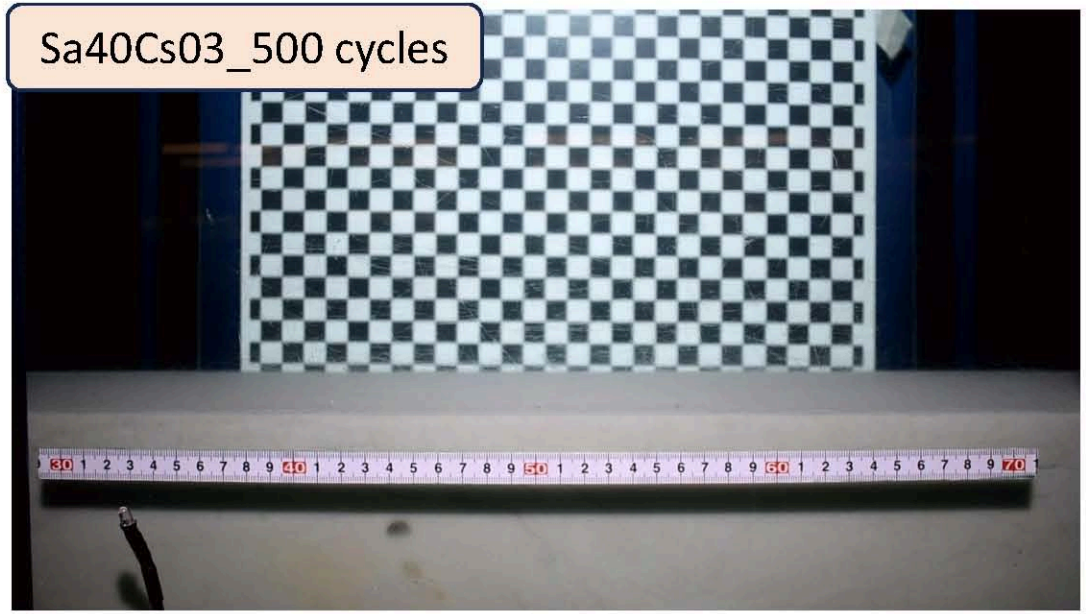

Sa40Ms03_600 cycles

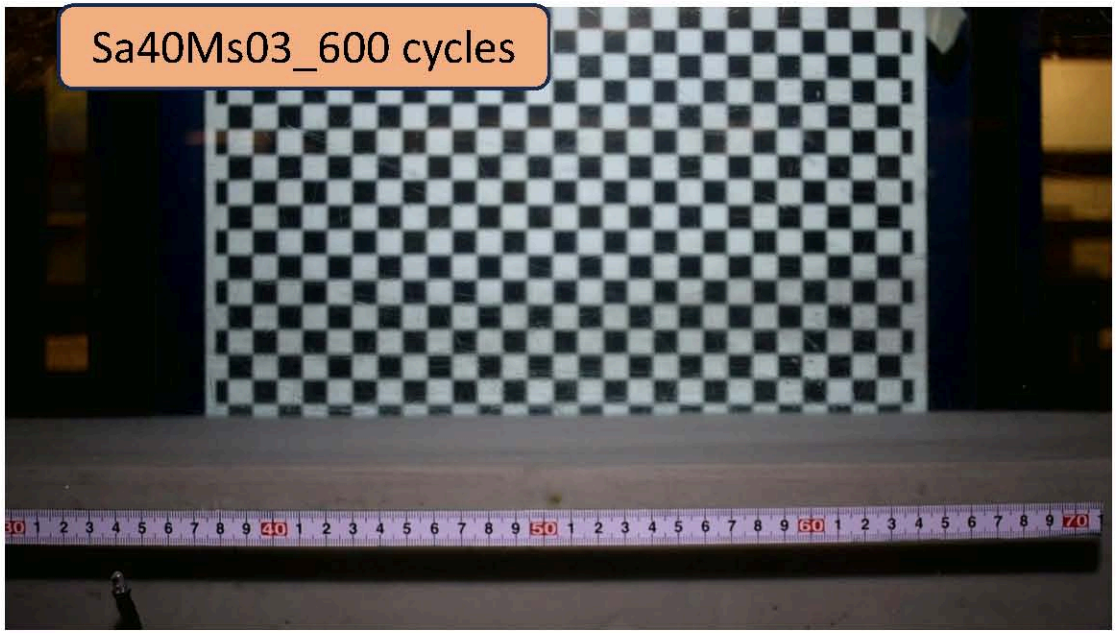

Sa03_600cycles

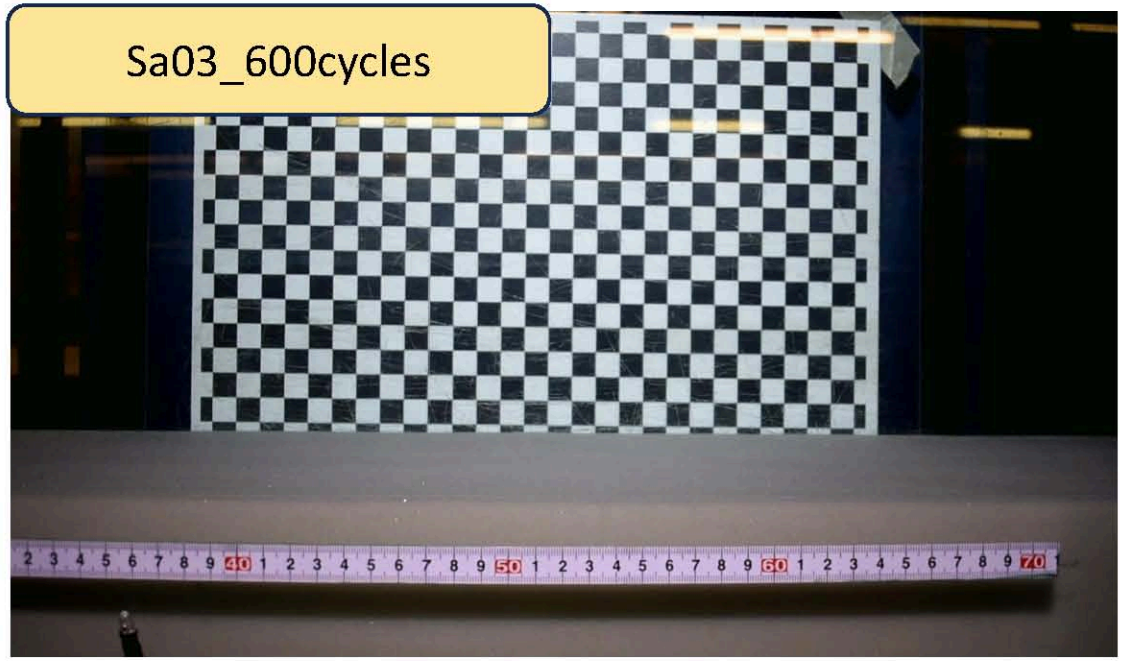

u_{rms} = 0.3 m/s condition

3. First result: ripples observations

Results from the SRP showing the ripple development of different mixtures in 0.2 m/s conditions.

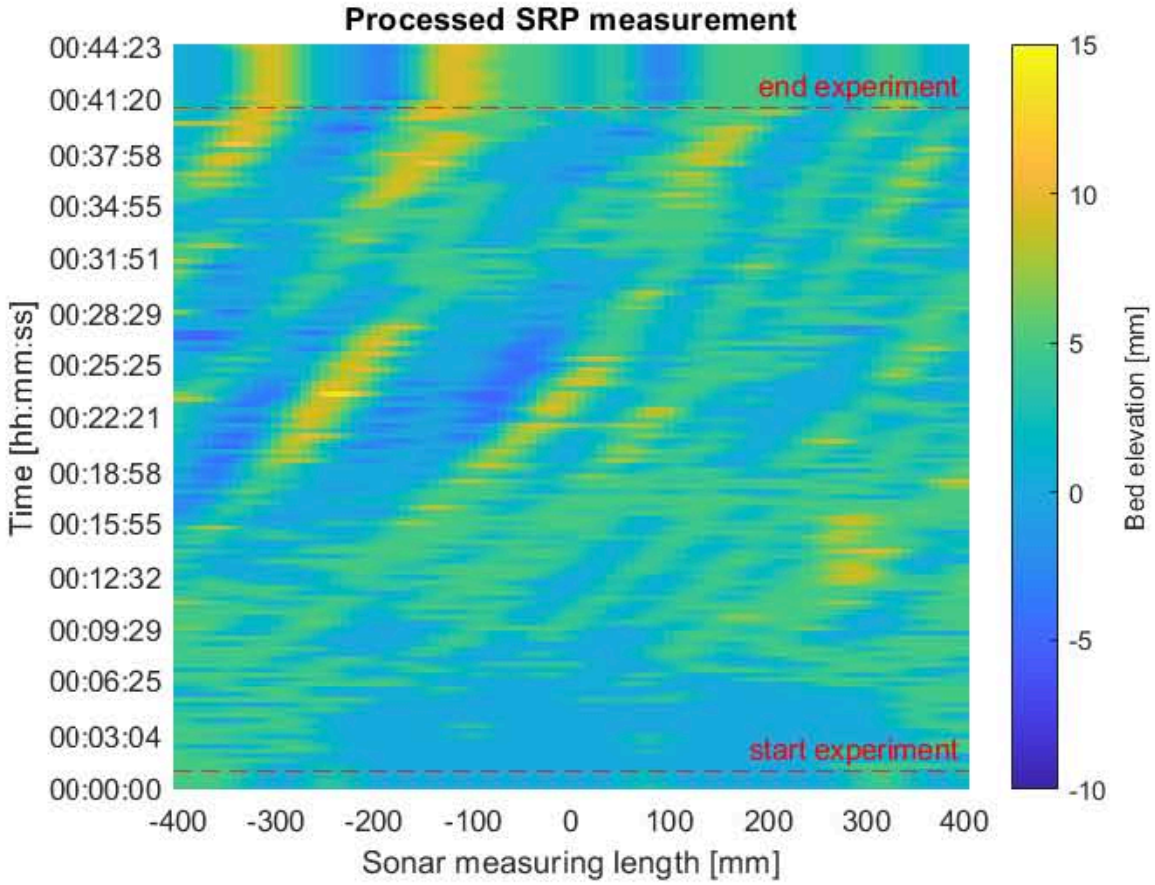

Sa02

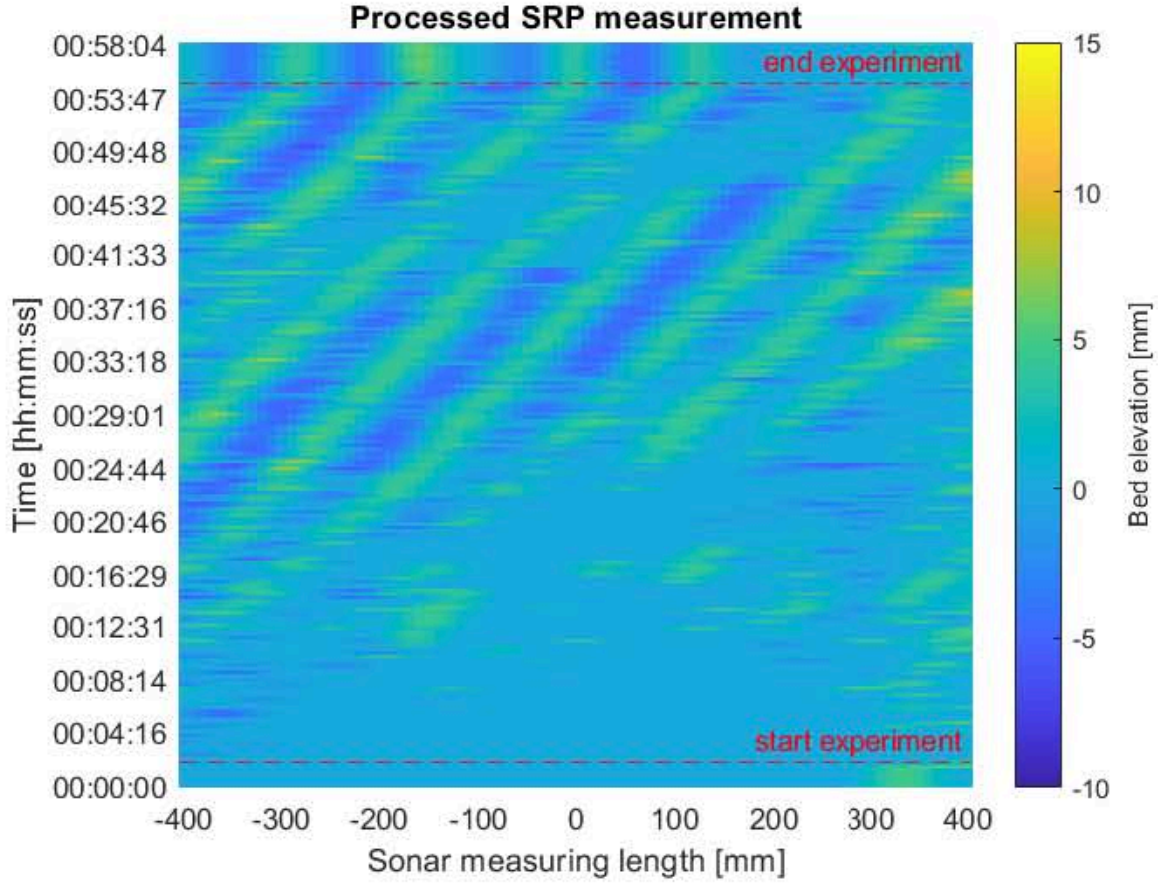

Sa20Cs02

3. First result: ripples observations

Sand

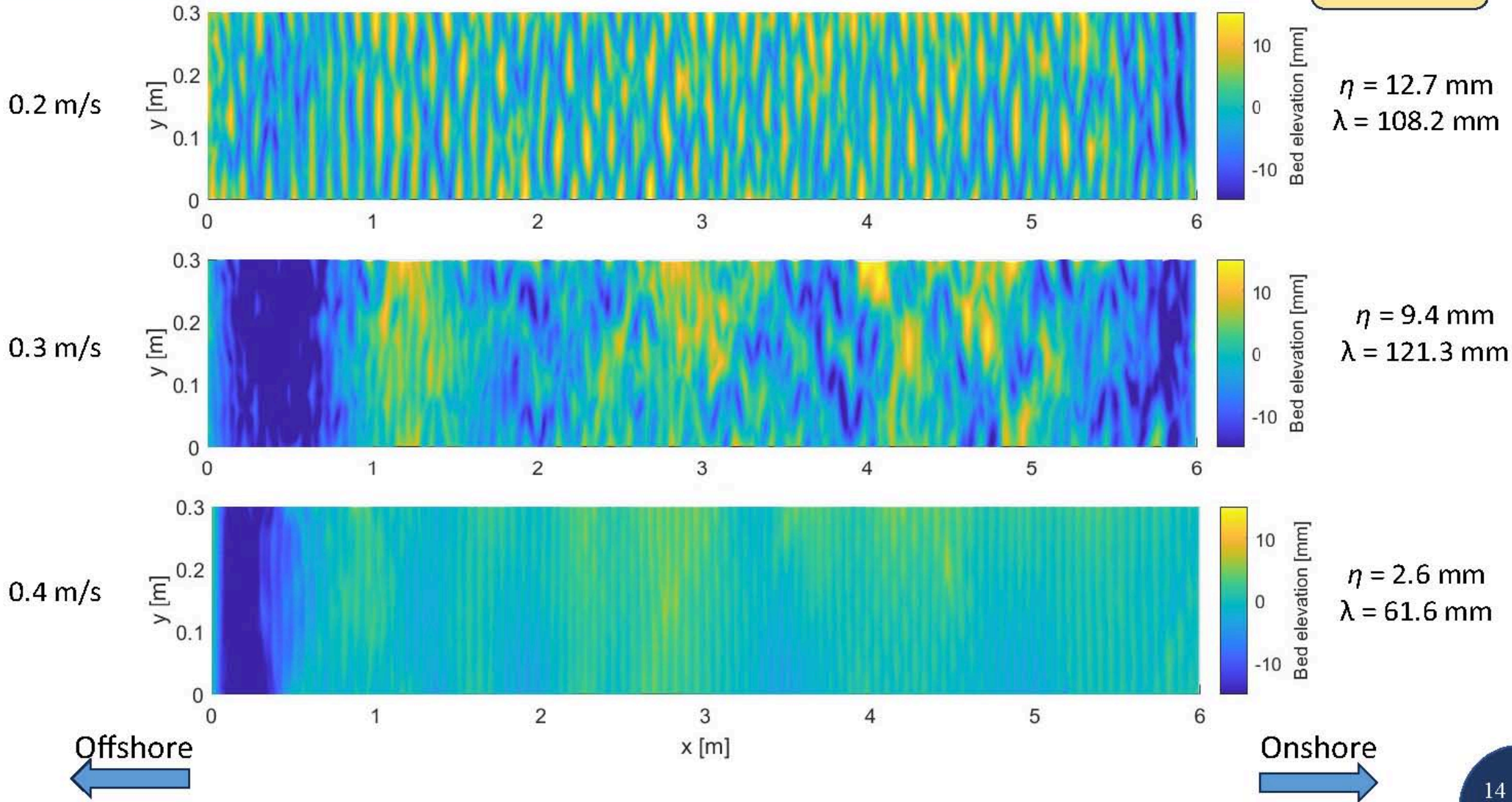

3. First result: ripples observations

Sa20Ms

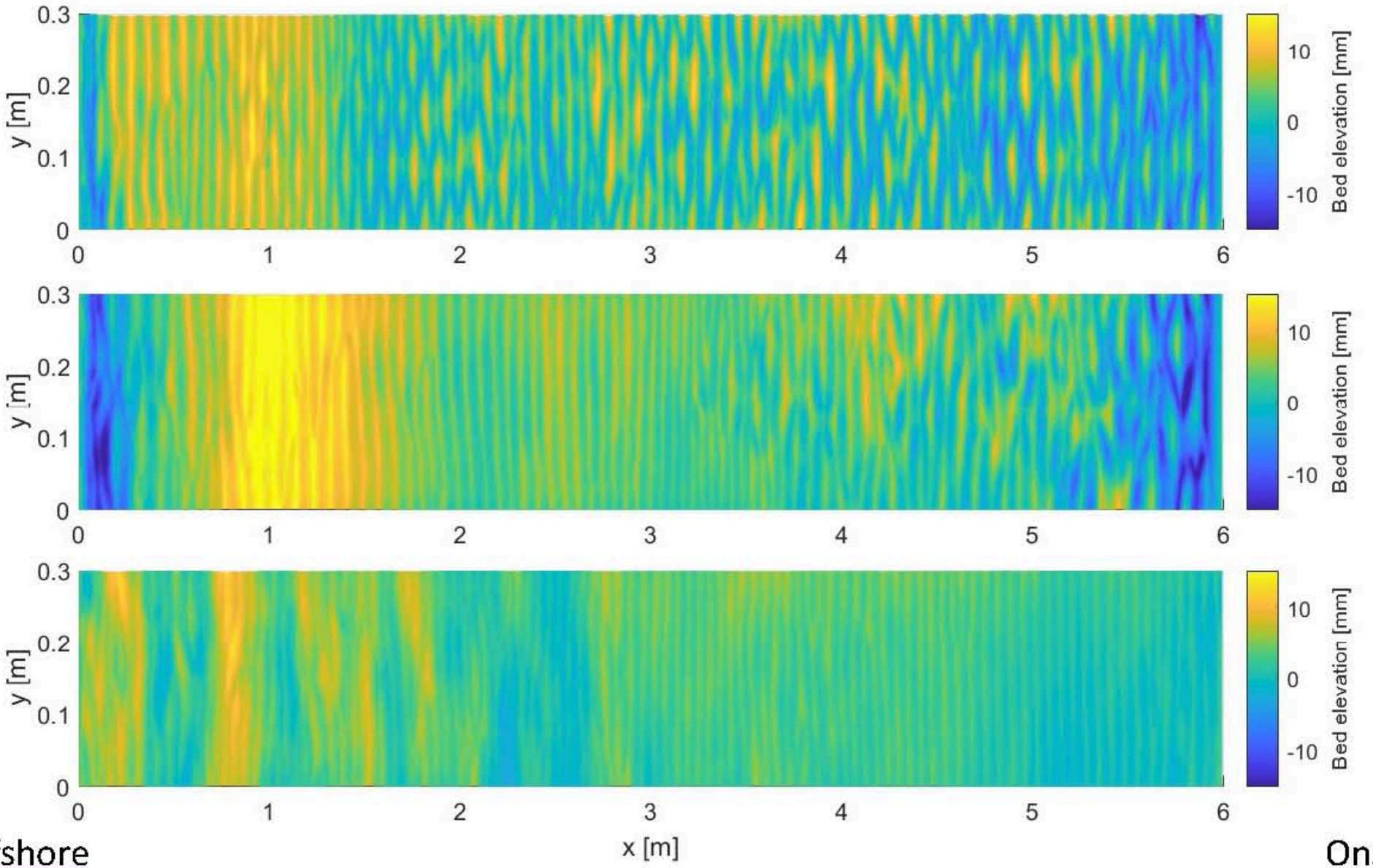

η = 8.4 mm
λ = 114.3 mm

η = 4.6 mm
λ = 80 mm

η = 3.5 mm
λ = 69 mm

Offshore

Onshore

4. Summary

1. **Finished the main experiment** in a full-scale oscillatory tunnel (AOFT)
2. Collected **good dataset** to study wave ripples and transport of various sand-silt mixtures.
3. **First nice observations on wave ripples**

Current and upcoming plans:

- Completing the deliverable for SEDIMARE project.
- Working on data analysis, particularly the ripples, and start writing the first paper.
- Supervising a master student who will have a defense on wave ripples topic this October.

Acknowledgment:

- *University of Aberdeen, in particular Dominic and the technical staff, for providing the facilities and great support during the experiment.*
- *Lukas, our master's student, for his valuable assistance with the experimental work.*
- *My supervisors, Pieter and Jebbe, for their continuous guidance and constructive advice.*

Source: freepik

Cross-shore hydro-morphodynamics in a beach protected by submerged vegetation meadow

2nd SEDIMARE Workshop at HR Wallingford

Presented by,

1) **Buckle Subbiah Elavazhagan** – Doctoral Researcher, IH Cantabria, Universidad de Cantabria
2) **Maria Maza** – Associate Professor, IH Cantabria, Universidad de Cantabria
3) **Javier Lara** – Full Professor, IH Cantabria, Universidad de Cantabria

Funded by the European Union

CONTENTS

INTRODUCTION

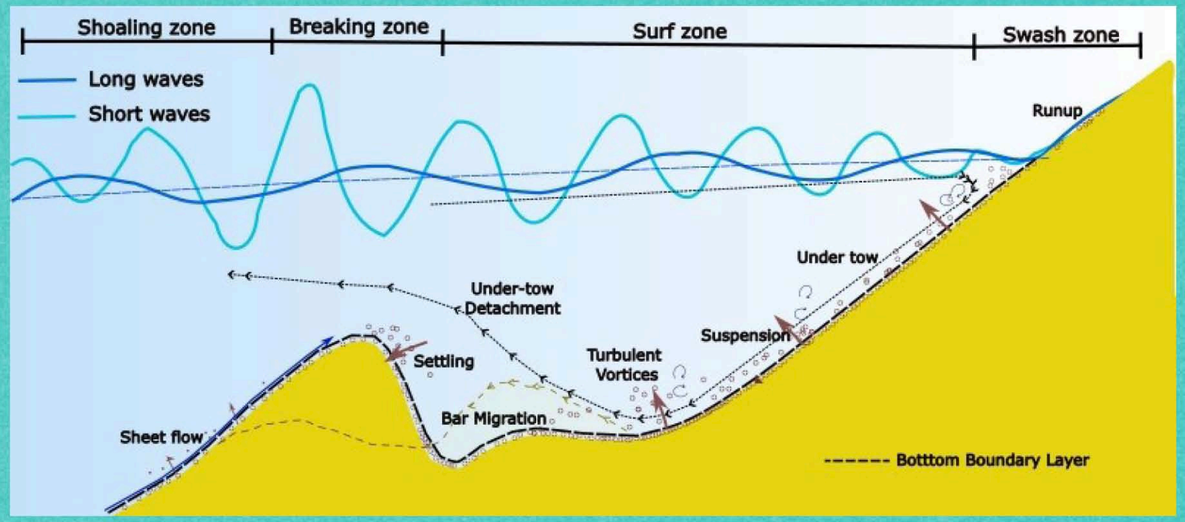

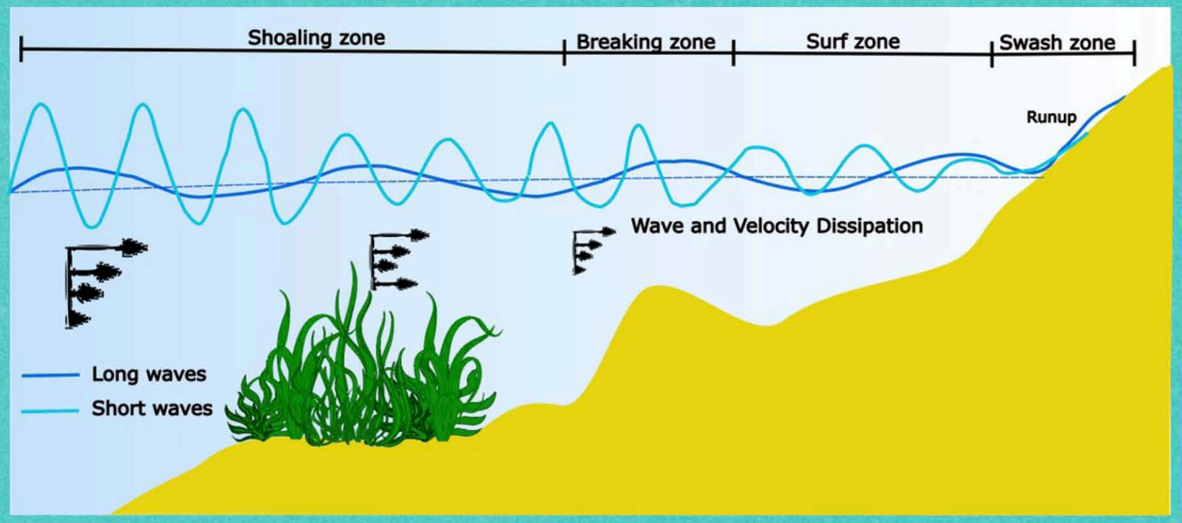

Why understanding cross-shore morphodynamics?

- ✓A comprehensive understanding of intrinsic of cross-shore hydrodynamics and morphodynamics is necessary for the sustainable management of the beaches as these processes are quite prevalent in storm conditions
- ✓Understanding this different cross-shore dynamics will result in better support to planning and managing the coastal protection measures like seawalls or nature based solutions.
- ✓Need for an efficient process based cross shore sediment transport model applicable to wide range of coastal applications

NUMERICAL MODEL

IH2VOF – SED : A RANS based 2DV sediment transport model

- ✓Turbulence is accounted using a k–ε closure model
- ✓Free surface reconstruction using Volume Of Fluid technique
- ✓Finite difference computational approach in a structured orthogonal mesh
- ✓Empirical formula by *Roulond et.al 2004* is used for Bed load estimation
- ✓Advective Diffusive equation is solved for Suspended load estimation
- ✓Two point friction velocity estimation is used utilizing log law approach

Friction velocity an important driver of the bed load

Turbulent viscosity an important driver of the suspended load

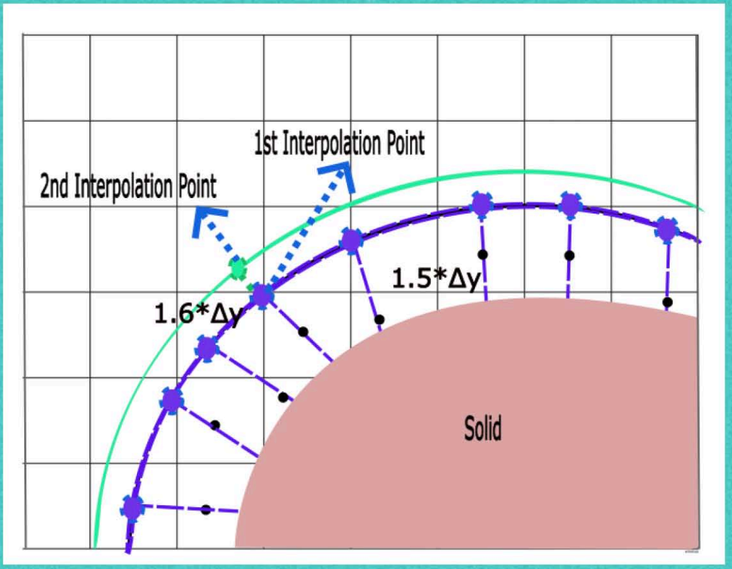

RECAP – BARE BEACH

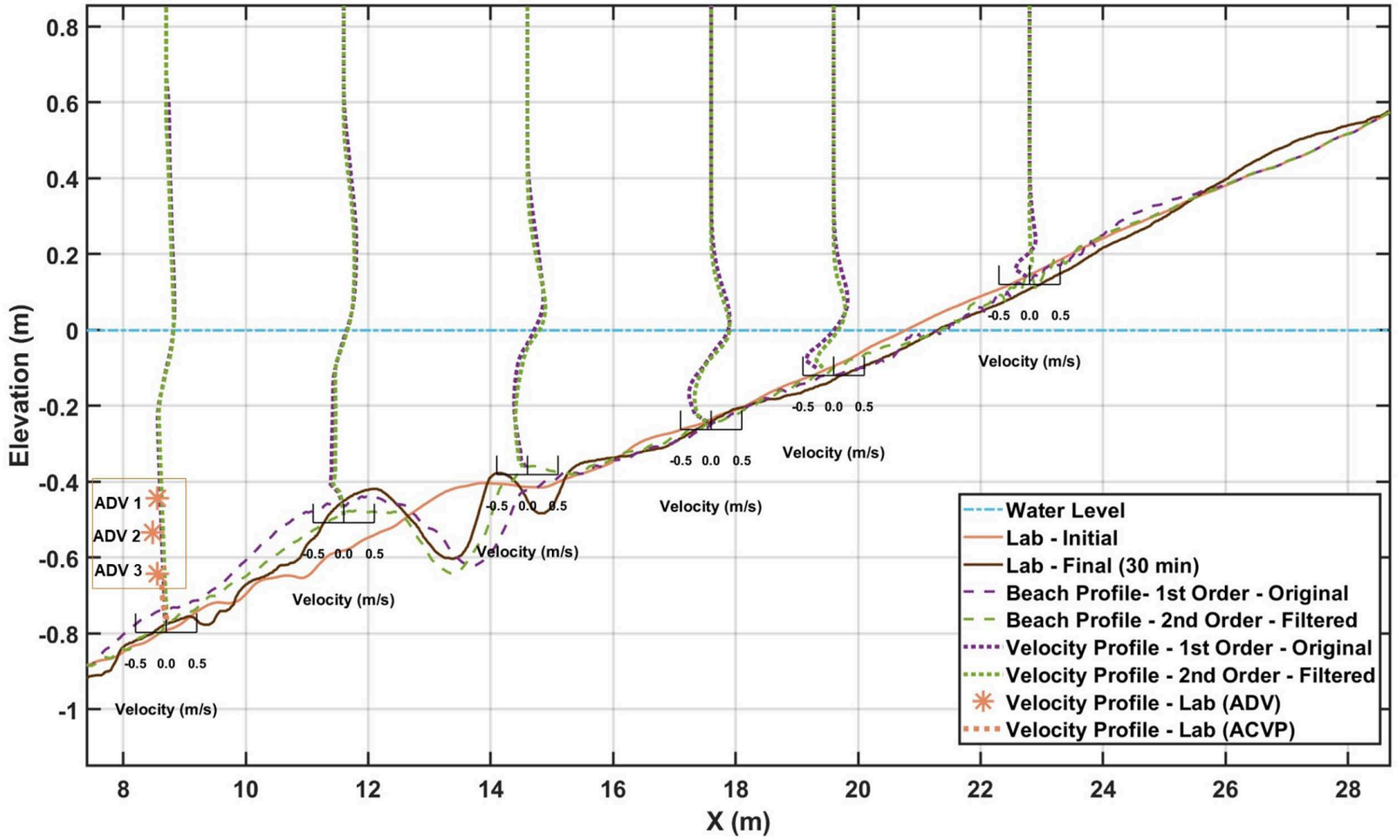

Horizontal Velocity – m/s

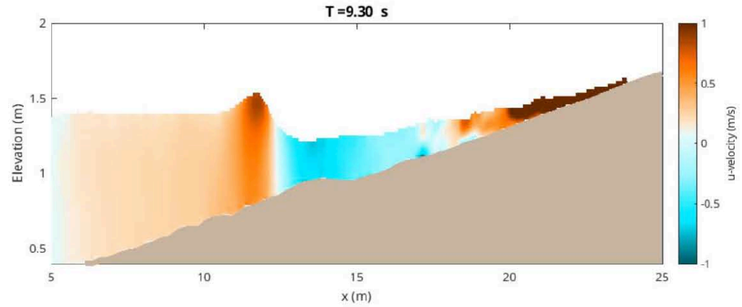

Volumetric sediment concentration – m3/m3

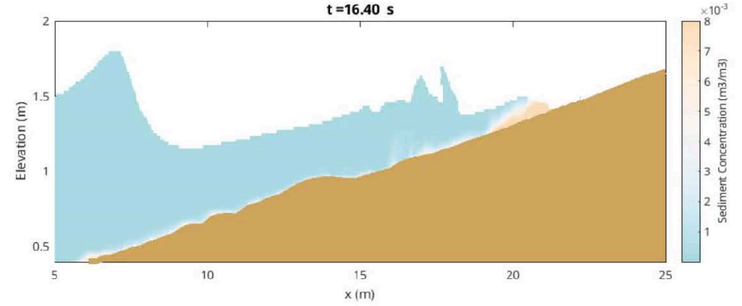

RECAP – BARE BEACH

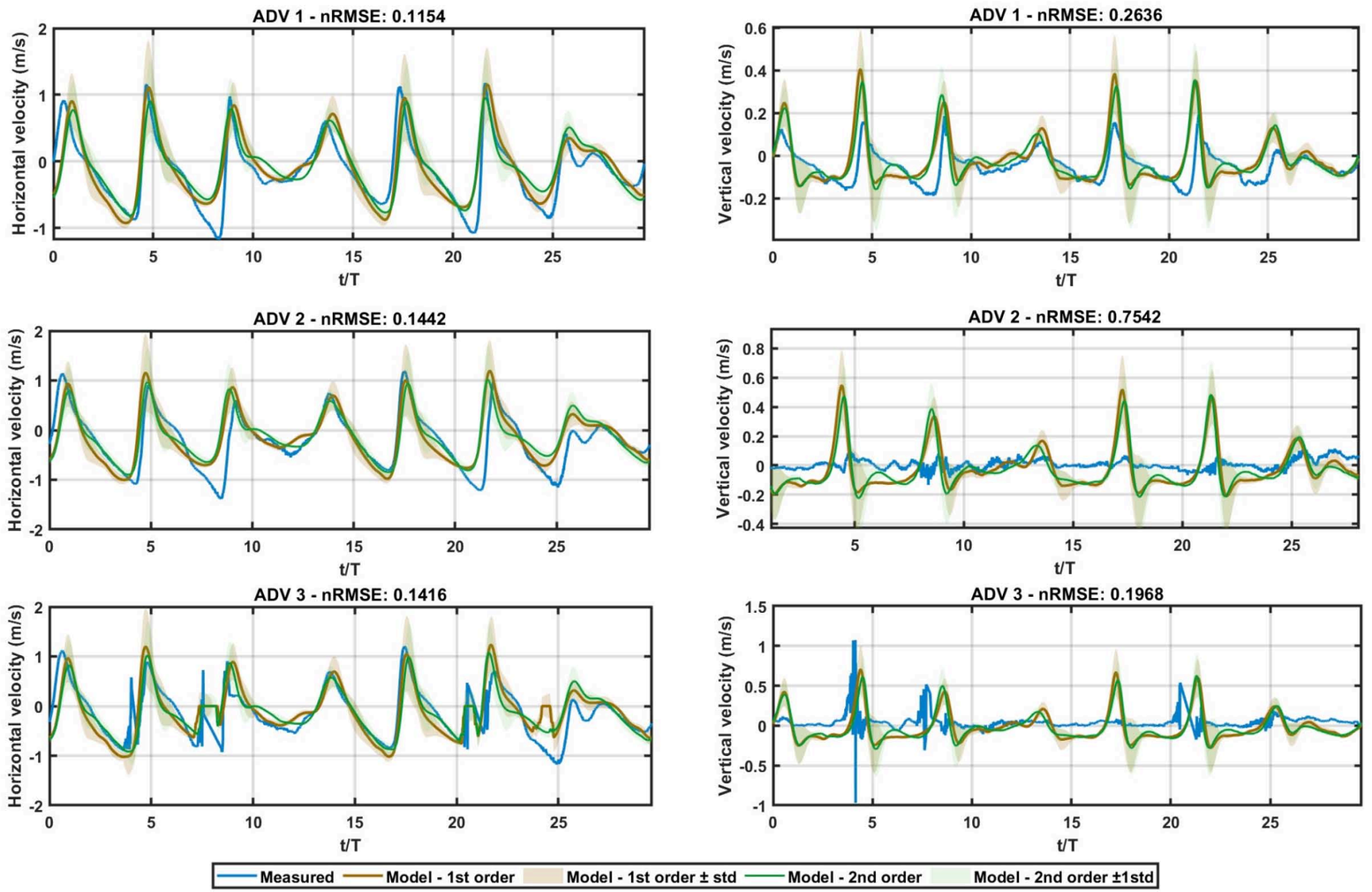

Horizontal Velocity – m/s

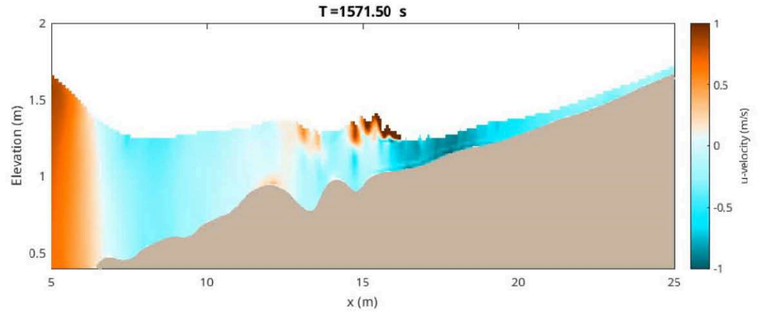

Volumetric sediment concentration – m3/m3

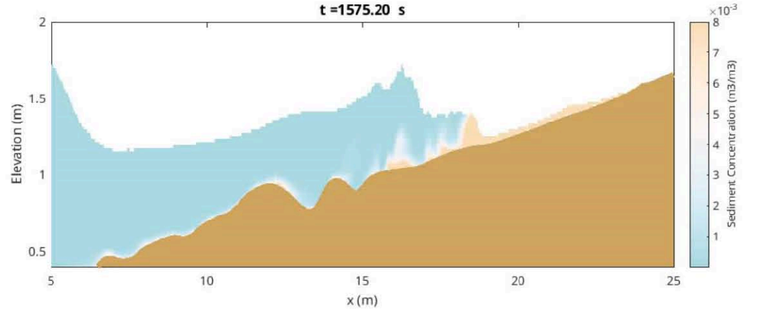

VEGETATION MODEL

Vegetation effect is modeled as a additional drag force term in the governing equation

- ✓Two additional source terms in the k–ε closure model to account for vegetation induced turbulence
- ✓Plant motion is resolved using Morrison equation
- ✓Multiple vegetation types in different meadow orientation possible

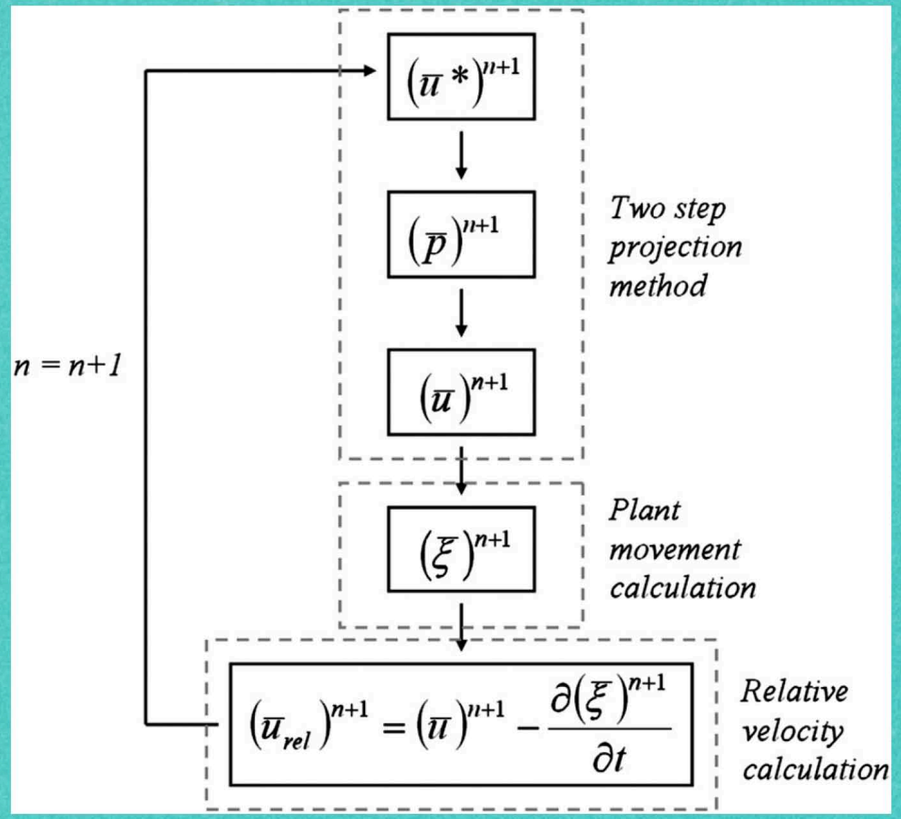

$$\frac{\partial \overline{u_i}}{\partial t} + \overline{u_j}\frac{\partial \overline{u_i}}{\partial x_j} = -\frac{1}{\rho}\frac{\partial \overline{p}}{\partial x_i} + g_i + \frac{1}{\rho}\frac{\partial \overline{\tau_{ij}}}{\partial x_j} - \frac{\partial \overline{(u_i' u_j')}}{\partial x_j} - \overline{F_{D,i}} \qquad \overline{F_{D,i}} = \frac{1}{2} C_D a N \overline{u_{rel,i}} \left|\overline{u_{rel,i}}\right|$$

$$\rho\frac{\partial k}{\partial t} + \rho\overline{u_j}\frac{\partial k}{\partial x_j} = \frac{\partial}{\partial x_j}\left[\left(\frac{\mu_t}{\sigma_k} + \mu\right)\frac{\partial k}{\partial x_j}\right] + \tau_{ij}\frac{\partial \overline{u_i}}{\partial x_j} - \rho\epsilon + \rho C_{kp} C_D a N \sqrt{\overline{u_{rel,i} u_{rel,i}}}\, k_w$$

$$\rho\frac{\partial \epsilon}{\partial t} + \rho\overline{u_j}\frac{\partial \epsilon}{\partial x_j} = \frac{\partial}{\partial x_j}\left[\left(\frac{\mu_t}{\sigma_\epsilon} + \mu\right)\frac{\partial \epsilon}{\partial x_j}\right] + C_{\epsilon 1}\frac{\epsilon}{k}\tau_{ij}\frac{\partial \overline{u_i}}{\partial x_j} - C_{\epsilon 2}\rho\frac{\epsilon^2}{k} + \rho C_{\epsilon p} C_D a N \sqrt{\overline{u_{rel,i} u_{rel,i}}}\, \epsilon_w$$

$$m_0\frac{\partial^2 \xi}{\partial t^2} + c\frac{\partial \xi}{\partial t} + \left(EI\frac{\partial^4 \xi}{\partial x^4}\right) = \frac{1}{2}\rho C_D a\left(\overline{u}\frac{\partial \xi}{\partial t}\right)\left(\overline{u} - \frac{\partial \xi}{\partial t}\right) + (\rho_a - \rho) g V_p \frac{\partial \xi}{\partial z} + \rho V_p \frac{\partial \pi}{\partial t} + \rho C_m V_p \left(\frac{\partial}{\partial t}\left(\frac{\partial \xi}{\partial t}\right)\right)$$

VEGETATED BEACH

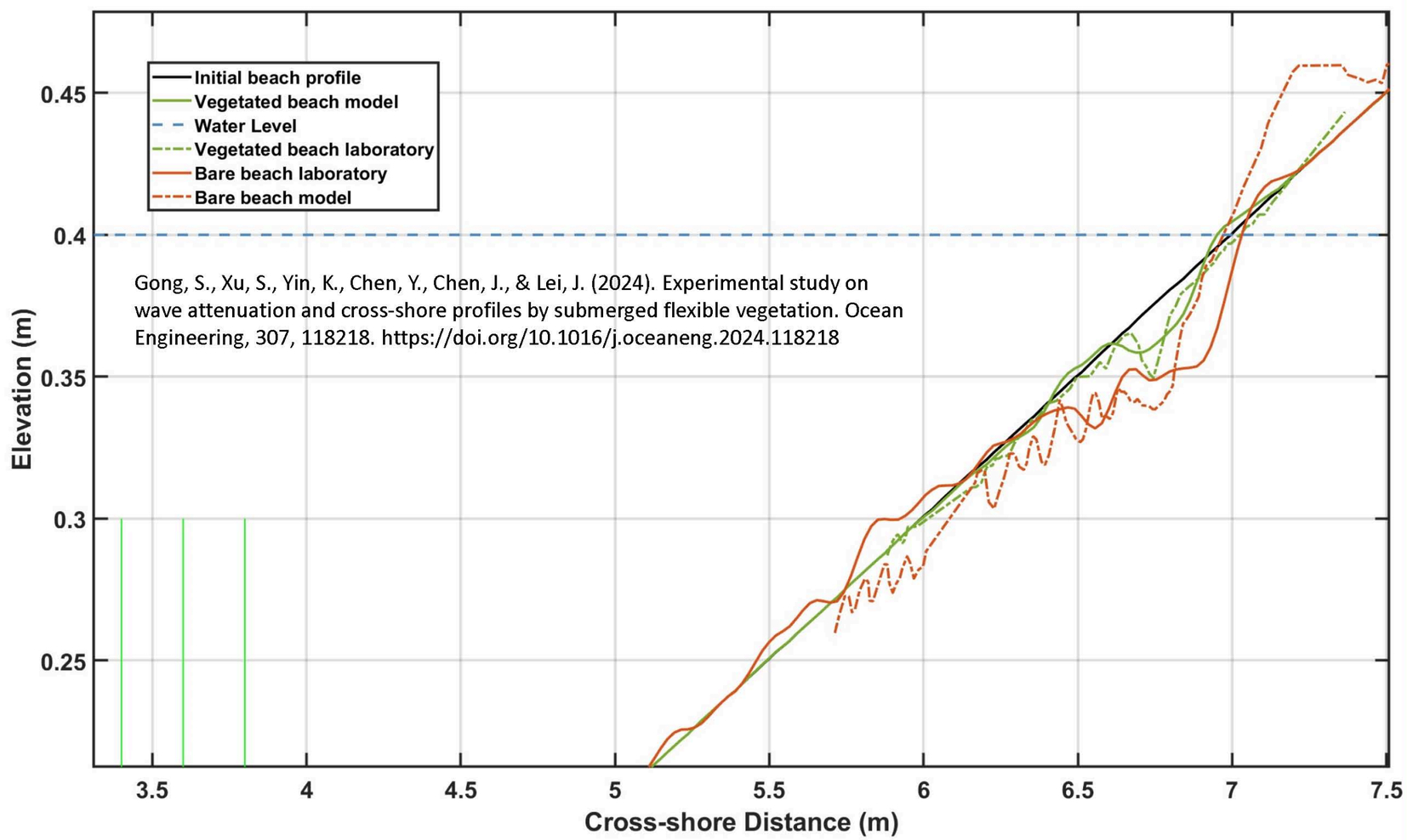

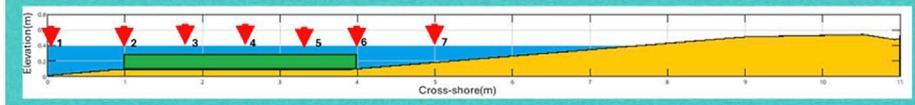

Beach Profile evolution to equilibrium state in a bare beach and a beach confined in the toe of the beach profile with a vegetation field

Vegetation mimic – S. alterniflora
Cd – 1.5
Water Depth – 0.4 m
Wave Height – 0.10 m
Wave Period – 1.5 s

VEGETATED BEACH

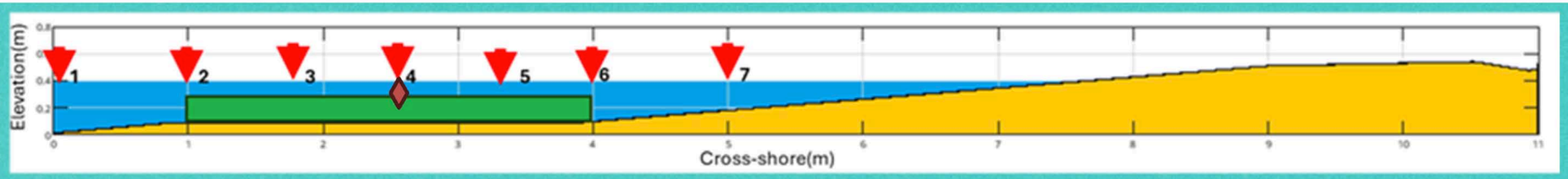

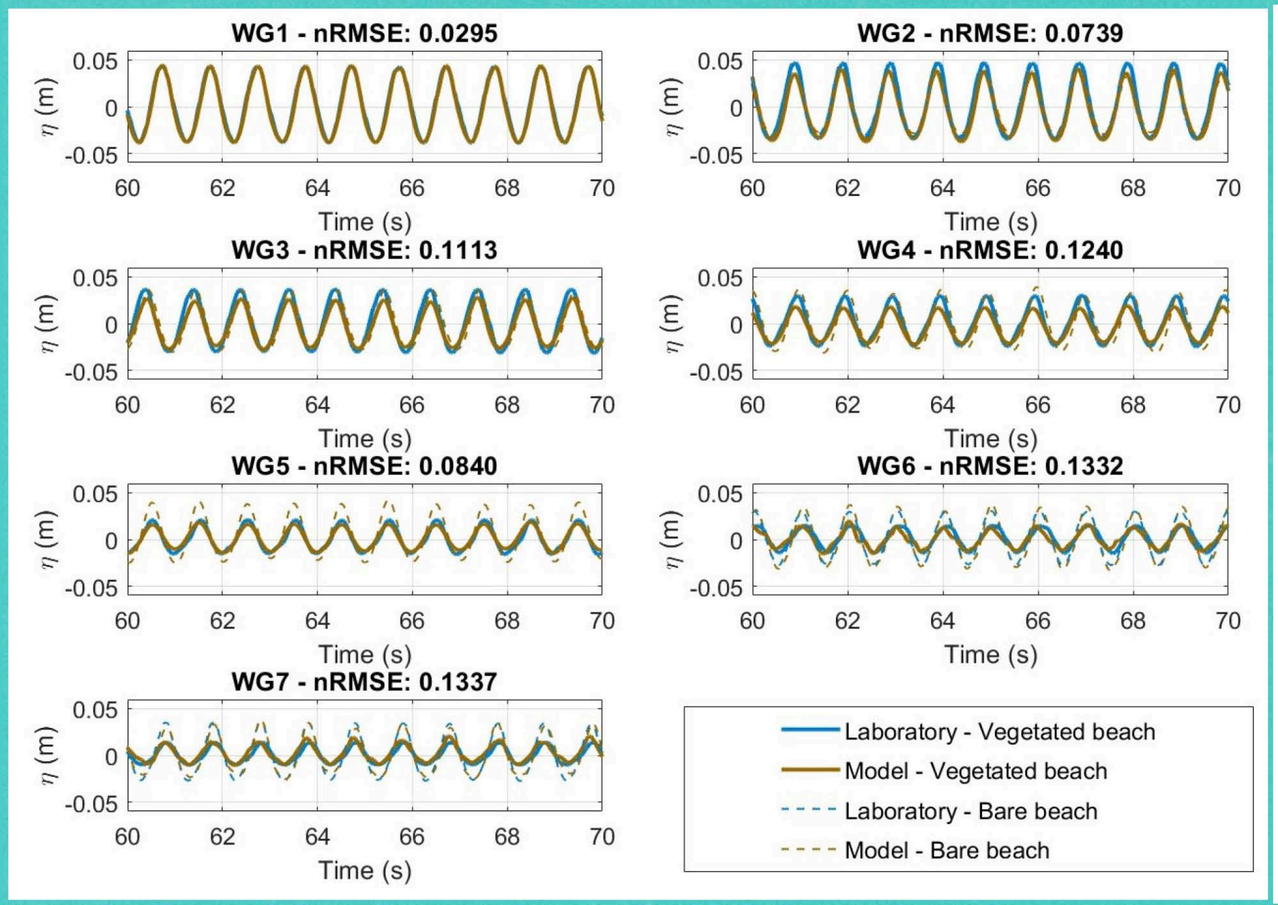

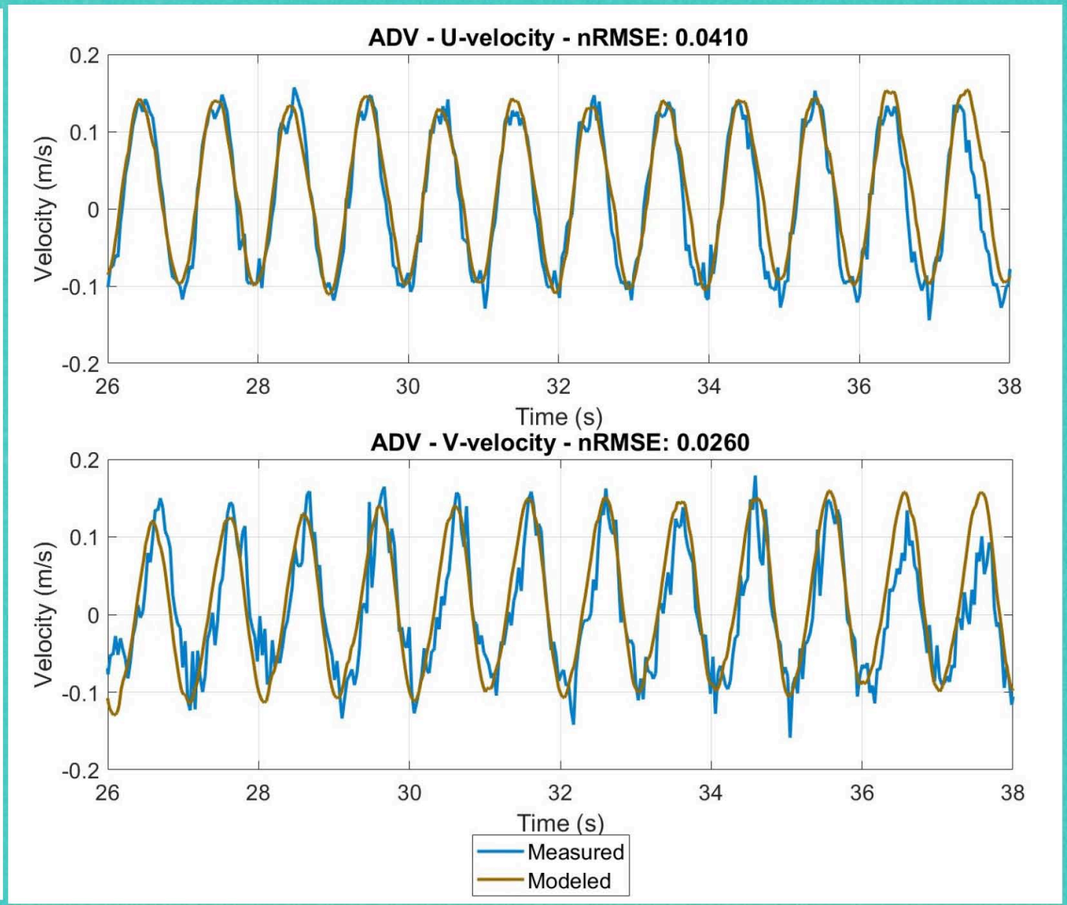

VEGETATED BEACH

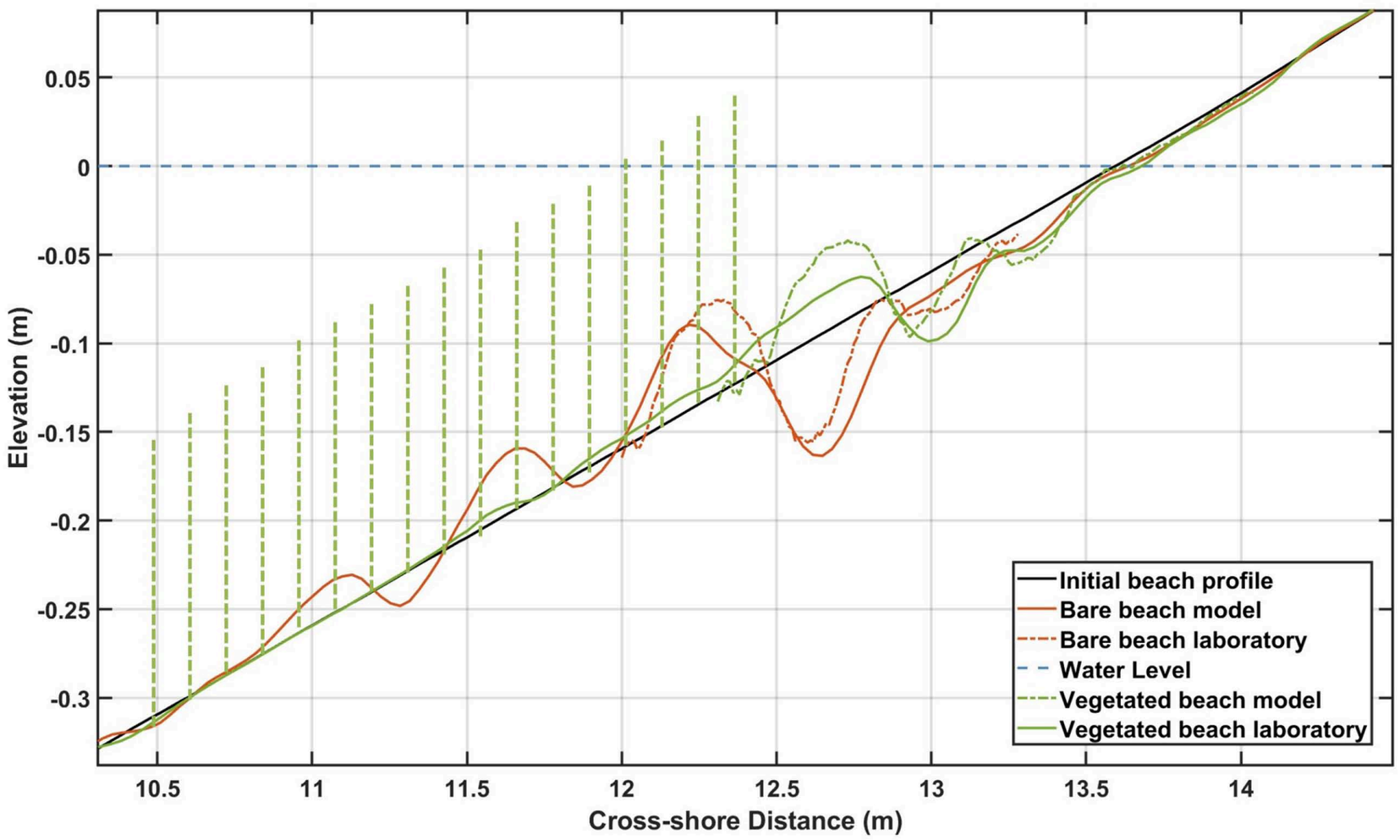

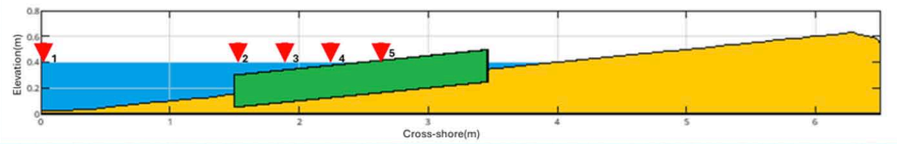

Beach Profile evolution to equilibrium state in a bare beach and a beach confined in the shoaling zone with a vegetation field

Vegetation mimic – P. Oceanica
Cd – 0.5
Water Depth – 0.45 m
Wave height – 0.12 m
Wave Period – 1.5 s

VEGETATED BEACH

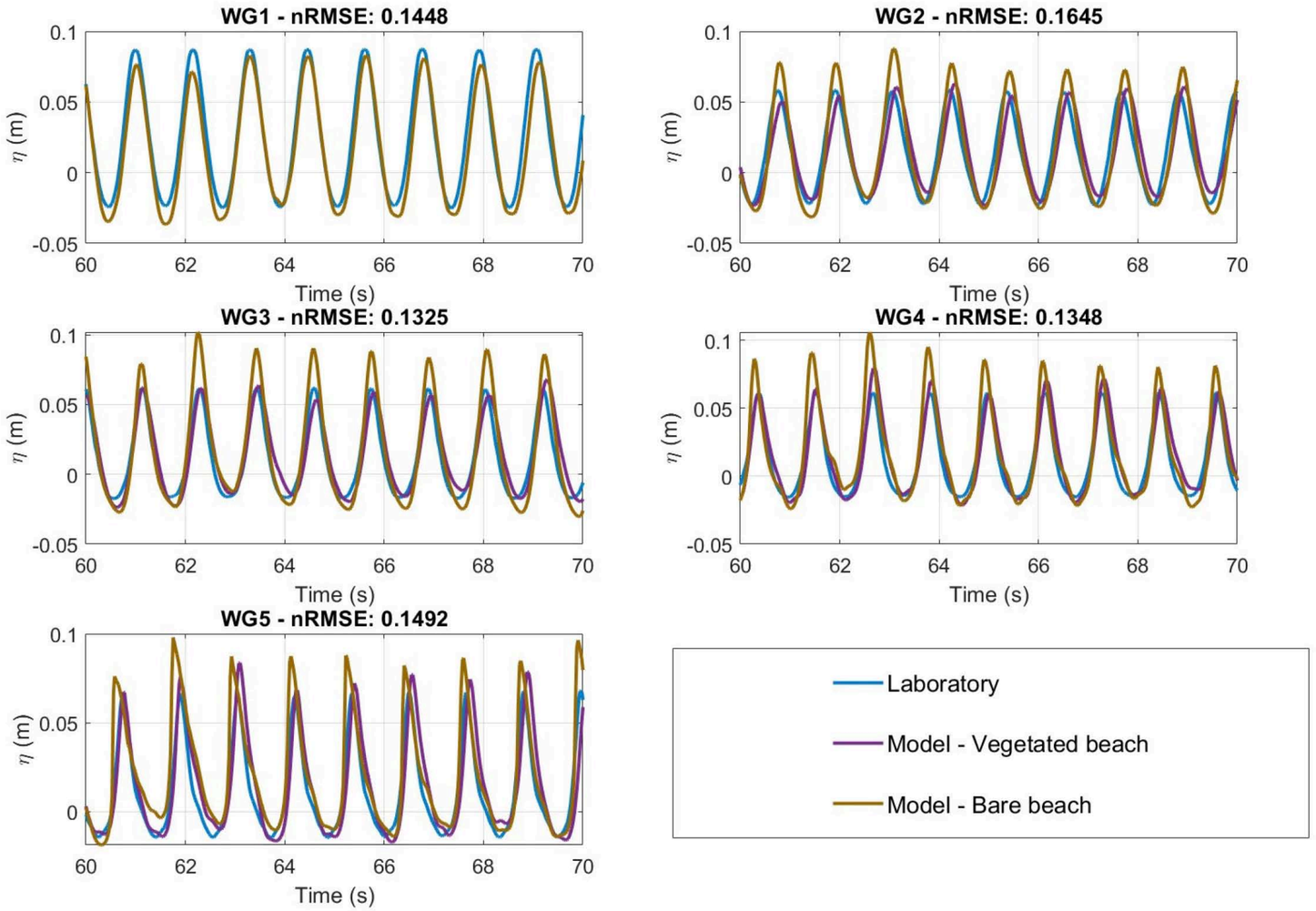

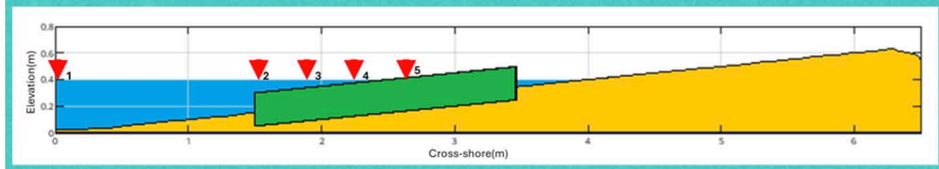

VEGETATED BEACH

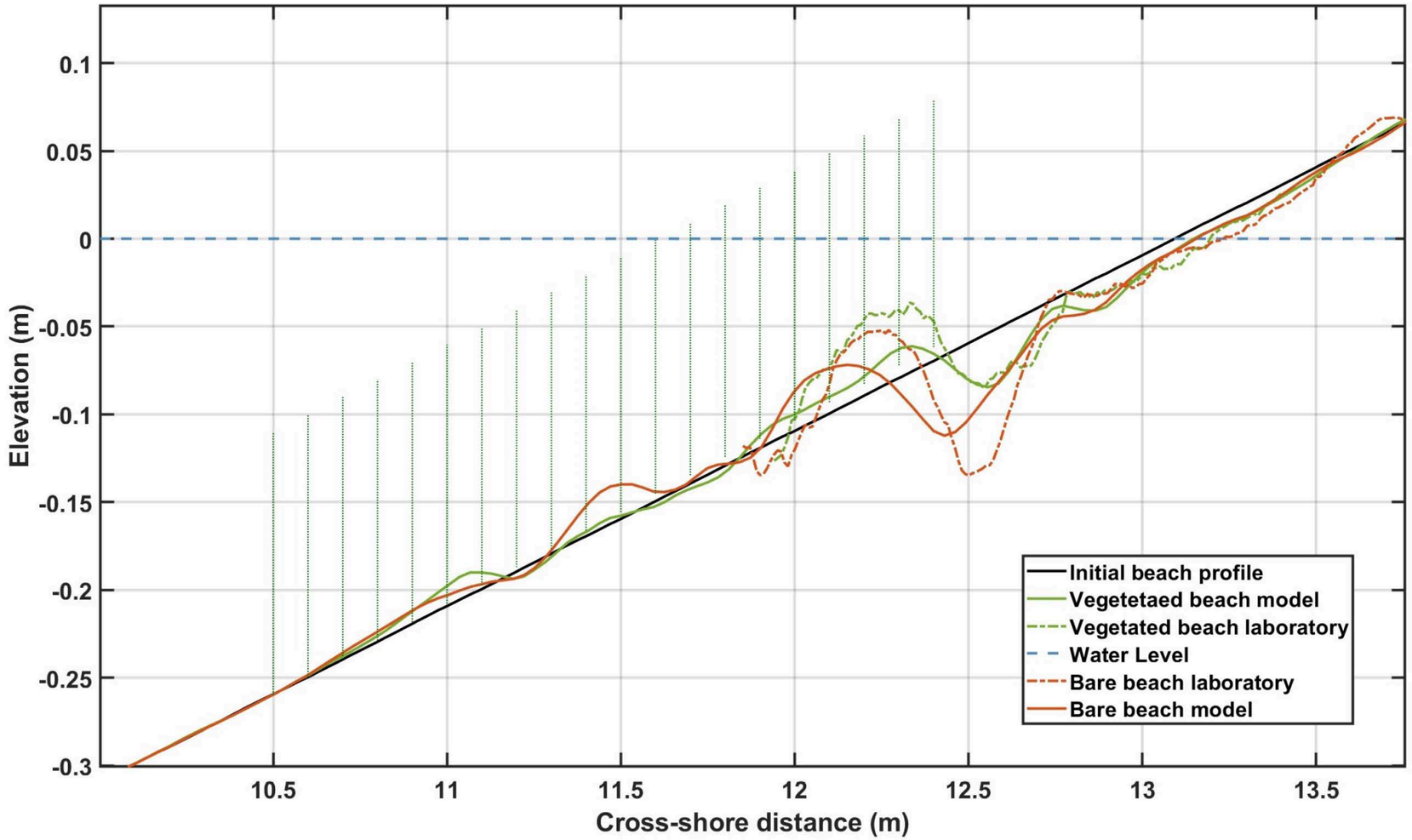

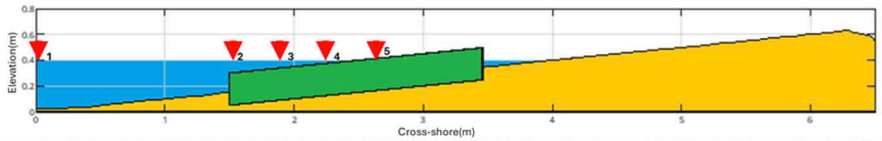

Beach Profile evolution to equilibrium state in a bare beach and a beach confined in the shoaling zone with a vegetation field

Vegetation mimic – P. Oceanica
Cd – 0.5
Water Depth – 0.40 m
Wave height – 0.12 m
Wave Period – 1.5 s

VEGETATED BEACH

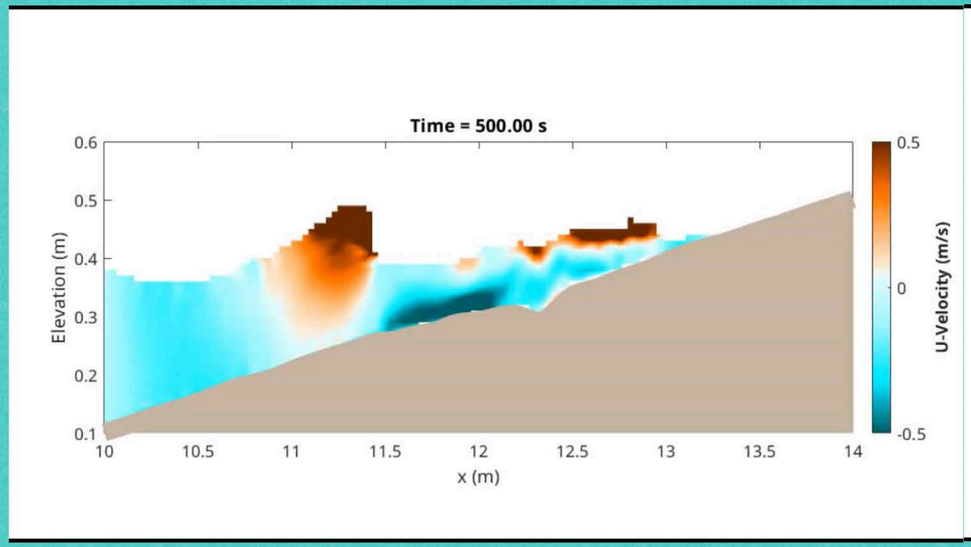

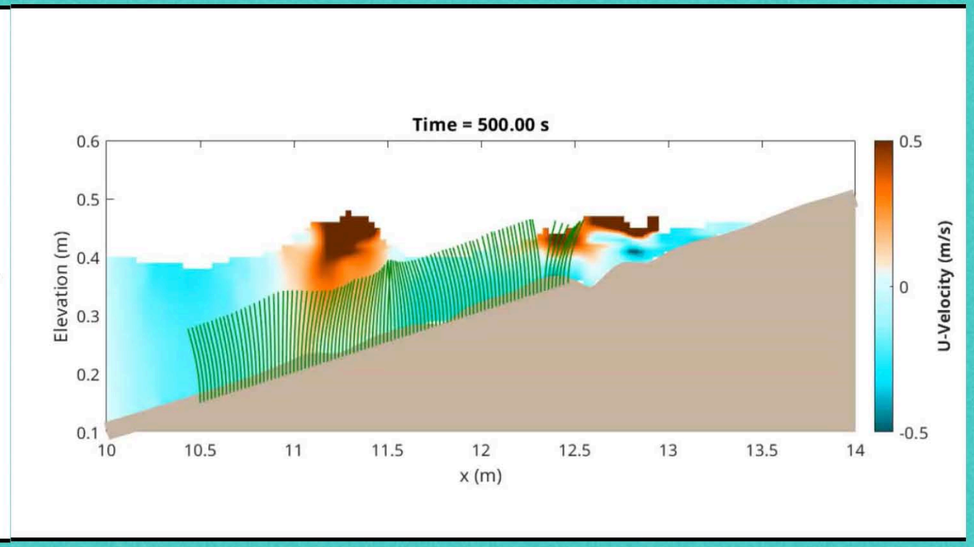

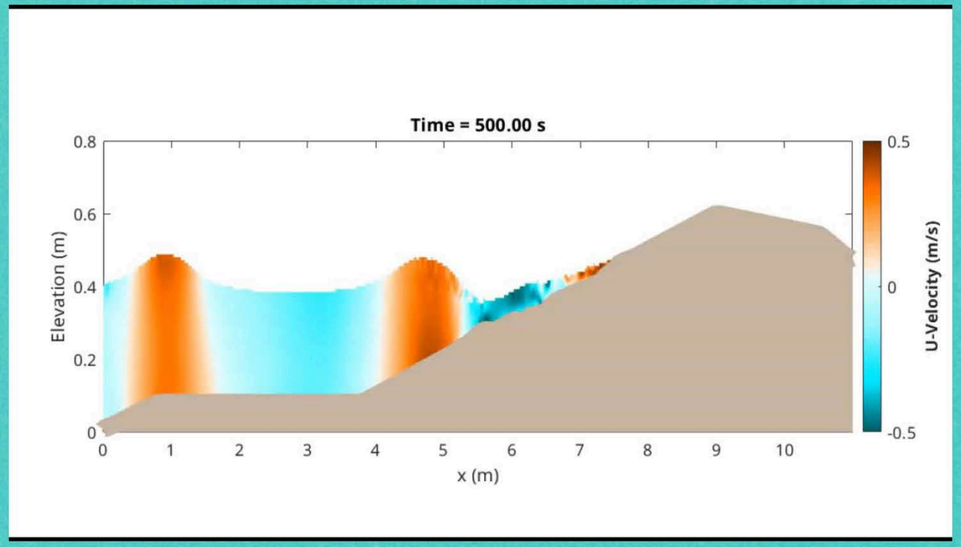

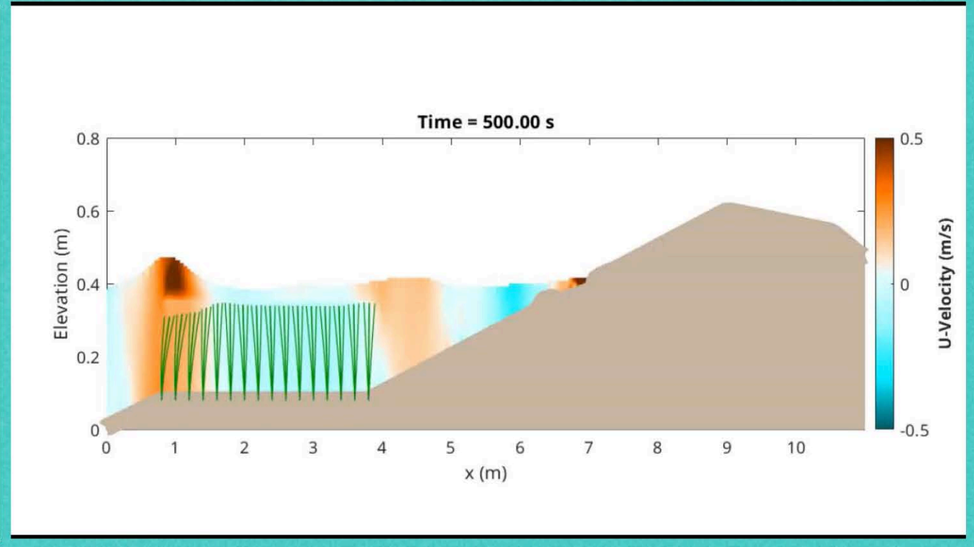

VEGETATED BEACH

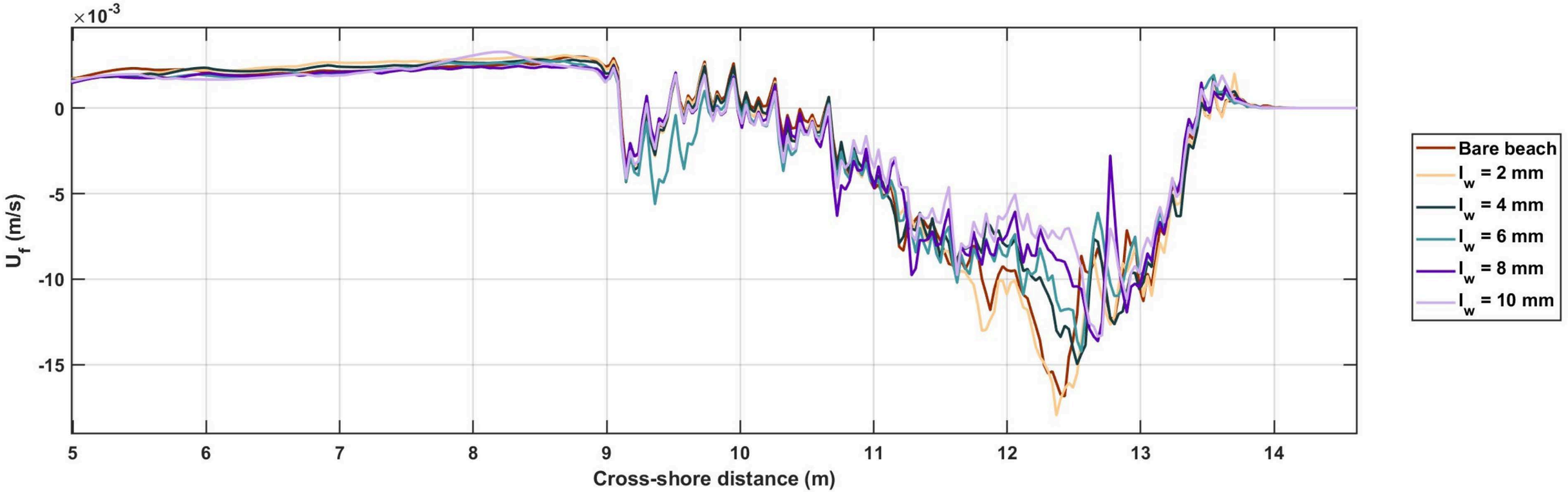

Friction velocity driving sediment transport under different lead width conditions

VEGETATED BEACH

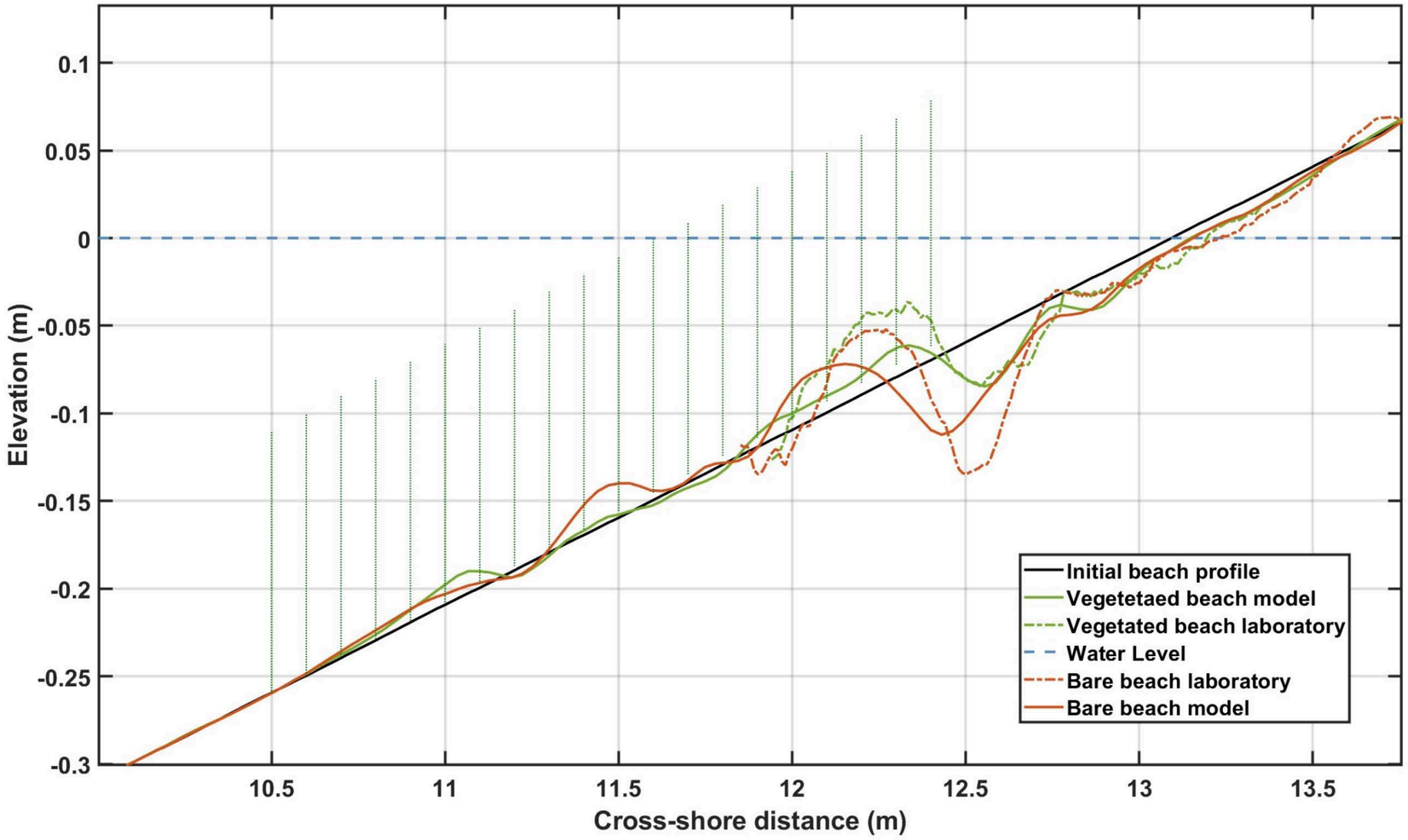

Vegetation mimic – P. Oceanica
Cd – 0.5
Water Depth – 0.40 m
Wave height – 0.12 m
Wave Period – 1.5 s

VEGETATED BEACH

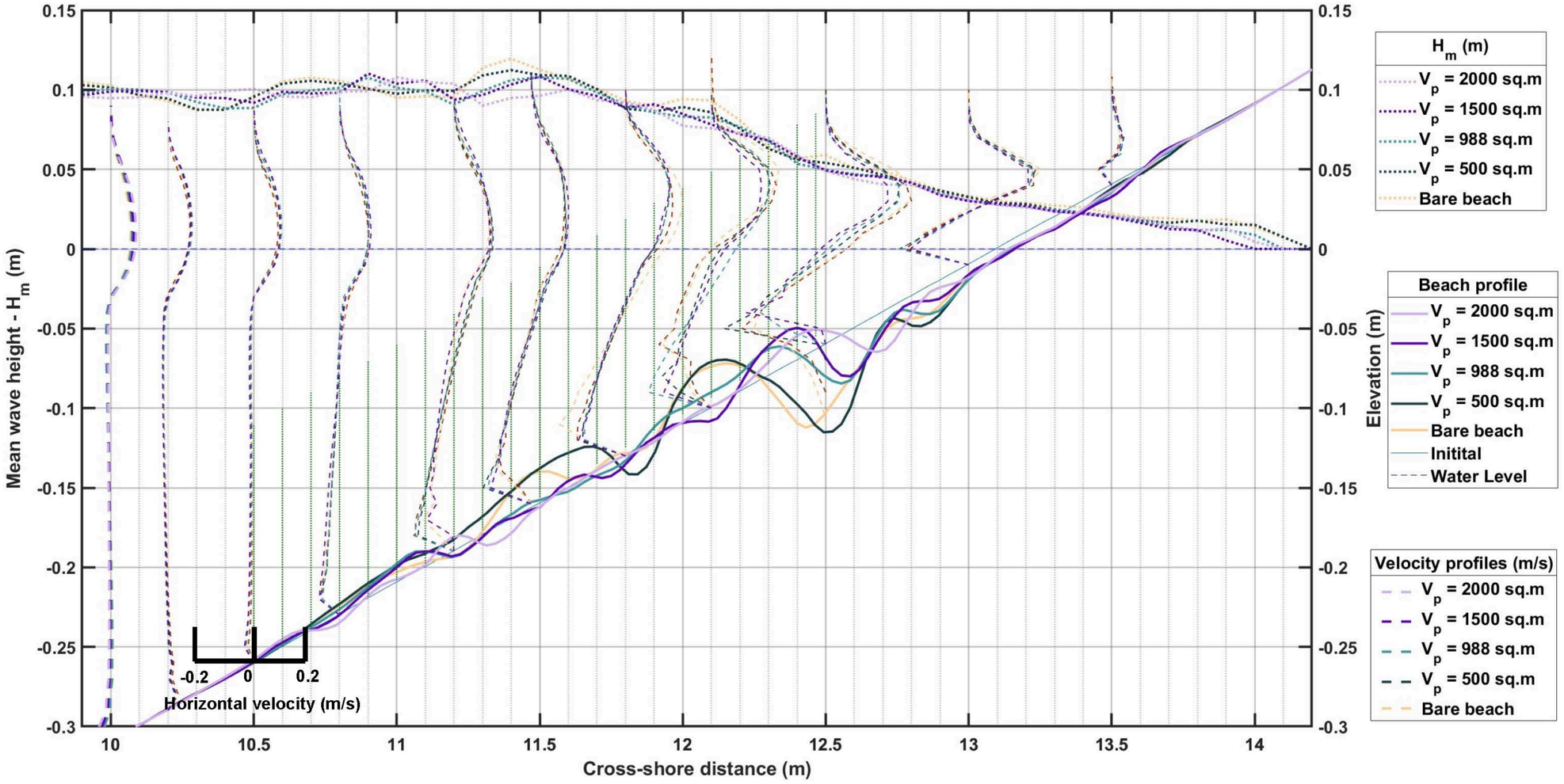

Bed evolution under different vegetation densities

VEGETATED BEACH

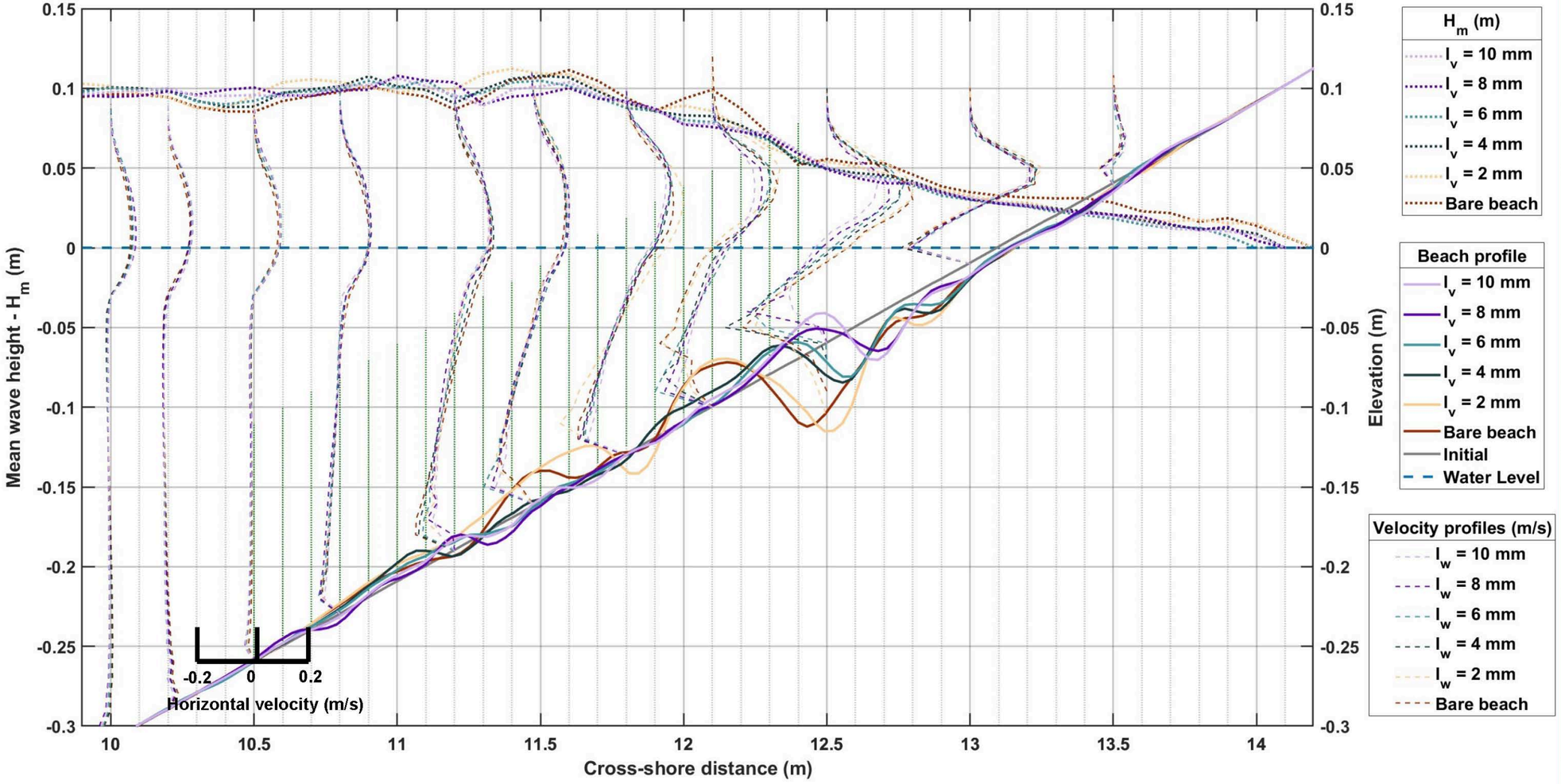

Bed evolution under different leaf width

VEGETATED BEACH

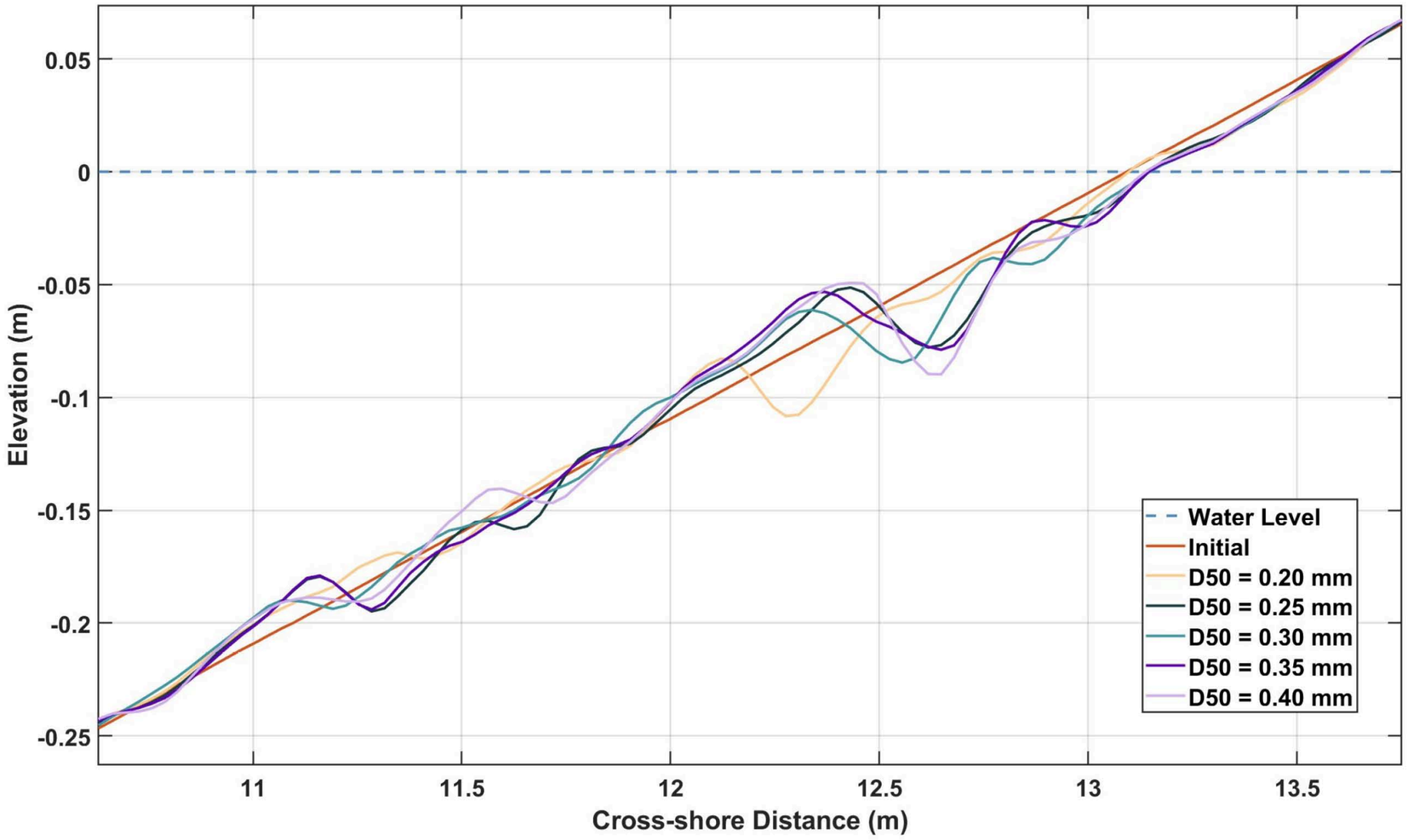

Bed evolution on different grain sizes

CONCLUSION

An efficient model capable of accurate prediction of Morphodynamic evolution for the given wave condition

- ✓No morphological and hydrodynamic calibration
- ✓Difficulty in accurately representing long waves as entirety of laboratory phenomena cannot be captured
- ✓Primary breaking point and the breaker bar evolution is predicted very well
- ✓Attenuation effects of vegetation are captured very well
- ✓Further validation with 2 additional cases of bare beach and vegetated beach before validating for scouring under a vertical seawall

Thank you !

For more information, please reach out to us.

Email

Buckle Subbiah Elavazhagan: subbiahb@unican.es
Maria Maza: mazame@unican.es
Javier Lara: lopezjav@unican.es

Website

www.ihcantabria.com

IH cantabria
INSTITUTO DE HIDRÁULICA AMBIENTAL
UNIVERSIDAD DE CANTABRIA

IH2O

UC
UNIVERSIDAD DE CANTABRIA
Escuela de Doctorado

SEDIMARE
Sediment Transport and Morphodynamics in Marine and Coastal Waters with Engineering Solutions

Funded by the European Union

Mathematical modeling and numerical simulations of water-saturated granular materials with emphasis to sediment transport

Evangelos Petridis

UCLouvain
Institute of Mechanics, Materials and Civil Engineering

Funded by the European Union

This project has received funding from the European Union's Horizon Europe research and innovation programme under the Marie Skłodowska-Curie grant agreement No 101072443.

Introduction

• Underwater dunes are dynamic sedimentary structures shaped by fluid flow. Their migration and evolution can strongly influence the seabed topography. At short term, local changes in dune height affect the flow and sediment transport. At long term, the cumulative motion of dunes can reshape the riverbed or seafloor, impacting ecosystems and engineering considerations such as navigation and flood management.

• Here, the evolution of underwater dunes is modelled using a 2-pressure, 2-velocity flow model for fluid-solid mixtures.

Fluid phase

Governing equations

$$\frac{\partial \phi_{\mathrm{f}}}{\partial t} + \nabla \cdot (\phi_{\mathrm{f}} u_{\mathrm{f}}) = 0,$$

$$\rho_{\mathrm{f}} \frac{\partial \phi_{\mathrm{f}} u_{\mathrm{f}}}{\partial t} + \rho_{\mathrm{f}} \nabla \cdot (\phi_{\mathrm{f}} u_{\mathrm{f}} \otimes u_{\mathrm{f}}) = \nabla \cdot \sigma_{\mathrm{f}} - f + \rho_{\mathrm{f}} \phi_{\mathrm{f}} g$$

Interphasial momentum exchange

$$f = p_{\mathrm{f}} \nabla \phi_{\mathrm{s}} + \delta (u_{\mathrm{f}} - u_{\mathrm{s}})$$

Stress tensor - Newtonian viscous stresses

$$\sigma_{\mathrm{f}} = -p_{\mathrm{f}} \phi_{\mathrm{f}} I + \tau_{\mathrm{f}},$$

For simple isotropic fluids, τ_{s} is further decomposed as the sum of a diagonal and a deviatoric component,

$$\tau_{\mathrm{f}} = \phi_{\mathrm{f}} \zeta_{\mathrm{f}} (\nabla \cdot u_{\mathrm{f}}) I + 2 \phi_{\mathrm{f}} \mu_{\mathrm{f}} D_{\mathrm{f}}^{\mathrm{d}},$$

Solid phase

Governing equations

$$\frac{\partial \phi_s}{\partial t} + \nabla \cdot (\phi_s u_s) = 0,$$

$$\rho_s \frac{\partial \phi_s u_s}{\partial t} + \rho_s \nabla \cdot (\phi_s u_s \otimes u_s) = \nabla \cdot \sigma_s + f + \rho_s \phi_s g$$

Interphasial momentum exchange

$$f = p_f \nabla \phi_s + \delta(u_f - u_s)$$

Stress tensor - Non - Newtonian viscous stresses

$$\sigma_s = -\phi_s p_s I + C_s + \tau_s .$$

Solid phase - Stress tensor

$$\sigma_{\mathrm{s}} = -\phi_{\mathrm{s}} p_{\mathrm{s}} I + C_{\mathrm{s}} + \tau_{\mathrm{s}} .$$

$$C_{\mathrm{s}} = \gamma_{\mathrm{s}} \nabla \phi_{\mathrm{s}} \otimes \nabla \phi_{\mathrm{s}} ,$$

where the coefficient γ_{s} accounts for the spatial distribution of the grains

$$\tau_{\mathrm{s}} = \left(\left(\zeta_{\mathrm{s}} + \zeta_{\mathrm{s}'} \right) \nabla \cdot u_{\mathrm{s}} + \chi_1 \right) \phi_{\mathrm{s}} I + 2 \left(\mu_{\mathrm{s}} + \mu_{\mathrm{s}'} \right) \phi_{\mathrm{s}} D_{\mathrm{s}}^{\mathrm{d}} + \chi_2 \phi_{\mathrm{s}} D_{\mathrm{s}} \cdot D_{\mathrm{s}}$$

where

$$\mu_{\mathrm{s}} = \mu_{\mathrm{f}} \left[\left(2.5 - \frac{2}{\phi_{\mathrm{m}}} \right) + \left(5.2 - \frac{3}{\phi_{\mathrm{m}}^2} \right) \phi_{\mathrm{s}} + \frac{\phi_{\mathrm{m}}^2}{\phi_{\mathrm{s}} \left(\phi_{\mathrm{m}} - \phi_{\mathrm{s}} \right)^2} - \frac{1}{\phi_{\mathrm{s}}} \right]$$

Solid phase - Stress tensor

In particular, all these parameters are nonlinear functions of the strain-rate tensor and read as follows,

$$\mu_{s'} = \frac{\mu_n}{\sqrt{2}} \frac{\det D_s}{(D_s : D_s)^{\frac{3}{2}}}, \qquad \zeta_{s'} = \frac{\mu_n \sqrt{2}}{3} \frac{\det D_s}{(D_s : D_s)^{\frac{3}{2}}},$$

$$\chi 1 = -\sqrt{2}\mu_n \left(2\sqrt{D_s^d : D_s^d} - \frac{3}{2} \frac{D_s^d : D_s^d}{\sqrt{D_s : D_s}} \right), \quad \chi 2 = -\frac{\sqrt{2}\mu_n}{\sqrt{D_s : D_s}},$$

Where

$$\mu_n = 0.75\, \mu_f \frac{\phi_s}{(\phi_m - \phi_s)^2}.$$

Compaction equation

The above system of balance laws is closed with an evolution equation for the volume fraction ϕ_{s}. This equation is referred to as *compaction equation*

$$\frac{\partial \phi_{\mathrm{s}}}{\partial t} + u_{\mathrm{s}} \cdot \nabla \phi_{\mathrm{s}} = Re \frac{\phi_{\mathrm{s}}\, \phi_{\mathrm{f}}}{\mu_{\mathrm{c}}} \left(p_{\mathrm{s}} - p_{\mathrm{f}} - \beta_{\mathrm{s}} + \nabla \cdot \left(\gamma_{\mathrm{s}} \nabla \phi_{\mathrm{s}} \right) \right)$$

β_{s} is the configuration pressure which is a logarithmic function of ϕ_{s} and ϕ_{max}. γ_{s} is related to the microstructure - power law function of ϕ_{s} .

Simulations

• The algorithm used to solve the equations is based on a predictor-corrector time-integration scheme with a generalized projection method for the phasic pressures.

• In the simulations, the images are shown in dimensionless form. The actual domain dimensions are 0.6 m in x and 0.3 m in y.

• A parabolic initial velocity profile and an appropriate pressure gradient along the x-axis are enforced.

• The initial solid volume fraction is set to $\phi_s = 0.59$.

• First, we present simulations with an initial velocity of 0.5 m/s for three different amplitudes. Next, we explore different velocities for the medium amplitude case.

Maximum initial velocity $u = 0.5$ m/s

Maximum initial velocity $u = 0.5$ m/s

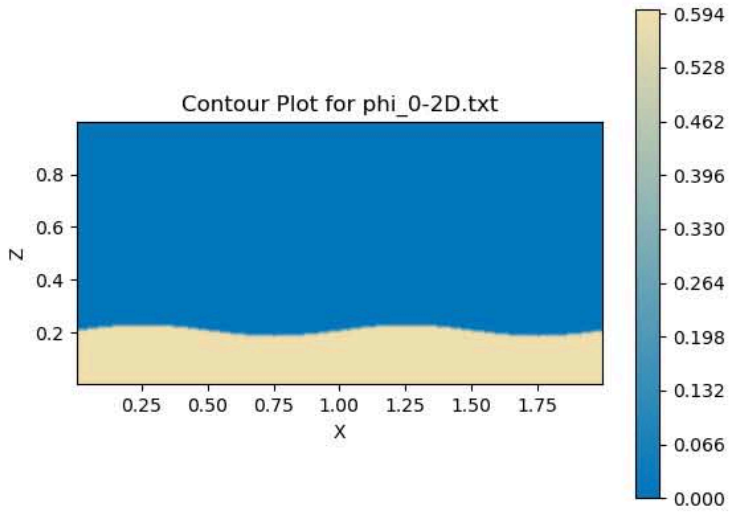

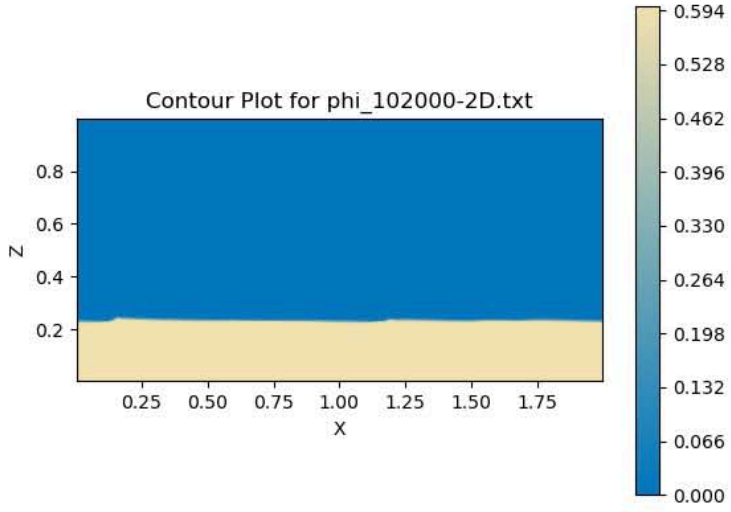

Maximum initial velocity $u = 0.5$ m/s

Maximum initial velocity $u = 0.5$ m/s

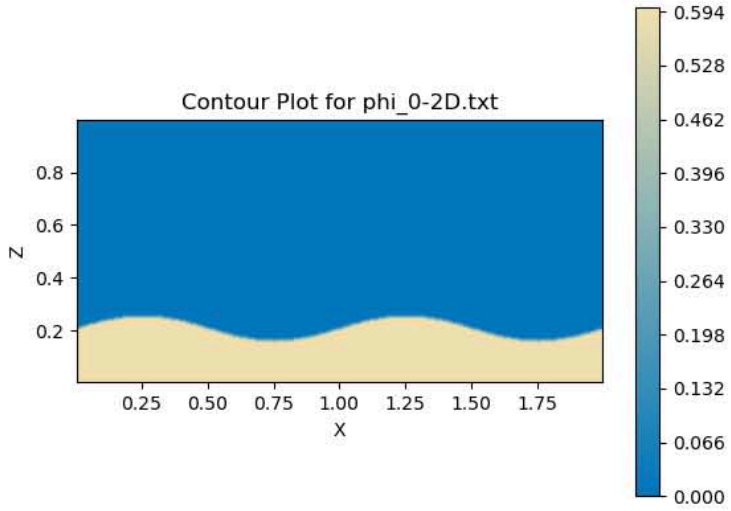

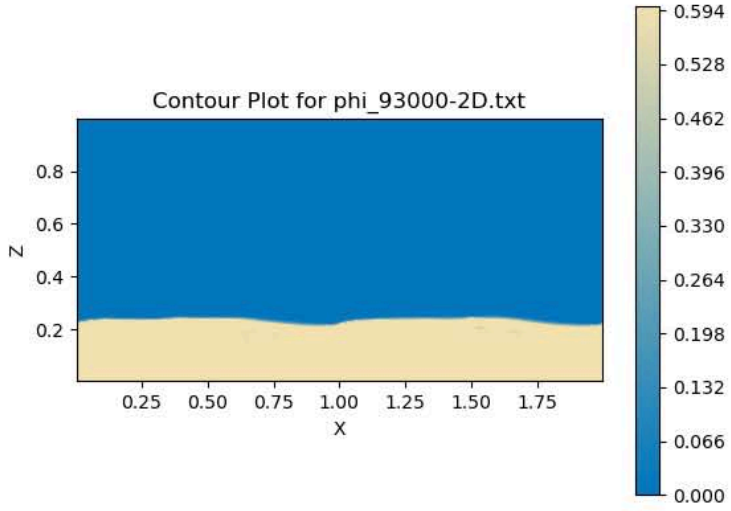

Maximum initial velocity $u = 0.5$ m/s

Maximum initial velocity $u = 0.5$ m/s

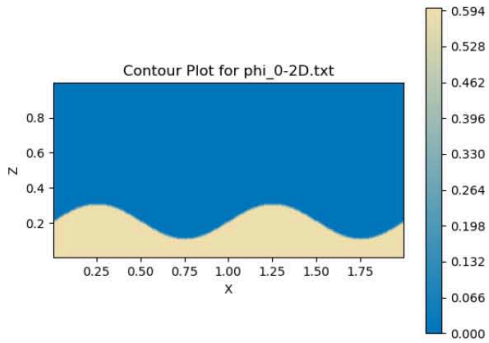

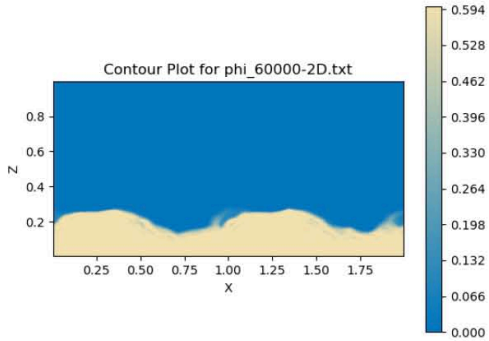

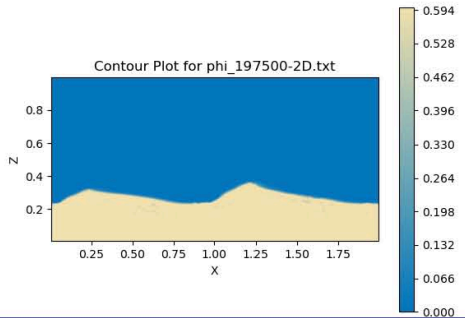

Velocity Field and Vorticity ($t = 1.5s$)

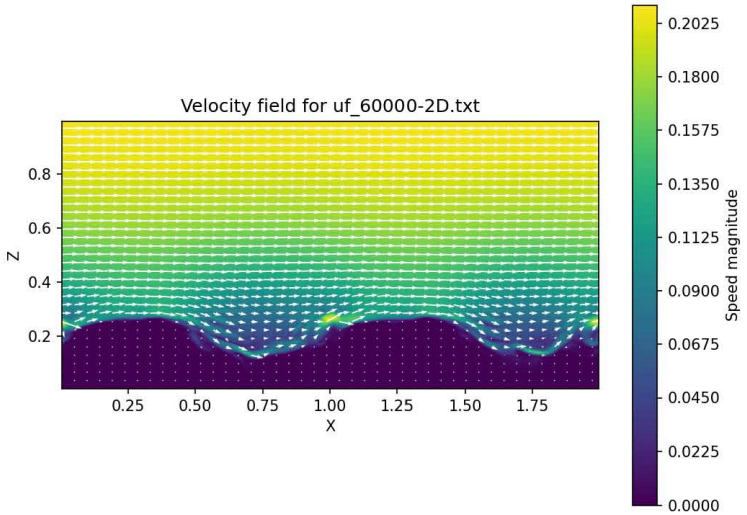

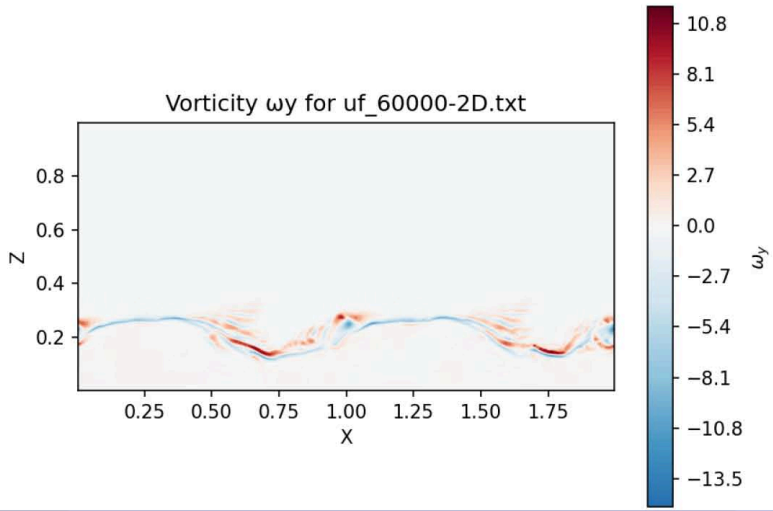

Velocity Field and Vorticity ($t = 5s$)

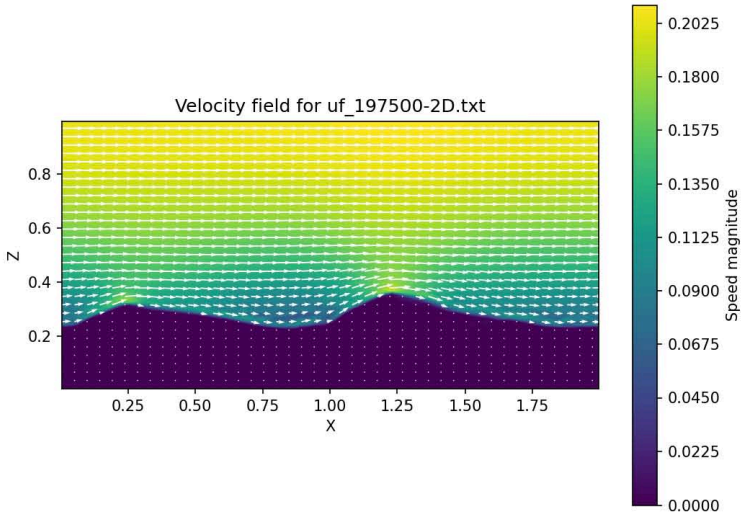

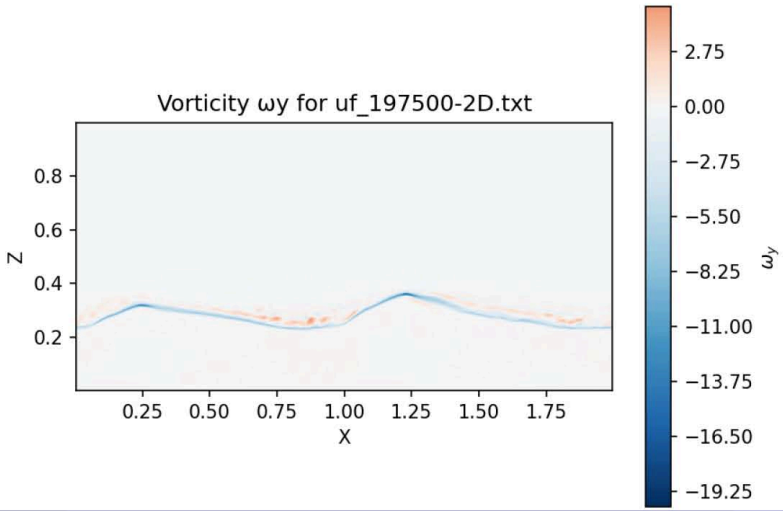

Maximum initial velocity $u = 1$ m/s

Maximum initial velocity $u = 1$ m/s

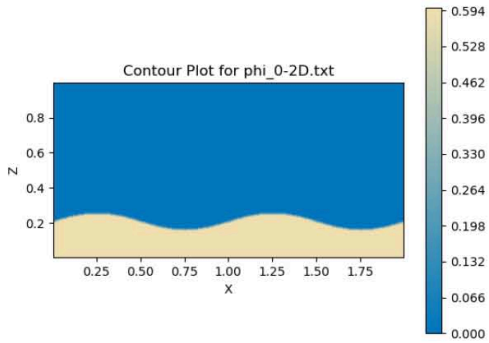

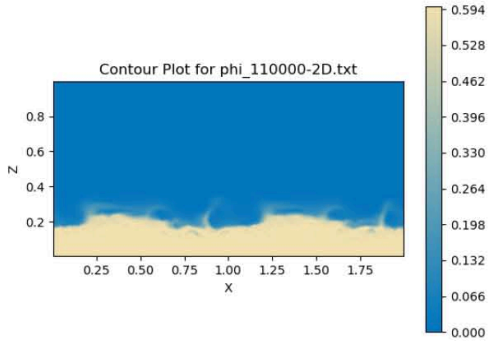

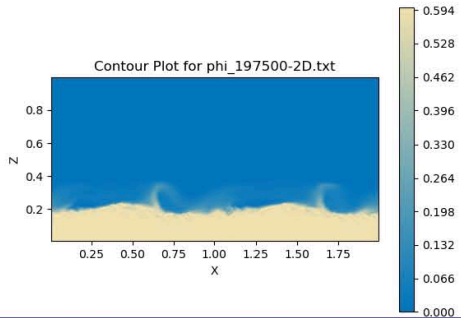

Maximum initial velocity $u = 1.5$ m/s

Maximum initial velocity $u = 1.5$ m/s

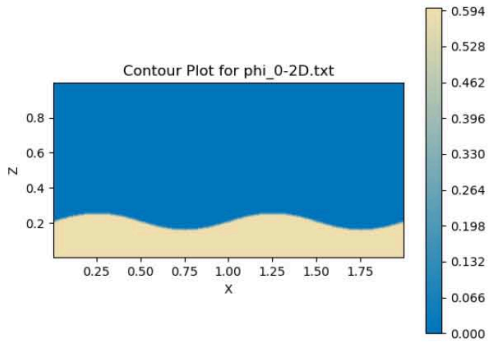

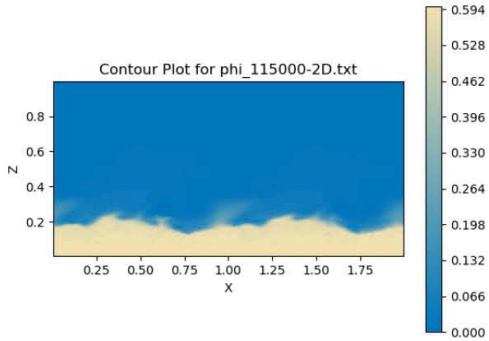

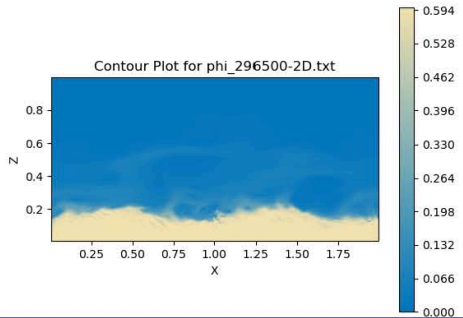

Velocity Field and Vorticity ($t = 3s$)

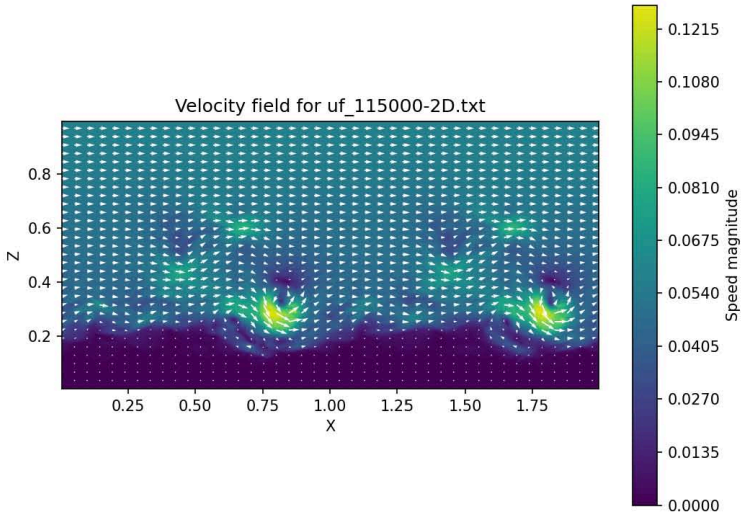

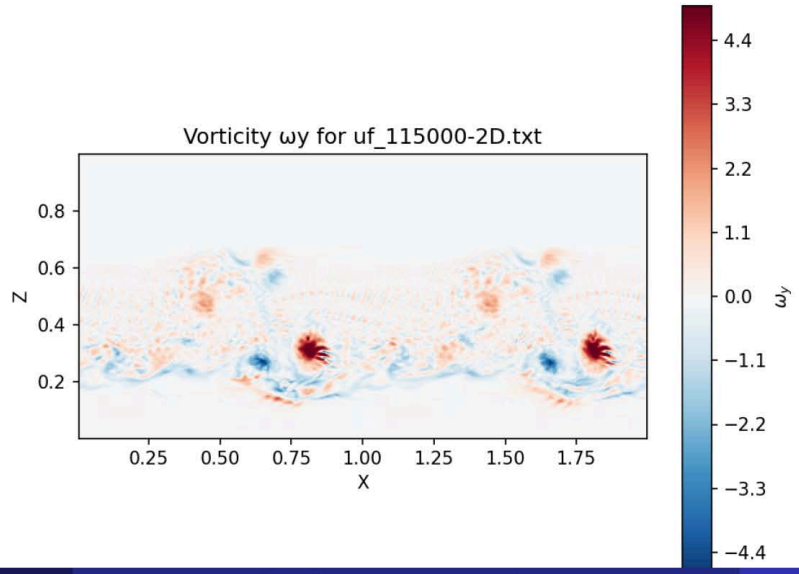

Velocity Field and Vorticity ($t = 7.5s$)

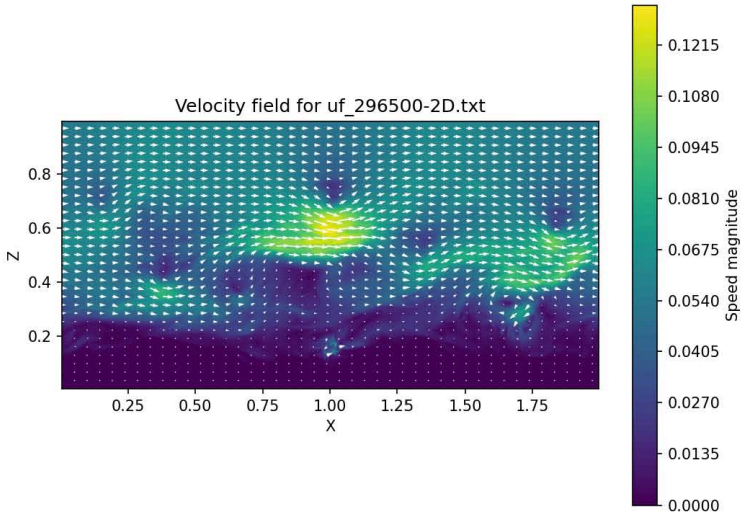

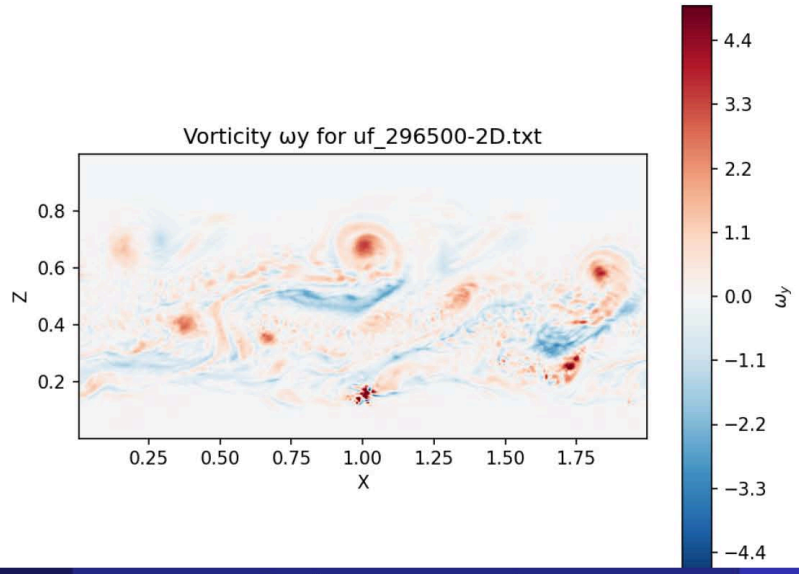

Future Work

- Extend the simulations to more realistic dune geometries, where the length is about 30–100$\times$ the height.
- Investigate subcritical flow regimes, focusing on cases with Froude number $\mathrm{Fr} < 0.3$.
- Eventually, compare the numerical results with previous experimental findings.

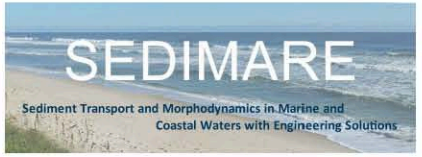

Erosion threshold of sand-silt-clay mixtures

P.S. Miranda, J.J. van der Werf, S.J.M.H. Hulscher

HR Wallingford – SEDIMARE Technical Workshop

Deltares UNIVERSITY OF TWENTE.

jowi.miranda@deltares.nl
p.s.miranda@utwente.nl

psmiranda

Funded by the European Union

Marie Skłodowska-Curie Actions

This study is financially support by the European Union's (EU) Horizon Europe Framework Programme (HORIZON) via SEDIMARE (Grant Agreement No. 101072443), an MSCA Doctoral Network (HORIZON-MSCA-2021-DN-01).

Sand-mud

- Sand-mud common type of sediments in estuaries, deltas, and ports.
- Sediment composition governs morphological development
- Key aspect: erosion threshold

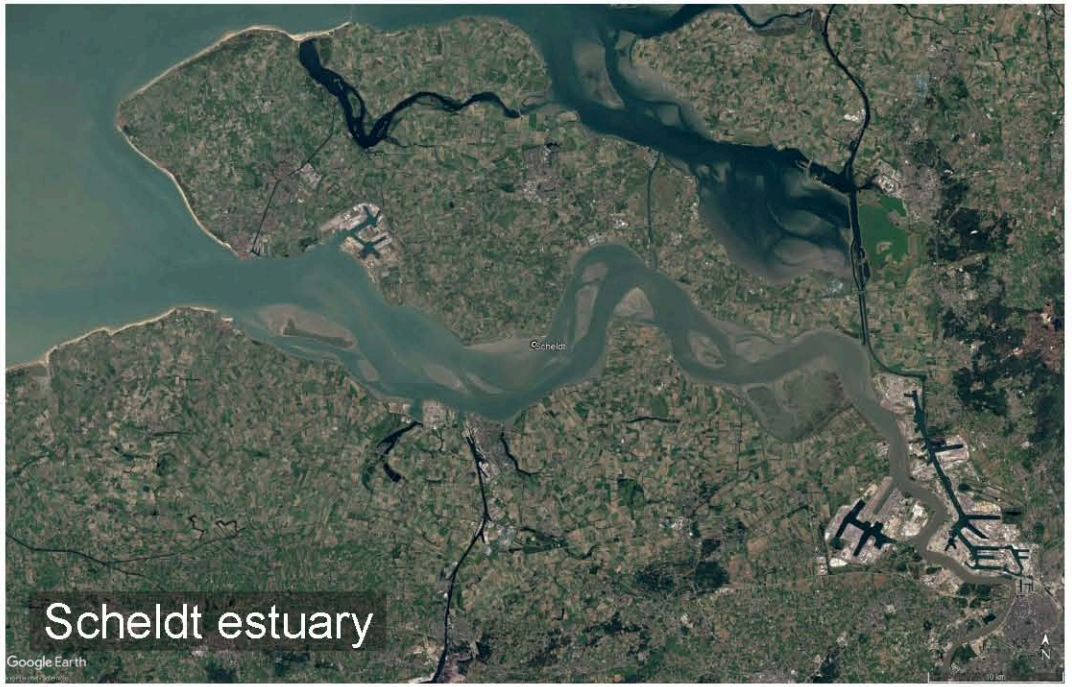

Funded by the European Union

Marie Skłodowska-Curie Actions

This study is financially support by the European Union's (EU) Horizon Europe Framework Programme (HORIZON) via SEDIMARE (Grant Agreement No. 101072443), an MSCA Doctoral Network (HORIZON-MSCA-2021-DN-01).

Study objectives

Integrated framework for the initiation of motion of sand-silt-clay based on bulk geotechnical parameters

1. Consolidate erosion threshold data from previous studies.
2. Classify data into 6 regimes, representing distinct erosion behavior
3. **Propose new erosion threshold equations using only bulk parameters**

Funded by the European Union

Marie Skłodowska-Curie Actions

This study is financially support by the European Union's (EU) Horizon Europe Framework Programme (HORIZON) via SEDIMARE (Grant Agreement No. 101072443), an MSCA Doctoral Network (HORIZON-MSCA-2021-DN-01).

Framework selection

- Van Ledden bed types (Van Ledden et al., 2004)
  - Cohesion

$$P_{clay} = 7\%$$

  - Network structure
    - Sand-dominated network structure:

$$\phi_{sand} \geq 40\%$$

    - Silt-dominated network structure:

$$\frac{\phi_{silt}}{(1-\phi_{sand})} \geq 40\%$$

    - Other network structures:
      1. Clay-water matrix
      2. Mixed structures

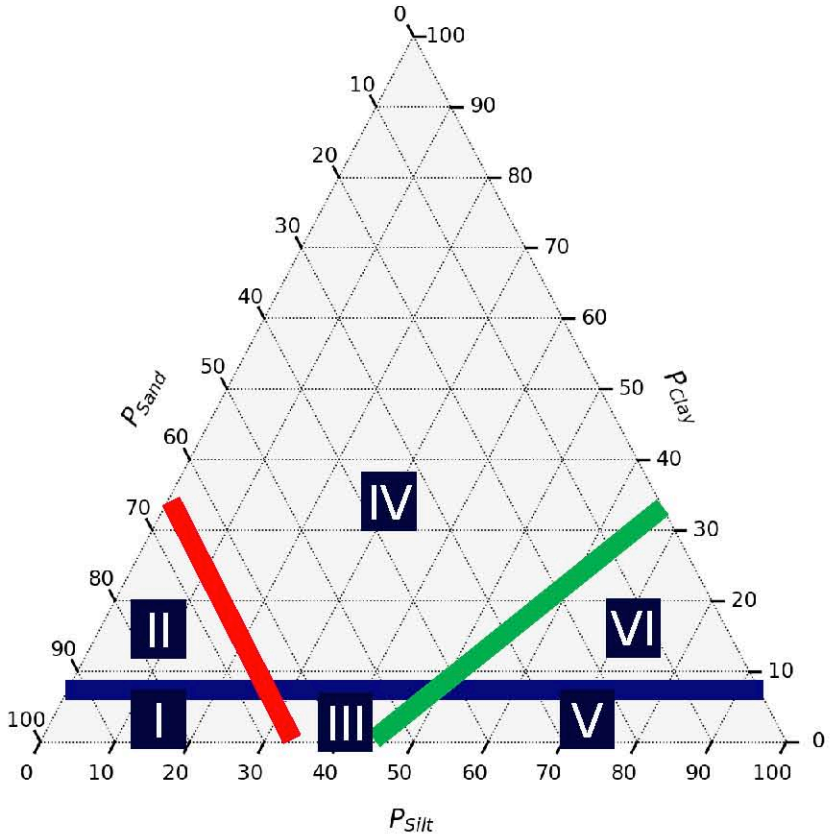

Mass fractions: $1 = P_{sand} + P_{silt} + P_{clay} = P_{sand} + P_{mud}$

Volume fractions: $1 = \phi_{sand} + \phi_{silt} + \phi_{clay} + \phi_{water}$

Funded by the European Union

Marie Skłodowska-Curie Actions

This study is financially support by the European Union's (EU) Horizon Europe Framework Programme (HORIZON) via SEDIMARE (Grant Agreement No. 101072443), an MSCA Doctoral Network (HORIZON-MSCA-2021-DN-01).

Compiled classified dataset

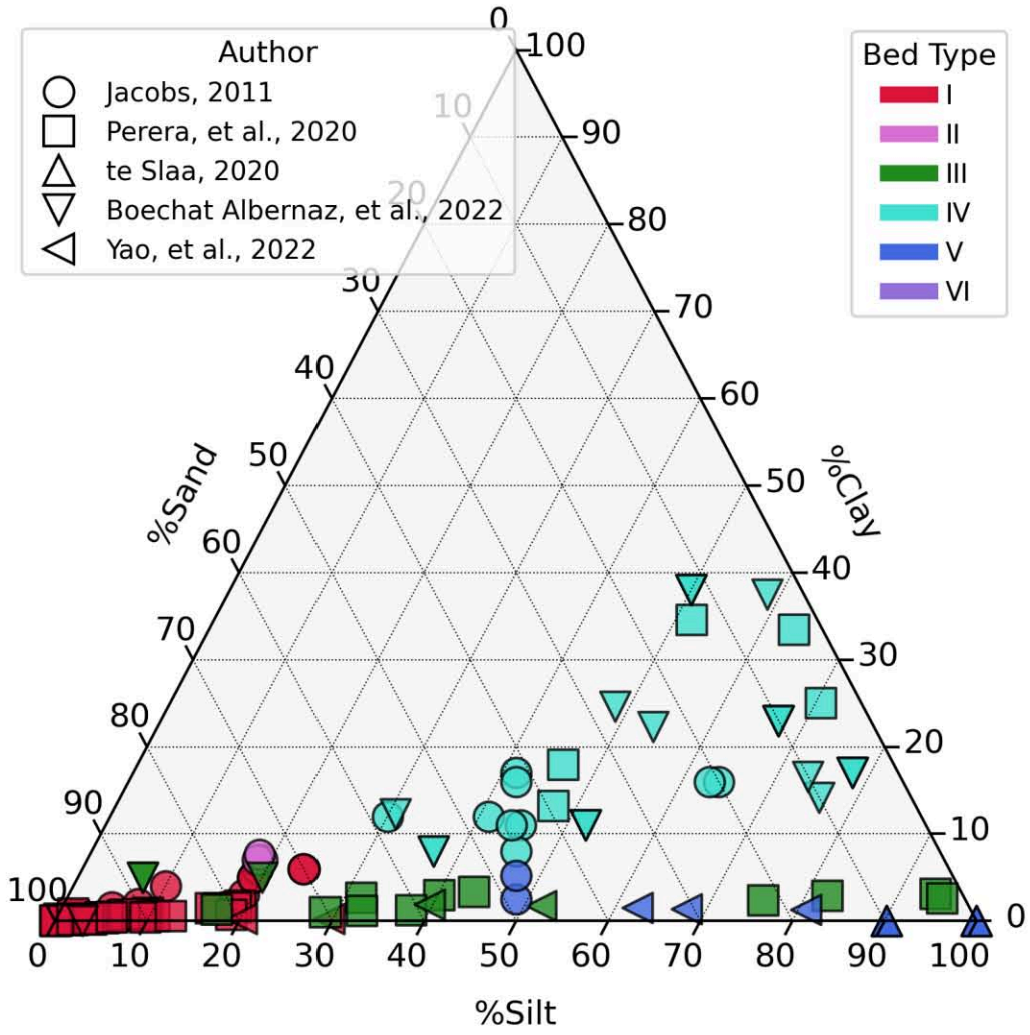

This study is financially support by the European Union's (EU) Horizon Europe Framework Programme (HORIZON) via SEDIMARE (Grant Agreement No. 101072443), an MSCA Doctoral Network (HORIZON-MSCA-2021-DN-01).

Regression analysis

SEDIMARE
Sediment Transport and Morphodynamics in Marine and Coastal Waters with Engineering Solutions

Target parameters

$$\theta_{cr} = \frac{\tau_{crit}}{(\rho_s - \rho_w) g d_{50}}$$

$$\tau^* = \frac{\tau_{crit}}{\tau_0}$$

$$\tau_c^* = \frac{\tau_{crit} - \tau_0}{\tau_0}$$

Features parameters

P_{silt}

P_{clay}

d_{50}/d_{sand}

$\rho_{dry}/\rho_{part.}$

$\rho_{bulk}/\rho_{part.}$

Regression forms

$y = ax + b$

$y = e^{ax+b}$

$y = ax^b$

$y = ax^b + c$

$y = a_1x_1 + a_2x_2 + \mathrm{b}$

$y = a{x_1}^{b_1}{x_2}^{b_2}$

$y = a{x_1}^{b_1}{x_2}^{b_2} + c$

Deltares UNIVERSITY OF TWENTE.

Funded by the European Union

Marie Skłodowska-Curie Actions

This study is financially support by the European Union's (EU) Horizon Europe Framework Programme (HORIZON) via SEDIMARE (Grant Agreement No. 101072443), an MSCA Doctoral Network (HORIZON-MSCA-2021-DN-01).

Mass fractions: $1 = P_{sand} + P_{silt} + P_{clay} = P_{sand} + P_{mud}$

Volume fractions: $1 = \phi_{sand} + \phi_{silt} + \phi_{clay} + \phi_{water}$

Regression selection

- Based on highest R^2 in terms of τ_{crit}
- Each feature parameter should align with R (Pearson correlation coefficient) of target and feature parameter

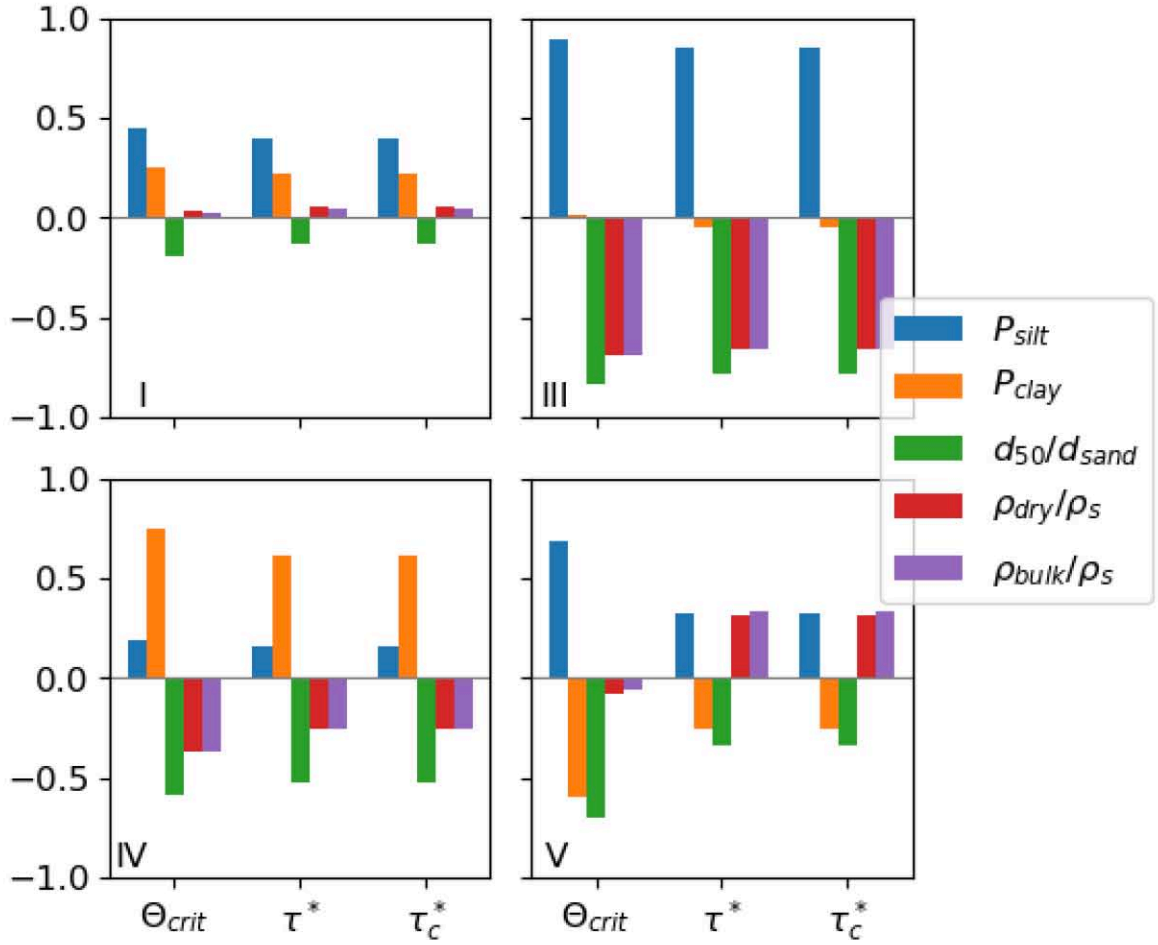

Funded by the European Union

Marie Skłodowska-Curie Actions

This study is financially support by the European Union's (EU) Horizon Europe Framework Programme (HORIZON) via SEDIMARE (Grant Agreement No. 101072443), an MSCA Doctoral Network (HORIZON-MSCA-2021-DN-01).

Erosion threshold equations

Bed type I, based on θ_{cr}:

$$\tau_{crit} = [0.06 + 0.35(P_{silt})^{0.3}](\rho_s - \rho)gd_{50}$$

Bed type III, based on τ^*:

$$\tau_{crit} = \left[4.3 + 6.5\left(\frac{d_{50}}{d_{sand}}\right)^{-1.1}\right]\tau_0$$

Bed type IV, based on τ^*:

$$\tau_{crit} = \left[24(P_{clay})^{0.4}\left(\frac{d_{50}}{d_{sand}}\right)^{-0.3}\right]\tau_0$$

Bed type V, based on τ_c^*:

$$\tau_{crit} = \left\{1 + \left[59.6(P_{silt})^{1.9}\left(\frac{\rho_{bulk}}{\rho_s}\right)^{9.3}\right]\right\}\tau_0$$

Funded by the European Union

Marie Skłodowska-Curie Actions

This study is financially support by the European Union's (EU) Horizon Europe Framework Programme (HORIZON) via SEDIMARE (Grant Agreement No. 101072443), an MSCA Doctoral Network (HORIZON-MSCA-2021-DN-01).

Erosion threshold equations per bed type

Recall:

$$\theta_{cr} = \frac{\tau_{crit}}{(\rho_s - \rho_w) g d_{50}}$$

$$\tau^* = \frac{\tau_{crit}}{\tau_0}$$

$$\tau_c^* = \frac{\tau_{crit} - \tau_0}{\tau_0}$$

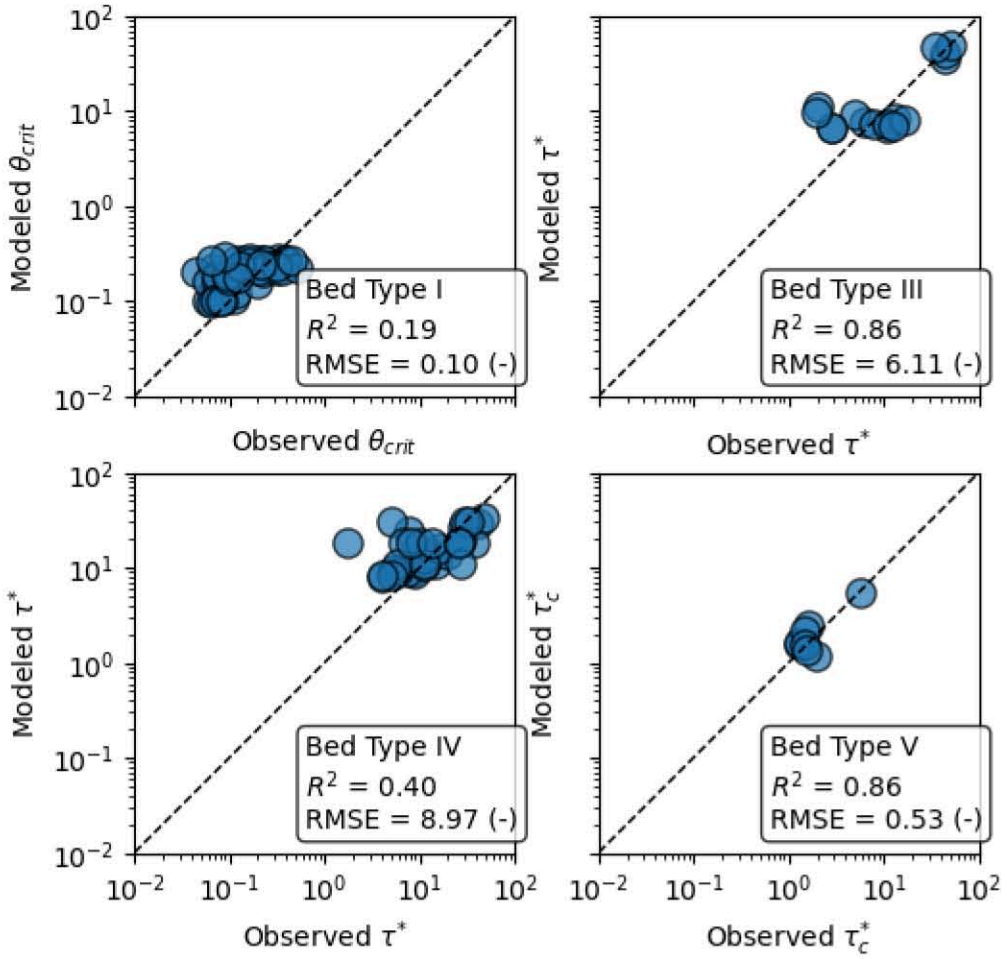

Funded by the European Union

Marie Skłodowska-Curie Actions

This study is financially support by the European Union's (EU) Horizon Europe Framework Programme (HORIZON) via SEDIMARE (Grant Agreement No. 101072443), an MSCA Doctoral Network (HORIZON-MSCA-2021-DN-01).

Erosion threshold equations per bed type

Recall,

I:

$$\tau_{crit} = [0.06 + 0.35(P_{silt})^{0.3}](\rho_s - \rho)g d_{50}$$

III:

$$\tau_{crit} = \left[4.3 + 6.5\left(\frac{d_{50}}{d_{sand}}\right)^{-1.1}\right]\tau_0$$

IV:

$$\tau_{crit} = \left[24(P_{clay})^{0.4}\left(\frac{d_{50}}{d_{sand}}\right)^{-0.3}\right]\tau_0$$

V:

$$\tau_{crit} = \left\{1 + \left[59.6(P_{silt})^{1.9}\left(\frac{\rho_{bulk}}{\rho_s}\right)^{9.3}\right]\right\}\tau_0$$

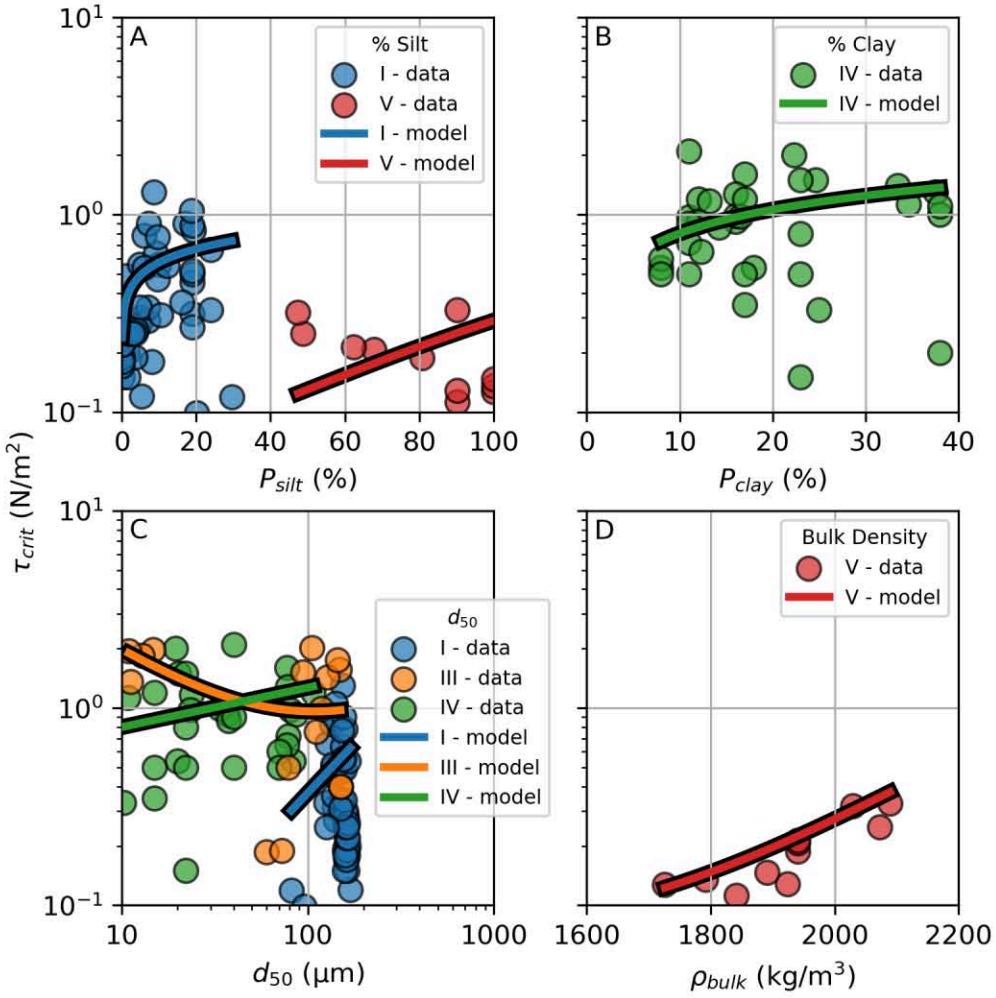

Funded by the European Union

Marie Skłodowska-Curie Actions

This study is financially support by the European Union's (EU) Horizon Europe Framework Programme (HORIZON) via SEDIMARE (Grant Agreement No. 101072443), an MSCA Doctoral Network (HORIZON-MSCA-2021-DN-01).

Comparison of erosion threshold equations

- Compared with formulas found in literature
  - Some formulas require site-specific parameters so assumptions were made

Mitchener et al., 1997

$$\tau_{crit} = 0.015(\rho_b - 1000)^{0.73}$$

Van Ledden, 2003

$$\tau_{crit} = \begin{cases} (1 + P_m)^{\beta}\tau_{cr,0} & P_m < \boldsymbol{P_{m,cr}} \\ \dfrac{\tau_{cr,0}\left(1 + P_{m,cr}\right)^{\beta} - P_{m,pu}}{1 - P_{m,cr}}(1 - P_m) + P_{m,pu} & P_m > \boldsymbol{P_{m,cr}} \end{cases}$$

Van Rijn, 2007

$$\tau_{crit} = \begin{cases} \left(1 + P_{clay}\right)^3 \tau_{cr,0} & : \quad d \geq 62\mu m \\ \left(\dfrac{c_{gel}}{c_{gel,s}}\right)\left(\dfrac{d_{sand}}{d_{50}}\right)^{\gamma} \tau_{cr,0} & : \quad d < 62\mu m \end{cases}$$

Wu et. al., 2018

$$\tau_{crit} = \begin{cases} 1.25P_{mud}\left(\tau_{cr,mud} - \tau_{cr,0}\right) + \tau_{cr,0} & P_{mud} < 5\% \\ \tau_{cr,L} + \left(\tau_{cr,mud} - \tau_{cr,L}\right)exp\left[-\alpha\left(\dfrac{P_{sand}}{P_{mud}}\right)^{\beta}\right] & 0 < P_{mud} < 100\% \\ 10.29\boldsymbol{r}^{1.7} & Pure\ mud \end{cases}$$

Yao et. al, 2022

$$\tau_{crit} = \begin{cases} \tau_{cr,0} & P_{silt} \leq 35\% \\ (1 + \beta_{ss})\tau_{cr,0} & P_{silt} > 35\% \end{cases}$$

Funded by the European Union

Marie Skłodowska-Curie Actions

This study is financially support by the European Union's (EU) Horizon Europe Framework Programme (HORIZON) via SEDIMARE (Grant Agreement No. 101072443), an MSCA Doctoral Network (HORIZON-MSCA-2021-DN-01).

Erosion threshold equations per bed type

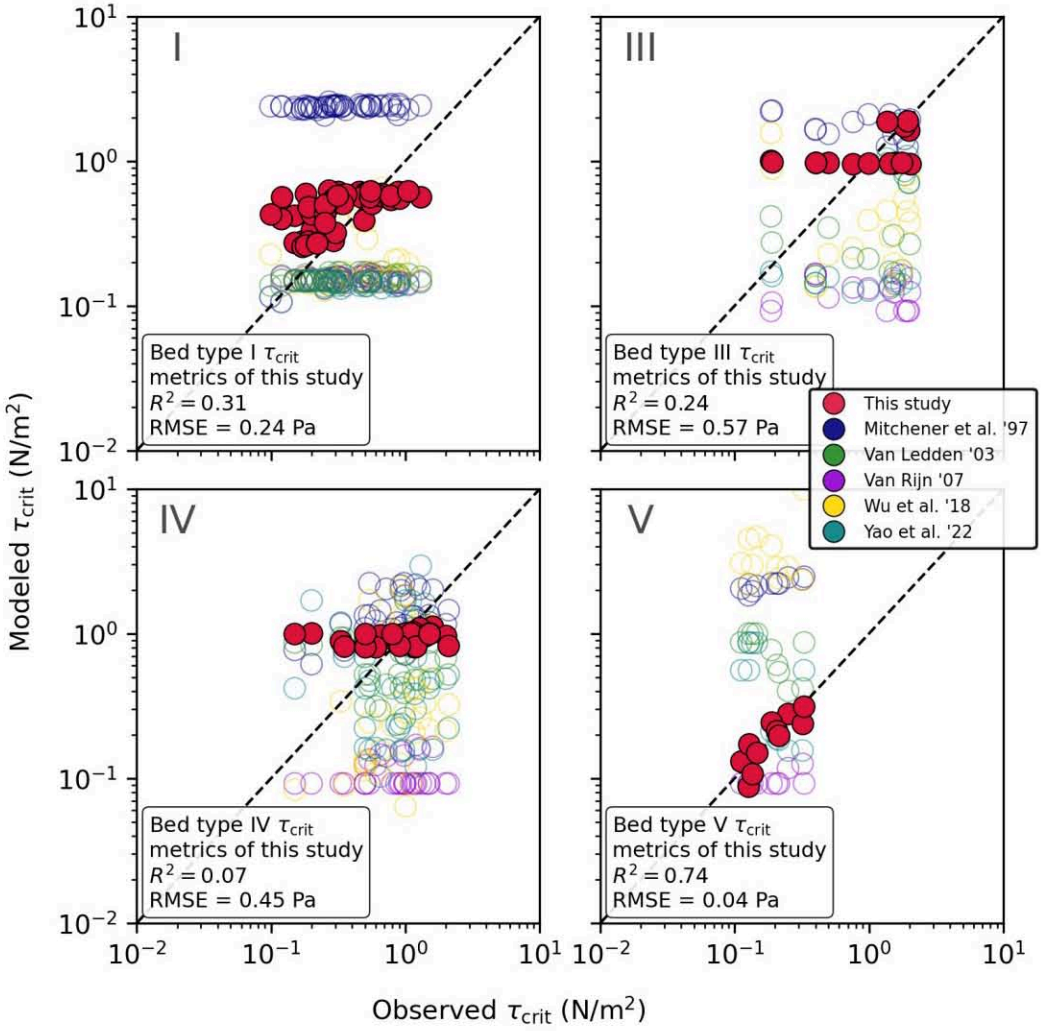

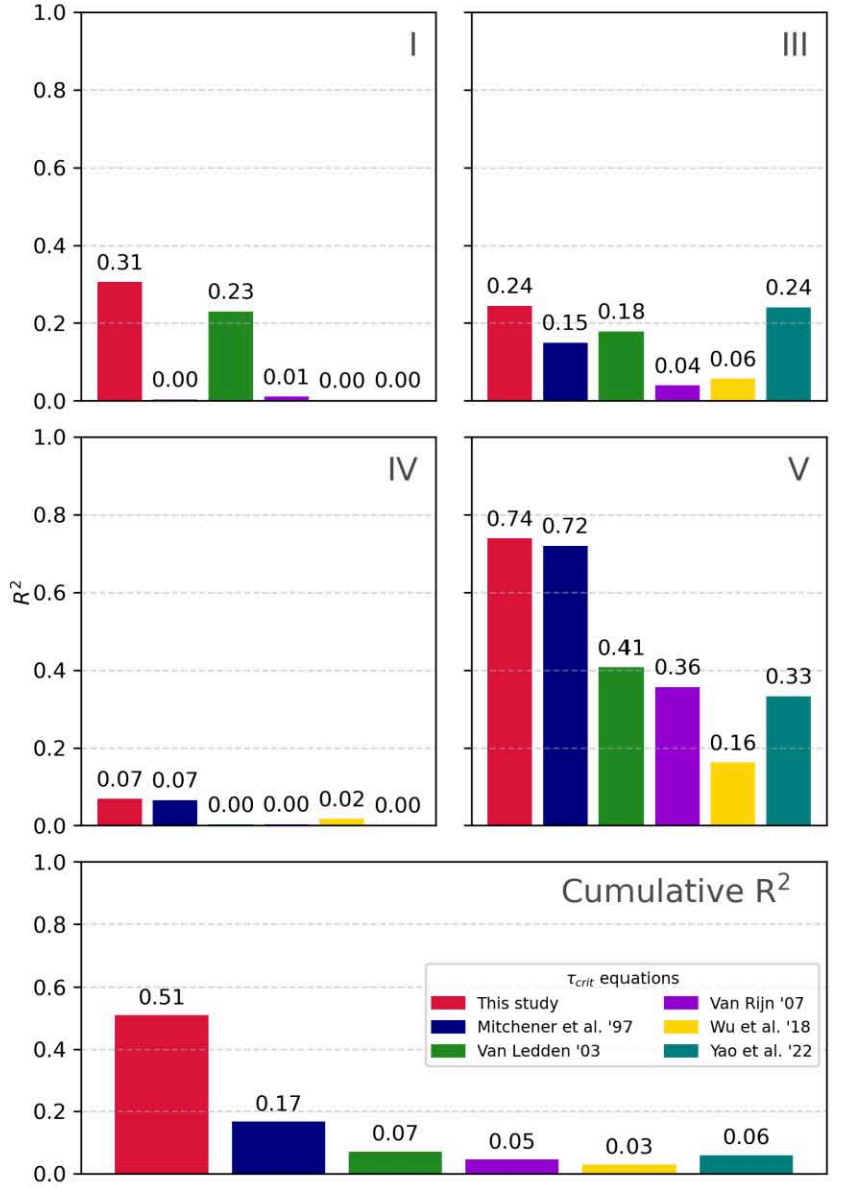

Deltares UNIVERSITY OF TWENTE.

Funded by the European Union

Marie Skłodowska-Curie Actions

This study is financially support by the European Union's (EU) Horizon Europe Framework Programme (HORIZON) via SEDIMARE (Grant Agreement No. 101072443), an MSCA Doctoral Network (HORIZON-MSCA-2021-DN-01).

Erosion threshold equations across bed type

- Generate synthetic data of different clay:silt ratios (CSR)
  - Western Scheldt (CSR 1:4)
  - Jiangsu coast, China (CSR 1:20)

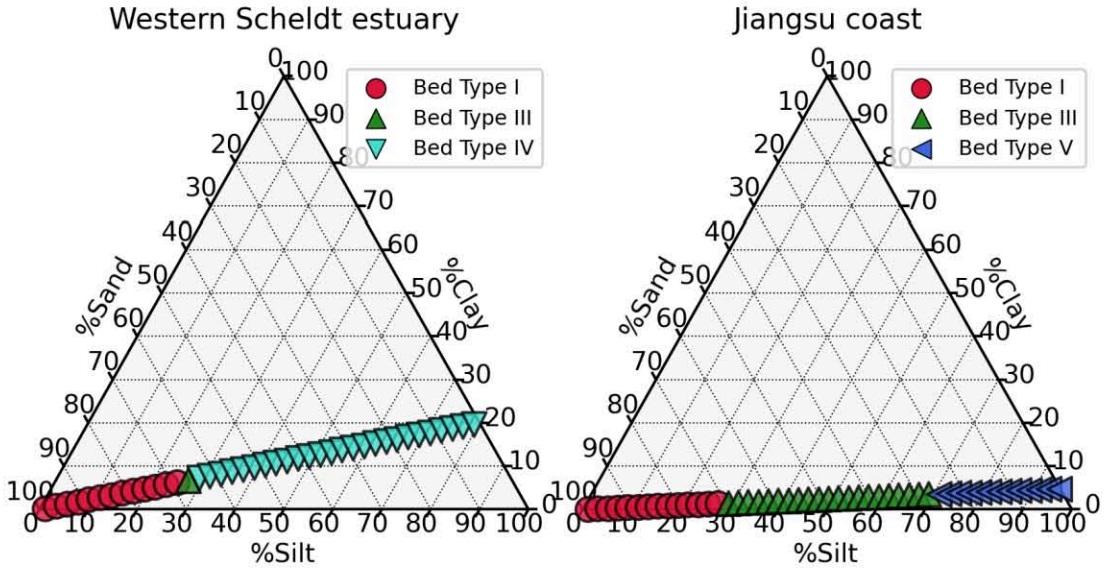

Funded by the European Union

Marie Skłodowska-Curie Actions

This study is financially support by the European Union's (EU) Horizon Europe Framework Programme (HORIZON) via SEDIMARE (Grant Agreement No. 101072443), an MSCA Doctoral Network (HORIZON-MSCA-2021-DN-01).

Erosion threshold equations across bed type

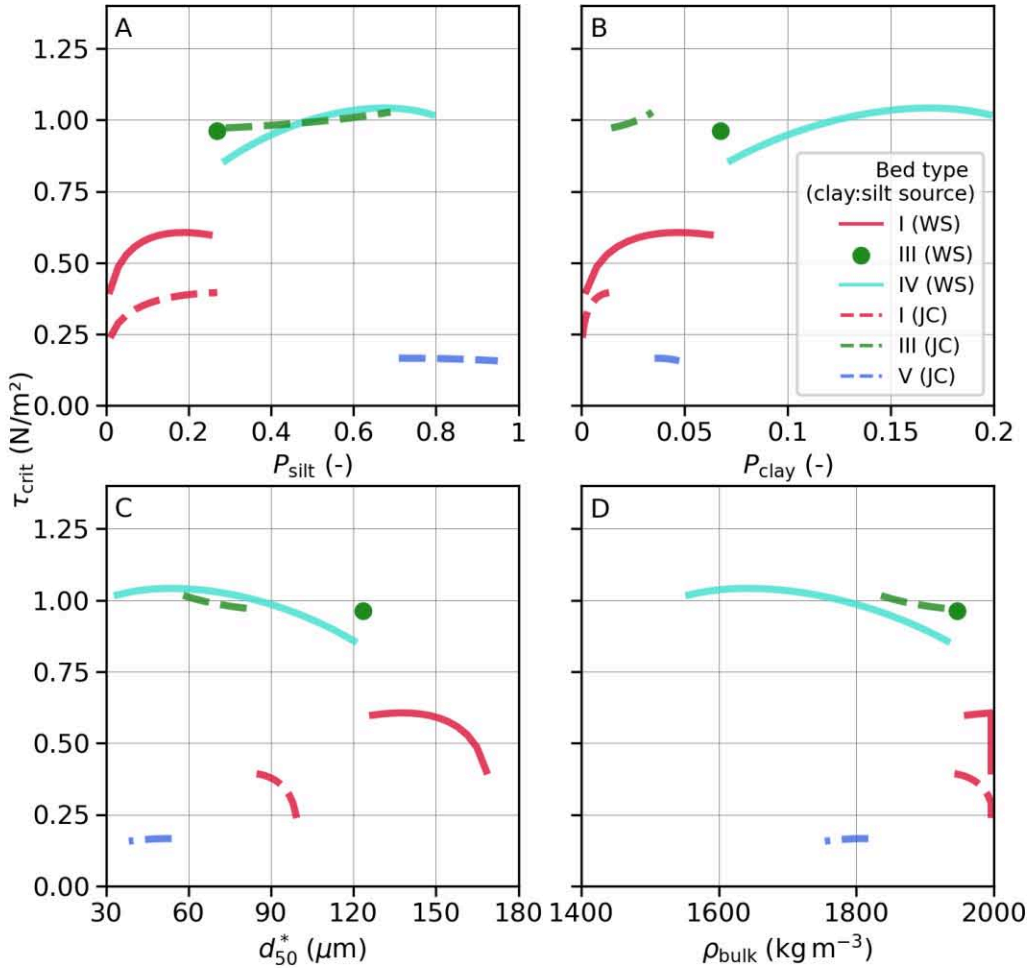

Funded by the European Union

Marie Skłodowska-Curie Actions

This study is financially support by the European Union's (EU) Horizon Europe Framework Programme (HORIZON) via SEDIMARE (Grant Agreement No. 101072443), an MSCA Doctoral Network (HORIZON-MSCA-2021-DN-01).

Conclusions

Erosion thresholds of sand-silt-clay mixtures can be **described within an integrated framework** using bulk geotechnical parameters. This framework **captures the distinct regimes of erosion behavior** across different bed types. Specifically:

- Erosion threshold measurements strongly depend on experimental setup, but **applying consistent criteria allows meaningful integration across studies**.

- The resulting six bed types indicate **changes in erosion behavior** of sand-silt-clay **cannot be described** by regimes **based on only 1 bulk parameter** (i.e. mud content, dry bulk density, median particle size, etc.).

- The four proposed erosion threshold equations reproduced observed data satisfactorily, suggesting they may **provide a practical tool in experimental work and numerical modeling**.

Funded by the European Union

Marie Skłodowska-Curie Actions

This study is financially support by the European Union's (EU) Horizon Europe Framework Programme (HORIZON) via SEDIMARE (Grant Agreement No. 101072443), an MSCA Doctoral Network (HORIZON-MSCA-2021-DN-01).

Future work

- Sand-silt-clay erosion (Partheniades) rate

$$E = M\left(\frac{\tau_b}{\tau_{crit}} - 1\right)$$

- Hindcast morphodynamic modeling using Scheldt estuary

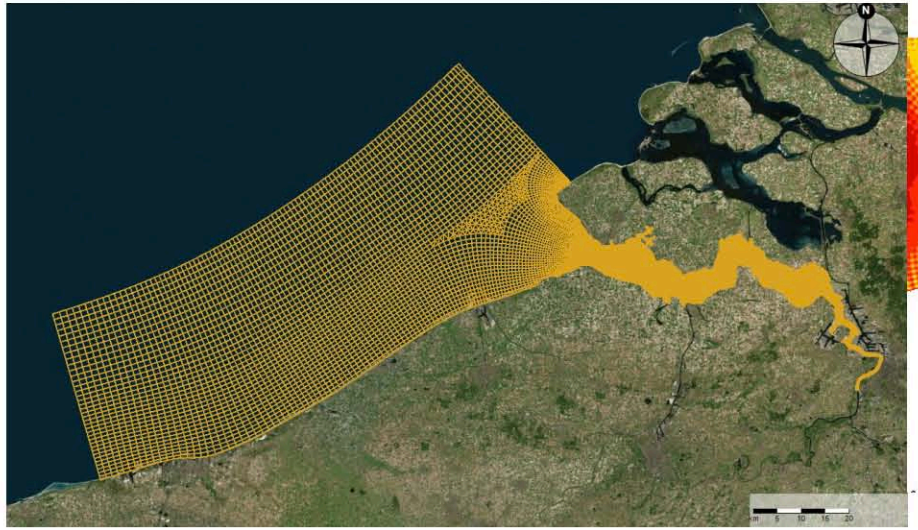

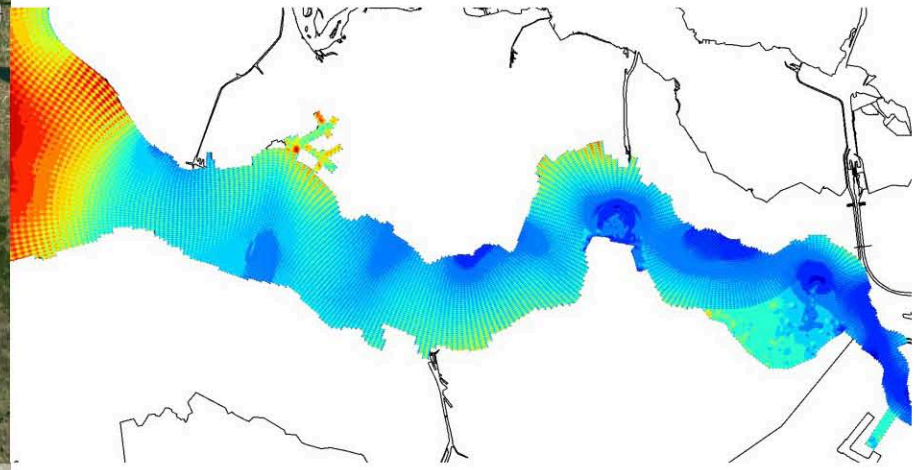

Funded by the European Union

Marie Skłodowska-Curie Actions

This study is financially support by the European Union's (EU) Horizon Europe Framework Programme (HORIZON) via SEDIMARE (Grant Agreement No. 101072443), an MSCA Doctoral Network (HORIZON-MSCA-2021-DN-01).

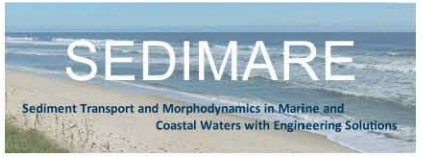

Erosion threshold of sand-silt-clay mixtures

P.S. Miranda, J.J. van der Werf, S.J.M.H. Hulscher

HR Wallingford – SEDIMARE Technical Workshop

Deltares UNIVERSITY OF TWENTE.

jowi.miranda@deltares.nl
p.s.miranda@utwente.nl

psmiranda

Funded by the European Union

Marie Skłodowska-Curie Actions

This study is financially support by the European Union's (EU) Horizon Europe Framework Programme (HORIZON) via SEDIMARE (Grant Agreement No. 101072443), an MSCA Doctoral Network (HORIZON-MSCA-2021-DN-01).

Modeling Debris Flow: A Multi-Layer Shallow Water Approach

D.C. 9 – Eloah Rosas

Promoter

PhD. Benoît Spinewine

PhD. Sandra Soares

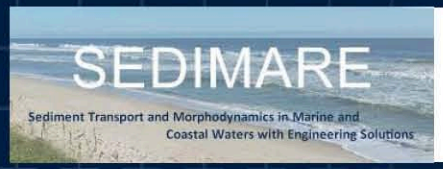

This project has received funding from the European Union's (EU) Horizon Europe Framework Programme (HORIZON) under Grant Agreement No 101072443 as a MSCA Doctoral Network (HORIZON-MSCA-2021-DN-01).

UCLouvain

FUGRO

High Sediment Laden Flow

Sediment-laden flow is characterized by unsteady, highly dense sediment concentrations and vertical stratification.

High-density sediment-laden flows is common in natural systems like rivers, deltas and coastal environments, and it can be initiated by natural or anthropogenic factors in the marine environment, such as:

Tsunamis, Earthquakes, Storms waves, Dredging.

Submarine Landslide

Some submarine landslides extend across 10,000 km² and mobilize over a million cubic meters of sediment in the seafloor

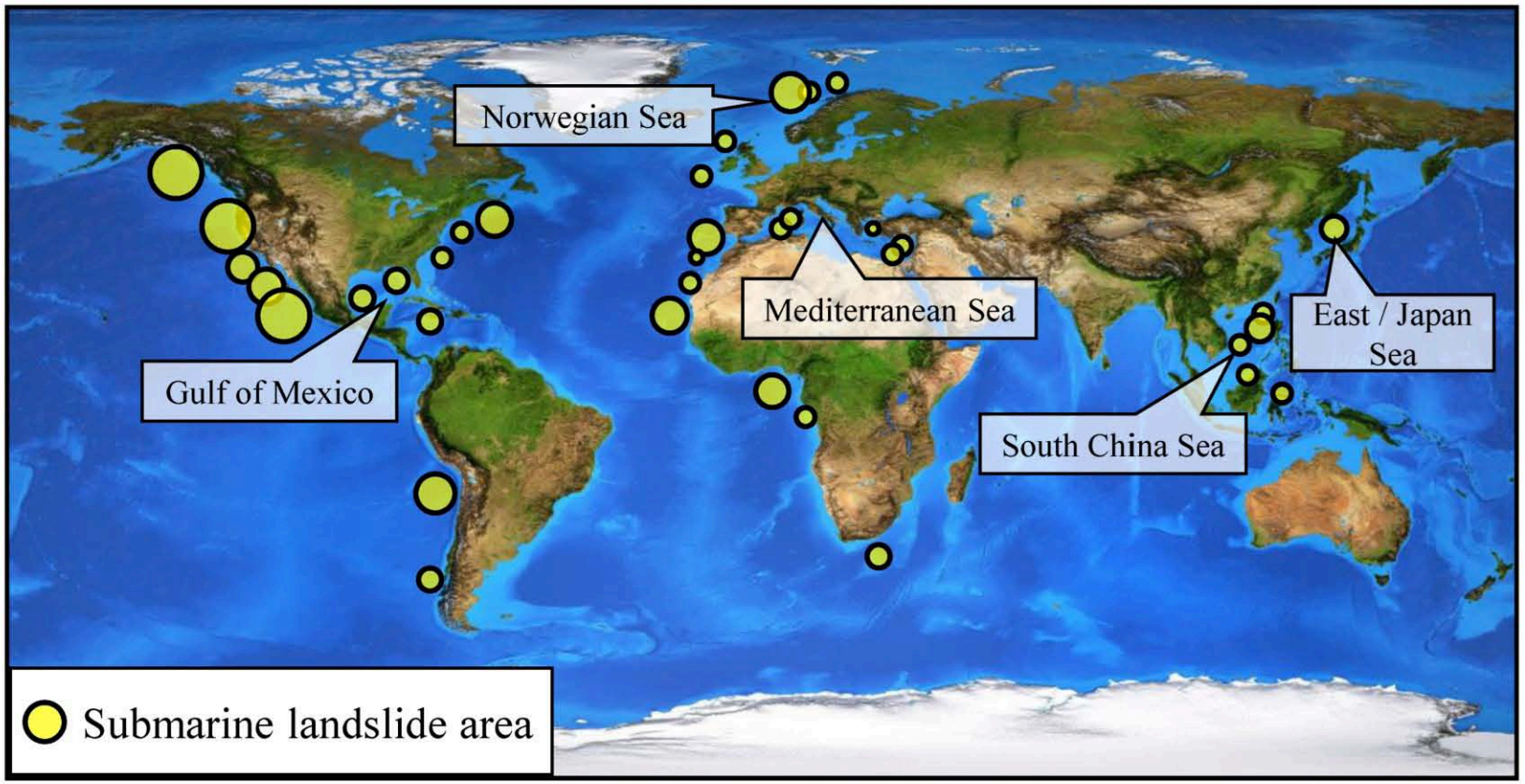

Evolution of Submarine Landslide

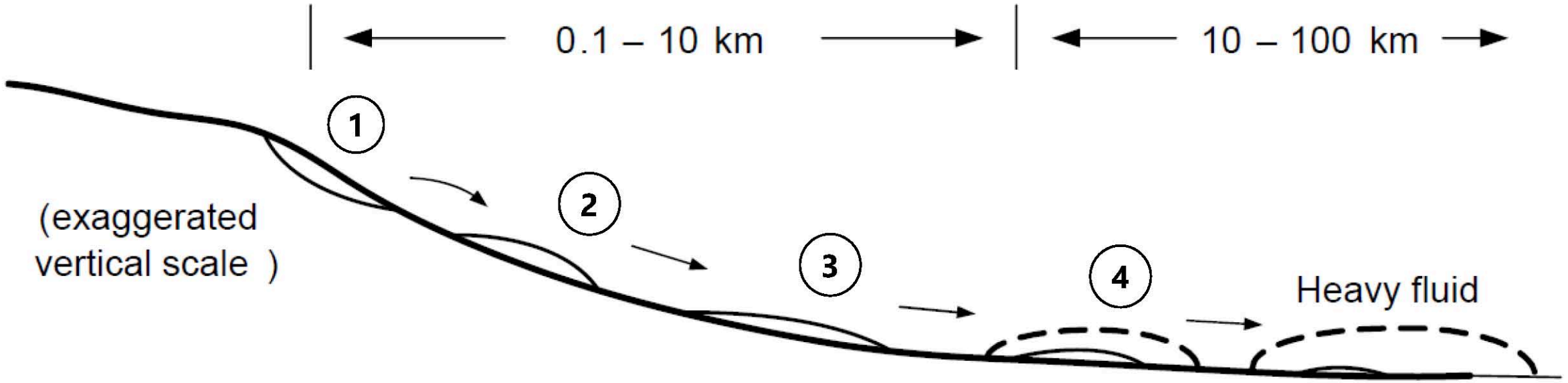

	1. Slope failure	**2.** Intact soil	**3.** Debris flow	**4.** Turbidity Flow
Soil Shear Strength	3-30 kPa	1 – 10 kPa	0.1 to 1 kPa	0.01 – 0.1 kPa
Bulk density	1300 – 1800 kg/m3		1000 – 1100 kg/m3	
Slide velocity	0	1-5 m/s	1 – 50 m/s	
Inertia – Strength ration	0	0.15	10 - 5000	

Rheology - Non-Newtonian flow

Debris Flow

- High Concentration of particles – Mud or Clay
- Minimum Stress – Yield Stress

Herschel-Bulkley Model

$$\tau = \tau_y + K\dot{\gamma}^n = \begin{cases} 0 & \text{if } |\tau| < \tau_y \\ \tau - \tau_y\dot{\gamma}^n & \text{if } |\tau| > \tau_y \end{cases}$$

$n = 1$ Bingham Flow (linear flow after field)

$n < 1$ Shear- thinning Flow (viscosity decreases with shear rate)

$n > 1$ Shear- thickening Flow (viscosity increases with shear rate)

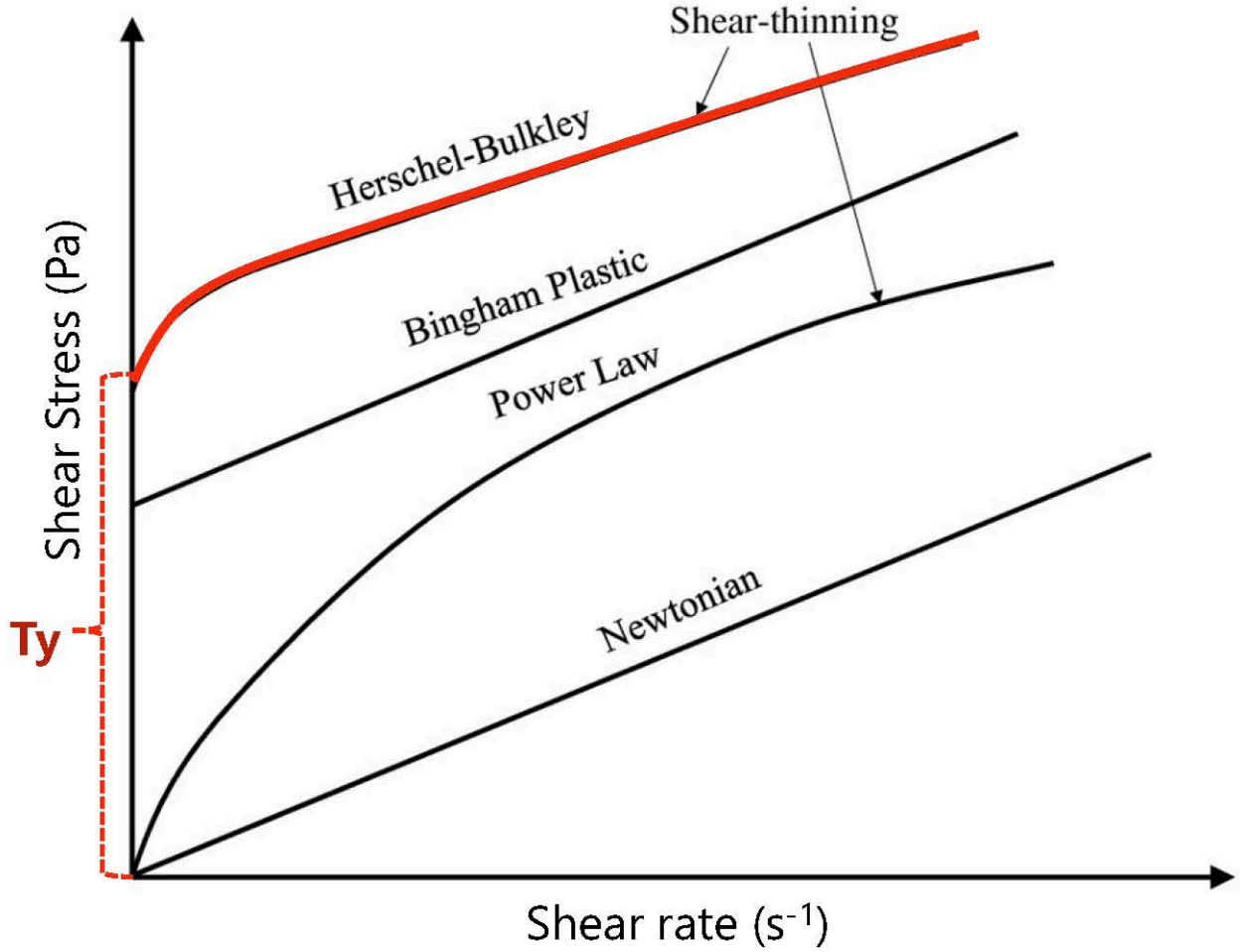

Rheological Models - Herschel-Bulkley Model

Once **yield stress** is exceeded, internal remodeling and strain accumulation reduce shear strength

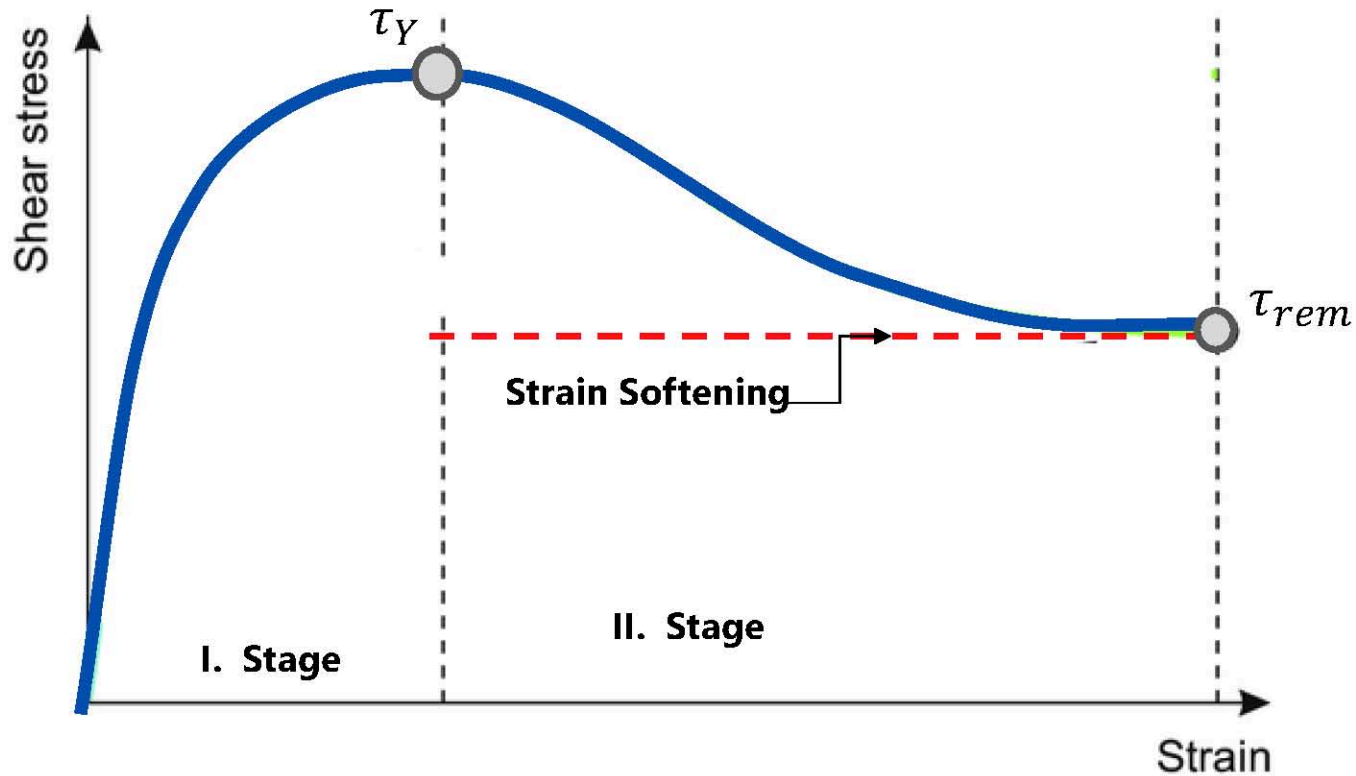

Rheology - Strain Softening

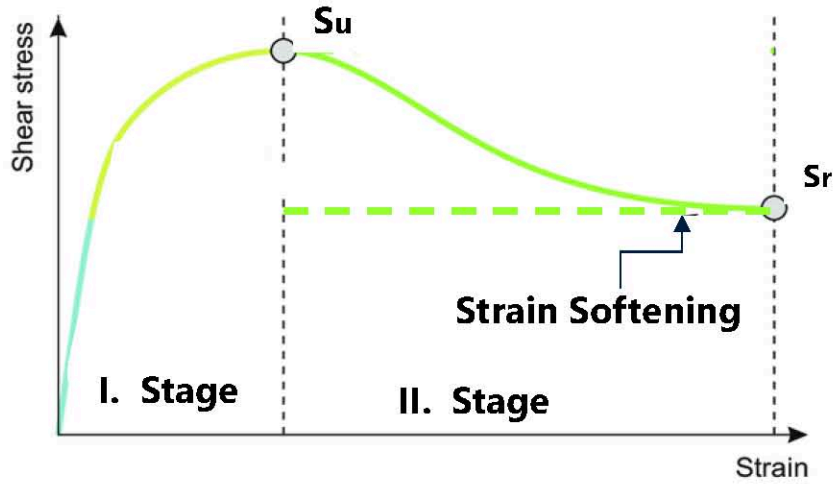

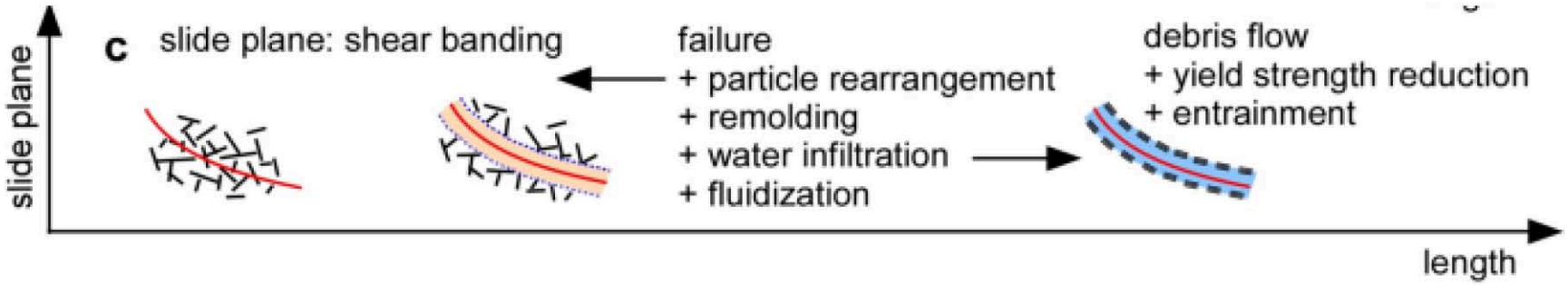

Rheology - Strain Softening

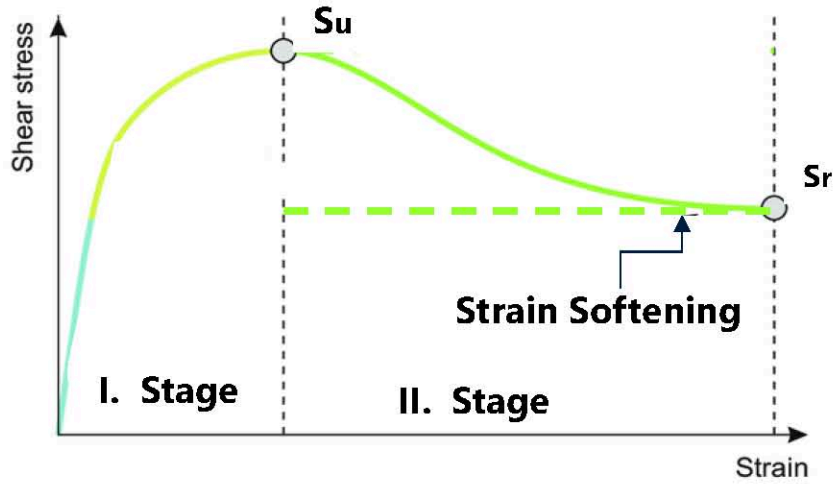

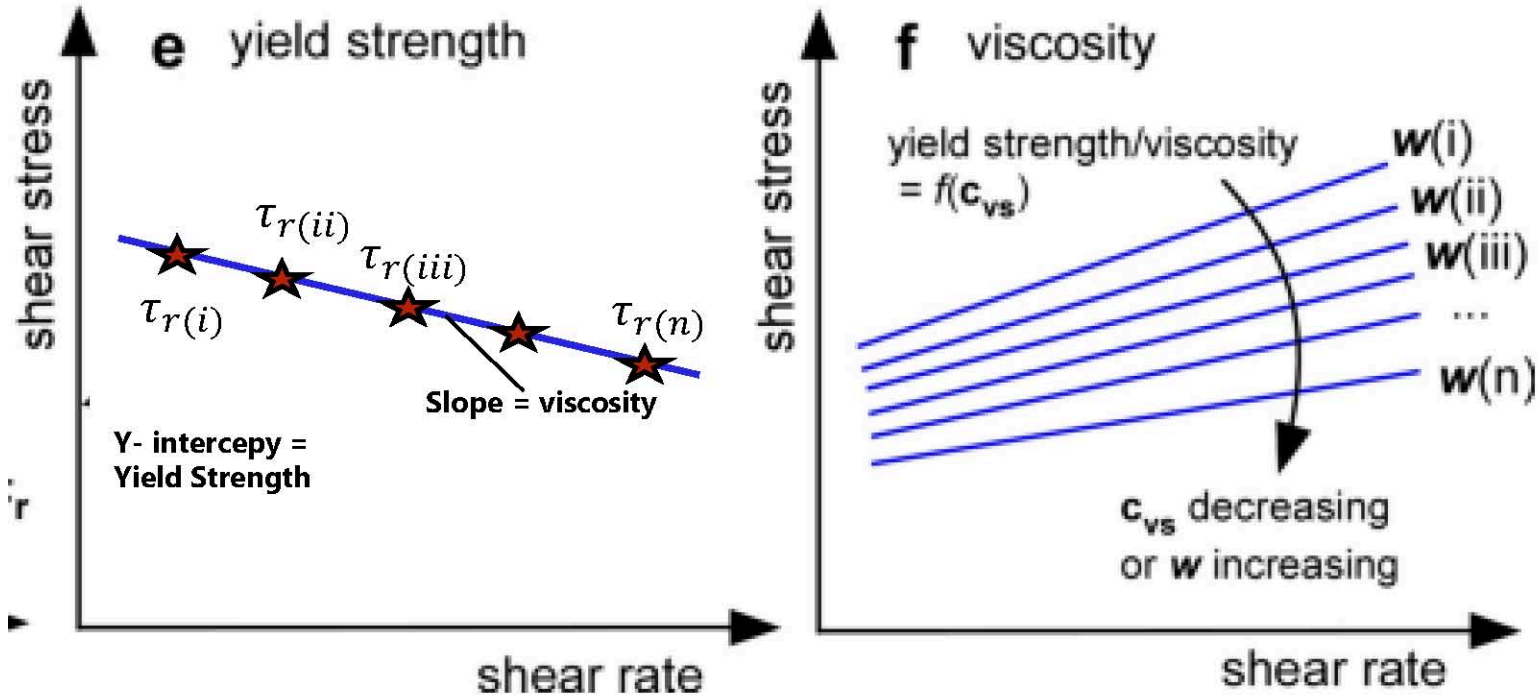

Rheology - Strain Softening

$$\tau_y = \tau_{rem} + (\tau_{int} - \tau_{rem}) e^{-\frac{3\gamma_{acc}}{\gamma_{95}}}$$

$$\gamma_{acc} = \int_0^t \left(-\frac{u\,(t)}{h_s} \right) dt$$

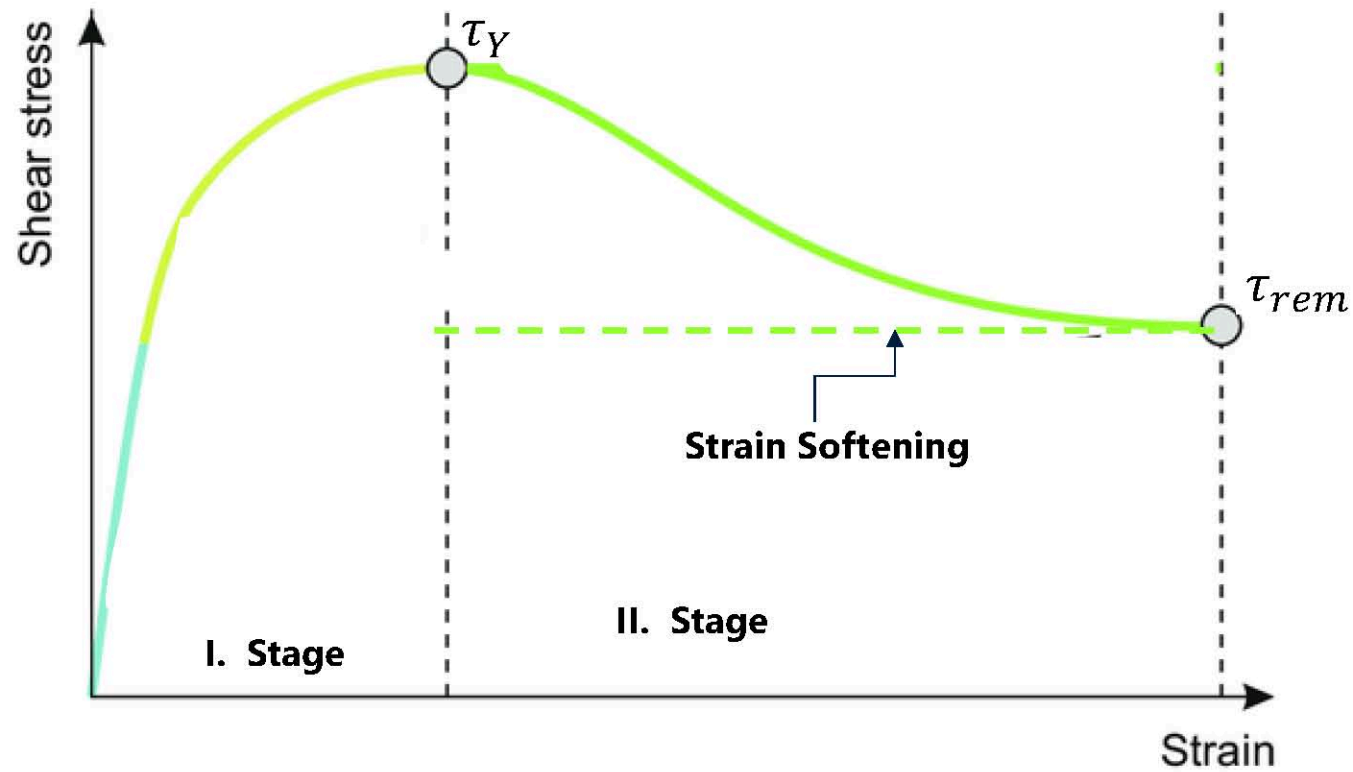

Numerical Model Framework

Shallow water depth-integrated

- Length Scale >> Vertical Scale
- Horizontal Velocity >> Vertical velocity

Flow idealised :

- **Plug Zone –** No internal shear rate → Constant plug velocity
- **Shear Zone –** Velocity varies from 0 at the seabed to v(p) at the plug layer

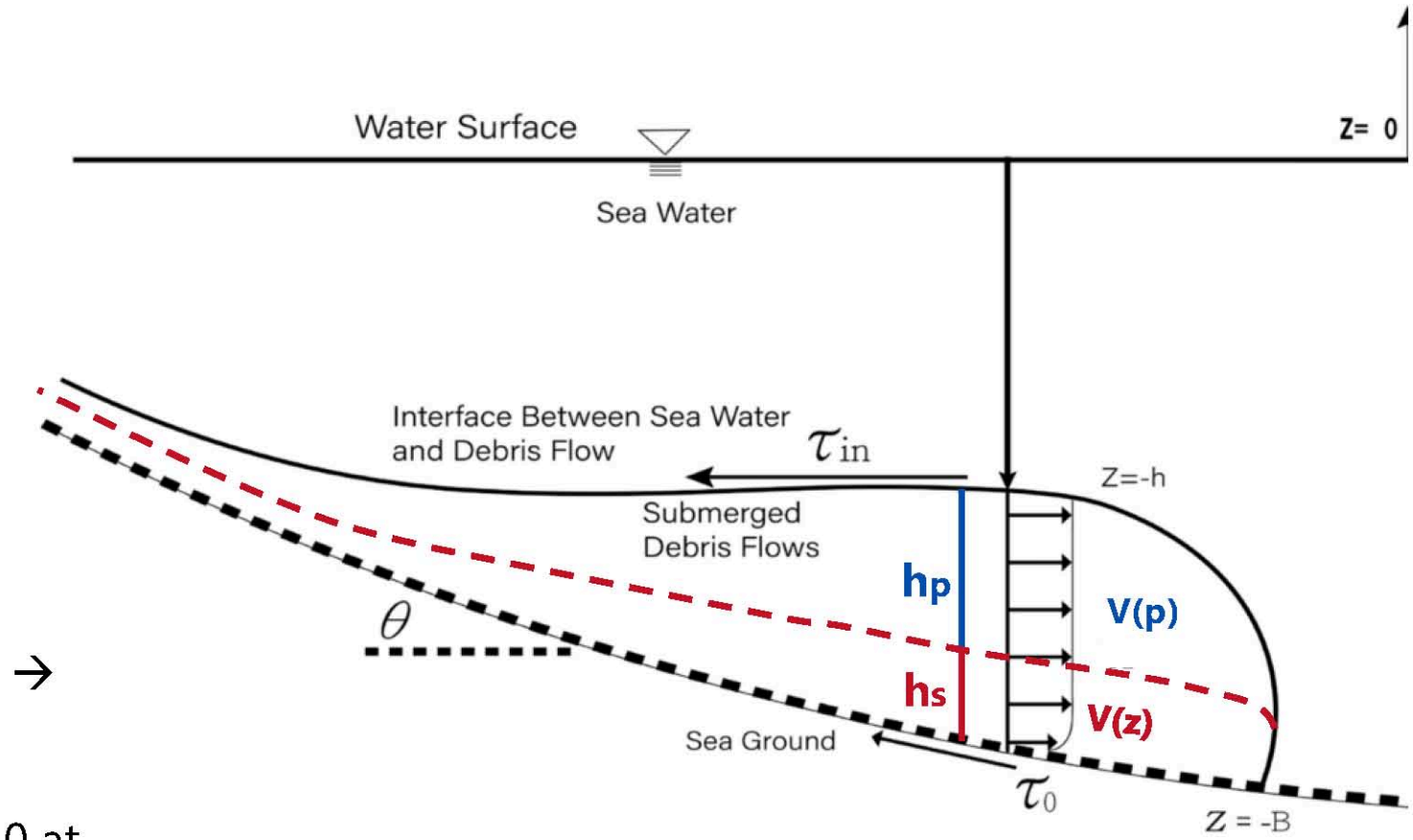

Shallow Water Debris Flow Framework

$$\frac{dh_s}{dt} + \frac{dh_s u_s}{dx} + \frac{dh_s v_s}{dy} = -eU_{rel}$$

$$\frac{dh_p}{dt} + \frac{dh_p u_p}{dx} + \frac{dh_p v}{dy} = \frac{\rho_s}{\rho_p} eU_{rel}$$

$$\frac{dC}{dt} + \frac{dCh_p u_p}{dx} + \frac{dCh_p v_p}{dy} = CeU_{rel}$$

$$\frac{dh_s u_s}{dt} + \frac{d(h_s {u_s}^2 + g\,{h_s}^2/2)}{dx} + gh_s \frac{dZ}{dx} + \frac{\rho_w}{\rho_p} gh_s \frac{d(RCh_p)}{dx}$$

$$\frac{dh_s u_s v}{dy} = \frac{\tau_{int} - \tau_{bed}}{\rho_s} - ueU_{rel}$$

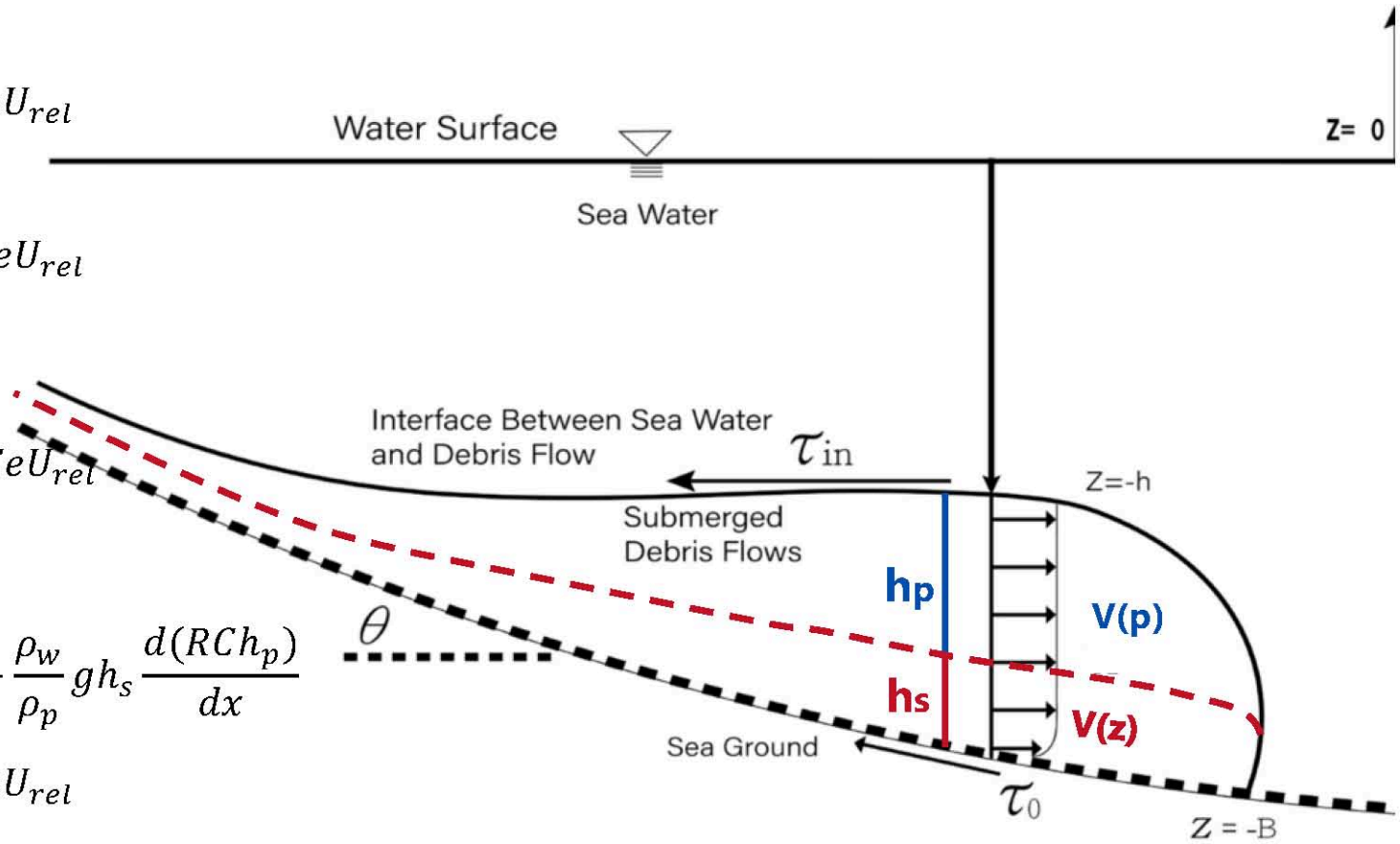

$$\frac{dh_p u_p}{dt} + \frac{d(h_p {u_p}^2 + RCg\,{h_p}^2/2)}{dx} + (RCgh_p)\frac{dZ}{dx} + \frac{dh_p u_p v_p}{dy} = -\frac{\tau_{int}}{\rho_p} + \frac{\rho_s}{\rho_p} ueU_{rel}$$

Sources SWDF2D

Sediment Erosion $\longrightarrow$ $E_s w_s$

- **Gacia and Parker, 1993**

$$E_s = \frac{1.3 \cdot 10^{-7} Z^5}{1 + \frac{1.3 \cdot 10^{-7} Z^5}{0.5}} \qquad Z = \alpha_1 u_* R_p^{\alpha_2}$$

$$\alpha_1 = \begin{cases} 1 & for \quad R_p > 2.36 \\ 0.586 & for \quad R_p \le 2.36 \end{cases}$$

$$\alpha_2 = \begin{cases} 0.6 & for \quad R_p > 2.36 \\ 1.23 & for \quad R_p \le 2.36 \end{cases}$$

- Akiyama and Fukushima (1984)

$$E_s = \begin{cases} 0.3 & for \quad Z > 13.2 \\ 3 \cdot 10^{-12} Z^{10} \left(1 - \frac{5}{Z}\right) & for \quad 5 > Z > 13.2 \\ 0 & for \quad Z < 5 \end{cases} \qquad Z = \frac{u_*}{w_s} R_p^{0.5}$$

Sources SWDF2D

- Water Entrainment

$$E_w = \frac{0.00153}{0.0204 + Ri}$$ Fukushima et al. 1985

- Sediment Dentrainment

$$Wd = KU_{rel}$$

$$\mathrm{K} = \begin{cases} 1 - (\frac{Ri - 0.2}{0.3 - 0.2}), & Ri < 3 \\ 0, & Ri \geq 3 \end{cases}$$

$$Ri_{gi} = -\frac{g(\partial\rho/\partial z)}{\rho(\partial u/\partial z)^2}$$

Multi-Layer Shallow Water

Mass Conservation Equation

$$\frac{dh_i}{dt} + \frac{dh_i u_i}{dx} + \frac{dh_i v_i}{dy} = S$$

Sediment mass conservation

$$\frac{dC_i}{dt} + \frac{dC_i h_i u_i}{dx} + \frac{dC_i h_i v_i}{dy} = CS$$

Momentum Conservation Equation

$$\frac{dh_i u_i}{dt} + \frac{d(h_i {u_i}^2 + g\,{h_i}^2/2)}{dx} + gh_i\frac{dZ}{dx} + \frac{\rho_{i-1}}{\rho_i} gh\frac{d(RC_i h_i)}{dx}$$

$$\frac{dC_i h_i v_i}{dy} = \frac{\tau_{int} - \tau_{bed}}{\rho_p} - u_i S$$

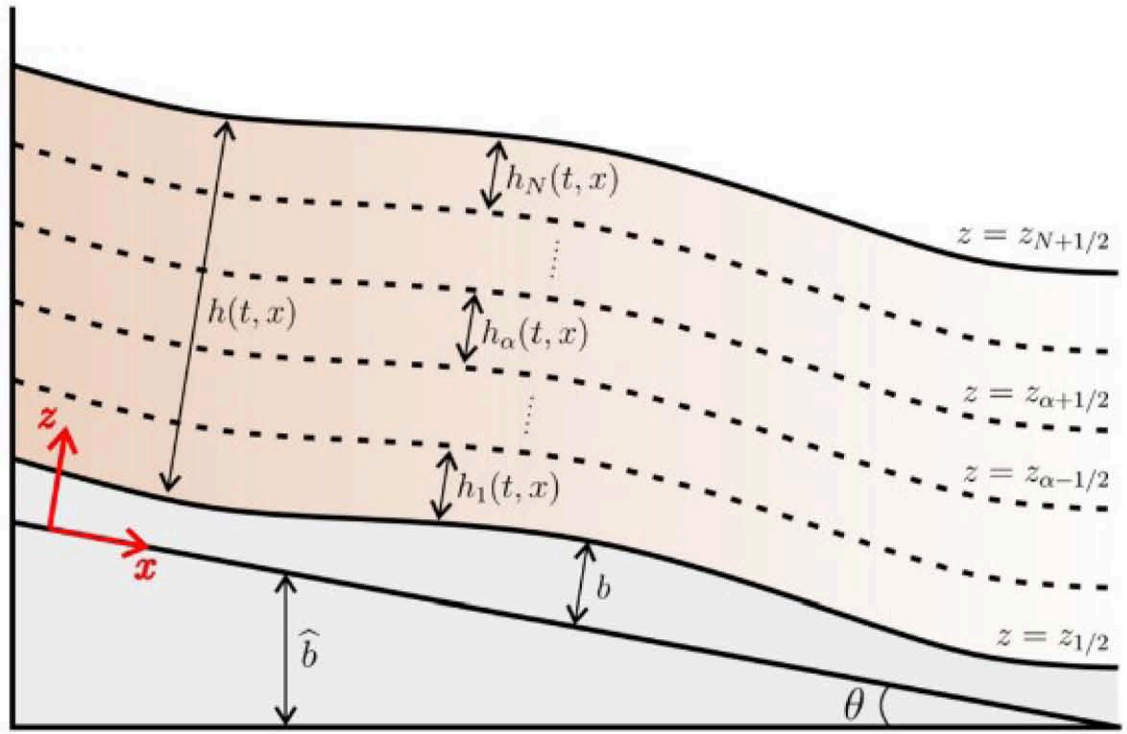

Fig. 1. Sketch of the multilayer configuration and notation.

HB Shear Stress

$$u(y) = \int \left(\frac{\tau - \tau_Y}{K}\right)^{1/n}$$

Shear Zone

$$u(y) = \frac{\boldsymbol{n}}{\boldsymbol{n}+1}\left(\frac{\boldsymbol{\rho g {h_s}^{n+1} sin\theta}}{\boldsymbol{K}}\right)^{1/\boldsymbol{n}}\left[1-\left(1-\frac{y}{h_s}\right)^{(\boldsymbol{n}+1)/\boldsymbol{n}}\right]$$

Plug Zone

$$u_p = \frac{\boldsymbol{n}}{\boldsymbol{n}+1}\left(\frac{\boldsymbol{\rho g {h_s}^{n+1} sin\theta}}{\boldsymbol{K}}\right)^{1/\boldsymbol{n}}$$

$$\tau_0 = \boldsymbol{\tau_y} + \boldsymbol{K}\left[\frac{1+(1/\boldsymbol{n})}{1-\ h_s\boldsymbol{n}/(2\boldsymbol{n}+1)\boldsymbol{h_1}}\right]^{\boldsymbol{n}}\left(\frac{|u_1|}{h_s}\right)^{\boldsymbol{n}}$$

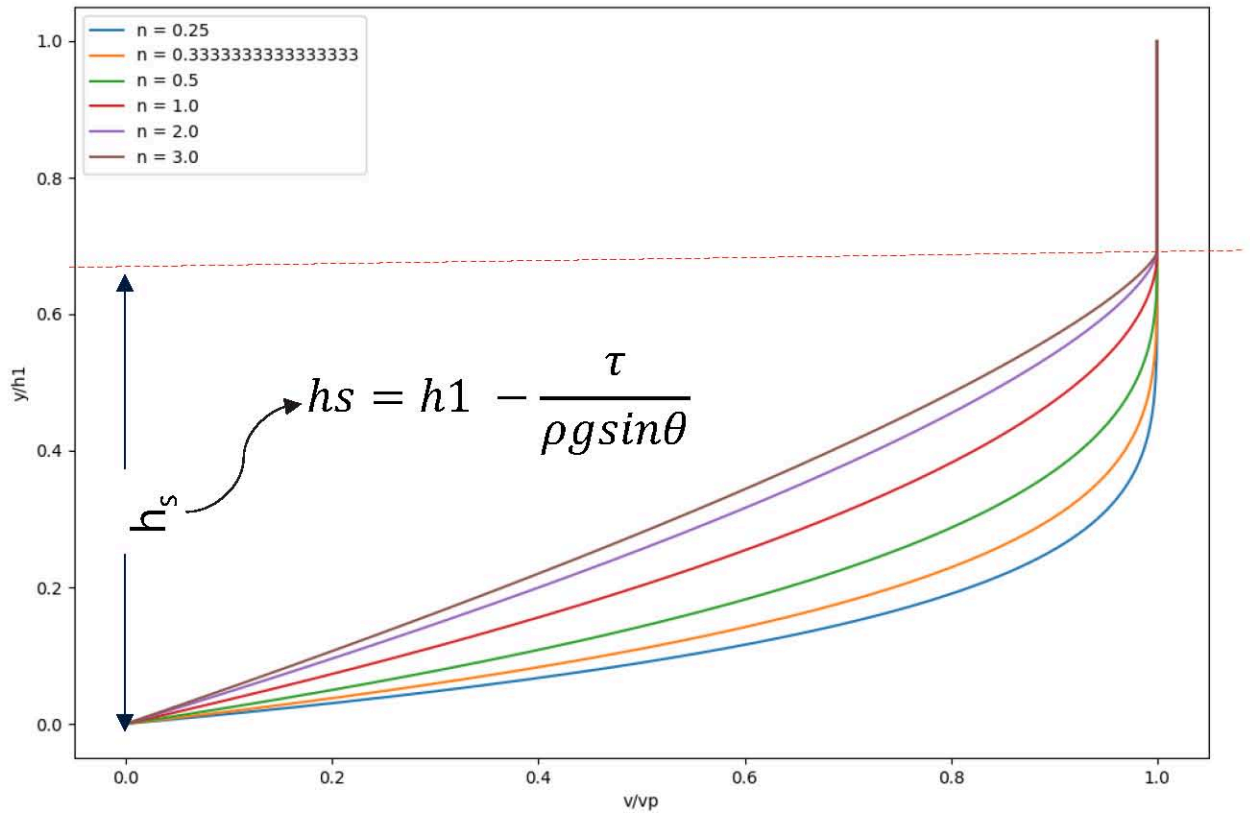

Chen et al. (2007)

Vertical Profiles with Multi-Layers

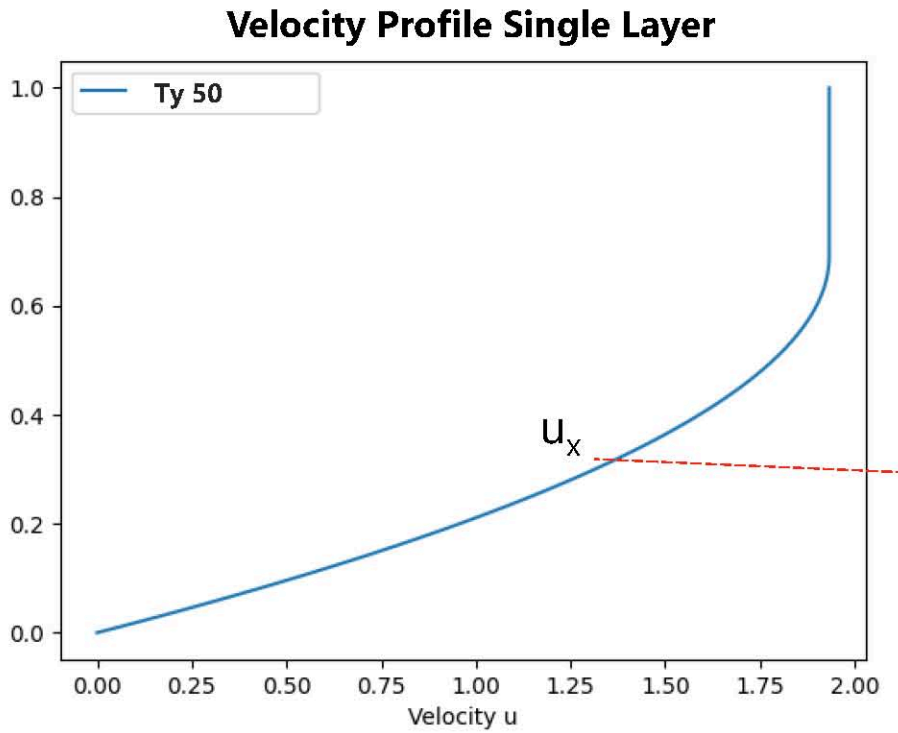

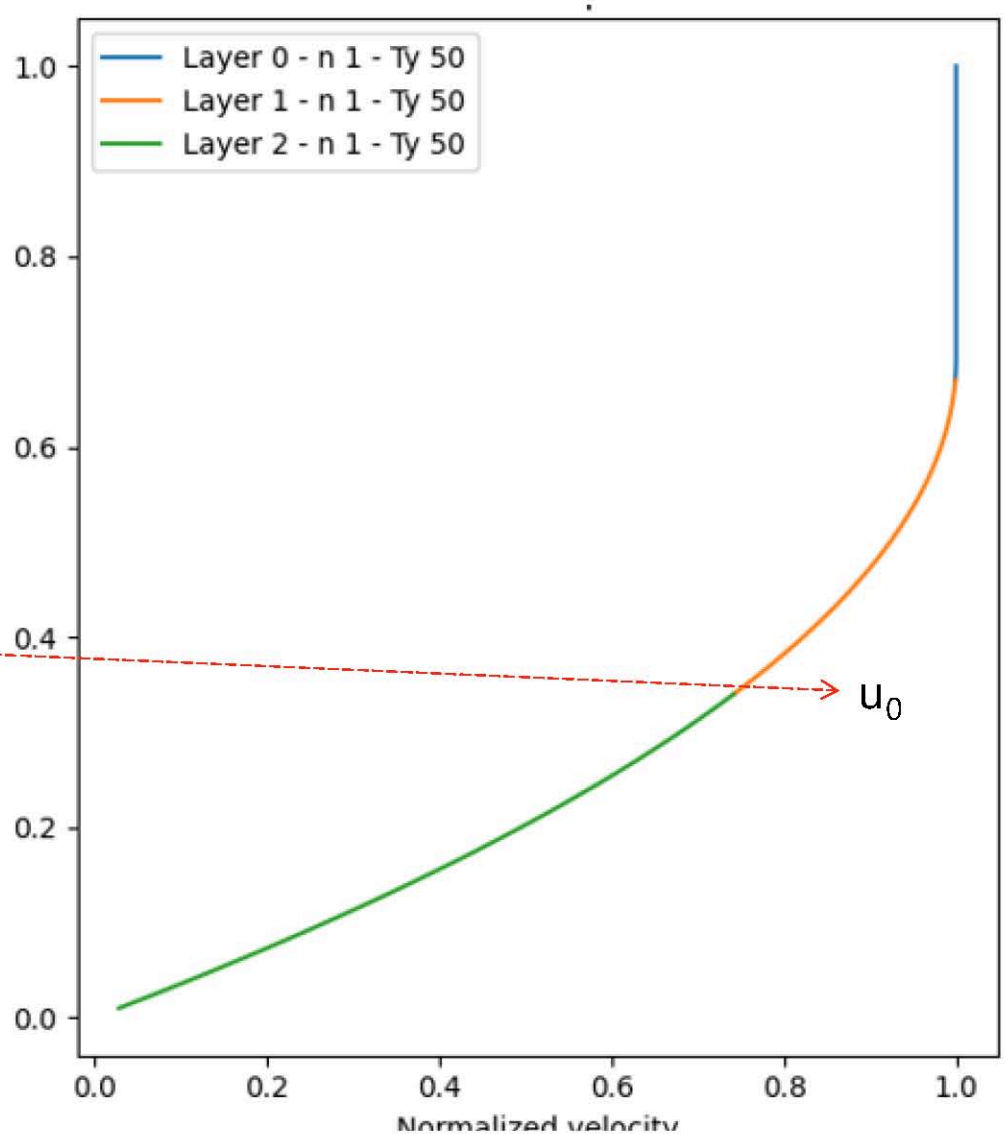

Vertical Profiles with Multi-Layers

Layer	τ_1	τ_b
1	0	53
2	54	108
3	108	162

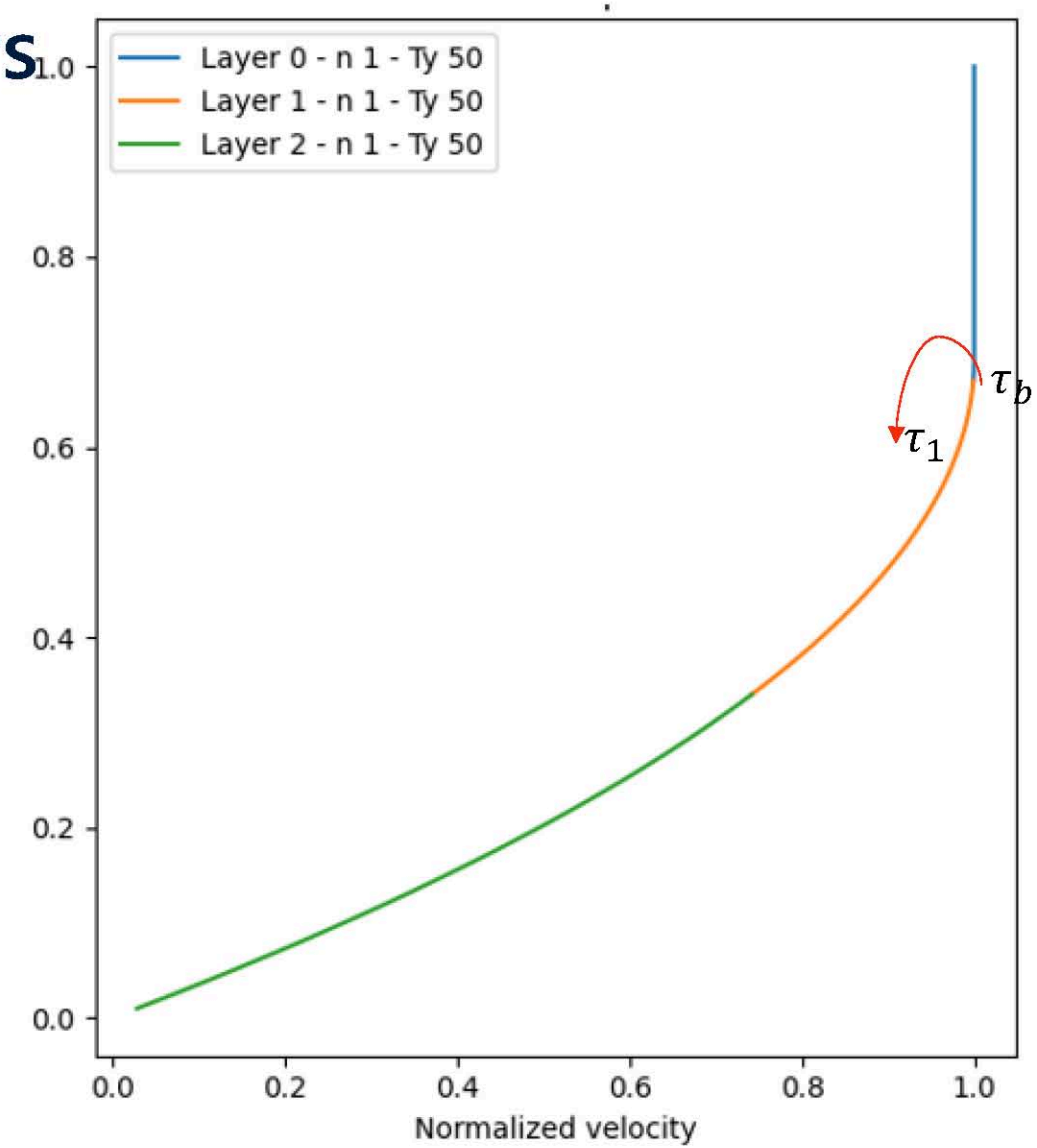

Variation in HB fluid layers

$\boldsymbol{\tau_b}$ = 16, 53, 108, 162

$$\tau(y) = \tau 0 \left(1 - \frac{y}{h1}\right)$$

$$u(y) = \int \left(\frac{\tau - \tau_Y}{K}\right)^{1/n}$$

τ_Y of layer 1 → 200, 150, 100, 50

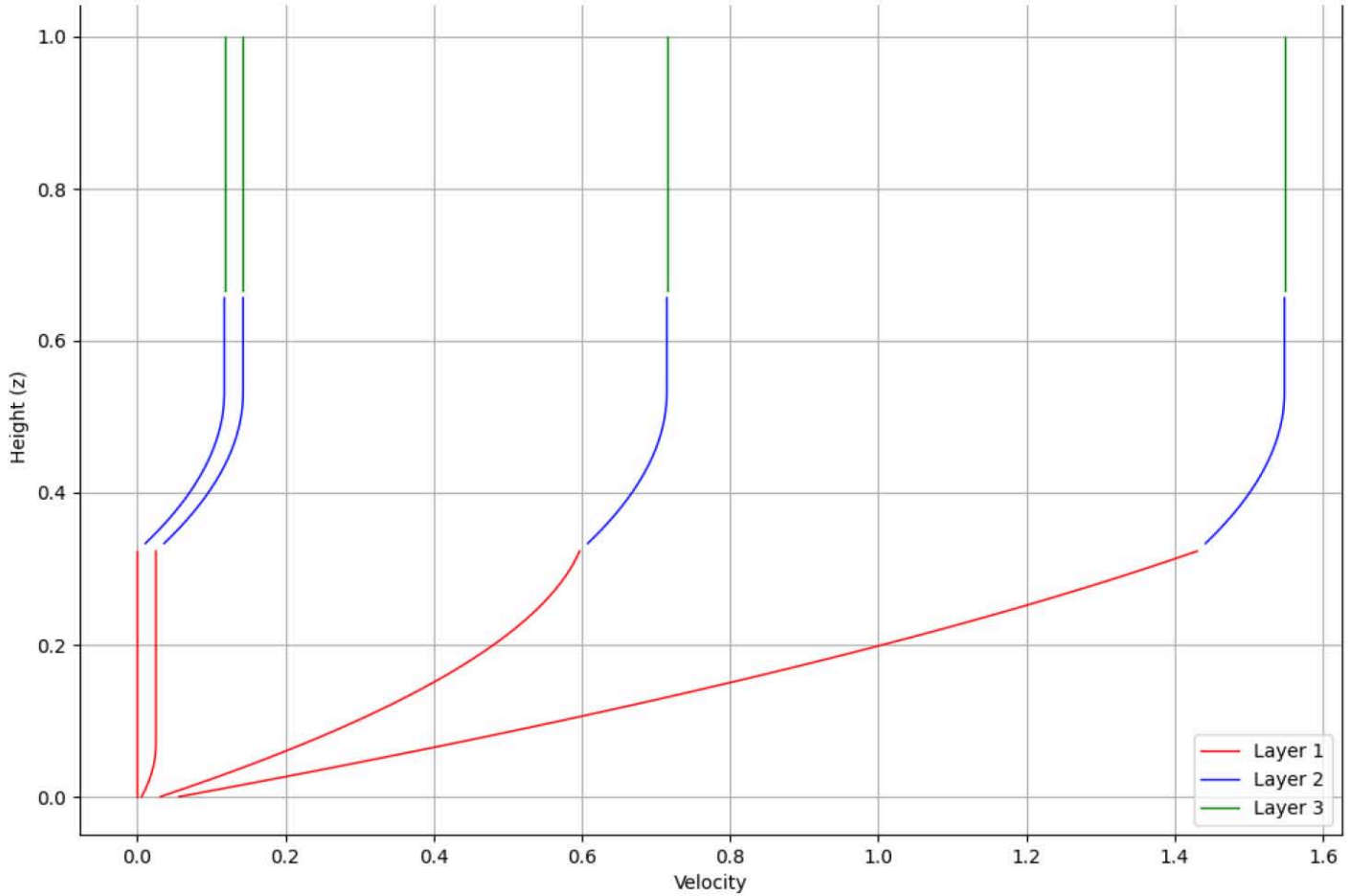

Strain rate and Softening effects

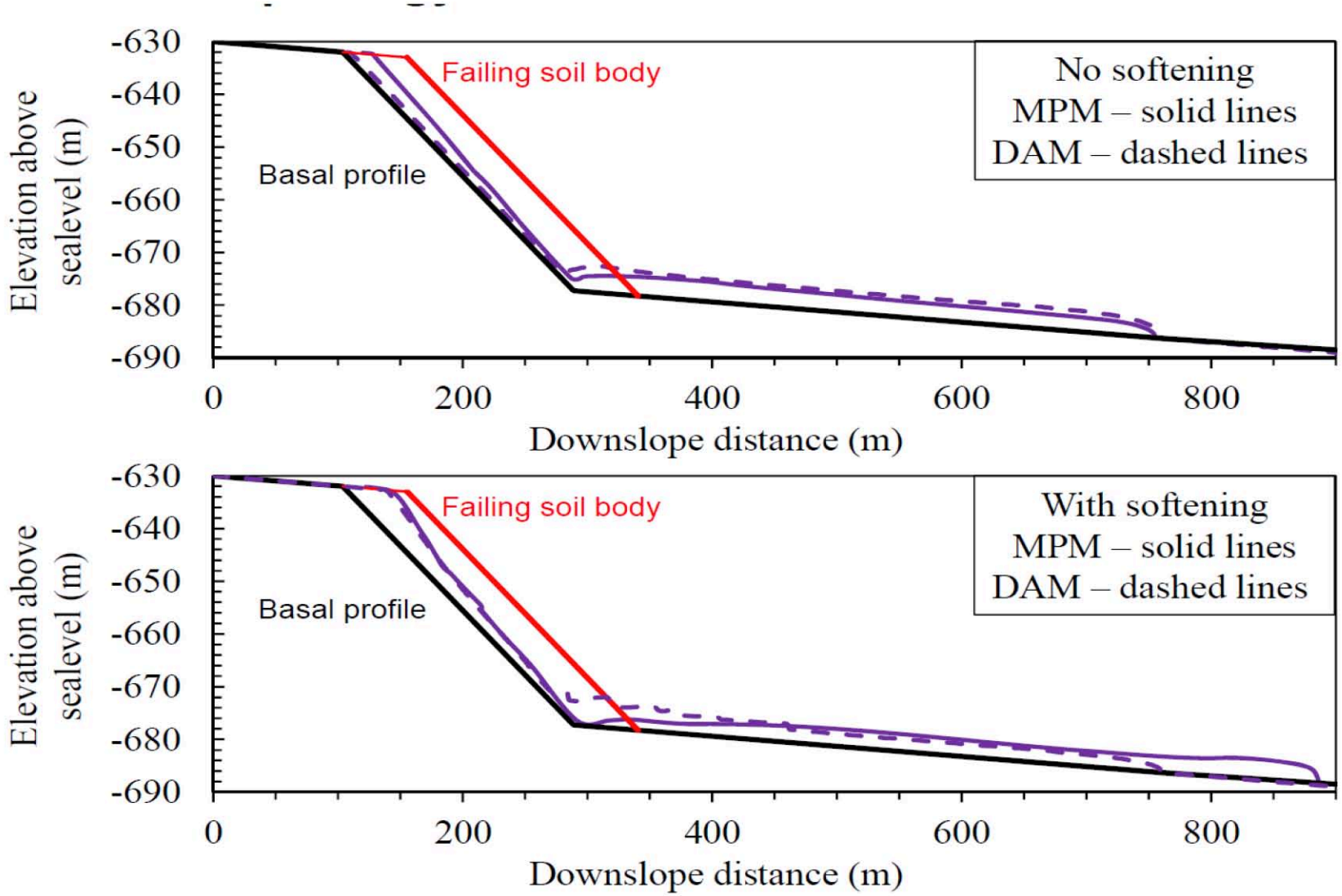

Longitudinal profiles of final strength

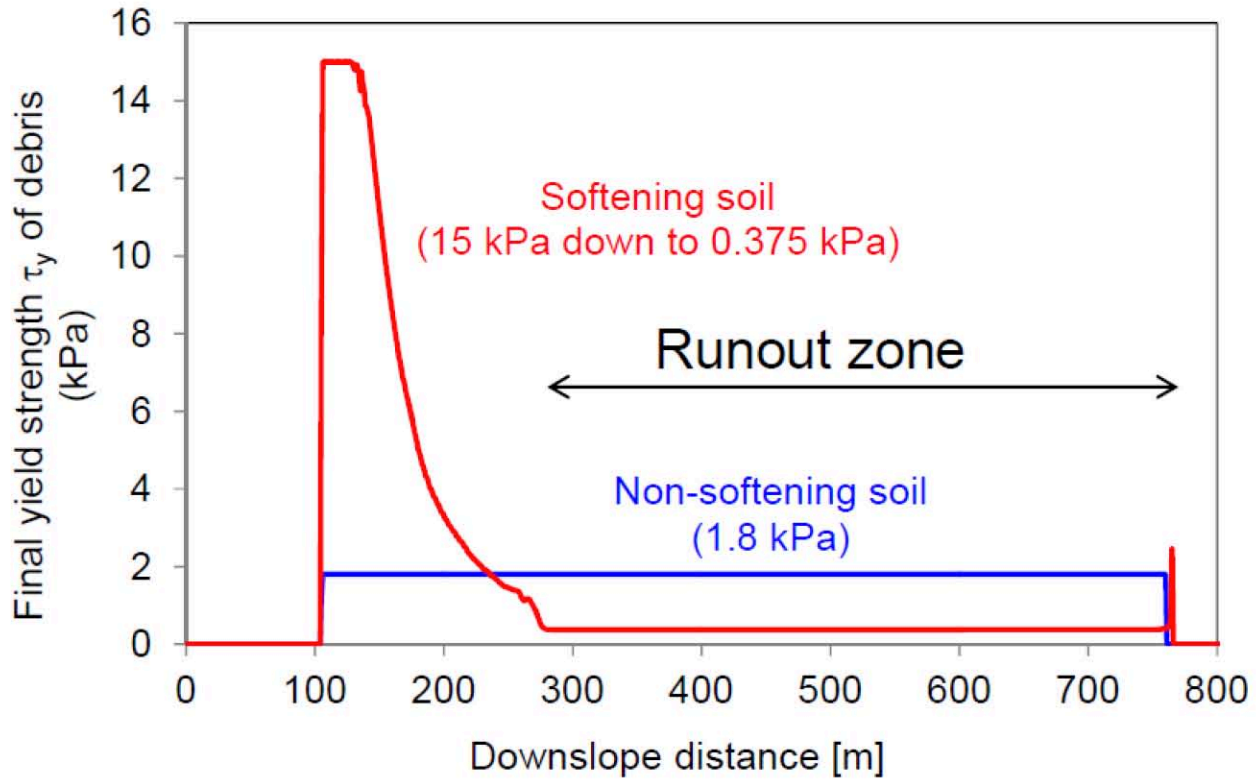

- Depth averaged analyses
- Softening analysis shows full remoulding over entire runout length

Next Step

- **Extend the Governing Equations**

Generalize the mass, momentum, and concentration equations to a multi-layer framework, allowing each layer to have distinct rheological properties.

- **Incorporate Rheological Evolution**

Integrate strain-softening behavior into the model by allowing
yield stress and viscosity parameters to evolve with strain or sediment remoulding.

- **Incorporate the HB shear stress**

FUGRO

FUGRO

Unlocking **Insights**
from **Geo-data**

Multi-Layer Shallow Water

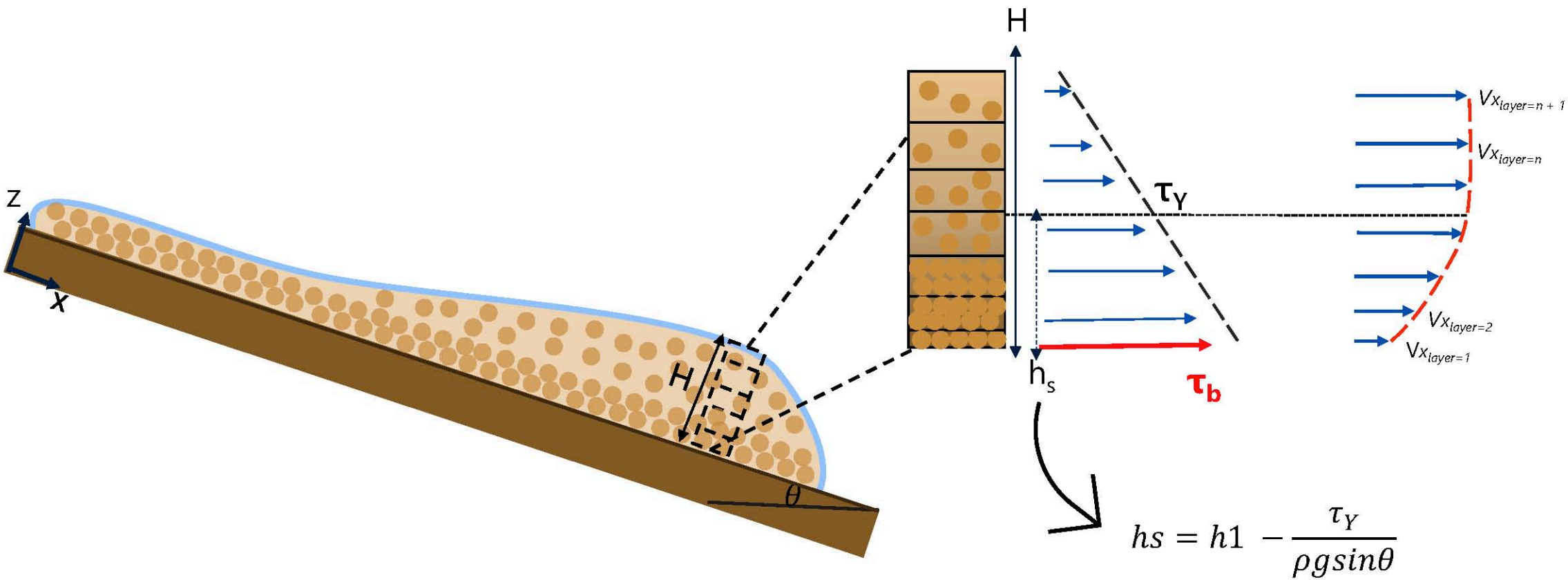

$$hs = h1 - \frac{\tau_Y}{\rho g sin\theta}$$

Overtopping Breakwater For Energy Conversion (OBREC)

Saeed Osouli

Supervisors:

Prof. Matteo Postacchini – UNIVPM

DR. Ivan Sabbioni – MAC

Prof. Maurizio Brocchini – UNIVPM

Prof. Gianluca Zitti – UNIVPM

SEDIMARE 2nd Workshop

HR Wallingford/ Howbery Park, Oxfordshire

10-11 September 2025

Motivations

- OBREC.
- Installing OBREC on attached Breakwaters (shore revetments).
- Comparing different convey systems in discharging water into the sea and behind the Device (inshore discharge).

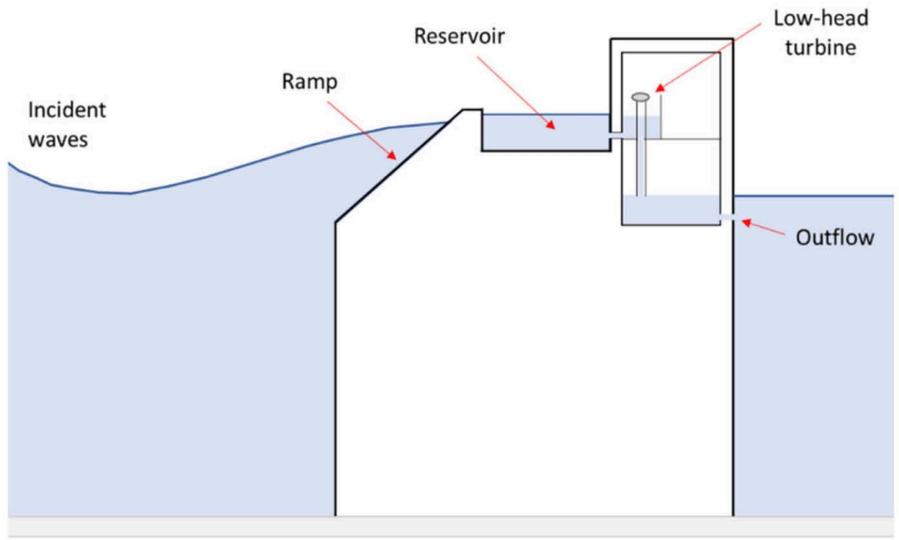

Scheme of the WEC integrated into a vertical caisson breakwater

Challenges

Water is discharged using two different conveyance systems: Pipe A and Pipe B.
Pipe A discharges directly into the sea, which can be challenging under storm conditions.
Pipe B discharges into the calm water behind the device.
The performance of the turbines in these two pipes will be compared

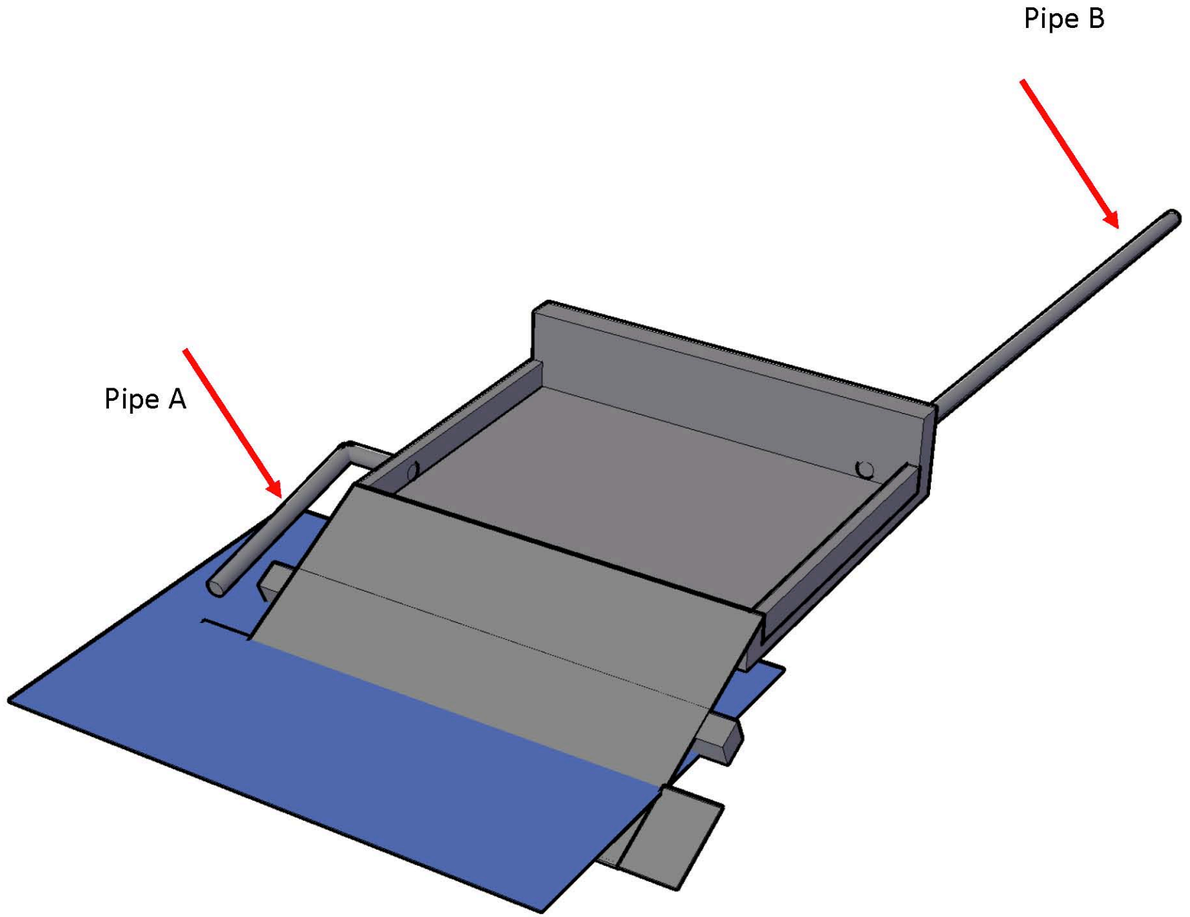

From the offshore to the port

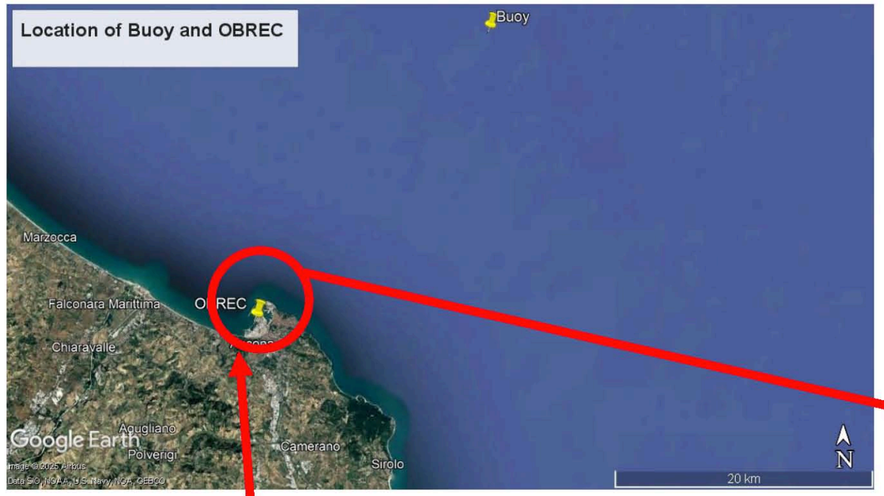

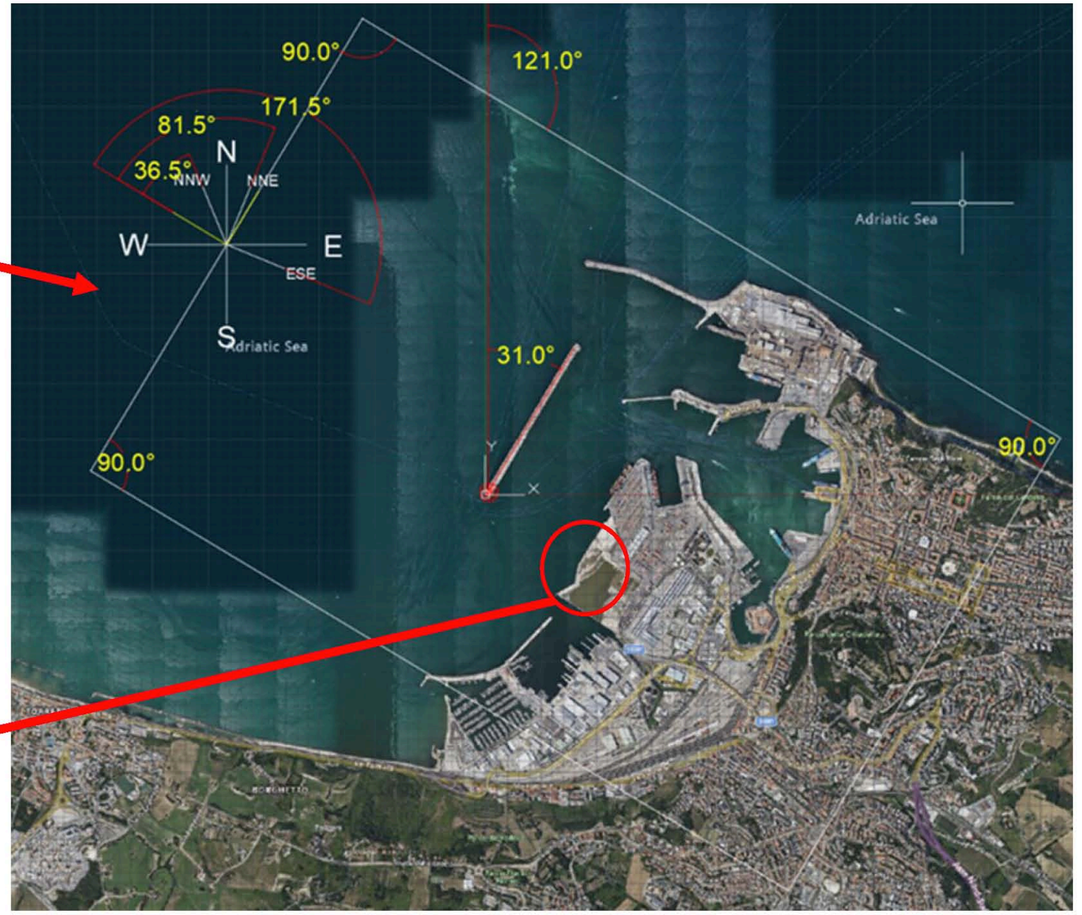

Inclination due to the boundary.

From the offshore to the port

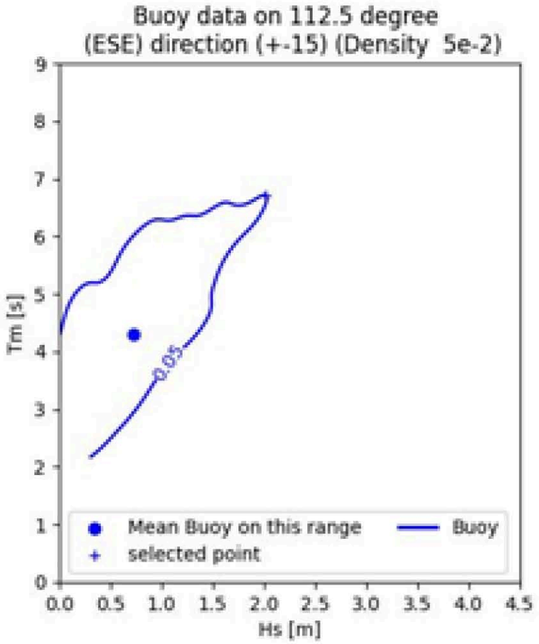

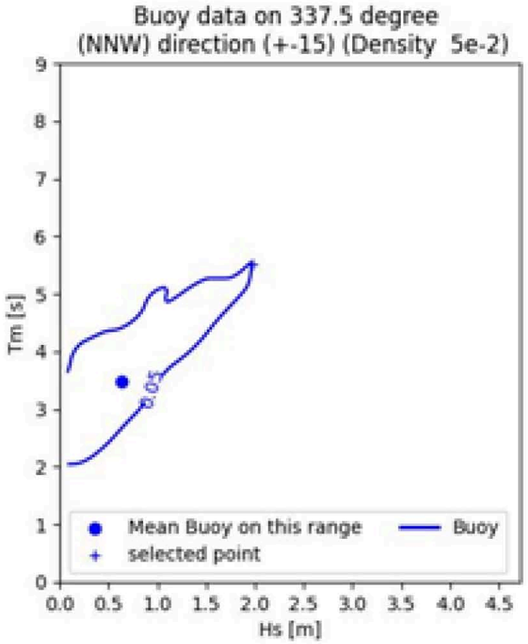

Applying Goda

Analytical approach

		NNE	NNW
Density 0.05	Hs (m)	2.53	1.67
	Tp (s)	7.81	6.51
	Tm (s)	6.62	5.52
	ap,h1 [°]	35.00	27.00
Density 0.005	Hs (m)	2.74	2.68
	Tp (s)	7.87	7.62
	Tm (s)	6.67	6.46
	ap,h1 [°]	35.00	23.00

FUNWAVE

FLOW-3D

FUNWAVE-TVD

- Bathymetry
- Simulation
- Outputs

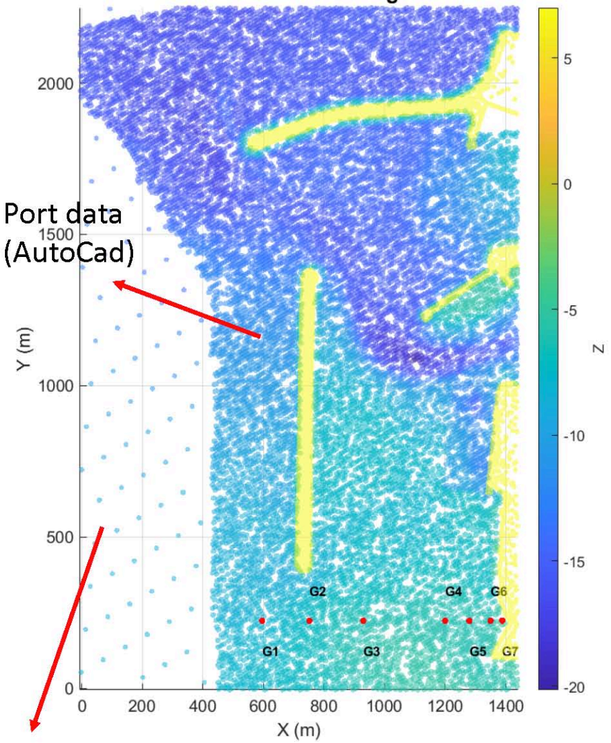

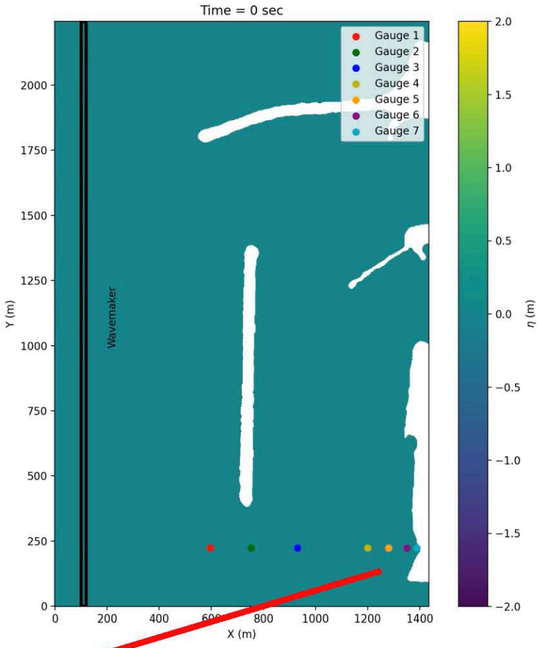

Density 0.005-NNE Waves

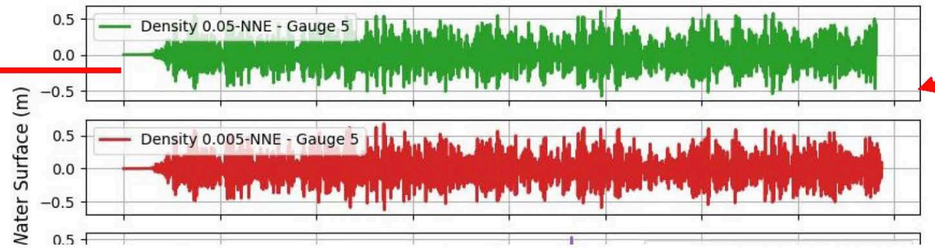

Free surface fluctuations

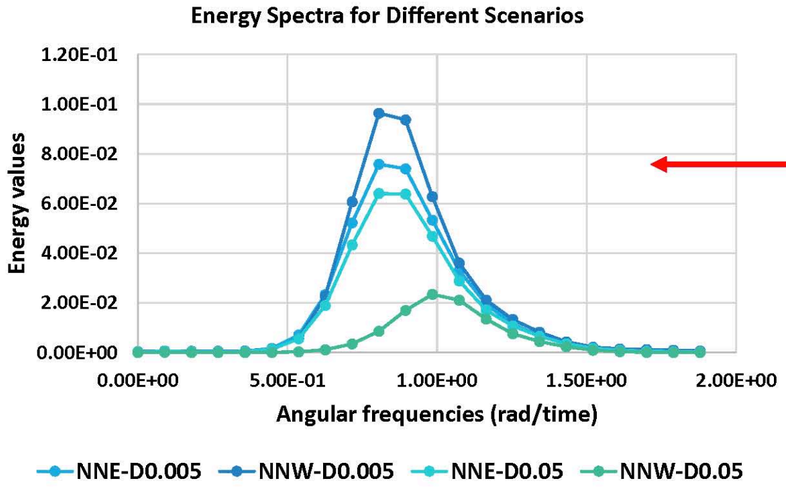

Results for different ramp slopes under different scenarios (freeboards, slopes)

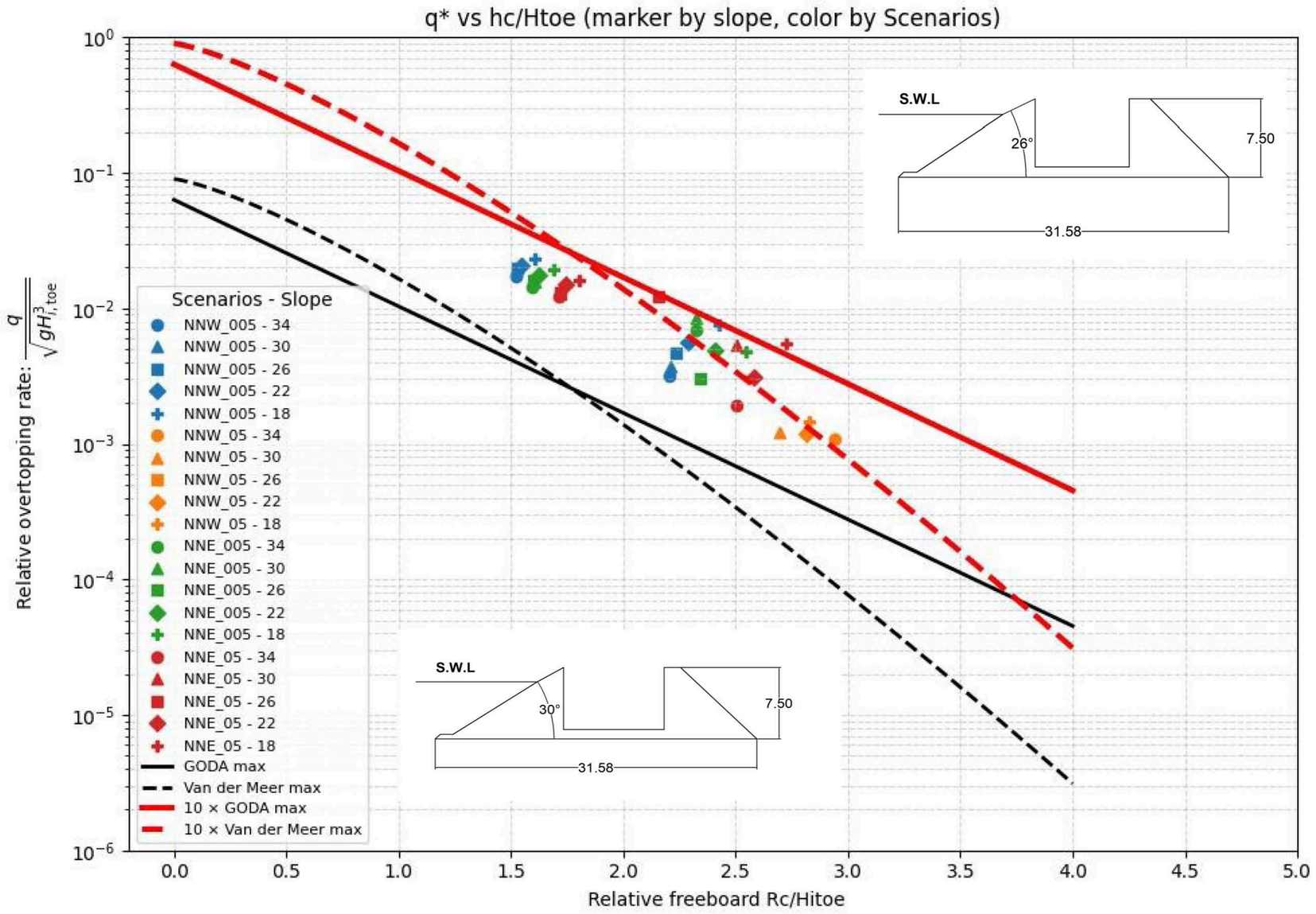

Goda (2009):

$$\frac{q}{\sqrt{gH_{s,toe}^3}} = q^* = \exp\left[-\left(A + B\frac{h_c}{H_{s,toe}}\right)\right]$$

$$A = A_0 \tanh\left\lfloor (0.956 + 4.44\tan\theta) \times (h_t/H_{s,toe} + 1.242 - 2.032\tan^{0.25}\theta)\right\rfloor \quad (17)$$

$$B = B_0 \tanh\left\lfloor (0.822 - 2.22\tan\theta) \times (h_t/H_{s,toe} + 0.578 + 2.22\tan\theta)\right\rfloor \quad (18)$$

with

$$A_0 = 3.4 \quad \text{and} \quad B_0 = 2.3 \quad (19)$$

Van der meer (2013) :

$$\frac{q}{\sqrt{g \cdot H_{m0}^3}} = 0.09 \cdot \exp\left[-\left(1.5\frac{R_c}{H_{m0} \cdot \gamma_f \cdot \gamma_\beta}\right)^{1.3}\right]$$

Numerical results overpredict in comparison to these equations.

Numerical results overpredict almost 10 times of these equations.

Reasons:

- number of waves
- Turbulence model
- Complete smooth ramp in numerical model

Results for different ramp slopes under different scenarios

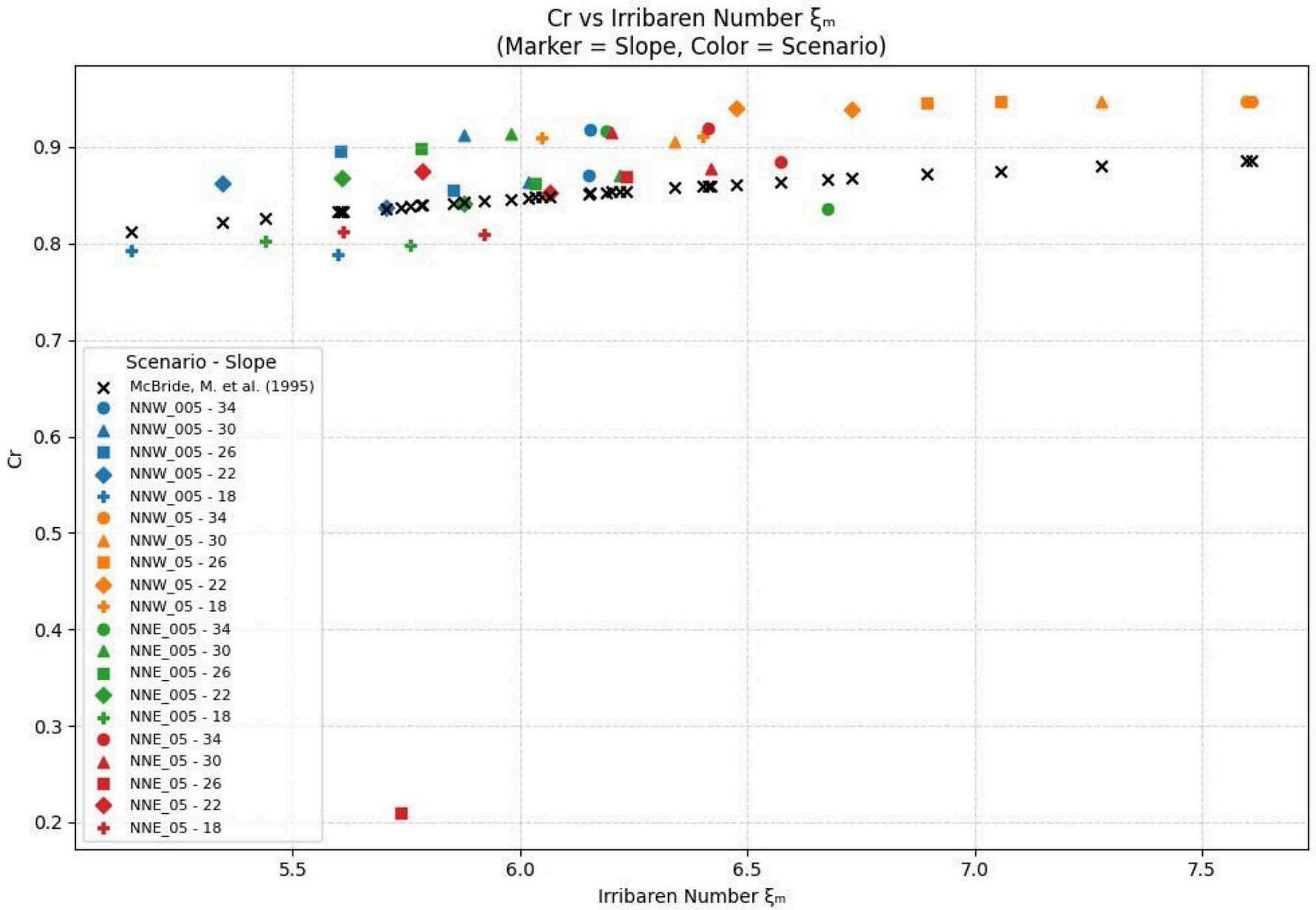

McBride, et al. 1995:

$$s_m = 2\pi H_s / g T_m{}^2$$
$$\xi = \tan\alpha / s_m{}^{0.5}$$
$$C_r = 0.96 \xi_m{}^2 / (4.8 + \xi_m{}^2)$$

Designing Turbine

D = 0.26 m in a 0.3 m pipe with 1.3 m head.

Numerically, controlling the rotation speed can increase both efficiency and output power. In the free rotation condition, the angular velocity is 62 rad/s, and it varies between 45 and 15 rad/s under other conditions.

P = ω*T

TSR = ω*R/v

Cp = P/Pav

Pav = Q*Δp

(Zitti et al.) 2020

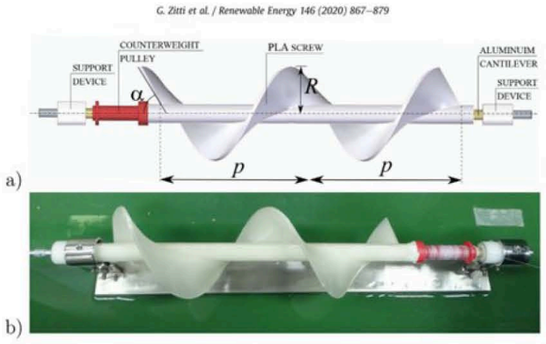

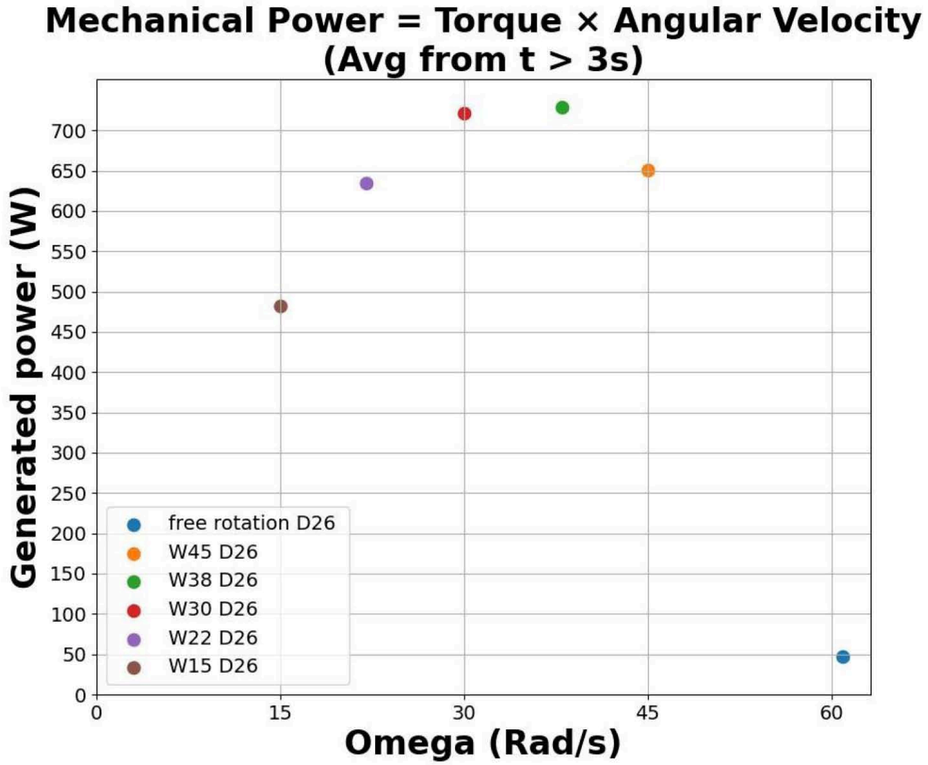

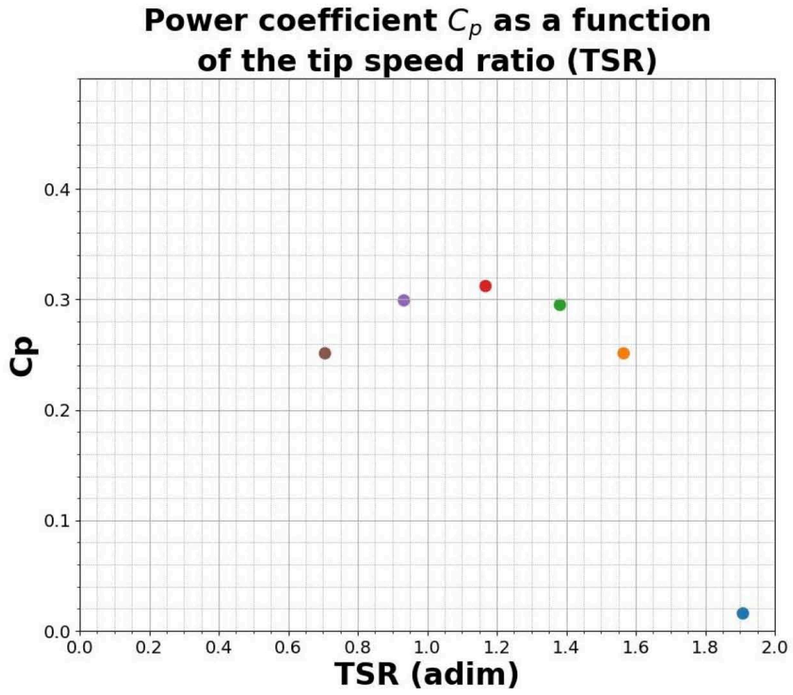

Turbulence pattern

The fluid velocity inside the pipe decreases as the rotation speed is reduced.

Free rotation	45 rad/s	30 rad/s	15 rad/s

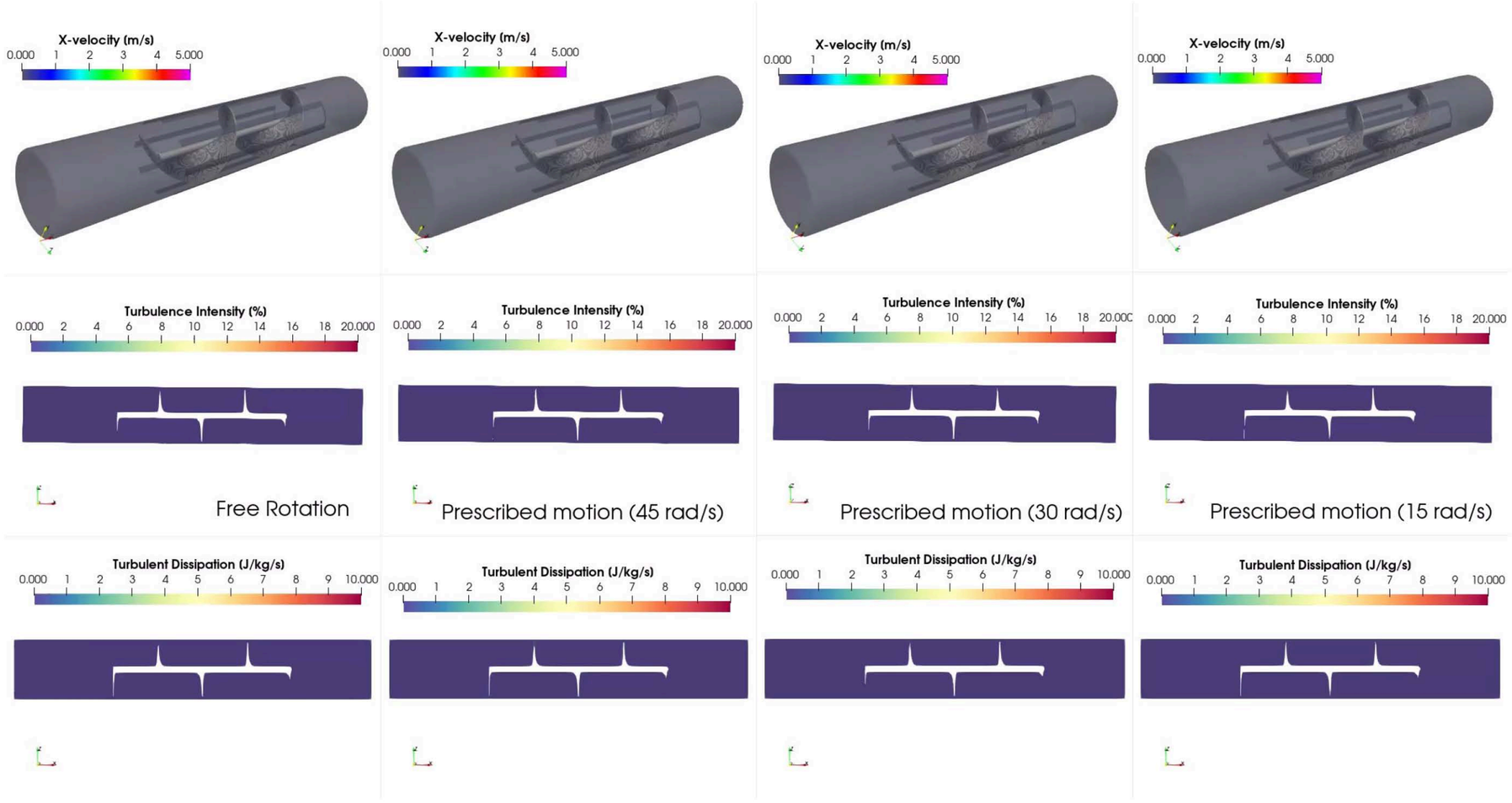

Energy across the system, considering different outlet pressures

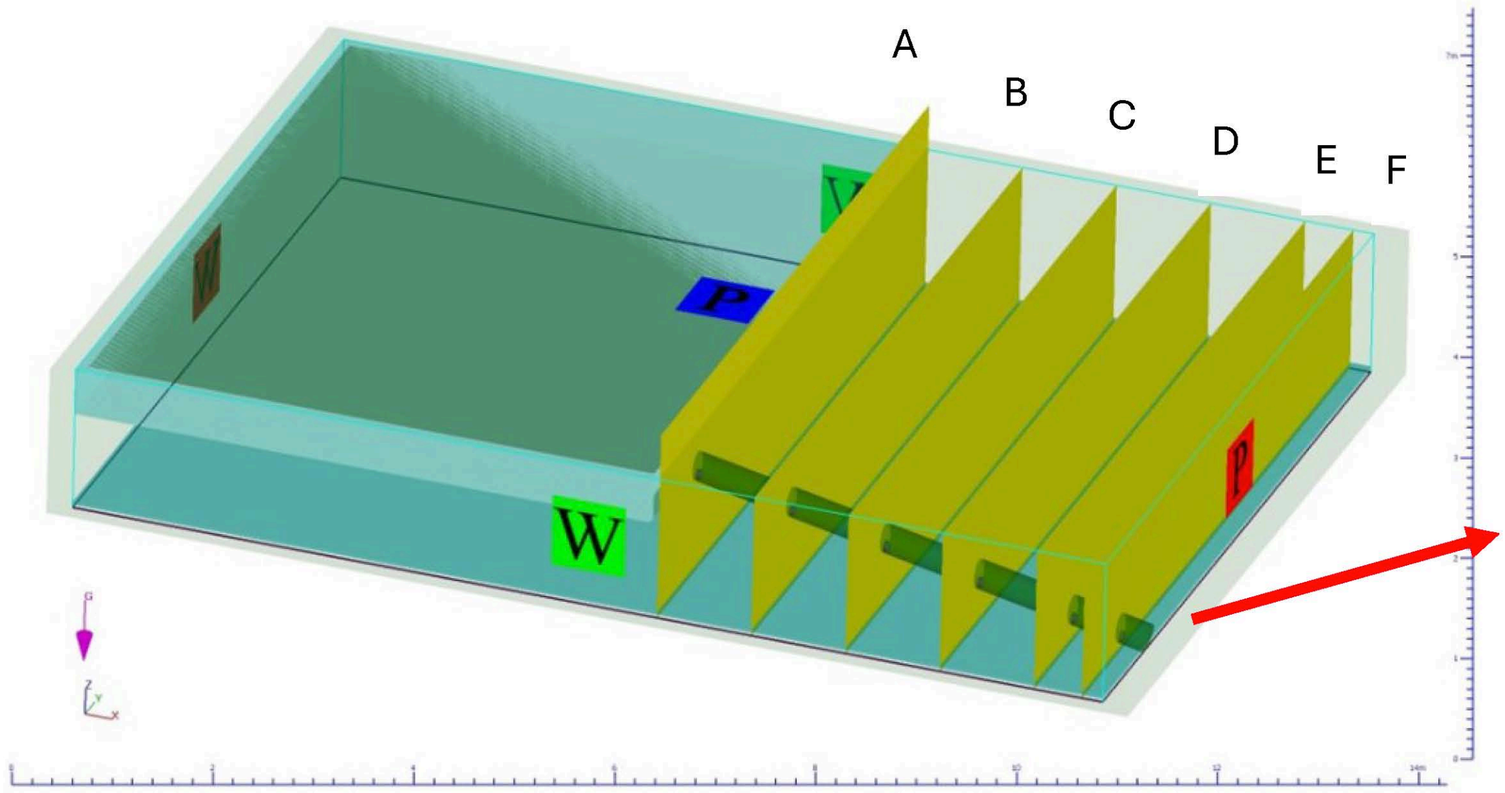

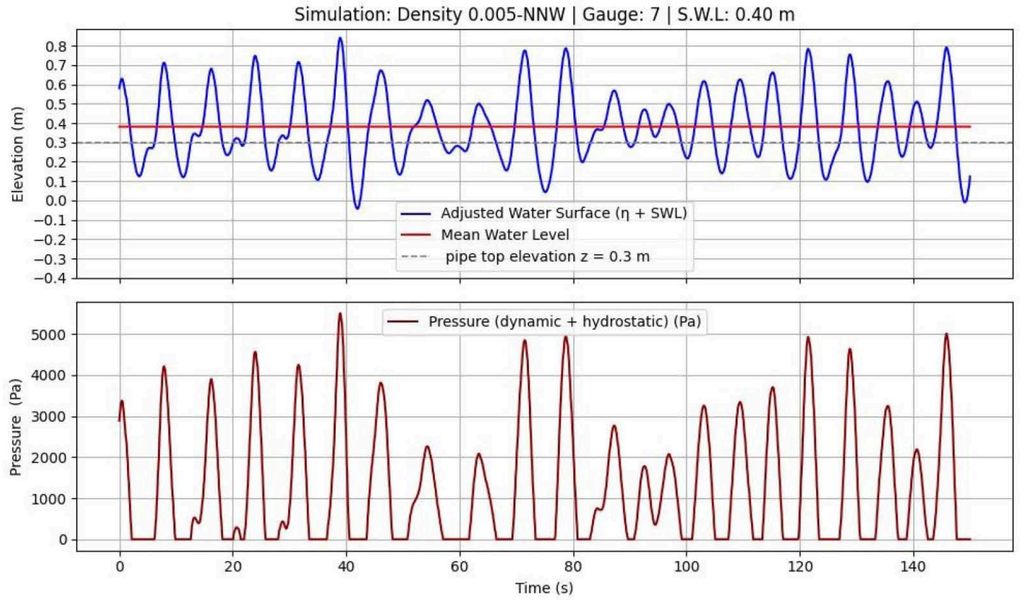

Hs =0.73 m near the outlet of pipe

kinetic energy : $P_f = \frac{1}{2}\rho A {v_{in}}^3$

A= $R^2 \arccos\left(1-\frac{h}{R}\right) - (R-h)\sqrt{R^2-(R-h)^2}$

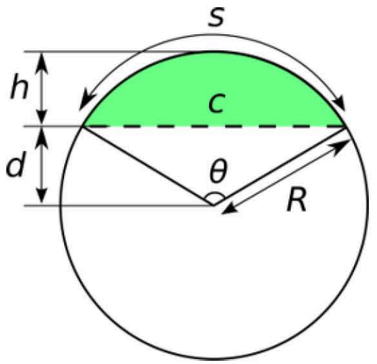

Energy across the system, considering different outlet pressures

Without Waves: mean energy at F: 720.7 w

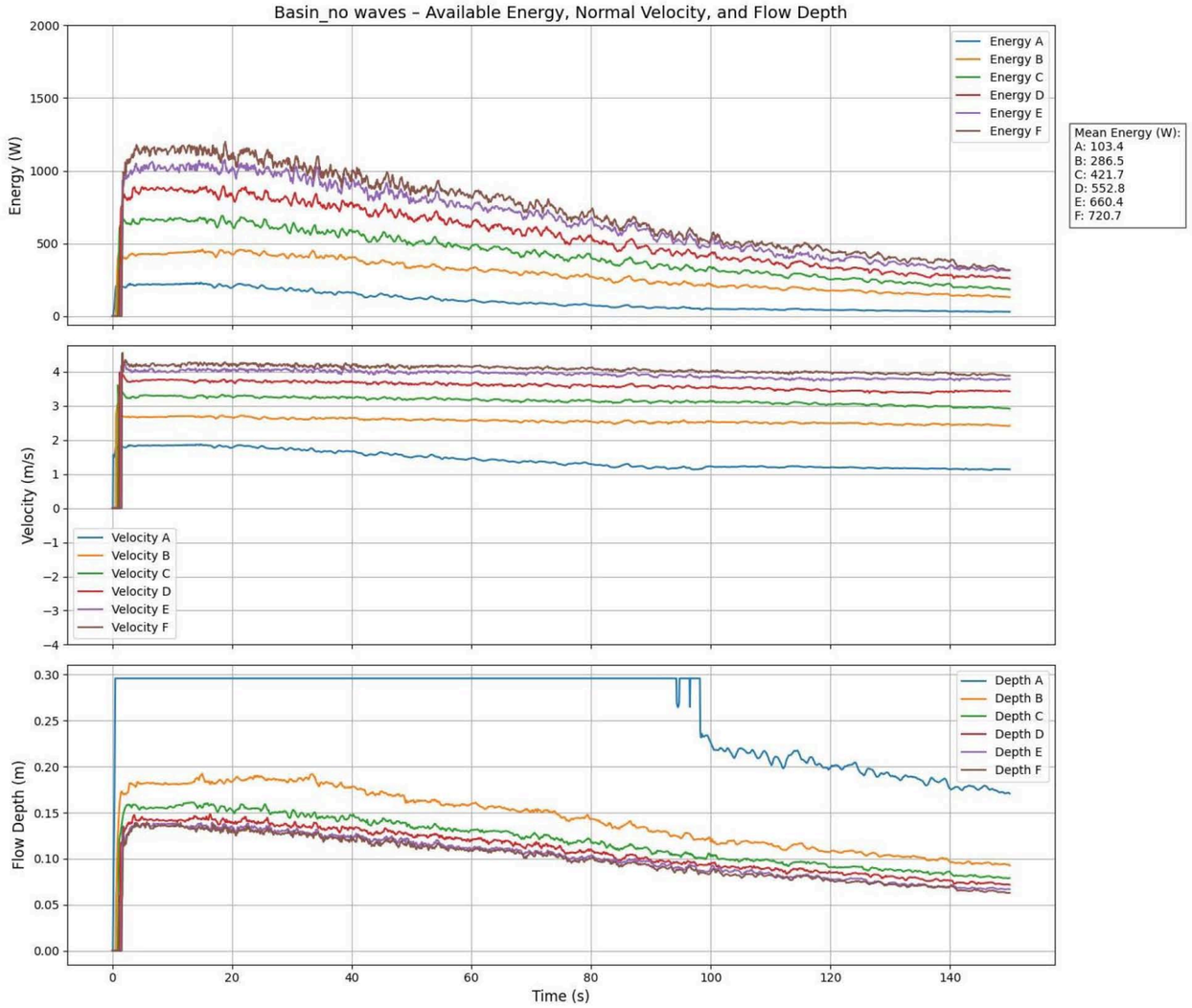

With Waves mean energy at F: 686.7 w

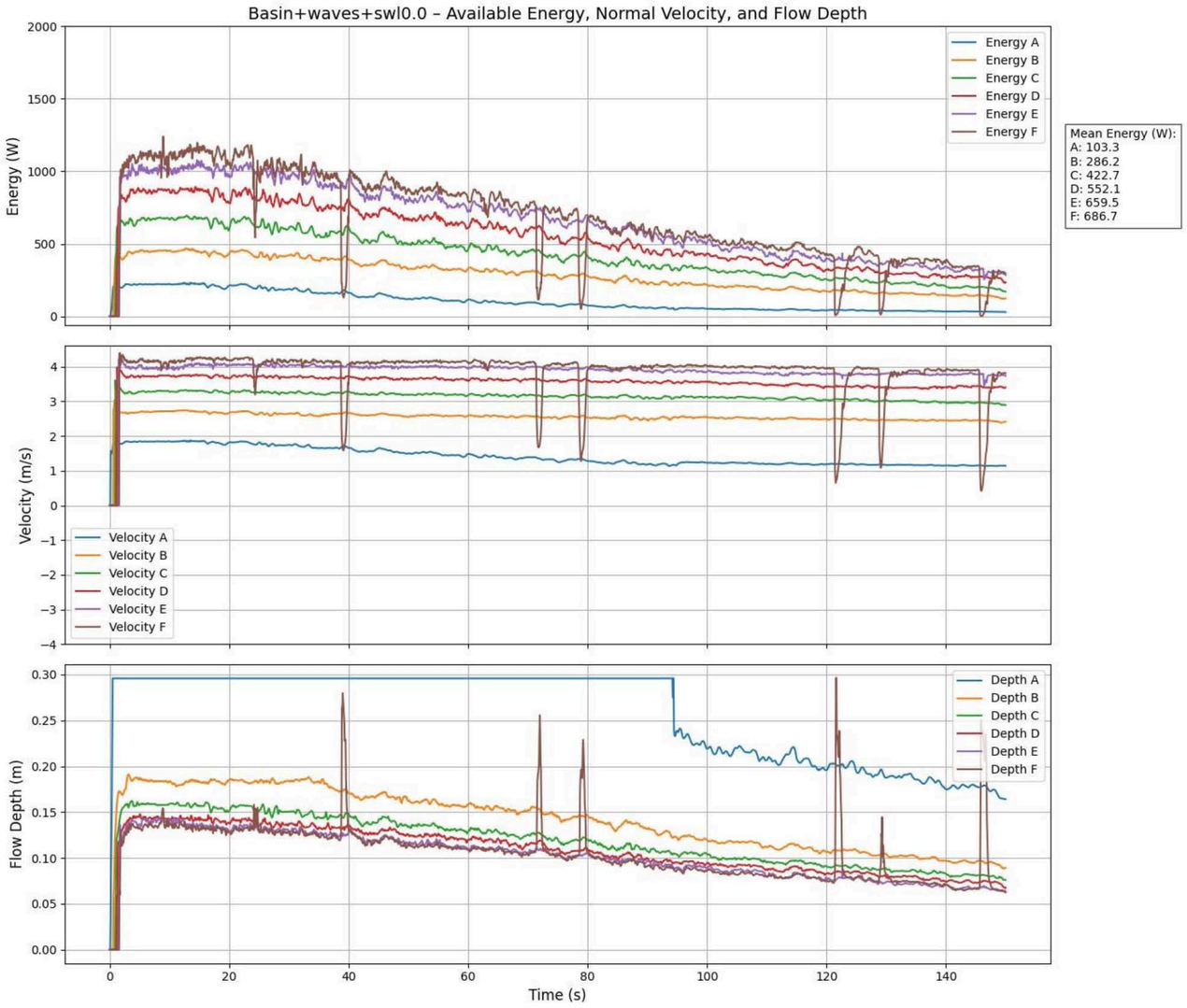

Conclusions

- Selecting waves based on 2 scenarios based on Buoy data.
- Transferring waves into Shallow water using Goda.
- Using FUNWAVE-TVD as the shallow water solver, its outputs were used as forcing waves in FLOW-3D.
- FLOW-3D is used to simulate wave and structure interaction as a CFD tool.
- Controlling the rotation speed for Turbine up to a specific value could increase the efficiency.

- **FUTURE WORK:**
  - Planned construction of ramp, basin and Turbine .
  - Monitoring the performance of the device.
  - Comparing 2 different convey systems.

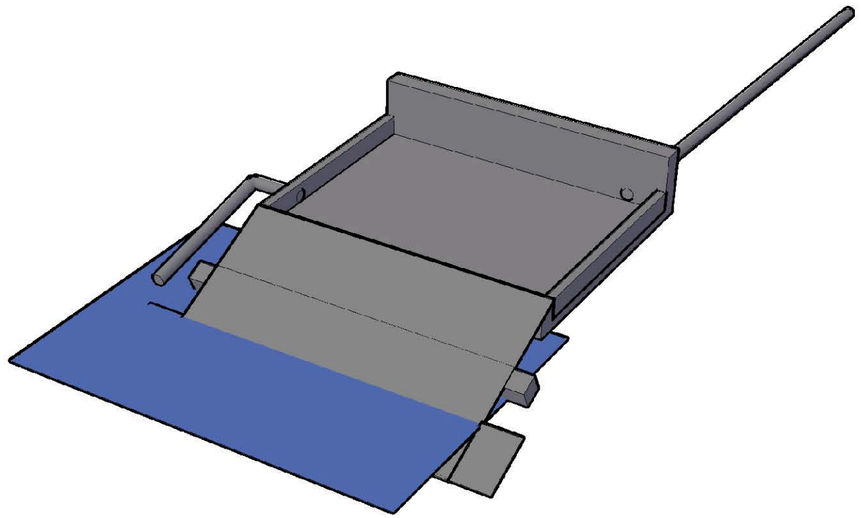

Thank you for your attention!

s.osouli@pm.univpm.it

Financial support has been provided by European Union's (EU) Horizon Europe Framework Programme (HORIZON) via SEDIMARE (Grant Agreement No. 101072443), an MSCA Doctoral Network (HORIZON-MSCA-2021-DN-01).

University of Nottingham
UK | CHINA | MALAYSIA

UK Research and Innovation

Marie Skłodowska-Curie Actions

SEDIMARE 2023-2027

Sediment Transport and Morphodynamics in Marine and Coastal Waters with Engineering Solutions

SEDIMARE 2nd Workshop

Wallingford, 10 – 11 Sep 2025

Numerical investigations of bottom boundary layer hydrodynamics under a dam-break-driven swash event

[1]**Quan T. Nguyen**, [3]Joost W.M. Kranenborg,

[1]Nicholas Dodd, [1]Riccardo Briganti, [2]Fangfang Zhu, [3,4]Jebbe J. van der Werf, [4]Pieter C. Roos

[1]University of Nottingham, UK

[2]University of Nottingham Ningbo Campus, China

[3]Deltares, Delft, The Netherlands

[4]University of Twente, Enschede, The Netherlands

This project has been funded by UKRI under the Horizon Europe guarantee scheme for the Marie Skłodowska-Curie Actions Doctoral Network grant (HORIZON-MSCA-2021-DN-01) under Grant Agreement No. 101072443.

Overview of the work

The swash zone

- **Wave run-up/run-down** impacts the sediment transport and the morphology of the bed
- **Bottom shear stress** in wave motion are one of the key parameters that affecting the mobilisation and transportation of sediment in the flow.
  - Depends on the **structure of the flow near the bottom**
- Standard hydrostatic models are efficient but struggle to accurately simulate swash zone dynamics where vertical water motions are significant (e.g., wave run-up, bore arrival)
  - Previous Bottom Boundary Layer (BBL) models by Briganti et al. (2011) did not include spatial acceleration terms.
  - Zhu et al. (2022) later incorporated horizontal spatial gradients.

The swash zone at El Sardinero beach in Santander, Spain

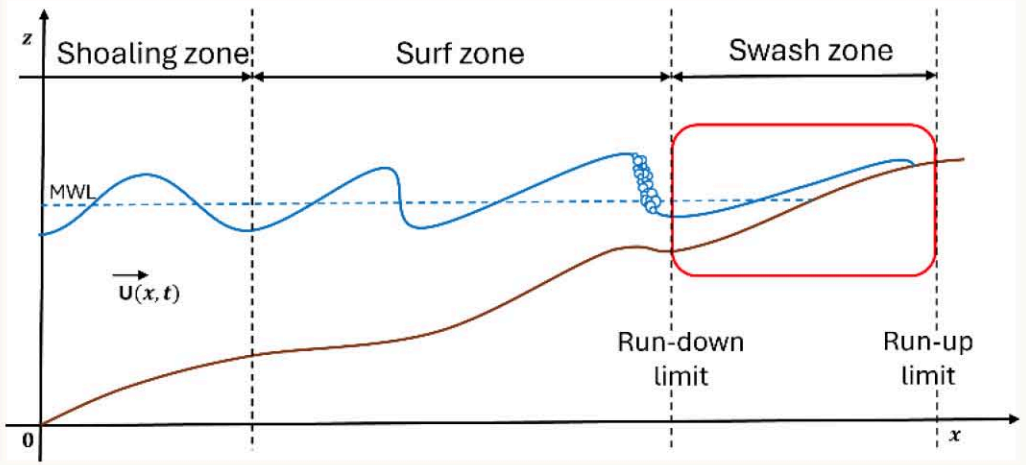

Schematic overview of the swash zone

Overview of the work

Motivation

Improving the representation of the velocity field within the bottom boundary layer (BBL) in the swash zones.

- Adding the description of **vertical velocity** inside the BBL

Investigating whether the non-hydrostatic terms are significant enough to be included in the NSWE

- Approximating the dynamic pressure gradients efficiently using a depth-averaging model equipped with a BBL sub-model

Overview of the work

Numerical modelling of swash processes

$B(x)$ is the bed level at location x;
z_0 is the bed roughness length;
δ is the bottom boundary layer thickness at location x;
κ is von Karman's constant;
U_0 is free stream velocity;
u_f is the friction velocity;
ρ is the water density.

- Wave-resolving, depth-averaged, fully-coupled model based on **1D nonlinear shallow water equations (NLSWEs)**
  - ✓ Description of bottom boundary layer (using the Momentum Integral Method)
    - ➢ Assumption inside the BBL:

$$u(x,z,t) = \frac{u_f(x)}{\kappa} ln\left(\frac{z - B(x)}{z_0}\right)$$

    - ➢ Integrating the momentum equation over the BBL thickness to compute the friction velocity u_f.
  - ✓ State of the art in modelling the evolution of BBL and description of vertical distribution of horizontal velocity inside the BBL for the **fixed** bed.
  - X **Not include the description of vertical velocity.**

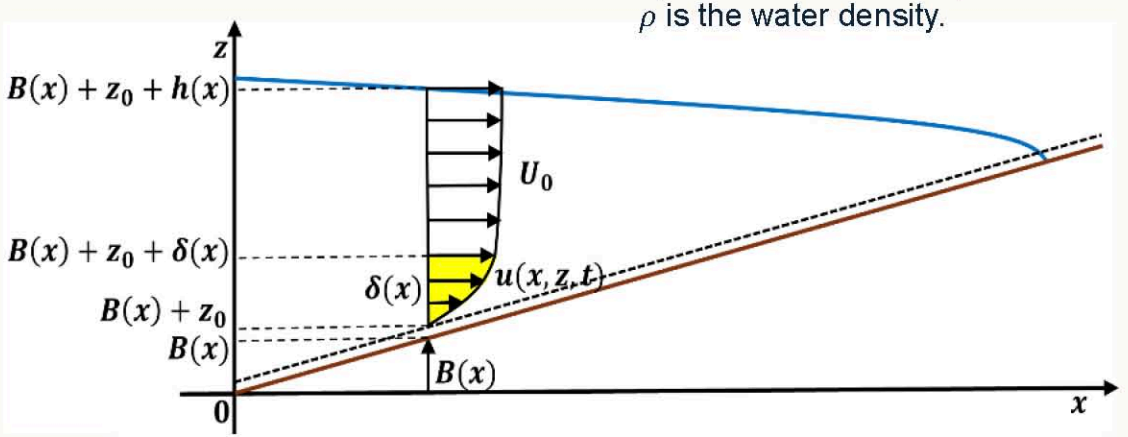

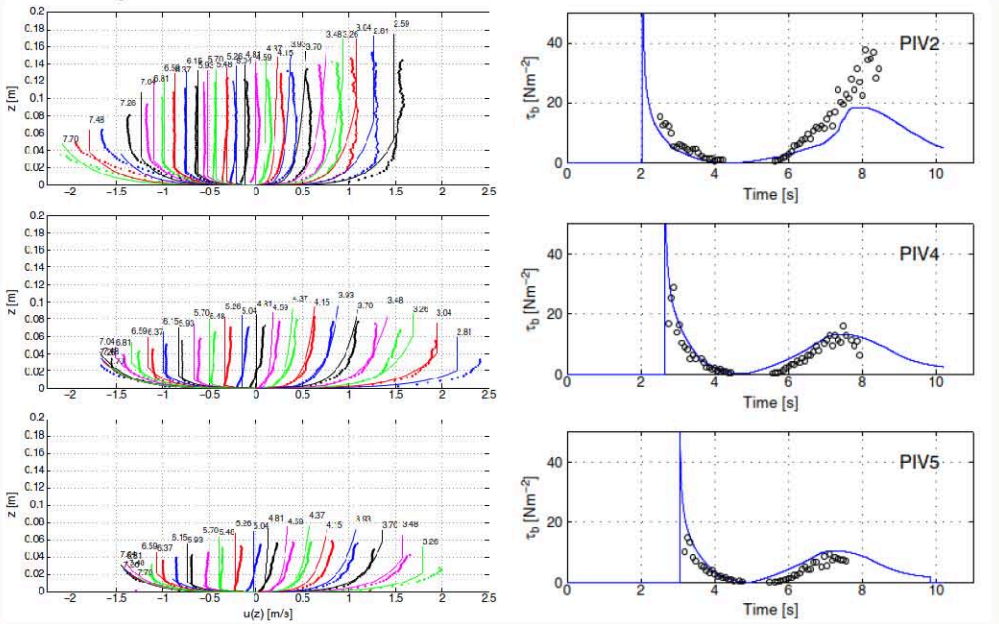

Prediction of vertical profile of horizontal velocity and bed shear stress (Briganti et el., 2011)

Research methodology

$B(x)$ is the bed level at location x;
z_0 is the bed roughness length;
δ is the bottom boundary layer thickness at location x;
κ is von Karman's constant;
U_0 is free stream velocity;
u_f is the friction velocity;
ρ is the water density.

Re-construct of vertical velocity

- Assumptions at the lower limit of BBL:

$$\begin{cases} u(x, z = B(x) + z_0, t) = 0 \\ w(x, z = B(x) + z_0, t) = 0 \end{cases}$$

- Integrating the 2D continuity equation $\left(\frac{\partial u}{\partial x} + \frac{\partial w}{\partial z} = 0\right)$ over the BBL: $\int_{B(x)+z_0}^{z} \frac{\partial w}{\partial x} dz = -\int_{B(x)+z_0}^{z} \frac{\partial u}{\partial x} dz$
  - Inside the BBL:

$$w(x,z) = -\frac{z_0}{\kappa}\frac{\partial u_f(x)}{\partial x}\left[\frac{z - B(x)}{z_0}\left(ln\left(\frac{z - B(x)}{z_0}\right) - 1\right) + 1\right]$$

  - At top of the BBL ($z = B(x) + z_0 + \delta(x)$):

$$w(x, z = B(x) + z_0 + \delta(x)) = -\frac{z_0}{\kappa}\frac{\partial u_f(x)}{\partial x}\left[\frac{z_0 + \delta(x)}{z_0}\left(ln\left(\frac{z_0 + \delta(x)}{z_0}\right) - 1\right) + 1\right]$$

  - Outside the BBL:

$$w(x,z) = w(x, z = B(x) + z_0 + \delta(x)) + \frac{\partial U_0}{\partial x}\left[z - \left(B(x) + z_0 + \delta(x)\right)\right]$$

Research methodology

Dynamic pressure gradient terms

$$p|_z \approx \rho g(\eta(x) - \hat{z}) + \rho \frac{\partial}{\partial t} \int_{\hat{z}}^{\eta(x)} w(x,z,t)dz + \rho \frac{\partial}{\partial x} \int_{\hat{z}}^{\eta(x)} u(x,z,t)w(x,z,t)dz$$

p_{Term1} p_{Term3} p_{Term3}

- From the BBL model:

$$w(x,z) = \begin{cases} -\frac{z_0}{\kappa}\frac{\partial u_f(x)}{\partial x}\left[\frac{z}{z_0}\left(ln\left(\frac{z}{z_0}\right) - 1\right) + 1\right], with\ z_0 \le z < z_0 + \delta(x) \\ w\left(x, z = z_0 + \delta(x)\right) - \frac{\partial U_0(x)}{\partial x}\left[z - \left(z_0 + \delta(x)\right)\right], with\ z_0 + \delta(x) \le z < z_0 + \eta(x) \end{cases}$$

$$u(x,z) = \begin{cases} \frac{u_f(x)}{\kappa} ln\left(\frac{z}{z_0}\right), with\ z_0 \le z < z_0 + \delta(x) \\ U_0(x), with\ z_0 + \delta(x) \le z < z_0 + \eta(x) \end{cases}$$

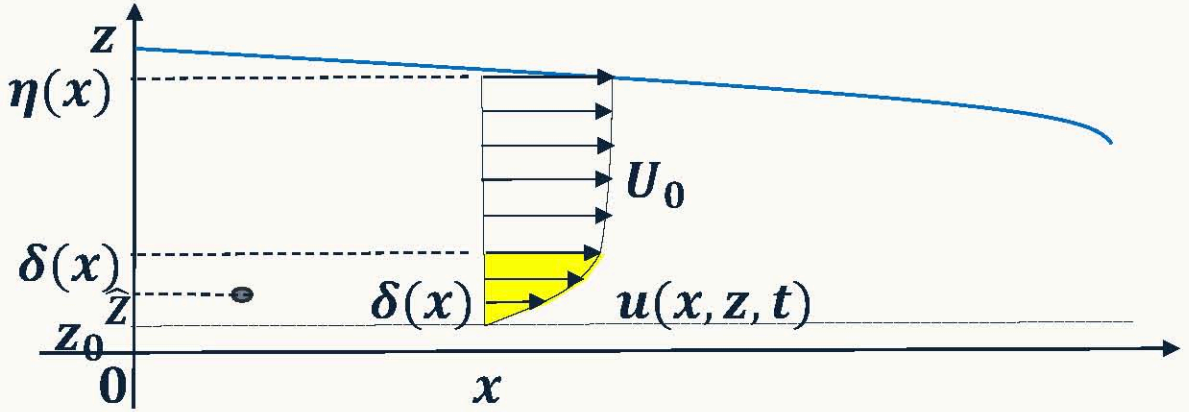

Research methodology

Numerical experiment set-up

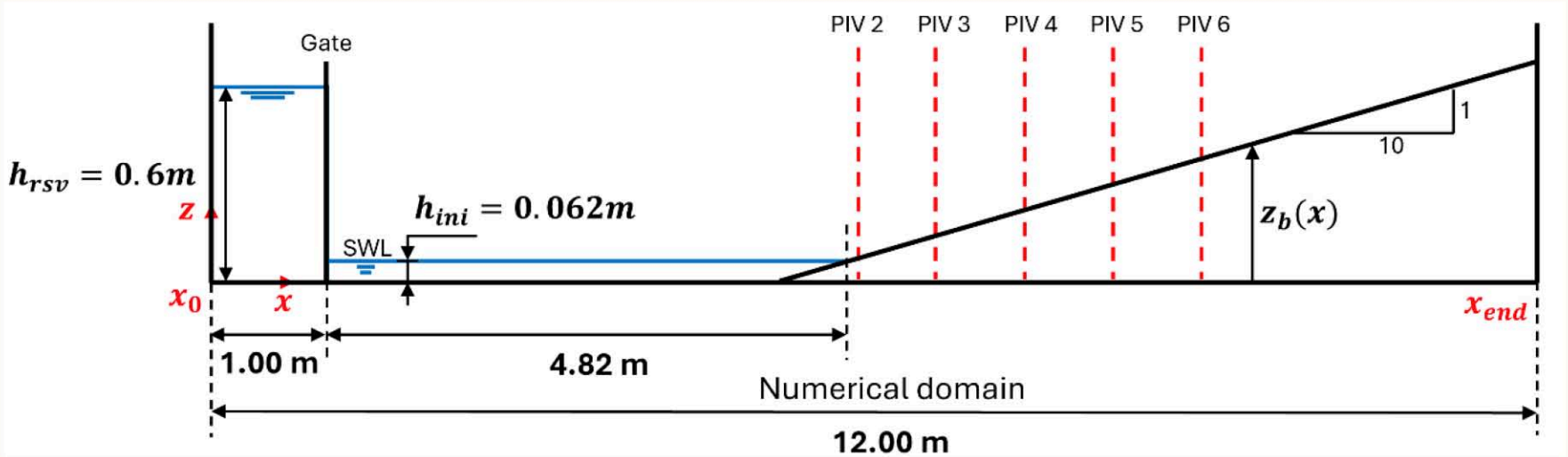

Schematic of the numerical setup based on the Aberdeen Swash facility.

- **Laboratory-based datasets for benchmarking**
  - Experimental study of bore-driven swash hydrodynamics on impermeable rough slopes (Kikkert et al., 2012).
- **Numerical-based datasets for comparison with depth-resolving model**
  - Corresponding simulation data for the same event, generated from a three-dimensional 2DV RANS (VOF) equation solver, denoting: J2DV/J3D-model (Kranenborg et al., 2022).

Research results - **Water depth**

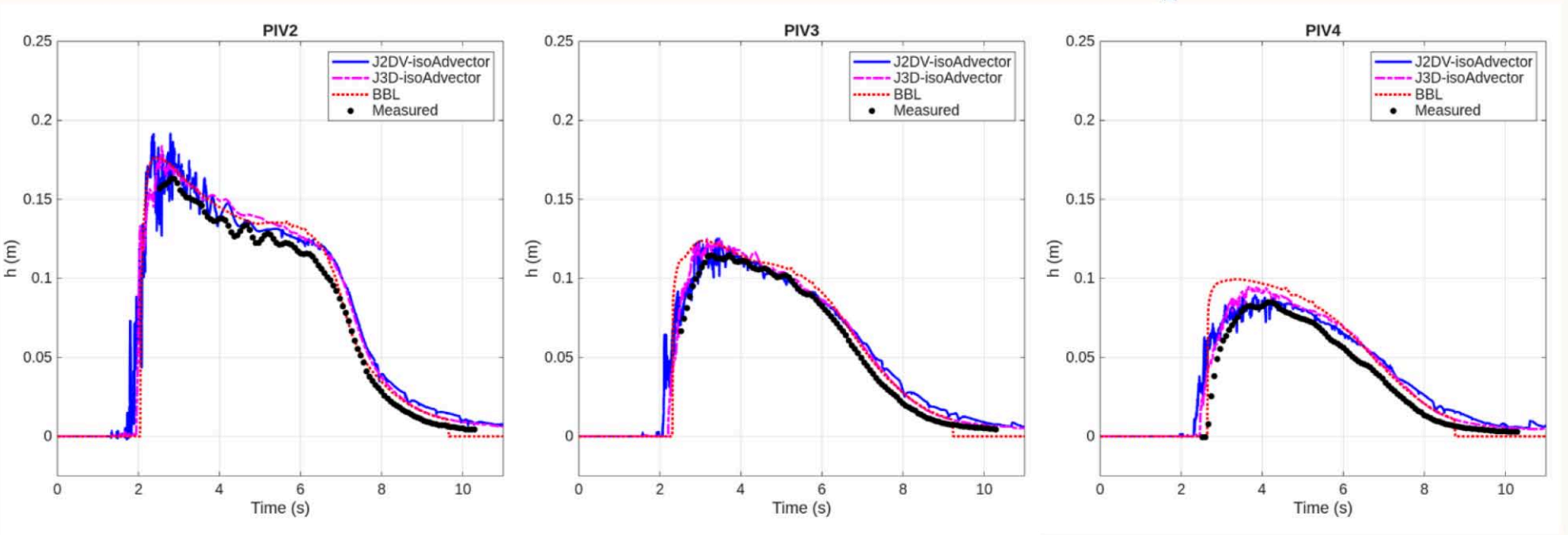

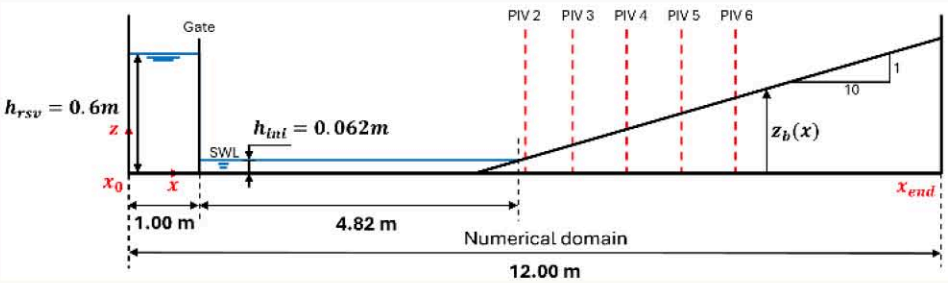

Research results - Depth-averaged velocity

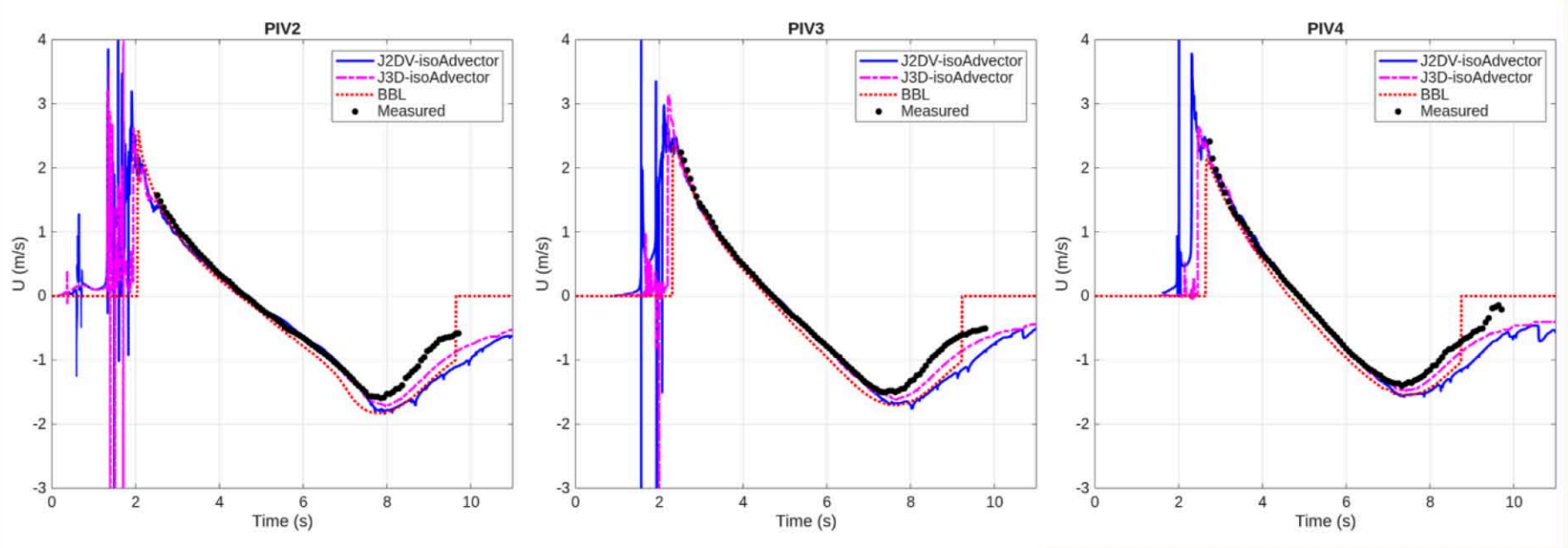

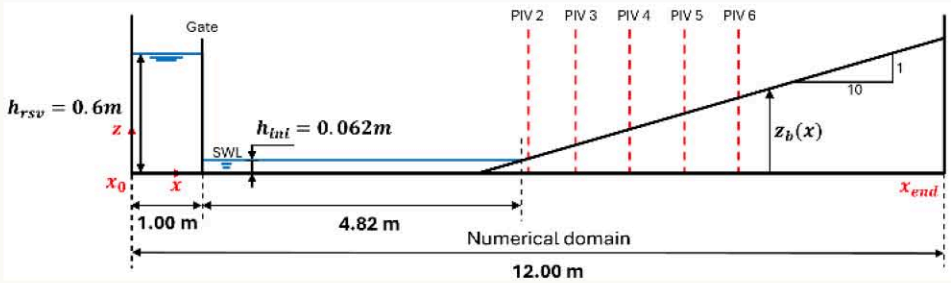

– Velocity profiles

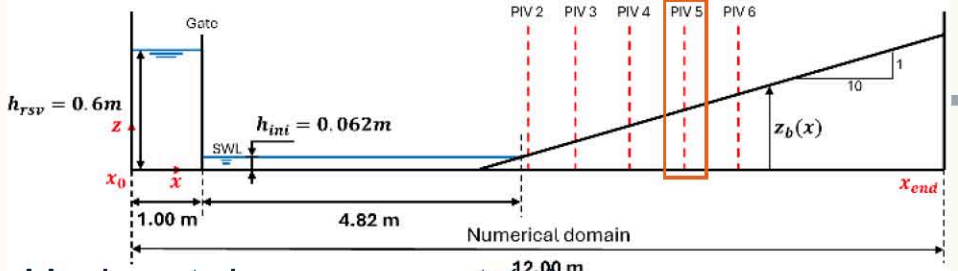

Horizontal component (u)

PIV5

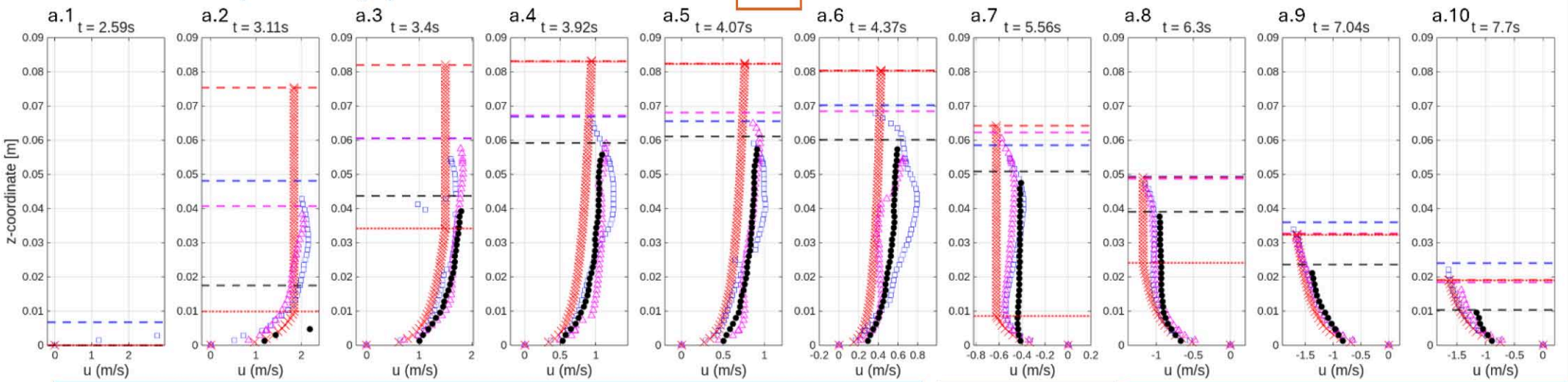

Up-rush phase | Flow reversal | Backwash phase

Vertical component (w)

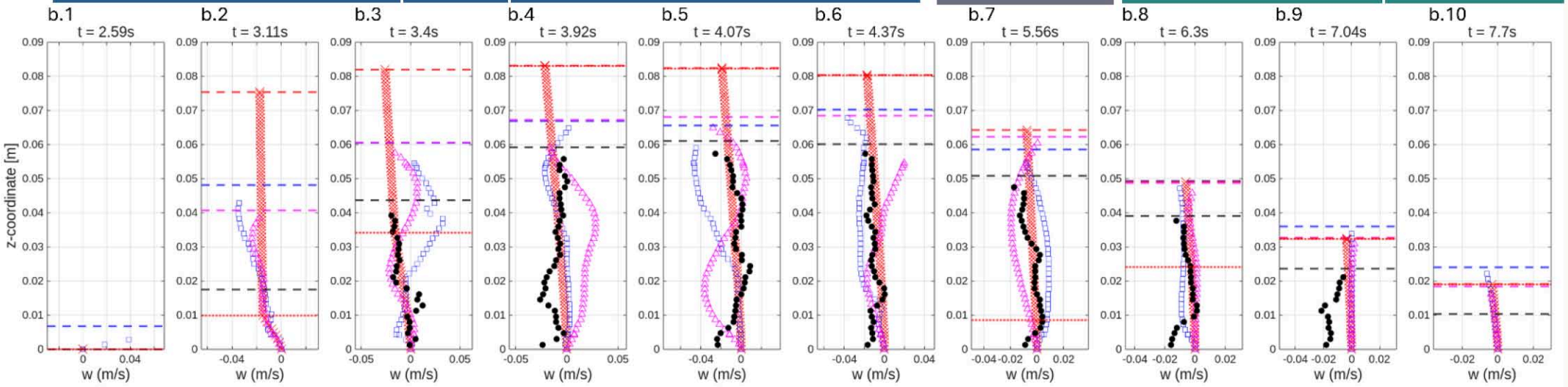

Research results – Pressure gradient terms

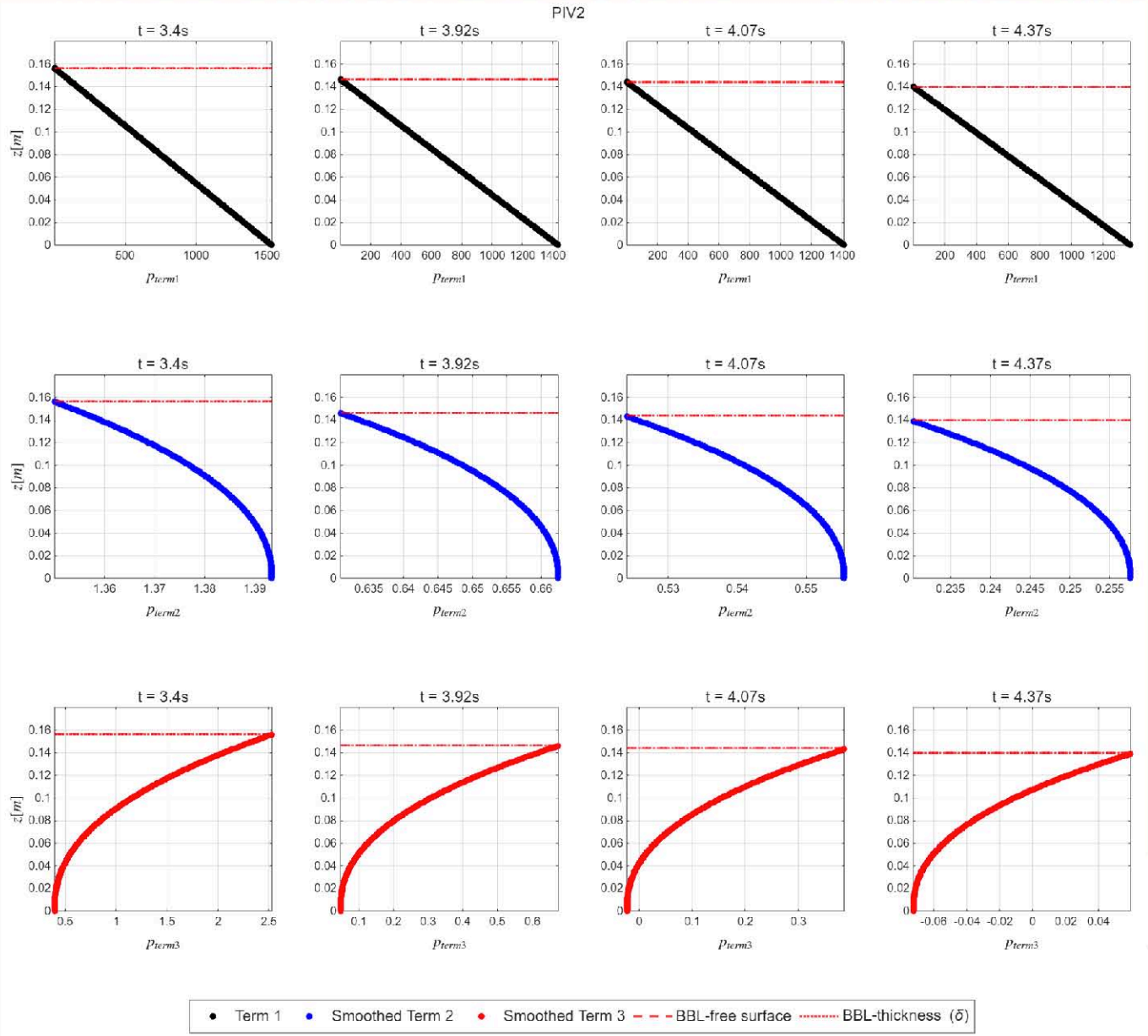

$$p_{Term1} = \rho g(\eta(x) - \hat{z})$$

$$p_{Term2} = \rho \frac{\partial}{\partial t} \int_{\hat{z}}^{\eta(x)} w(x,z,t)dz$$

$$p_{Term3} = \rho \frac{\partial}{\partial x} \int_{\hat{z}}^{\eta(x)} u(x,z,t)w(x,z,t)dz$$

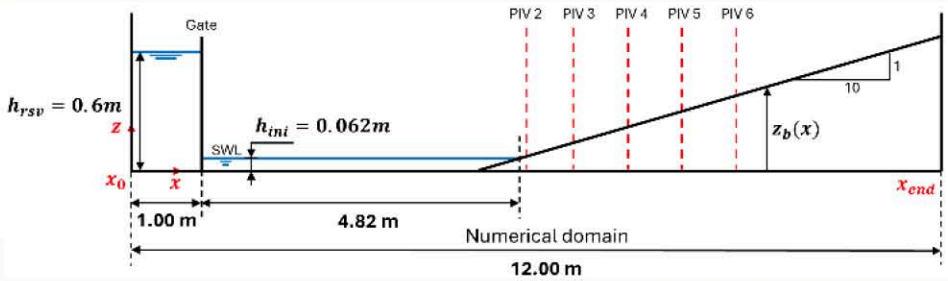

Research results – Pressure gradient terms

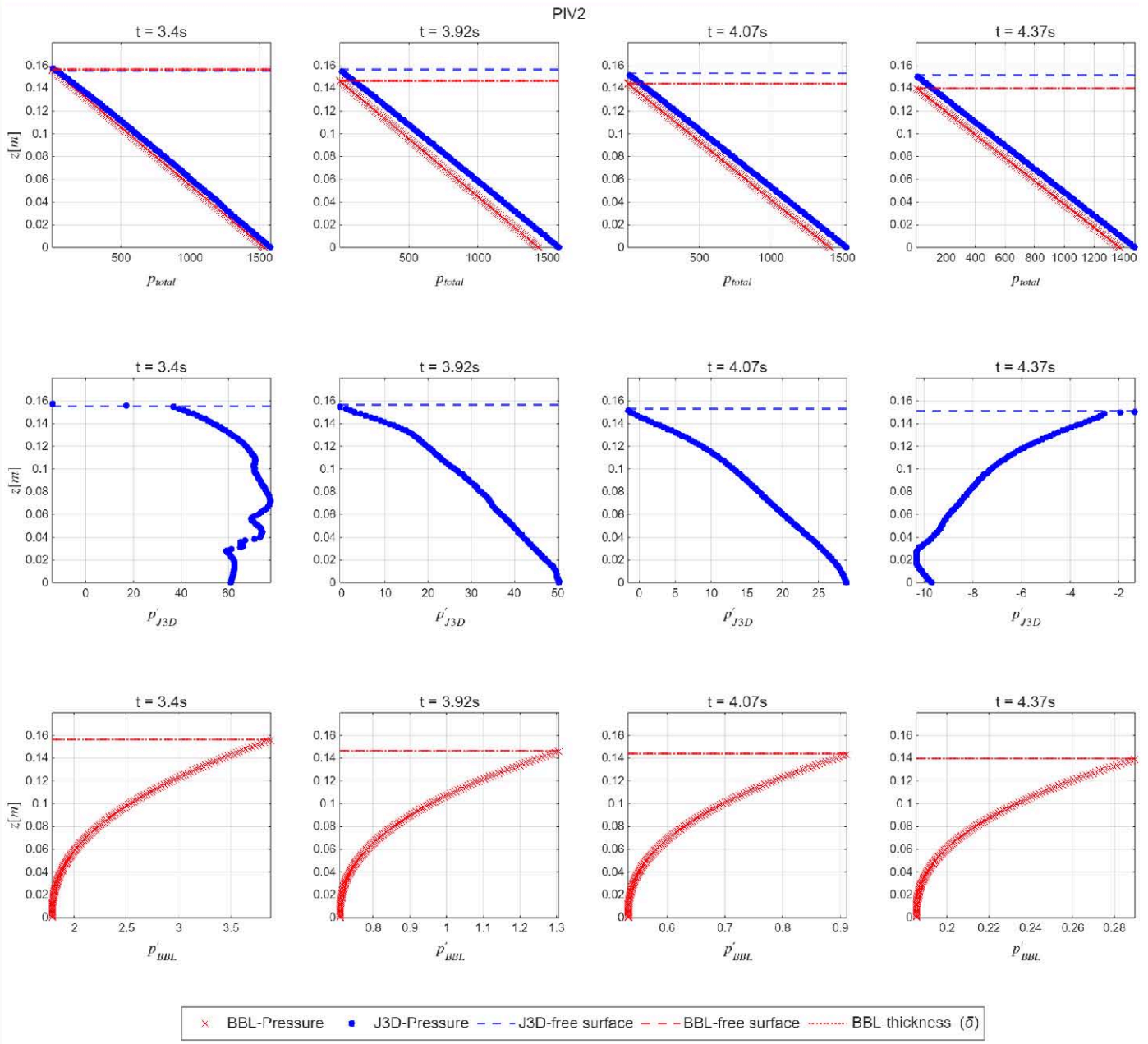

$$p_{Total}$$

$$p'_{J3D} = p_{Total} - \rho g(\eta(x) - \hat{z})$$

$$p'_{BBL} = p_{Term2} + p_{Term3}$$

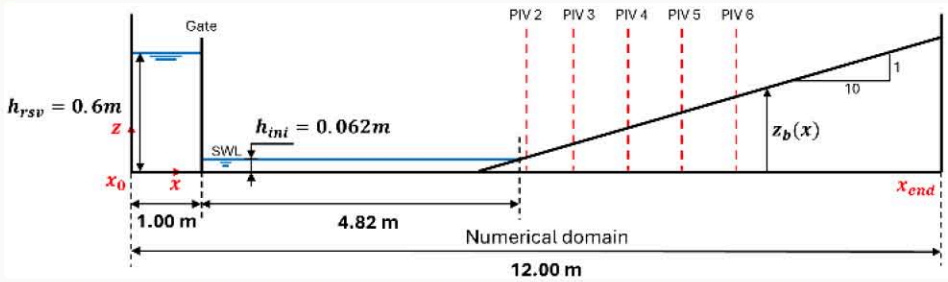

Conclusions

Model advancements and Limitations

Variables	BBL-model vs Measurements	BBL-model vs Depth-resolving model
Water depth (h)	✓ Well-predicted the bore arrival time X Overprediction	X Overprediction
Depth-averaged velocity (U)	✓ Accurate simulation for the run-up phase and the time of flow reversal X Overprediction in the backwash phase	✓ In close agreement
Horizontal-component of velocity (u)	✓ Accurate simulation for the velocity outside the BBL X Overprediction the BBL thickness	✓ Closer to the measurements for the run-up and backwash phase X Not accuracy at the flow reversal time
Vertical-component of velocity (w)	✓ Well-predicted X Not accuracy prediction near the toe of the beach	✓ Closer to the measurements
Dynamic pressure gradient		X Generally smaller

Conclusions

- The model successfully reconstructed vertical velocity
- The enhanced BBL model outperformed more complex 2DV/3D models in predicting vertical velocity, demonstrating the value of this approach.
- Reconstructed vertical acceleration terms contribute minimally to the overall pressure gradient, and the hydrostatic term are several orders of magnitude higher..
- The model's accuracy is reduced during highly dynamic events (bore arrival, uprush), and data smoothing at discontinuities remains a challenge.

Future work

- Adaptive Smoothing: Develop algorithms that can detect and handle discontinuities (like the swash tip) to avoid generating non-physical values during the smoothing process.
- Improved w Reconstruction: Explore higher-order continuity equations to better capture vertical mixing, especially during bore impact.
- Finalise the formu Non-Hydrostatic Pressure: Incorporate higher-order pressure terms into the governing equations if necessary.

University of Nottingham
UK | CHINA | MALAYSIA

UK Research and Innovation

Marie Skłodowska-Curie Actions

SEDIMARE 2023-2027

Sediment Transport and Morphodynamics in Marine and Coastal Waters with Engineering Solutions

Thank you for your attention!

This project has been funded by UKRI under the Horizon Europe guarantee scheme for the Marie Skłodowska-Curie Actions Doctoral Network grant (HORIZON-MSCA-2021-DN-01) under Grant Agreement No. 101072443.

Marie Skłodowska-Curie Actions

SEDIMARE

Sediment Transport and Morphodynamics in Marine and Coastal Waters with Engineering Solutions

hrwallingford

Multi-model approach to scour in dynamic areas

Nishchay Tiwari
HR Wallingford, UK

Supervisors and Advisors:
Michiel A.F. Knaapen
Sina Haeri
Richard Whitehouse

Marie Curie Grant Agreement Number: 101072443

UNIVERSITY OF PATRAS
UNIVERSITÀ POLITECNICA DELLE MARCHE
UNIVERSITY OF TWENTE.
UCLouvain
Deltares
FUNDACION
FUGRO
MENTUCCIAldo impresa di costruzioni
Flanders Hydraulics
Flanders State of the Art
The University of Nottingham

Contents

- Scour Phenomenon
- Scour Analysis with wave current interaction
  - Methodology
  - Three-phase Governing Equations
  - Computational Domain
  - Monopile scour with currents
  - Flume Wave analysis (University of Patras)
  - Flume Reflection analysis
  - Monopile scour under wave-current interaction
- Update on Cofferdam Scour
- Conclusion & Future Work

Scour Mechanisms around structures

Hydrodynamic Forces

- *Flow Acceleration :*
  - Structures disrupt flow, creating high-velocity zones and turbulence.
  - Flow accelerates around the structures, increasing bed shear stress.
- *Vortex Formation :*
  - Horseshoe vortices form at the base, enhancing local scour.
  - Wake vortices downstream contribute to scour hole deepening.

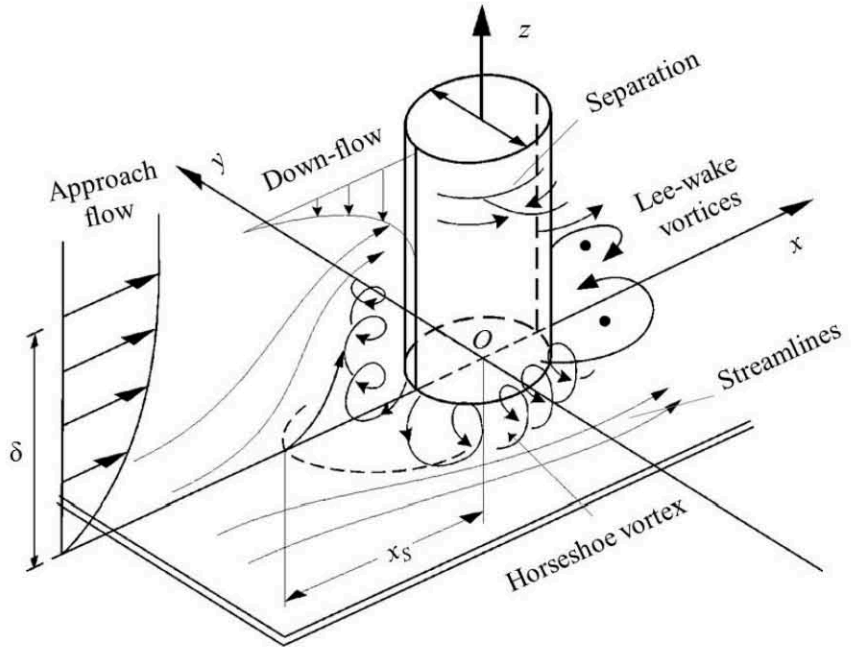

Sediment Transport Dynamics

- *Erosion :* High shear stress lifts sediment particles into suspension.
- *Deposition :* Sediment settles in low-energy zones (e.g., downstream of structures).

SedInterFoam Methodology

Inputs

Experimental Data

- *Transport properties* of sand and water (Flumes Experiment)
- *Geometrical dimensions* of flume and monopile
- *Input flow velocity, wave parameters*

Solver

Three-phase Eulerian RANS OpenFOAM

- **3D domain Creation**
- **SedInterFoam Implementation**:
  - *VOF* for water-air interface
  - *Granular Rheology* properties (muI)
  - Transport & Interfacial properties
  - Wave Properties

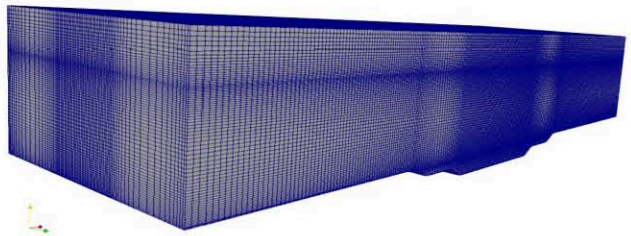

Outputs

Scour Depth

- **Wave spectrum** validation
- Prediction of **scour depth** using volume fraction of water and sand.

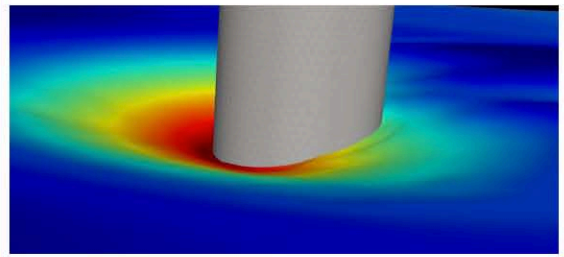

Three-phase Eulerian Governing Equations

- The continuity equations for sediment and fluid(water and air) phase

$$\frac{\partial \phi}{\partial t} + \frac{\partial}{\partial x_i}[\phi u_i^s] = 0$$

$$\frac{\partial}{\partial t}[\gamma(1-\phi)] + \frac{\partial}{\partial x_i}[\gamma(1-\phi)u_i^l] = 0$$

$$+$$

$$\frac{\partial}{\partial t}[(1-\gamma)(1-\phi)] + \frac{\partial}{\partial x_i}[(1-\gamma)(1-\phi)u_i^g] = 0$$

$$=$$

$$\frac{\partial \gamma}{\partial t} + \frac{\partial}{\partial x_i}[\gamma u_i^f] - \gamma\frac{\partial u_i^f}{\partial x_i} = 0$$

$$u_i^f = \gamma u_i^l + (1-\gamma)u_i^g$$

ϕ Volume Fraction of Sediment Phase

γ Fluid Indicator Function: Volume Fraction of Liquid Phase

Velocity of the fluid phase, a weighted average of water and air velocities

Three-phase Eulerian Governing Equations

- The momentum equations for the sediment and fluid phase

$$\frac{\partial}{\partial t}[\rho^s \phi u_i^s] + \frac{\partial}{\partial x_i}[\rho^s \phi u_i^s u_j^s] = \frac{\partial}{\partial x_i}\Sigma_{ij}^s + \phi \rho^s g_i + \phi f_i + M_i$$

The momentum exchange term, representing forces between the sediment and fluid phases.

Solid-phase effective stress tensor.

Fluid-phase effective stress tensor.

$$\frac{\partial}{\partial t}[\rho^f (1-\phi) u_i^f] + \frac{\partial}{\partial x_i}[\rho^f (1-\phi) u_i^f u_j^f] = \frac{\partial}{\partial x_i}\Sigma_{ij}^f + (1-\phi)\rho^f g_i + (1-\phi) f_i - M_i + \sigma\kappa\frac{\partial \gamma}{\partial x_i}$$

The surface tension force at the air-water interface, proportional to the surface tension coefficient σ and the interface curvature κ

Stress Tensors & Rheology

- Stress Tensors

$$\Sigma_{ij}^f = -P^f \delta_{ij} + T_{ij}^f$$
$$\Sigma_{ij}^s = -P^s \delta_{ij} + T_{ij}^s$$

$$T_{ij}^f = \rho^f (1-\phi) \left[\left(v^{\text{mix}} + v_t^f \right) \left(\frac{\partial u_i^f}{\partial x_j} + \frac{\partial u_j^f}{\partial x_i} - \frac{2}{3} \frac{\partial u_k^f}{\partial x_k} \delta_{ij} \right) - \frac{2}{3} \lambda^f \delta_{ij} \right]$$

$$v^f = \gamma v^l + (1-\gamma) v^g$$

Fluid-phase eddy (turbulent) viscosity, modeling turbulence effects

$k - \omega$

$$T_{ij}^s = \rho^s \phi \left[(v^s + \cancel{v_t^s}) \left(\frac{\partial u_i^s}{\partial x_j} + \frac{\partial u_j^s}{\partial x_i} - \frac{2}{3} \frac{\partial u_k^s}{\partial x_k} \delta_{ij} \right) - \frac{2}{3} \lambda^s \delta_{ij} \right]$$

Solid-phase viscosity, modelled using kinetic theory for granular flows or μ(I) rheology.

$$\nu_s = \frac{\mu(I) \bar{p}^s}{\rho^s \| \mathbf{S}^s \|}$$

$$\mu(I) = \mu_s + \frac{\mu_2 - \mu_s}{I_0 / I + 1}$$

Computational Domain Setup

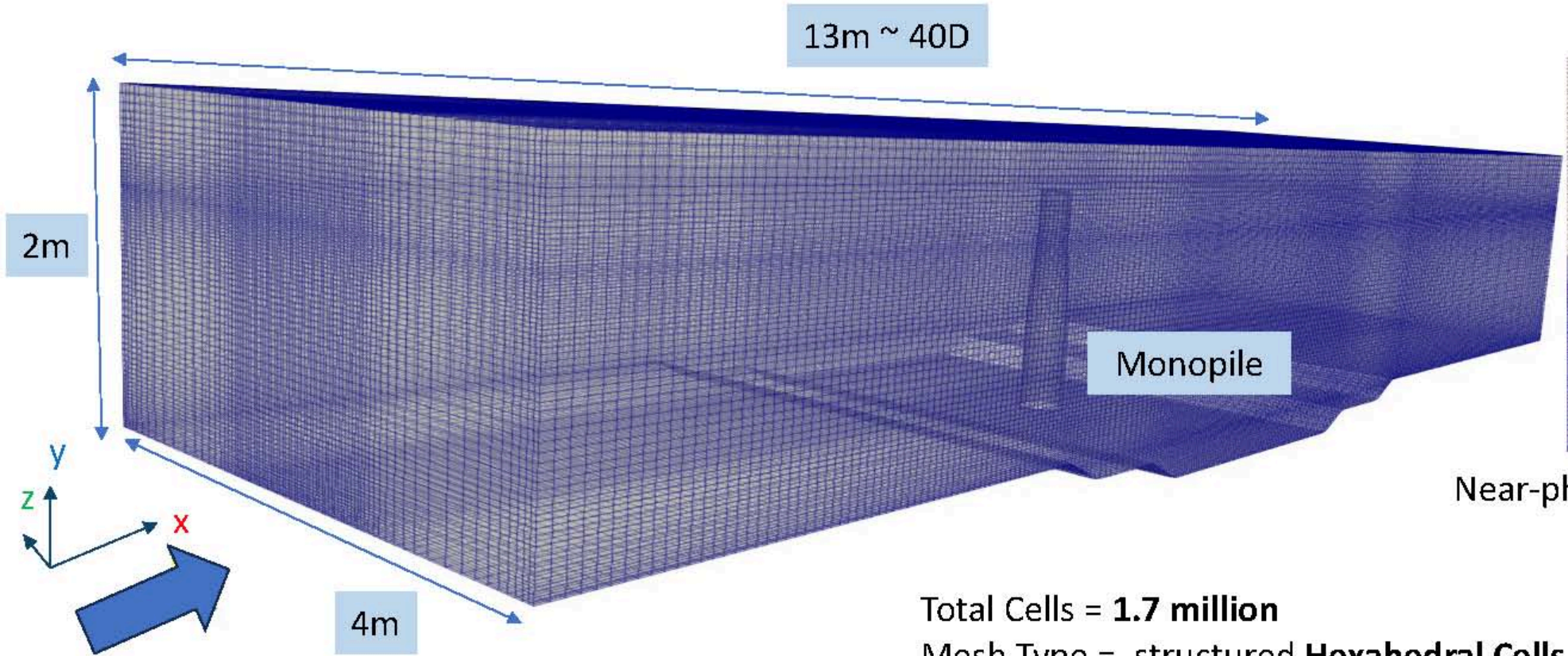

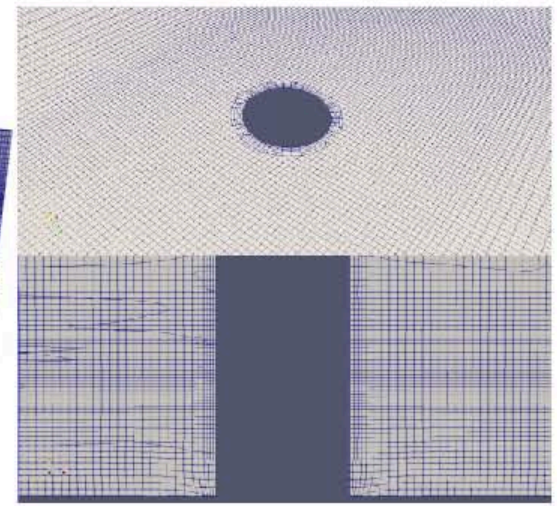

Near-phase resolution $\Delta y_1 \approx 6$ mm

Total Cells = **1.7 million**
Mesh Type = structured **Hexahedral Cells** *with hybrid interface*
Dimensions based on Flumes Experiments (with shorter Flume Length)
Monopile Diameter (D)= **0.35m**
Monopile Height= **2m**

Boundary and Initial conditions

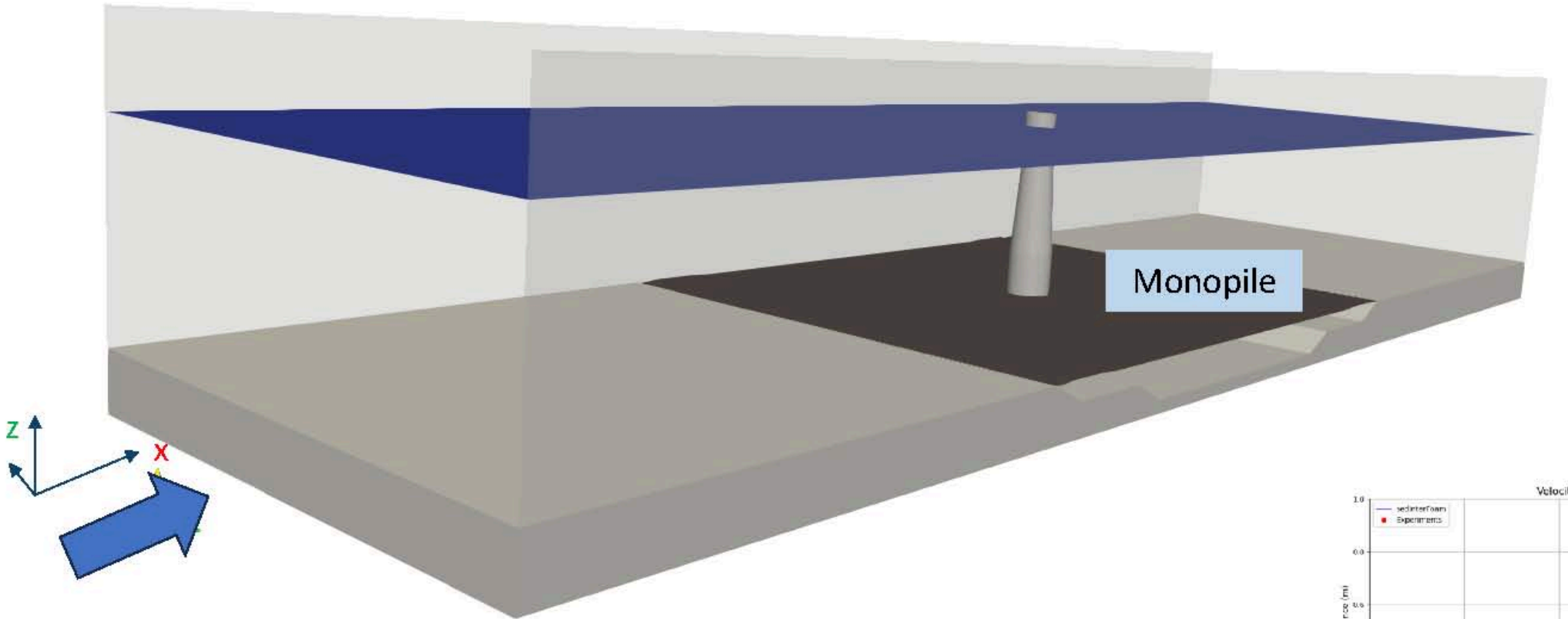

ϑ_t= Wall Function
k = Wall Function
ω = Wall Function
U = 0 [m/s]

walls

α_{sand} = 0.635
α_{fluid} = 0.365

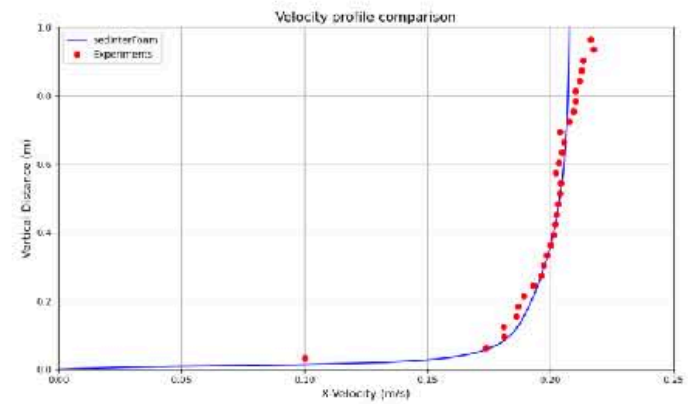

Monopile with currents

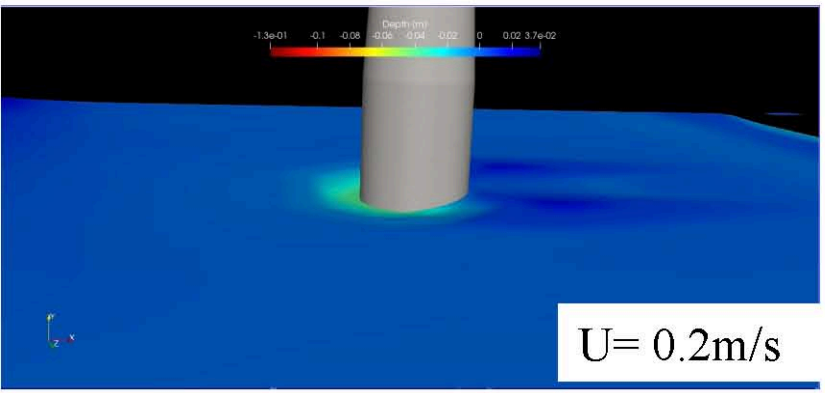

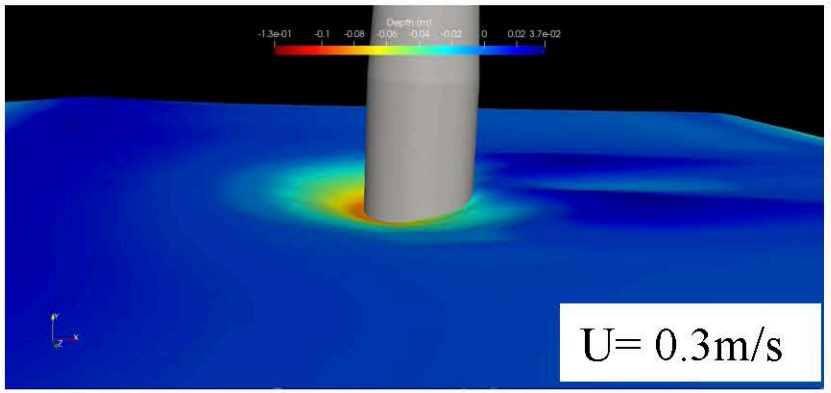

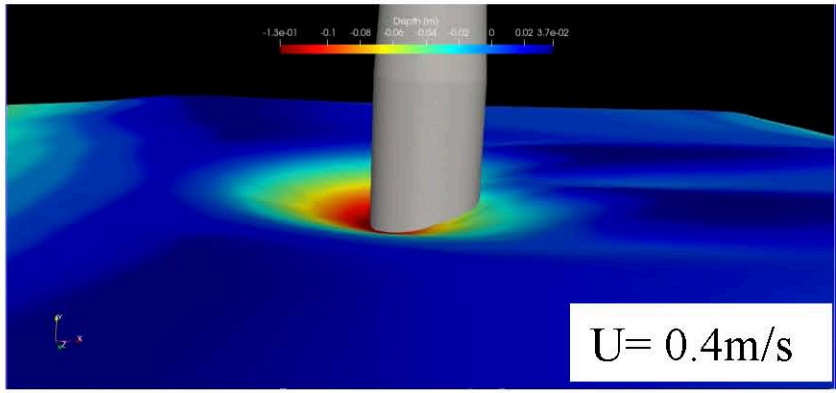

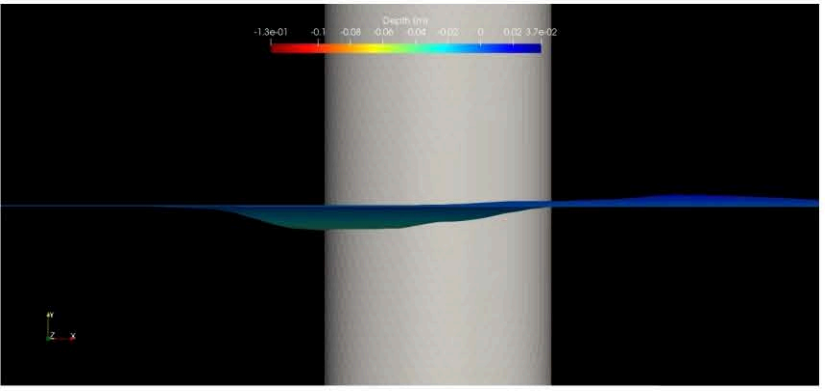

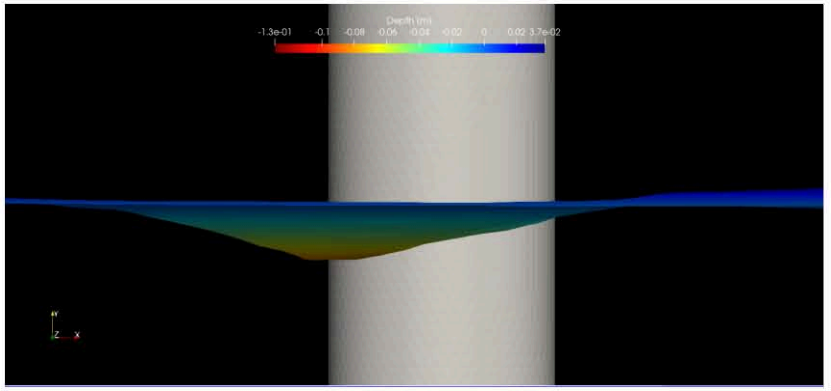

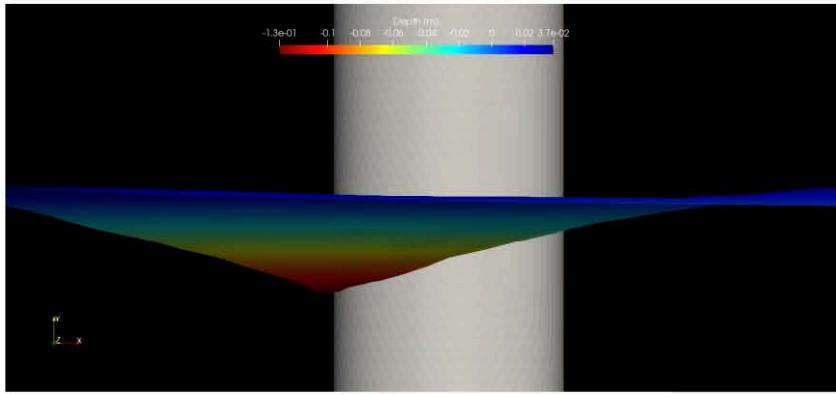

$$D_* = d_{50}\left(\frac{(s-1)g}{\nu^2}\right)^{1/3} \approx 5.06 \qquad \theta_{cr} = \frac{0.30}{1+1.2D_*} + 0.055\left[1-e^{-0.020D_*}\right] \approx 0.0477 \qquad u_*^{cr} = \sqrt{\theta_{cr}(s-1)gd_{50}} \approx 0.0124\,\mathrm{m/s} \qquad \bar{U}_{cr} = \frac{u_*^{cr}}{\kappa}\left[\ln\left(\frac{h}{z_0}\right)-1\right] \Rightarrow \bar{U}_{cr} \approx 0.313\,\mathrm{m/s}$$

Monopile with currents

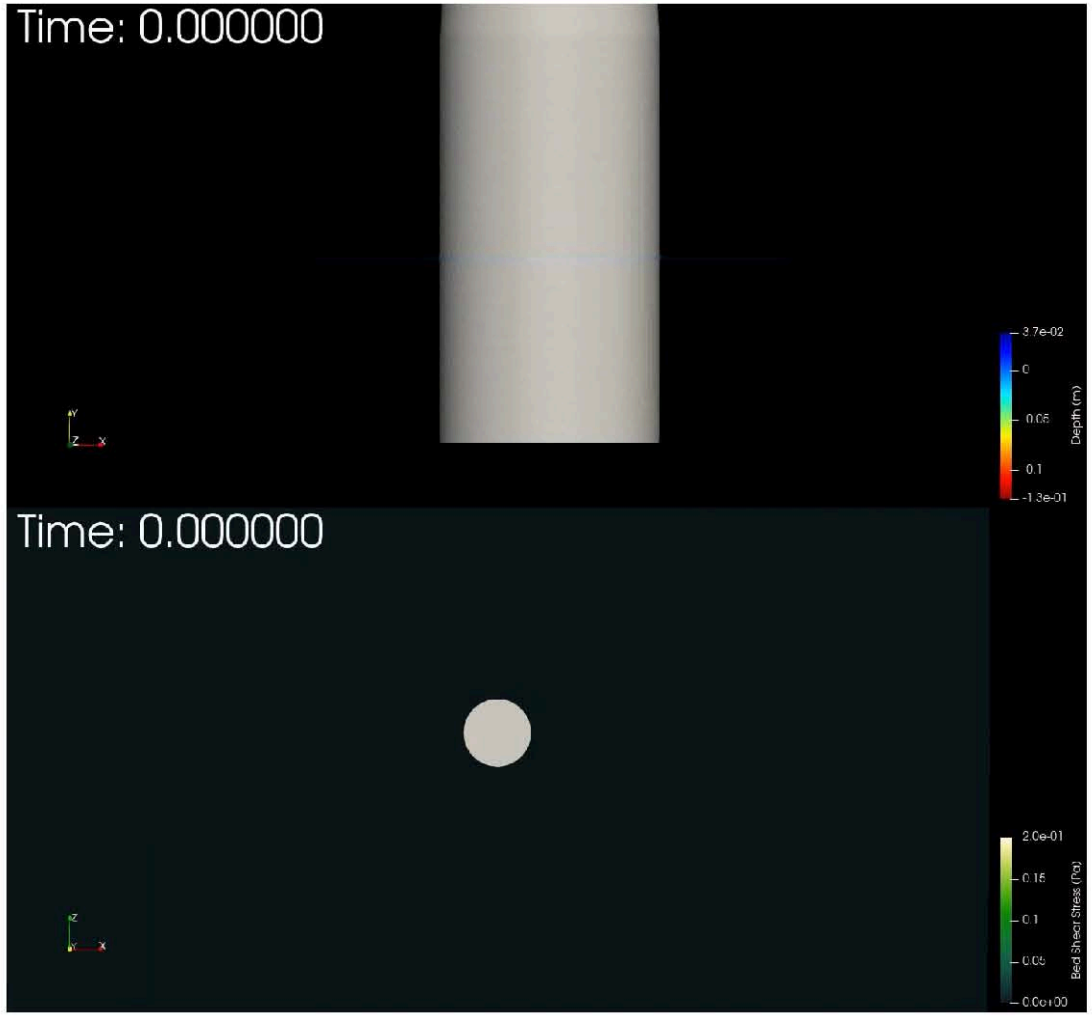

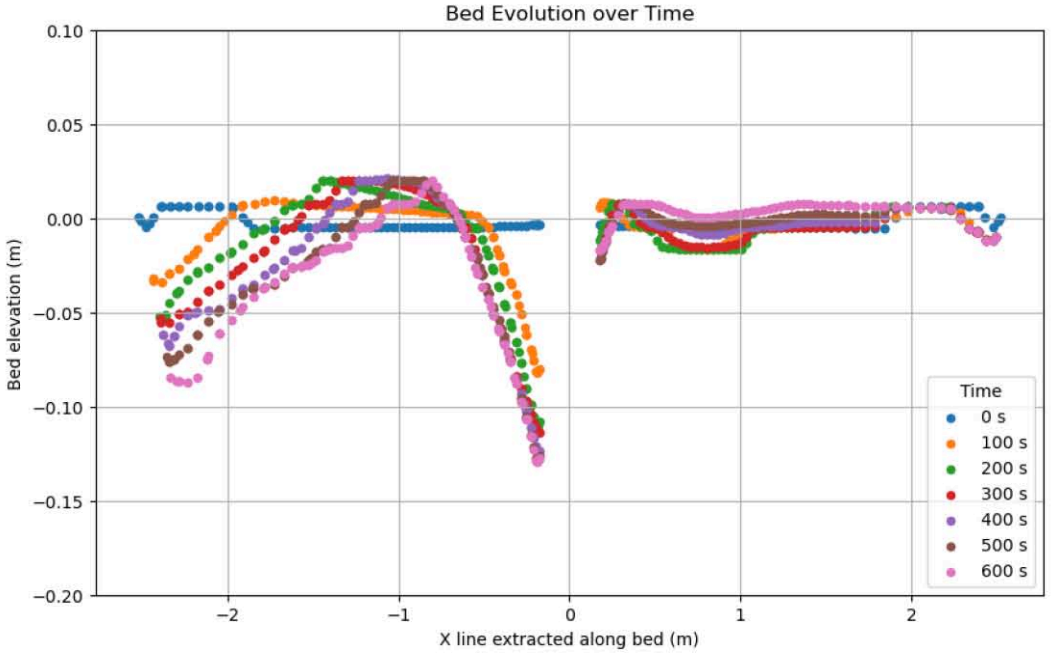

$$\boldsymbol{\tau} = \mu \left[\nabla \mathbf{u} + (\nabla \mathbf{u})^T \right]$$

$$\boldsymbol{\tau}_{\tan} = \mathbf{t} - (\mathbf{t} \cdot \mathbf{n})\mathbf{n}$$

$$\tau_b = |\boldsymbol{\tau}_{\tan}|$$

$$\tau_{cr} = \theta_{cr}(\rho_s - \rho)gd$$

Wave Flume CFD setup

Array Spacings	Ref_01	Ref_02	Ref_03	Ref_04
Array_01	0.00	0.40	0.90	2.40

Relaxation Zone INLET

Relaxation Zone OUTLET

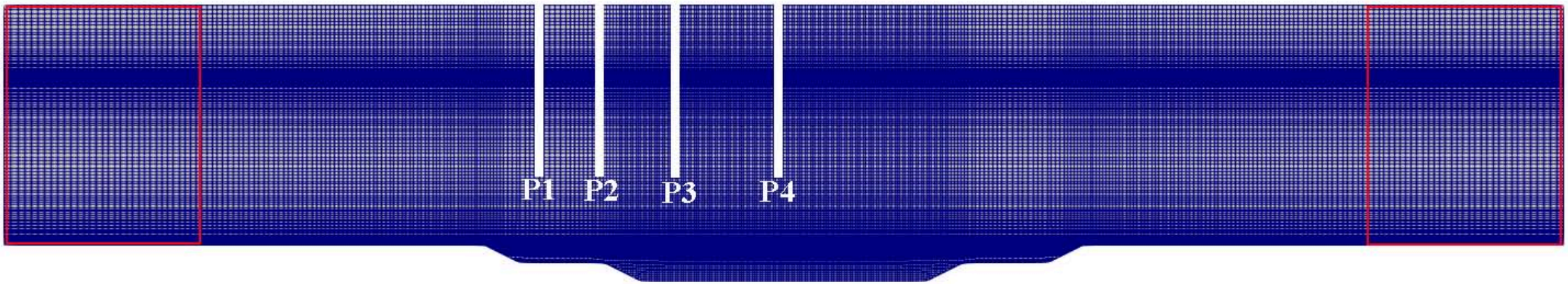

Parameter	*Value*
Wave Type	**Irregular**
Spectrum	**JONSWAP**
Significant Wave Height (Hs)	**0.271 m**
Peak Wave Period (Tp)	**2.194 s**
JONSWAP Gamma (γ)	**2**
Water Depth	**1.395 m**

Number of Frequency Components (N)	**1000**
Phase Method	**Random Phase**
Seed for Random Phases	**10**
Frequency Axis	**Equidistant**
Lower Frequency Cutoff	**0.15 Hz**
Upper Frequency Cutoff	**1.3 Hz (includes peak at ~0.455 Hz)**

Waves analysis (standard vs weighted)

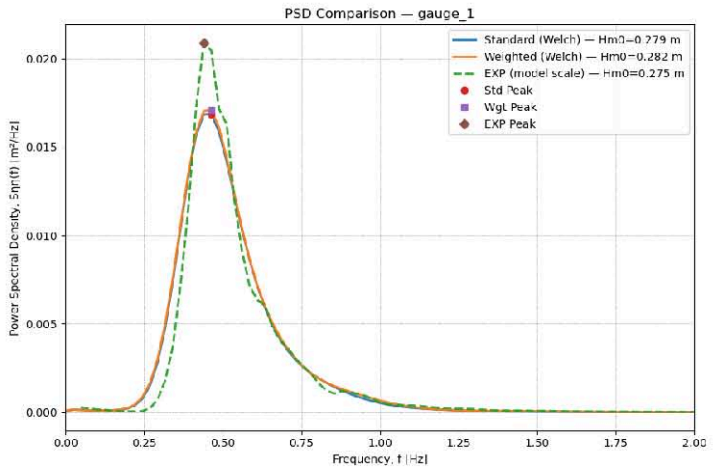

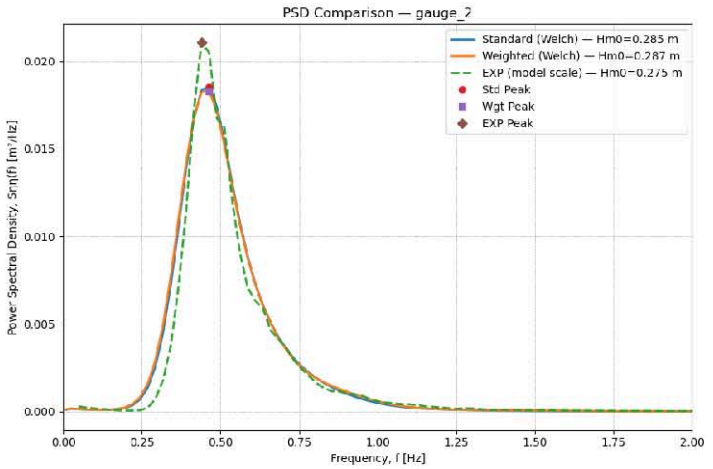

Reconstruction from CFD

$$\eta_i(t)$$

$$\eta_{\mathrm{SWL}} = 1.395\,\mathrm{m} \qquad \eta_i'(t) = \eta_i(t) - \eta_{\mathrm{SWL}}$$

$$\Delta t = t_{k+1} - t_k$$

$$S_{\eta\eta}(f) = \frac{1}{N}\left|\mathcal{F}\{\eta'(t)\}\right|^2$$

$$m_0 = \int_0^\infty S_{\eta\eta}(f)\,df \qquad H_{m0} = 4\sqrt{m_0}$$

EXP $\quad n_L = 31.4$

$$f_{\mathrm{model}} = f_{\mathrm{proto}}\sqrt{n_L}$$

$$S_{\eta\eta,\mathrm{model}}(f_{\mathrm{model}}) = \frac{S_{\eta\eta,\mathrm{proto}}(f_{\mathrm{proto}})}{n_L^{2.5}}$$

$$m_0 = \int_0^\infty S_{\eta\eta}(f)\,df \qquad H_{m0} = 4\sqrt{m_0}$$

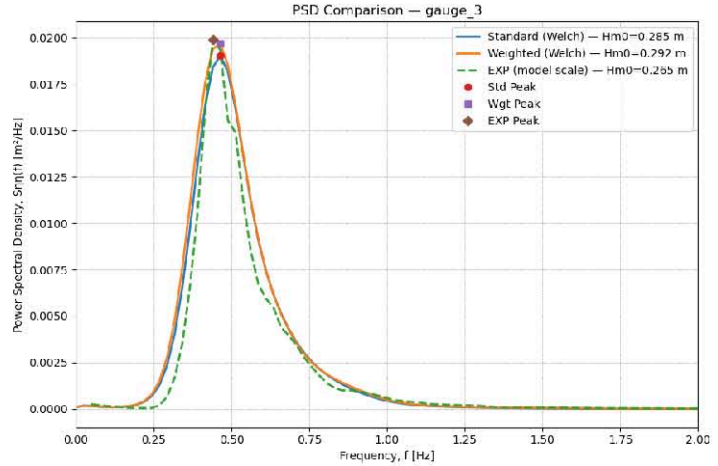

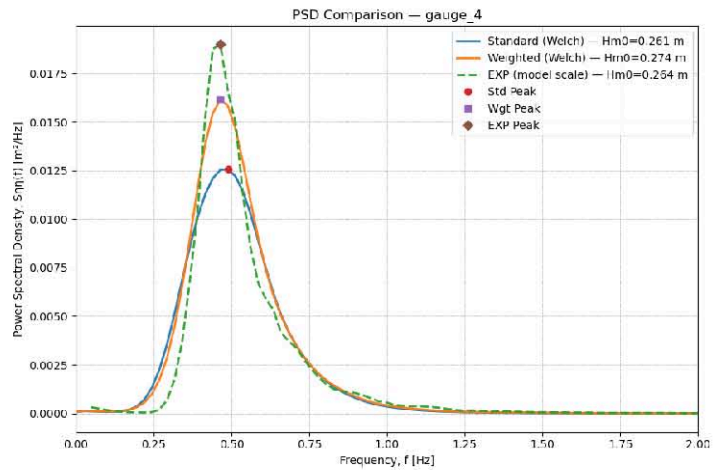

Reflection analysis

$\eta_i(t)$

$\tilde{\eta}_j(t) = \eta_j(t) - \eta_{\mathrm{SWL}}$

$\omega^2 = g\,k\,\tanh(kh)$

Phase for incident waves

Phase for reflected waves

$$G_{ij}(f) = S^+(f)\, e^{+ik(f)\Delta x_{ij}} + S^-(f)\, e^{-ik(f)\Delta x_{ij}}$$

$$\mathbf{Hs} \approx \mathbf{y}$$

Least Square System

$$\mathbf{H}(f) = \begin{bmatrix} e^{+ik\Delta x_{i_1 j_1}} & e^{-ik\Delta x_{i_1 j_1}} \\ \vdots & \vdots \\ e^{+ik\Delta x_{i_{N_p} j_{N_p}}} & e^{-ik\Delta x_{i_{N_p} j_{N_p}}} \end{bmatrix} \quad \mathbf{s}(f) = \begin{bmatrix} S^+(f) \\ S^-(f) \end{bmatrix} \quad \mathbf{y}(f) - \begin{bmatrix} G_{i_1 j_1}(f) \\ \vdots \\ G_{i_{N_p} j_{N_p}}(f) \end{bmatrix}$$

$S^+(f)$

$S^-(f)$

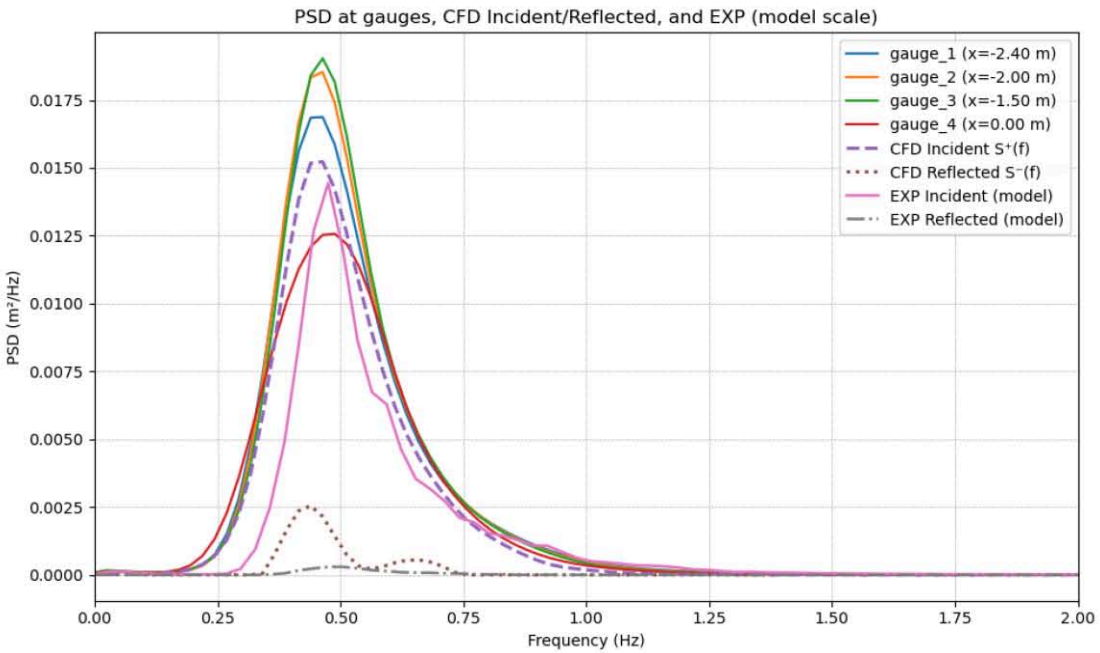

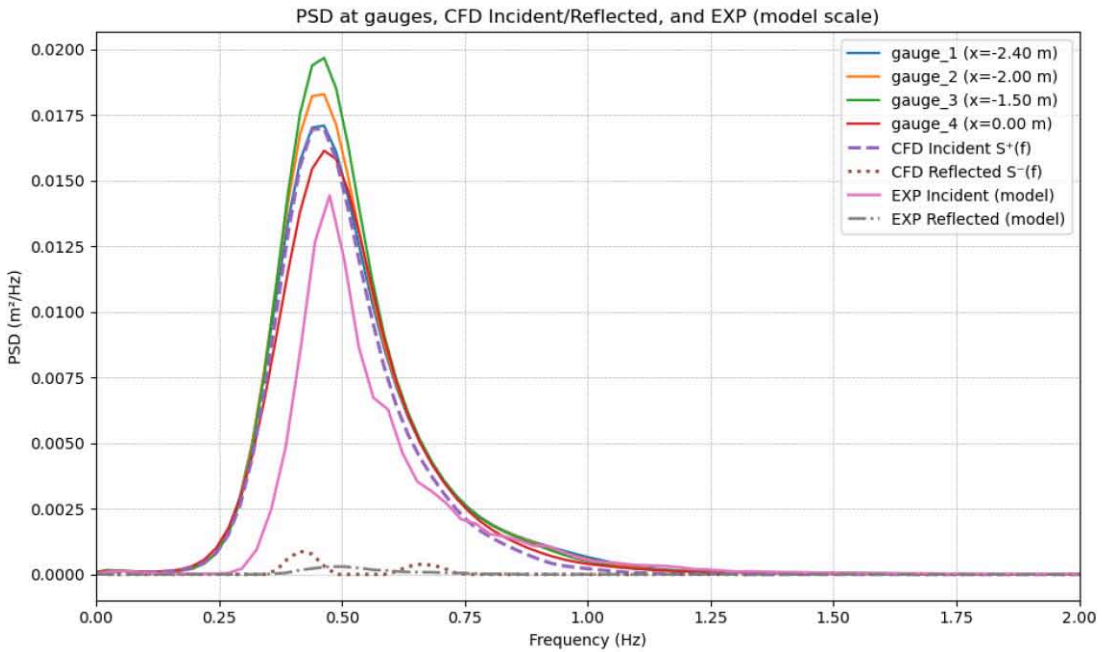

Reflection analysis

Significant wave heights (CFD)
gauge_1 @ x= -2.40 m : Hm0 = 0.2791 m
gauge_2 @ x= -2.00 m : Hm0 = 0.2851 m
gauge_3 @ x= -1.50 m : Hm0 = 0.2850 m
gauge_4 @ x= 0.00 m : Hm0 = 0.2611 m
Incident (S+) : **Hm0 = 0.2563 m**
Reflected (S-) : **Hm0 = 0.0770 m**

Significant wave heights (EXP, model scale)
EXP Incident : **Hm0 = 0.2275 m**
EXP Reflected : **Hm0 = 0.0313 m**

$$m_0 = \int_0^\infty S_{\eta\eta}(f)\, df$$

$$H_{m0} = 4\sqrt{m_0}$$

Significant wave heights (CFD)
gauge_1 @ x= -2.40 m : Hm0 = 0.2821 m
gauge_2 @ x= -2.00 m : Hm0 = 0.2867 m
gauge_3 @ x= -1.50 m : Hm0 = 0.2916 m
gauge_4 @ x= 0.00 m : Hm0 = 0.2741 m
Incident (S+) : **Hm0 = 0.2689 m**
Reflected (S-) : **Hm0 = 0.0411 m**

Significant wave heights (EXP, model scale)
EXP Incident : **Hm0 = 0.2275 m**
EXP Reflected : **Hm0 = 0.0313 m**

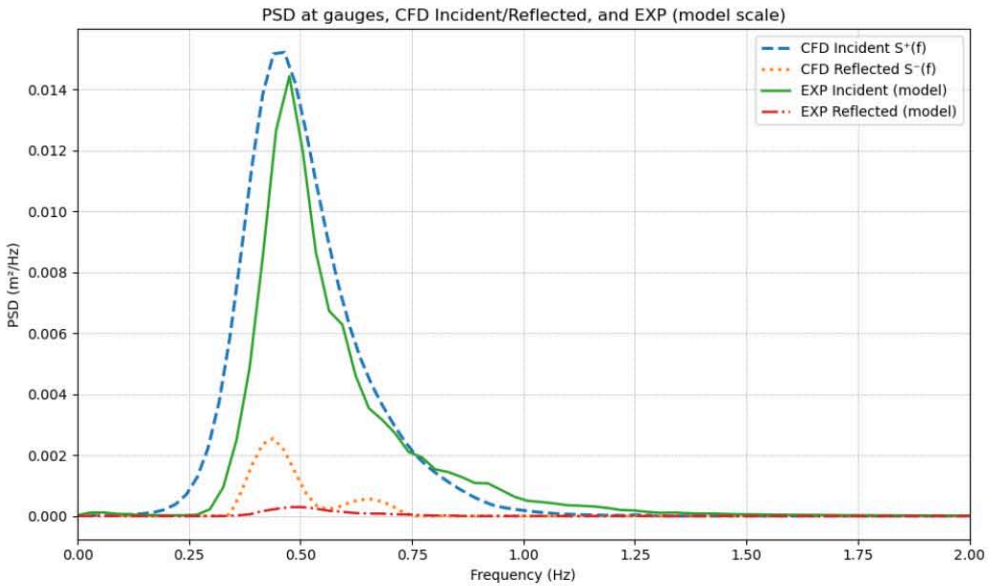

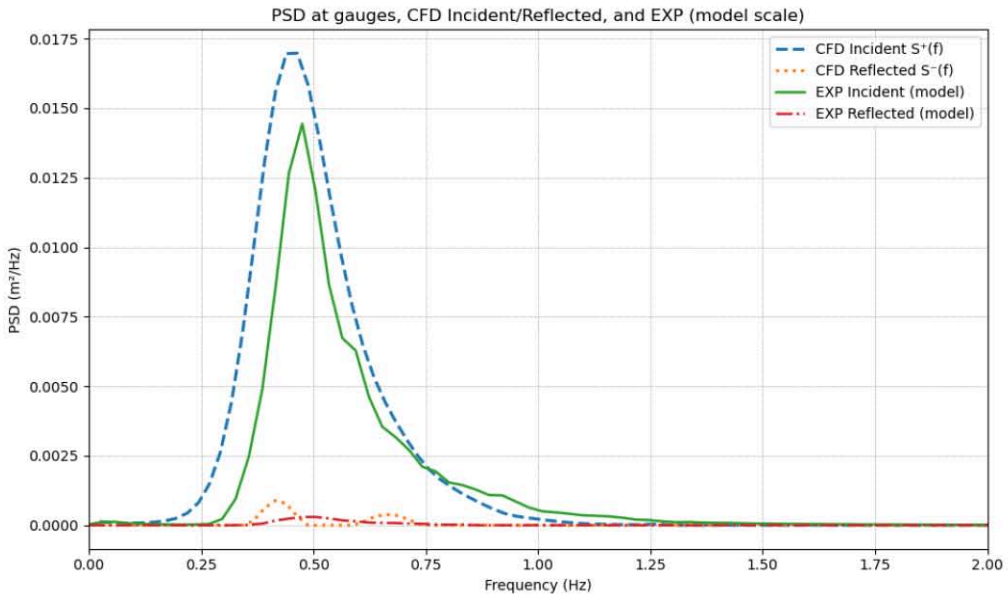

Reflection analysis (adjusted)

Significant wave heights (CFD)
gauge_1 @ x= -2.40 m : Hm0 = 0.2491 m
gauge_2 @ x= -2.00 m : Hm0 = 0.2545 m
gauge_3 @ x= -1.50 m : Hm0 = 0.2547 m
gauge_4 @ x= 0.00 m : Hm0 = 0.2328 m
Incident (S+) : **Hm0 = 0.2296 m**
Reflected (S-) : **Hm0 = 0.0683 m**

Significant wave heights (EXP, model scale)
EXP Incident : **Hm0 = 0.2275 m**
EXP Reflected : **Hm0 = 0.0313 m**

$$m_0 = \int_0^\infty S_{\eta\eta}(f)\, df$$

$$H_{m0} = 4\sqrt{m_0}$$

Significant wave heights (CFD)
gauge_1 @ x= -2.40 m : Hm0 = 0.2421 m
gauge_2 @ x= -2.00 m : Hm0 = 0.2455 m
gauge_3 @ x= -1.50 m : Hm0 = 0.2495 m
gauge_4 @ x= 0.00 m : Hm0 = 0.2346 m
Incident (S+) : **Hm0 = 0.2315 m**
Reflected (S-) : **Hm0 = 0.0332 m**

Significant wave heights (EXP, model scale)
EXP Incident : **Hm0 = 0.2275 m**
EXP Reflected : **Hm0 = 0.0313 m**

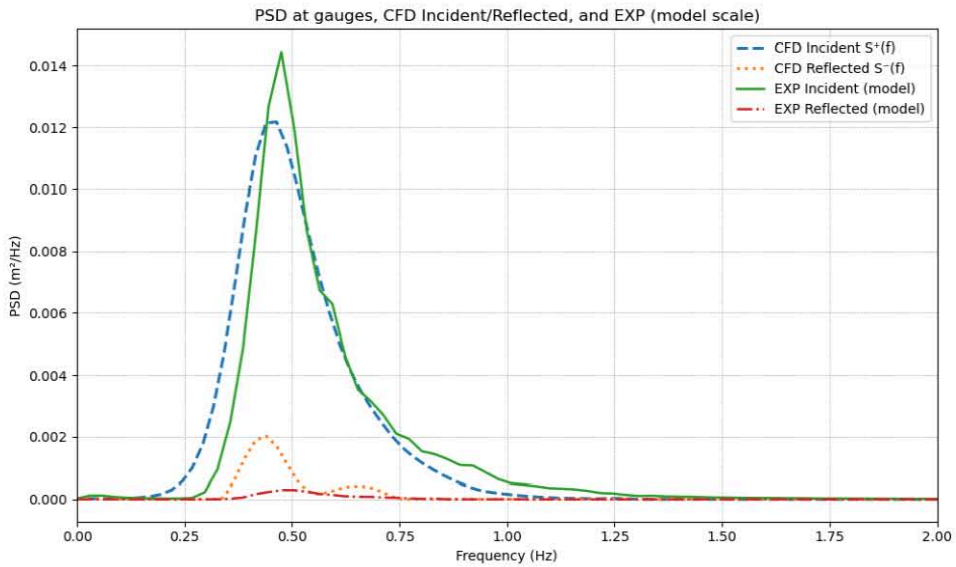

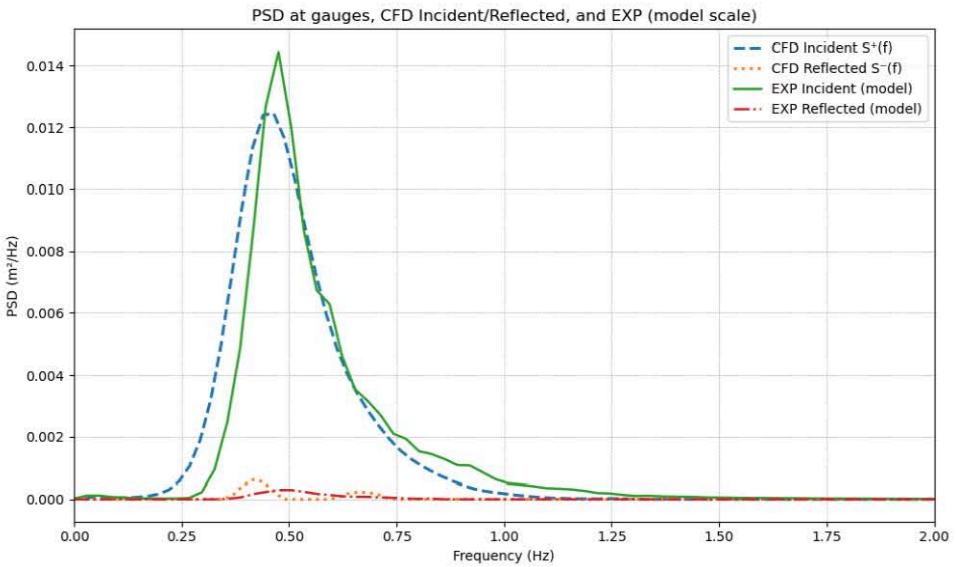

Monopile scour under waves & currents

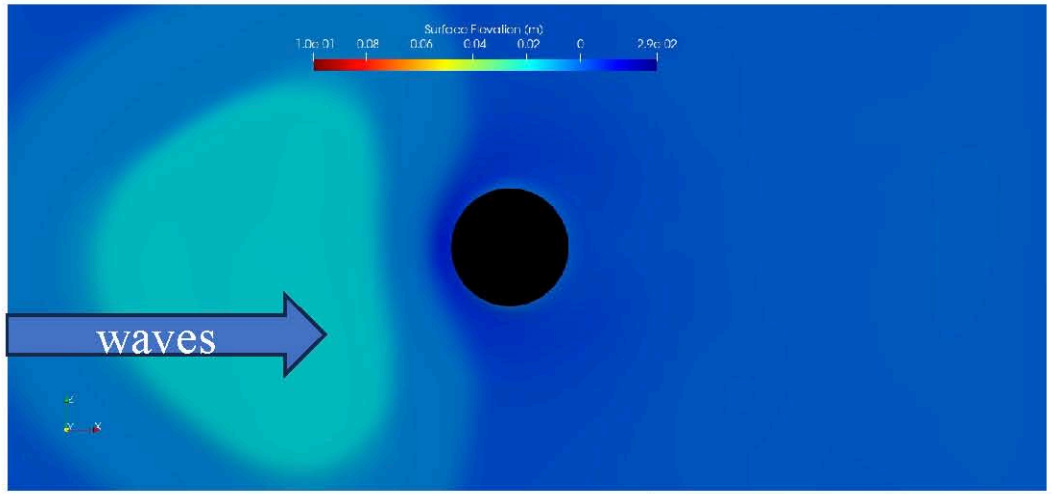

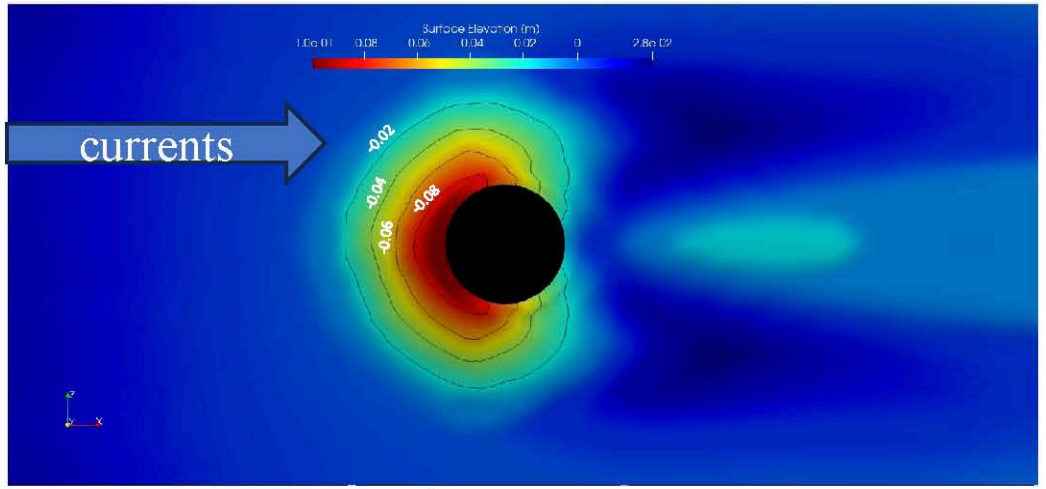

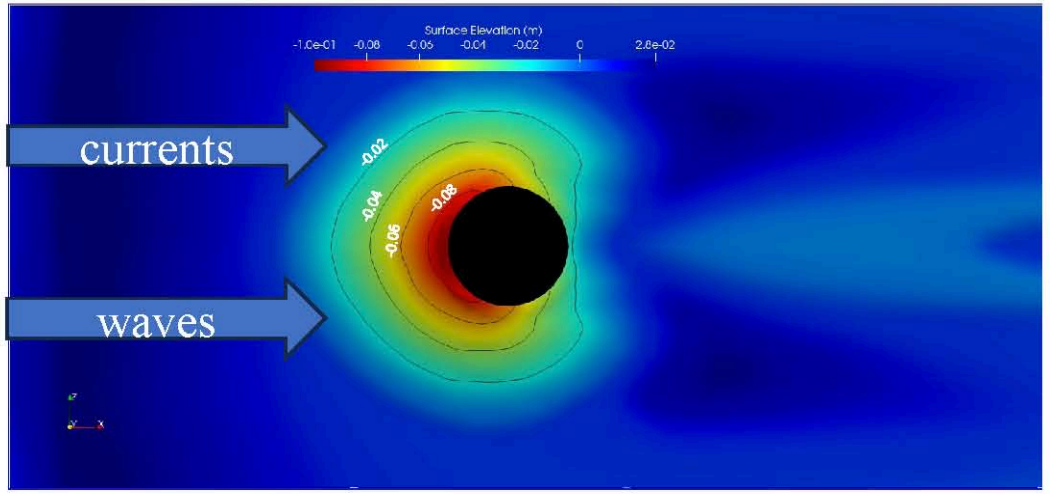

Update on Cofferdam Case

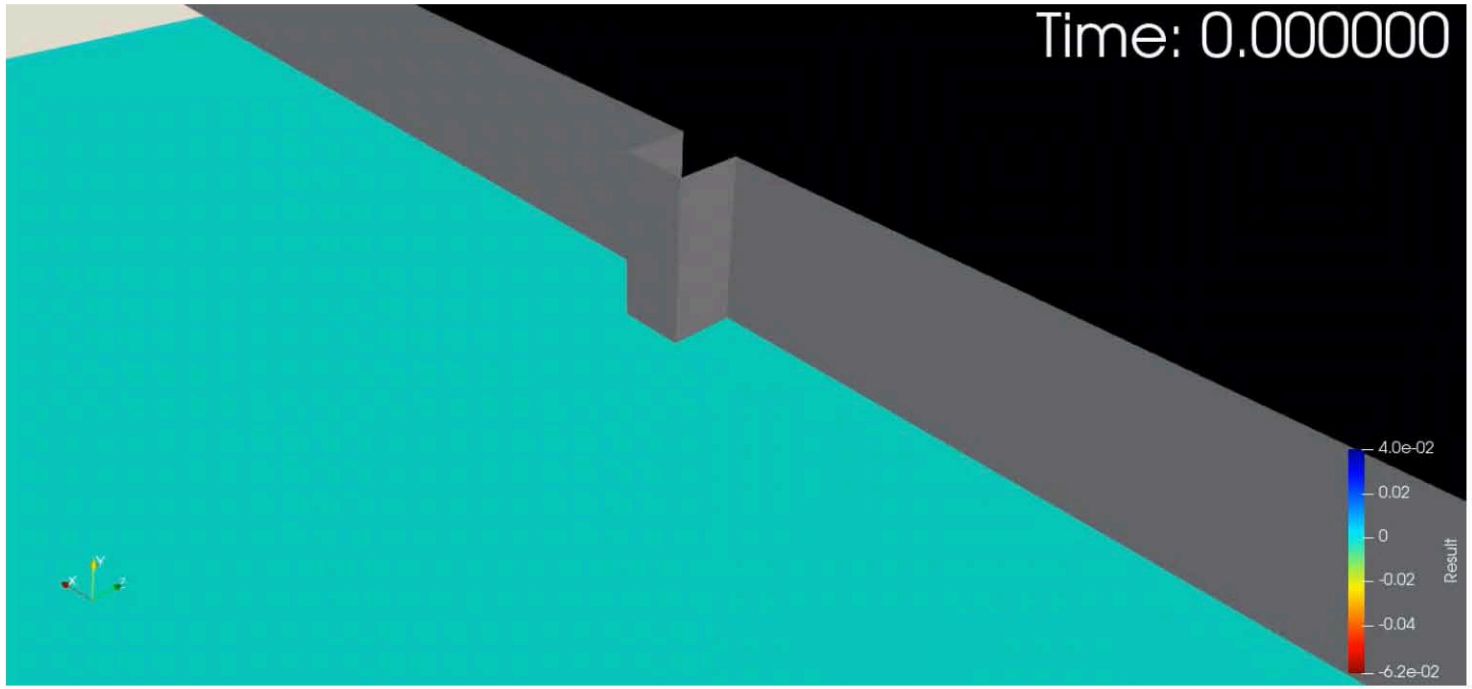

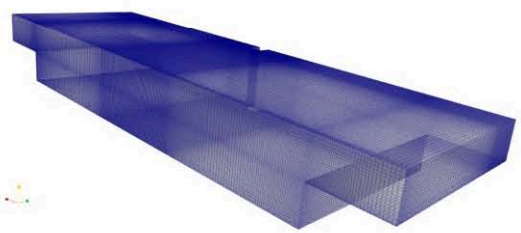

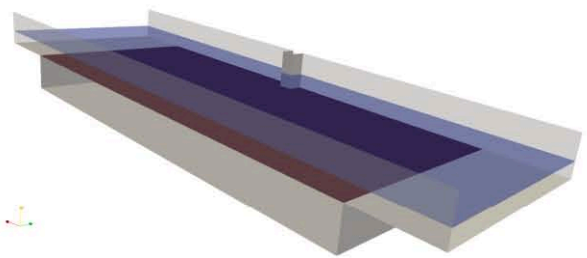

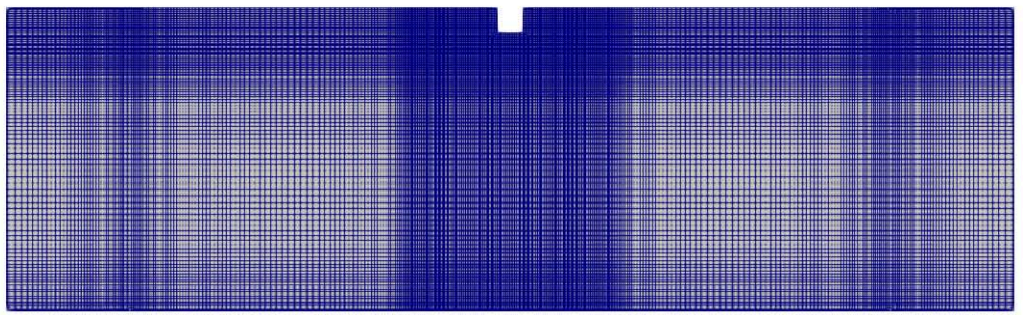

Rheology Parameters

Dynamic Friction Coefficient (high shear limit)

$$\mu(I) = \mu_s + \frac{\mu_2 - \mu_s}{\frac{I_0}{I} + 1}$$

Static friction Coefficient

Transitional Inertial Number

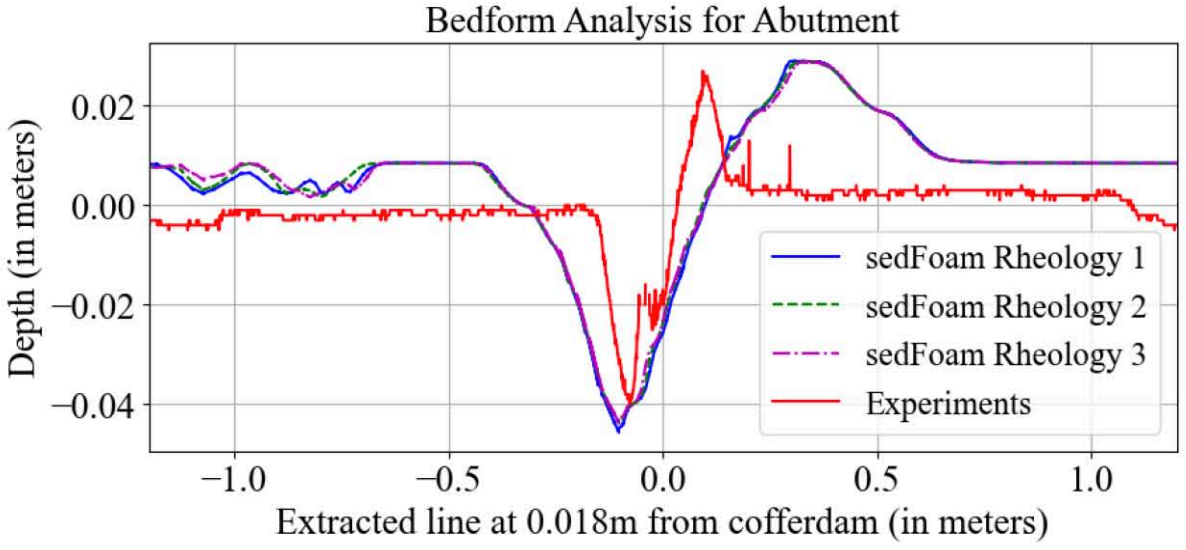

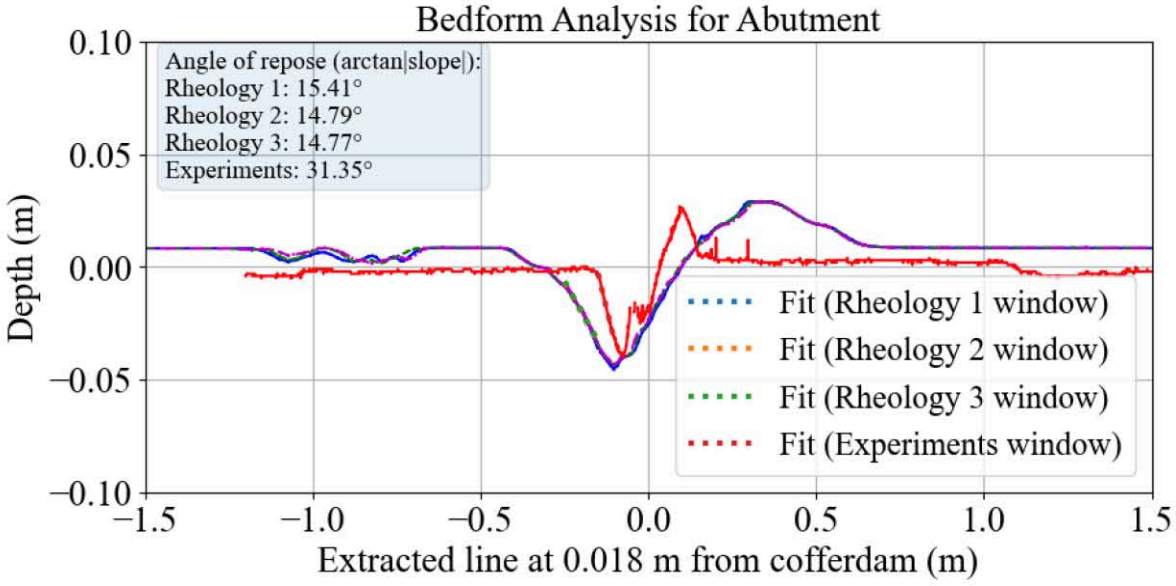

Bed Shear Stress

Recommended alpha.solid cut-off: (from literature) 0.001-0.01

$$\boldsymbol{\tau} = \mu \left[\nabla \mathbf{u} + (\nabla \mathbf{u})^T\right]$$

$$\boldsymbol{\tau}_{\tan} = \mathbf{t} - (\mathbf{t} \cdot \mathbf{n})\mathbf{n}$$

$$\tau_b = \left|\boldsymbol{\tau}_{\tan}\right|$$

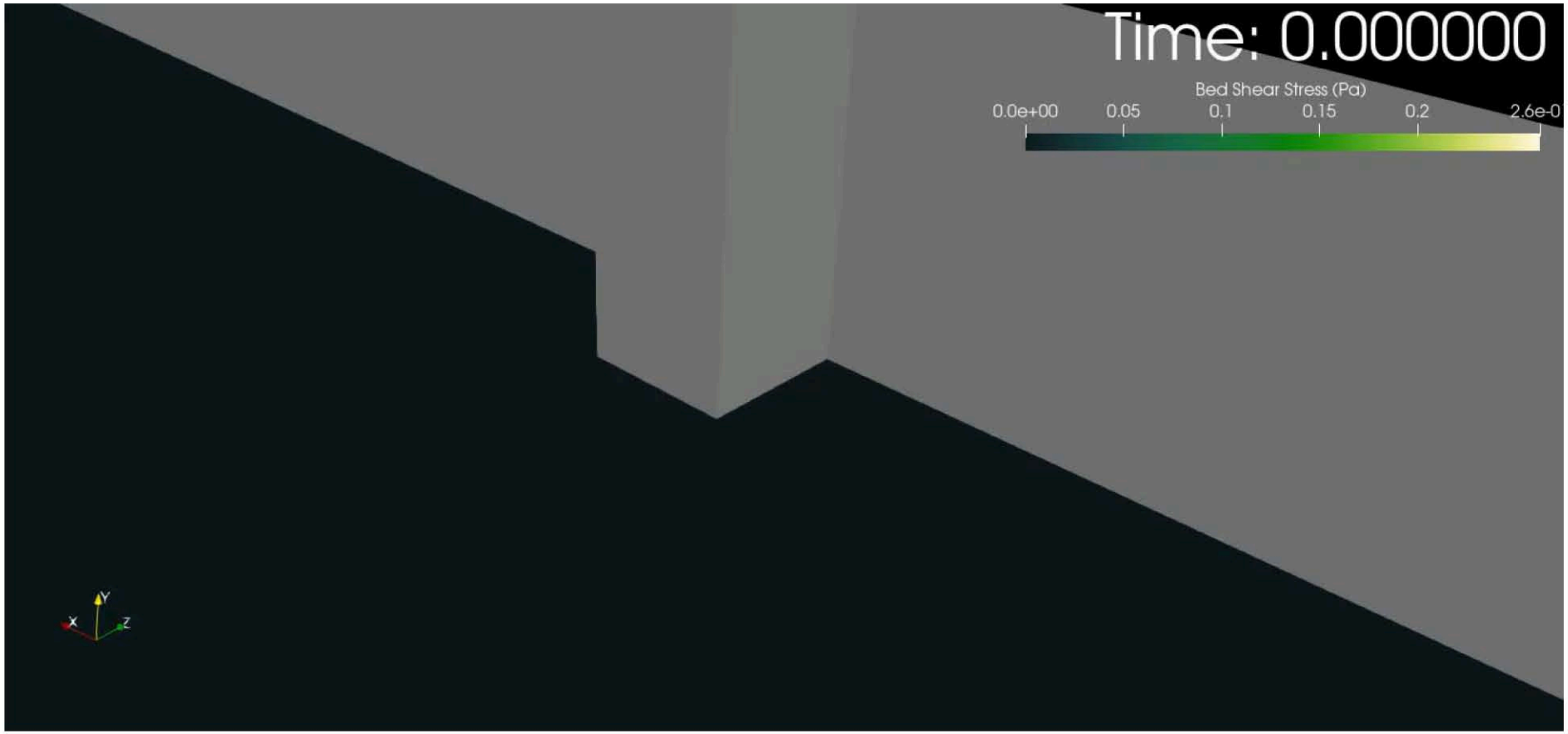

Conclusions and Future Work

Key Findings

- **Wave2Foam** reproduced experimental spectra reliabily.
- **Wave-current interaction**: Simulations showed that combined forcing changes the scour pattern.
- The model captured scour depth evolution with good agreement to flume experiments (cofferdam case).
- A structured mesh with $\Delta y = 5 * d_{50}$is recommended for accurately resolving the bed; it consistently outperforms unstructured meshes.
- The model successfully captured sediment transport around the structure near and above the critical threshold velocity:
  - At U ≈ U_cr = 0.3 m/s (onset of sediment motion)
  - At U > U_cr = 0.4 m/s (fully mobilized bed)

Future Work

- Detailed analysis of vorticity generation and turbulence under wave–current interaction.
- Implementation heterogeneity (mixed grain sizes) in the code.
- Extend the approach to prototype-scale offshore structures.
- Improve Rheology Implementation to reproduce realistic angle of repose.

Dissemination

- **Conference Presentations and Proceedings**
  - Paper presentation at Coastal Dynamics 2025, Aveiro, Portugal. Tiwari, N., Knaapen, M., Haeri, S., & Whitehouse, R. (2025, April 7–11). Numerical modelling for scour near cofferdams using Eulerian two-phase flow model.
  - Presentation at DMPCO 2025, Patras, Greece. Tiwari, N., Knaapen, M., Haeri, S., & Attili, T. (2025, May 7–9). Numerical Investigation of Scour Evolution around Monopile structures using sedInterFoam.

- **Secondment at University of Patras, Greece**
- **Planned Presentations and Journal Papers**
  - ICE Maritime Engineering Journal Article
  - Presentation at ICCE 2026

- **Outreach Activities**
  - United Nations SDG Innovation Project

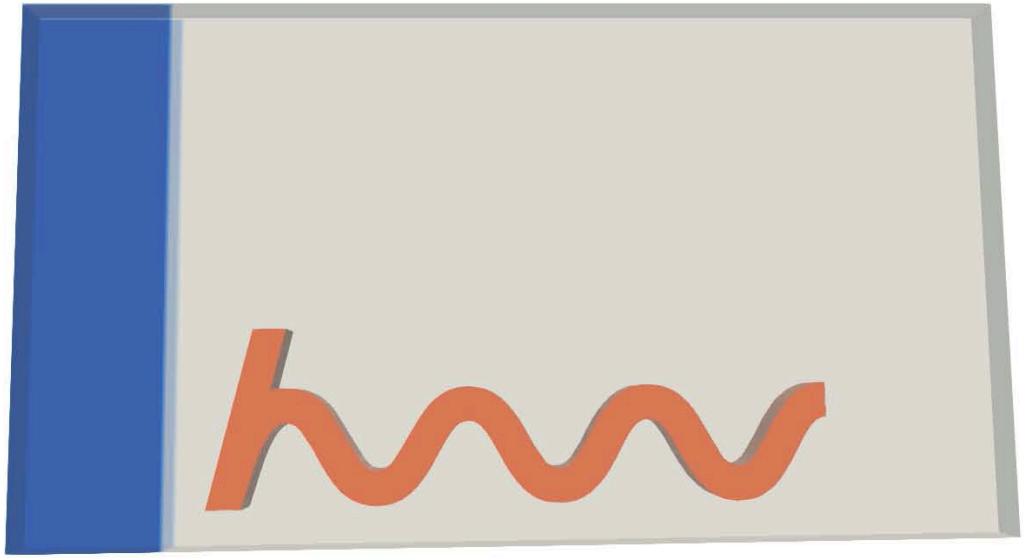

Thank You

The project is part of the EU Sedimare project (Horizon Europe Marie Skłodowska-Curie Actions, Grant Agreement no. 101072443), funded by the UKRI through the Horizon Europe guarantee (ref. EP/X02802X/1)

SEDIMARE

Funded by the European Union

UK Research and Innovation

Marie Skłodowska-Curie Actions

hr wallingford